DISSERTATION

# PHOTOPROTECTION AND CHLOROPLAST REGULATION IN THE GREEN ALGAE *CHLAMYDOMONAS REINHARDTII*

Submitted by

Michael Cantrell

Department of Biology

In partial fulfillment of the requirements

For the Degree of Doctor of Philosophy

Colorado State University

Fort Collins, Colorado

Spring 2019

Doctoral Committee:

Advisor: Graham Peers

Marinus Pilon
A.S.N Reddy
Christie Peeble

ABSTRACT

PHOTOPROTECTION AND CHLOROPLAST REGULATION IN THE GREEN ALGAE *CHLAMYDOMONAS REINHARDTII*

Absorbed light energy in excess of a cell's photosynthetic capacity can lead to production of reactive oxygen species (ROS) causing cell damage and death. Plants and algae have evolved conserved photoprotective responses that, at the level of light harvesting, are collectively measured as non-photochemical quenching (NPQ) of chlorophyll fluorescence. The major components of NPQ are thermal dissipation of excess light energy (excitation dependent quenching, qE), the migration of antenna complexes from PSII to PSI (state transitions, qT) and inactivation of PSII by damage (photoinhibition, qI). Excess reductant generated during light harvesting can also be dissipated by auxiliary electron transport (AET). The following dissertation aimed to characterize the role of qE in acclimation to saturating and sinusoidal light regimes in the model green algae *Chlamydomona*s *reinhardtii*, to characterize potential energy dissipating mechanisms that may occur in absence of qE and identify factors regulating the expression of the chloroplast encoded photosystem I subunit, *psaA,* using a forward genetic screen. In chapter 2 I show that the qE mutant, *npq4lhcsr1*, displays decreased growth under a sinusoidal light regime mimicking natural oscillations in irradiance. This reduction in growth rate occurs without a significant impact on carbon accumulation, accumulation of oxidized lipids or impairment of photosynthetic rate. We hypothesized that this was due to increased consumption of excess energy by AET pathways and the results of this investigation are presented in chapter 3. We found that absence of qE in *Chlamydomonas* did not significantly

impact AET associated with light dependent oxygen consumption. The *npq4lhcsr1* mutant instead appears to experience less acceptor side limitation downstream of Photosystem I and have a greater capacity for state transitions. This in the absence of any evidence for increased light dependent oxygen consumption in the *npq4lhcsr1* mutant indicates that *Chlamydomonas* compensate for the absence of qE by increasing cyclic electron transport around Photosystem I, which generates additional ATP at the cost of NADPH. In my final chapter I use a positive selectable marker to generate a library of 400 putative *psaA* mutants, present preliminary flanking sequence characterization for 29 of these mutants and discuss possible roles they may be playing in *psaA* regulation. Together these chapters expand our understating of the role of qE in long term acclimation to saturating and sinusoidal light regimes and provide a library of putative chloroplast regulatory mutants that, with further characterization, will refine our understanding of chloroplast genome regulation in green algae.

# ACKNOWLEDGEMENTS

First, I would like to thank my advisor Graham Peers for his ongoing mentorship and support over the last seven years. Graham has provided invaluable advice, learning opportunities, and environment for my personal growth and development as a scientist. He aided in my development as a writer, public speaker, scientist and more generally as a person. His positive impact on my life is incalculable. I have come to appreciate and value all my experiences in the Peers lab and look forward to applying what I've learned in my future career.

I would also like to thank my committee members, Marinus Pilon, A.S.N. Reddy and Courtney Jahn for their feedback during committee meetings and genuine interest in my academic development. Additionally, I'd like to think Christie Peebles for stepping in as an outside committee member on short notice.

The Peers lab has been a second home for me and I wouldn't be where I am today without the support and comradery of its various members over the years. This includes of Denis Jallet, Matt Youngblood, Alexandra Gallina, and David Xing, Nate Sindt, Alex Hughes, Björn Andersson, Annah Holmberg, Mark Layer, and Laura Hantzis. I'd like to especially thank Max Ware. Our runs were both an excellent break from the daily science grind, and perfect brainstorming sessions for solving problems and developing hypotheses.

I would also like to thank several undergraduates who have facilitated directly or indirectly my research: Tiffany Wong, Brittany Wetzel, Katrina Lems, Natalie Moler Taylor Bailey and many more. I'd like to especially thank Julia Kendrick. She, through her hard work and dedication, was involved directly or indirectly in generation of most of the data generated in chapter #4. I'd have another year or more of graduate school without her assistance.

Finally, I'd like to thank my family and friends for endless support over the last 7 years. My family and friends have been a constant source of support and encouragement – especially during rough patches during my PhD. Mustering the persistence and mental fortitude needed to finish my PhD would have been possible without you.

TABLE OF CONTENTS

LIST OF TABLES

LIST OF FIGURES

# CHAPTER 1: INTRODUCTION

## Photosynthesis – Light and Dark reactions

The biological diversity on our planet today is a product of life's ability to capture solar energy. The earth's surface receives approximately 1000 J/($m^2 \cdot s$) of sunlight (Qiang, 2003; Ruban 2012). This abundance of free energy has driven the evolution of photosynthesis. This has ultimately shaped terrestrial and aquatic environments through the primary production of organic matter through conversion of sunlight and abundant atmospheric molecules, Carbon dioxide ($CO_2$) and water ($H_2O$), into complex and high energy carbohydrates ($C_m(H2O)_n$) (Blankenship, 2002b). This occurs through light dependent and independent reactions, that by their ubiquitous prevalence and importance in terrestrial and aquatic environments, reflect the most important biochemical suite of reactions on the planet.

Light dependent reactions

Oxygenic photosynthesis in Eukarya occurs in the chloroplast through the capture of light energy and its stabilization in the form chemical bonds. Chloroplasts contain an extensive membrane system, called the Thylakoids, separating an outer stromal compartment from an inner, lumenal compartment (Figure 1.1). Pigments vital for photosynthesis are contained in the thylakoid membrane. The photosynthetic pigments, chlorophylls and carotenoids, are incorporated within two photosystems and their associated light harvesting complexes (LHCs) and facilitate the absorption of light. These photosystems, consisting of a reaction center and an associated antenna (LHCs) are spatially separated: photosystem II localizes to stacked (grana) regions whereas photosystem I is present in unstacked (stroma lamella) regions of the thylakoid membrane (Figure 1.1). The four stages of photosynthesis are light absorption, primary electron

transport in each respective reaction center, energy stabilization and synthesis and export of phosphorylated sugars used to support autotrophic cellular metabolism.

Chlorophyll, upon photon absorption, goes from a ground state to an excited state. This excited state can be passed to adjacent chlorophylls between light harvesting complexes, by Förster resonant energy transfer, until it reaches a reaction center. Light energy is mainly collected at the level of the antennae and is funneled towards the reaction centers where primary electron transport occurs (Blankenship, 2002b). This organization of light harvesting proteins allows the adjustment of the absorption cross section or antenna size associated with each reaction center allowing acclimation to different light intensities (Bonente *et al.*, 2012).

Primary electron transport begins when this excited state is transferred to a reaction center chlorophyll molecule generating a strong reducing species. This reducing species, either $P680^*$ in PSII or P700* in PSI, donates an electron to a proximal acceptor within the photosystem leading to a to a charge separated state ($P^+ A^-$) (Blankenship, 2002a). To avoid loss of this energy through charge recombination by reduction of the primary chlorophyll, electrons are rapidly (within picoseconds) transferred through secondary acceptors that spatially separate positive and negative charges (Falkowski and Raven, 2007). This effectively captures excitation energy through chemical reduction. These steps apply to all photosynthetic reaction centers and mediate the conversion of light energy into chemical energy.

Stabilization of this energy occurs through linear transport of electrons. Electrons transferred in this process are harvested by PSII through the oxidation of water to oxygen and hydrogen ions. Two electrons derived from PSII are then used to reduce plastoquinone (PQ) to plastoquinol ($PQH_2$). The cytochrome $b_6f$ complex oxidizes plastoquinol, releasing protons to lumen. At this point, linear electron transport has effectively coupled the transport of electrons

with the generation of a pH gradient across the thylakoid membranes. This electrochemical gradient is used to drive the synthesis of ATP. Electrons at the cytochrome *b*$_6$*f* complex are then passed to plastocyanin in the lumen. Plastocyanin (PC) subsequently reduces the primary chlorophyll pair in PSI, where upon excitation, these electrons are transferred through PSI associated secondary acceptors to ferredoxin in the stroma. Ferrredoxin then primarily reduces $NADP^+$ to NADPH by the ferredoxin $NADP^+$ reductase but can also mediates redox regulation through thioredoxin reduction (Figure 1.1; Michelet *et al.*, 2013b).

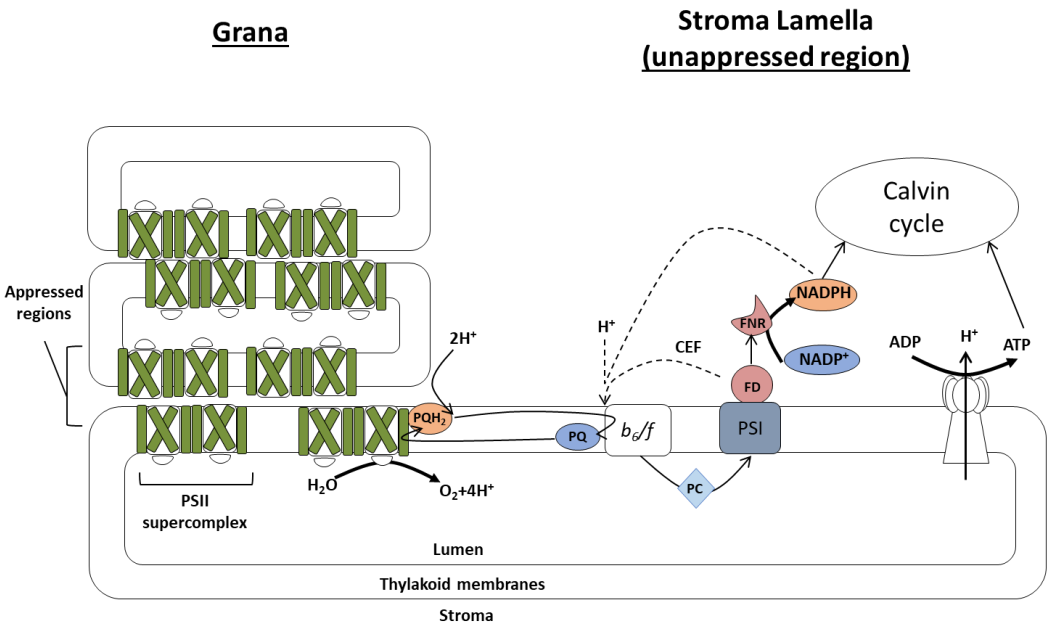


**Figure 1.1 Light reactions of photosynthesis.**
Representation of a side view for the chloroplast thylakoids with depictions of classical linear electron transport from PSII super complexes, localized in the appressed regions of the thylakoid grana, through the thylakoid associated plastoquinone cytochrome *b*$_6$*f* (*b*$_6$*f*) complex to the luminal localized plastocyanin (PC). During these steps protons are generated in the lumen by water oxidation and pumped from the stroma through the cytochrome *b*$_6$*f*. PC then reduces PSI which in turn, upon excitation can reduce ferredoxin. Ferredoxin then reduces either its stromal reducing partner, like ferredoxin NADPH reductase, or alternately is believed to participate in cyclic electron transport for the conversion of reductant to ATP by the generation of additional proton motive force (*pmf*; Blankenship, 2002a)

Light independent reactions

The synthesis and export of phosphorylated sugars used to support autotrophic cellular metabolism are generated by $CO_2$ assimilation in the Calvin-Benson cycle (C3 cycle). Although this stage is called light-independent, it occurs during daylight, and requires the production of NADPH which is directly reduced from $NADP^+$ at PSI. The C3 cycle has three phases: carboxylation, reduction and regeneration of metabolite intermediates. In the first stage, Rubisco binds and carboxylates ribulose 1,5-bisophosphate (RuBP) - capturing inorganic carbon. The six carbon enediol-enzyme complex that forms is unstable and leads to the immediate split into two 3-phosphoglycerates (3-PGA). During reduction, two ATP are used to phosphorylate the two 3-PGA to generate 1,3-bisphosphoglycerate (1,3BPGA). 1,3BPGA is than reduced to glyceraldehyde 3-phosphate (G3P) by NADPH, generating oxidized $NADP^+$ which acts as a primary acceptor, as mentioned above, for PSI. In the final stage, regeneration, RuBP is regenerated from the 6 G3P in a complex series of reactions. During the regeneration of the RuBP pool during this step carbohydrates are generated, most commonly hexose ($C_6H_{12}O_6$) (Blankenship, 2002a). This cycle consumes three ATP and two NADPH (ATP/NADPH ratio of 1.5) in the process of $CO_2$ assimilation into phosphorylated sugars (Kramer and Evans, 2011). To maximize the rate of carbon assimilation, the ratio of ATP and NADPH in the chloroplast is tightly regulated, mechanisms for which are discussed below (Johnson and Alric, 2013b; Kramer and Evans, 2011)

The balancing act between Sink and Source

The stoichiometry of ATP and NADPH production during linear electron transport cannot sustain the Benson-Calvin cycle alone. Based on the ratio of protons per ATP produced during ATP synthesis it's estimated that linear electron transport produces an ATP/NADPH ratio

of 1.3(Kramer and Evans, 2011; Vollmar *et al.*, 2009). To adjust this ratio to meet the demand for $CO_2$ fixation alone, cyclic electron transport around PSI is proposed to recycle 10% of electrons through a ferredoxin quinone reductase (Figure 1.1; Allen, 2003). This involves recycling of reductant generated at PSI, either as ferredoxin or NADPH, back into the plastoquinone pool through mechanisms described in detail below. In the chloroplast, ATP demand outside of $CO_2$ fixation varies depending on the environmental condition and metabolic state (Adams Iii *et al.*, 2002; Adams *et al.*, 2016; Johnson and Alric, 2012, 2013a). For example, low $CO_2$ levels or increased rates of photosystem damage increase ATP demand due to ATP dependent $CO_2$ transporters and costs of ATP-dependent translation (Lucker and Kramer, 2013a; Miyata *et al.*, 2012; Raven, 2011b).

**Photosynthesis in a dynamic light environment**

Photoacclimation

Photosynthetic organisms have evolved in light environments that vary both spatially and temporally necessitating mechanisms for optimizing light harvesting under fluctuating sink and source demands (Demmig-Adams *et al.*, 2012). Fluctuations in irradiances in terrestrial environment depend on the environmental niche occupied – ranging from the shady undergrowth in forest to direct sunlight in the top of a canopy. These environments experience short fluctuations in light due to sunflecks – a brief exposure of a plant in the understory to direct sunlight due to canopy leaf movement – to long term fluctuations driven by cloud cover and seasonal changes (Figure 1.2A; Jallet *et al.*, 2016b; Mathur *et al.*, 2018). Aquatic environments experience similar fluctuations in irradiance to terrestrial environment and additionally deal with variability due to mixing in the water column and wave focusing – were irradiances can be magnified by surface water by up to 5-fold (Dera, 1992). Photosynthetic organisms alter their

light harvesting architecture to acclimate to both light limiting and saturating light environments as well as the rapid fluctuations in irradiance found in nature.

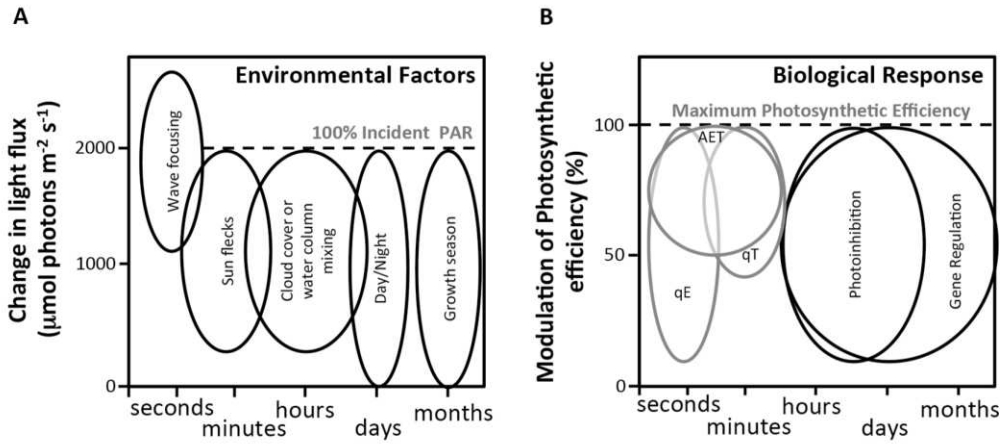


**Figure 1.2 Time scales of environmental mediators of the change in light flux and consequent biological responses in photosynthetic organisms.**
(A) Time scales and ranges of irradiance due environmental factors provided as a percentage of incident photosynthetic active radiation (PAR). (B) Time scales of biological responses associated with acclimation to photosynthesis and approximate ranges of their impact on the ability to modulate photosynthetic efficiency (Jallet *et al.*, 2016b).

When light is limiting photosynthetic organisms increase their ability to absorb light by increasing chlorophyll content and accumulating light harvesting complexes to increase light absorption. This is observed as a decrease in the ratio of Chlorophyll a to chlorophyll b. Chlorophyll b is enriched in accessory LHCs and low ratios of chlorophyll a to b consequently suggests the increase in reaction center absorption cross section by the accumulation of LHCs This functionally increases light absorption capacity and facilitates growth in low light environments in both plants and algae (Anderson *et al.*, 2008; Anderson *et al.*, 1988; Cantrell and Peers, 2017; Falkowski and Raven, 2013; Jia *et al.*, 2012). Additional acclimation occurs through structural changes in chloroplast architecture. Chloroplast in the shade tend to be larger, have more thylakoid per chloroplast, increased thylakoid membranes per grana and consequently

more chlorophyll per chloroplast (Anderson *et al.*, 1988; Bonente *et al.*, 2012; Cantrell and Peers, 2017; Falkowski and Raven, 2013; Kouril *et al.*, 2013).

In light saturating conditions excess light absorbed has many potential fates (Figure 1.3). Light use capacity is set by the utilization of ATP and NADPH by the Calvin-Benson cycle. $CO_2$ fixation saturates at a fraction of natural sunlight (Figure 1.3; Willhelm *et al.*, 2011; Falkowski and Raven, 2013). When in light is in excess of its utilization, it increases the probability of reactive oxygen species (ROS) generation. This can occur at either PSII by the generation and reaction between a long lived chlorophyll triplet states and oxygen (Pospíšil, 2012; Rinalducci *et al.*, 2004) or by reduction of oxygen during electron transport by PSI (Asada, 1999a). In either case, excess ROS generated during light harvesting ultimately reduces the rate of photosynthesis by damaging photosynthetic machinery through a process termed photoinhibition – described in more detail below (Falkowski and Raven, 2007). To avoid photoinhibition plants undergo chloroplast modifications that reduce light absorption and induce photoprotective mechanism that collectively reduce the probability of ROS generation (Figure 1.2B). In contrast with low light acclimation, plants and algae acclimate to high light by reduction in chlorophyll content, accessory LHCs, Grana stacks, and chloroplast size, which all effectively reduce light absorption (Anderson *et al.*, 1988; Bonente *et al.*, 2012; Cantrell and Peers, 2017; Falkowski and Raven, 2013; Kouril *et al.*, 2013).

Photoprotection describes mechanisms involved in both ROS mitigation and reduction. Photosynthetic organisms have specific chloroplast localized enzymes involved in ROS detoxification. These include superoxide dismutases (SODs) and ascorbate peroxidases (APXs) which effectively detoxify ROS generated during excess light exposure and their regulation is described in more detail below (Mittler, 2002). ROS reduction is achieved by regulating both

light absorption and reductant downstream of light harvesting. Light absorption is regulated by mechanisms collectively measured by the decrease in PSII associated fluorescence between a dark and illuminated state – collectively termed non-photochemical quenching of chlorophyll fluorescence (NPQ). NPQ associated mechanisms effectively quench singlet excited states through, in most cases, interactions with protein or pigment effectors and are characterized by their time scales of activation and relaxation (Magdaong and Blankenship, 2018). Downstream of light harvesting alternative electron transport (AET) facilitates reductant dissipation and conversion to ATP (Alric and Johnson, 2017). NPQ and AET are proposed to act synergistically for the energetic control of photosynthesis during short- and long-term exposures to excess light, but many questions remain in their roles and function overlap. Each are described in more detail below (Figure 1.3).

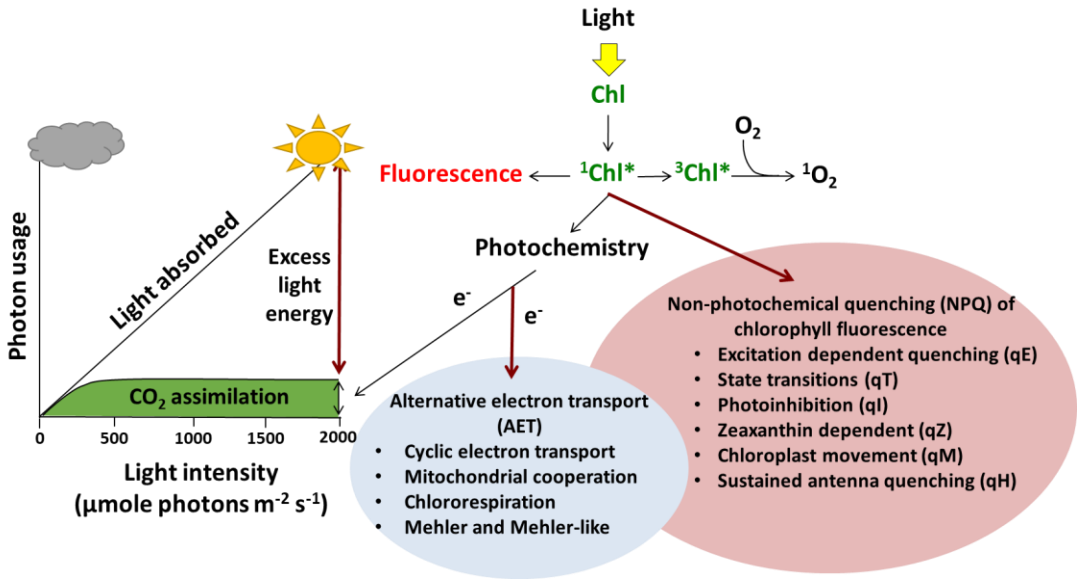


**Figure 1.2 Fates of excess light energy.**
Representation of the fates of light energy after chlorophyll (Chl) excitation. The chlorophyll singlet excited state is primarily quenched by linear electron transport – which drives CO2 assimilation through primary photochemistry. When light exceeds the capacity of its utilization by CO2 assimilation the chlorophyll singlet excited state can either (1) undergo radiative decay by emission of a red shifted photon, (2) generate reactive oxygen species after undergoing intersystem crossing to a triplet state, (3) be dissipated at the level of light harvesting through mechanisms collectively measured as the Non-photochemical quenching of chlorophyll fluorescence, and (4) generate excess reductant that is than dissipated downstream of light harvesting through AET. Adapted and expanded from Willhelm *et al.* 2011.

Non-photochemical quenching

*qE -Excitation dependent quenching*

Energy dependent quenching (qE) is often considered to be the main sink for excess energy within NPQ-based photoprotection (Ruban, 2017). It occurs through the regulated quenching of a chlorophyll excited state by the light dependent activation of affecter proteins. This subsequently increases the probability quenching of a chlorophyll excited state as heat (Goss and Lepetit, 2015). Many photosynthetic eukaryotes have light harvesting antenna compromised by membrane-intrinsic pigment-protein complexes called light harvesting complexes (LHCs). Excitation-dependent quenching in these systems relies on xanthophyll dependent NPQ associated with specialized members of the LHC protein superfamily (Goss and

Lepetit, 2015). The two major xanthophyll cycles are the violaxanthin-antheraxanthin-zeaxanthin (VAZ) cycle found in green algae and higher plants (Yamamoto *et al.*, 1962) and diadinoxanthin-diatoxanthin cycle in stramenopile algae (Olaizola *et al.*, 1994). qE activation requires the formation of, zeaxanthin. antheraxanthin or diatoxanthain which are generated following luminal acidification by thylakoid associated xanthophyll deapoxidases (Funk *et al.*, 1995). In higher plants qE requires photosystem II subunit S (PsbS). Green algae and stramenopiles qE requires a stress related light harvesting complex (LHCSR) or the evolutionarily related LHCX protein (Goss and Lepetit, 2015), respectively. PsbS is constitutively expressed in plants and initiates qE in photosystem II antenna upon lumenal acidification (Bergantino *et al.*, 2003). PsbS does not bind pigments, but it does activate a quenching state by inducing confirmation changes and aggregation of PSII LHCs (Betterle *et al.*, 2009; Johnson *et al.*, 2011; Sacharz *et al.*, 2017). In the model green algae *Chlamydomonas reinhardtii* qE depends on the light induced expression of two LHCSR proteins – LHCSR3 ( encoded by *LHCSR3.1* and *LHCSR3.*2 genes) and LHCSR1 which shares 87% protein sequence identity (Dinc *et al.*, 2016; Peers *et al.*, 2009). Upon luminal acidification both LHCSR3 and LHCSR1 become protonated and undergo a conformational shift to a quenching state (Ballottari *et al.*, 2016; Dinc *et al.*, 2016). LHCSR proteins can associated with either photosystem and mediate quenching of fluorescence during luminal acidification (Girolomoni *et al.*, 2019). *Chlamydomonas reinhartii* also expresses PsbS transiently under high light, low CO2 availability and UV-B exposure (Allorent *et al.*, 2016; Correa-Galvis *et al.*, 2016a; Tibiletti *et al.*, 2016). Unlike plants, PsbS alone is insufficient to induce qE and instead appears to regulate NPQ capacity and LHCSR3 accumulation (Correa-Galvis *et al.*, 2016b). The moss *Phycomitrella patens*, often used as a model evolutionary intermediate between land plants and their

streptophyte algal ancestors, express LHCSR and PsbS proteins that function as additive contributors to NPQ (Gerotto *et al.*, 2011, 2012; Rensing *et al.*, 2008).

*qT -State transitions*

State transitions (qT) balance light absorption between the photosystems by adjusting the relative absorption capacity of PSII and PSI. State 1 refers to conditions in which the plastoquinone pool is oxidized and LHCII are associated with PSII (Fleischmann *et al.*, 1999). State 2 refers to conditions when the plastoquinone pool is reduced, which induces phosphorylation of LHCII causing their dissociation from PSII. In *Chlamydomonas*, qT is regulated by the serine-threonine thylakoid kinase STT7 that phosphorylates PSII associated LHCs (LHCII) upon plastoquinone pool reduction (Depège *et al.*, 2003). Once phosphorylated these LHCIIs can migrate to PSI increasing the rate of it turnover (Drop *et al.*, 2014) or undergo a conformation change to a quenching state (Nagy *et al.*, 2014b). The STT7 kinase protein abundance is regulated post-translationally, with increased protein degradation occurring in high light (Lemeille *et al.*, 2009a). STT7, unlike its *Arabidopsis* ortholog STN7, phosphorylates a greater percent of LHCII (up to 80% -Delsome, 1996 vs. 15-20% - Forti and Fusi, 1990). This difference has been proposed to allow enhancement of cyclic electron transport around PSI (Cardol *et al.*, 2009). Alternatively, the recent observation that phosphorylated LHCII can remain associated with PSII in a quenched state suggests that state transitions may cooperate with excitation dependent quenching in dissipating excess light energy absorbed by PSII antenna (Nagy *et al.*, 2014b).

*qI - Photoinhibition*

Photoinhibition primarily occurs when the rate of PSII damage exceeds the rate of its repair (Aro *et al.*, 1993b; Nishiyama *et al.*, 2006). Damage to PSII is proposed to occur in two

steps (Ohnishi *et al.*, 2005). In the first step the oxygen evolving complex is becomes damaged. This is followed by oxidation of amino acids within the D1 subunit by either oxidized P680 or reactive oxygen species generated by P680 (Ohnishi *et al.*, 2005). This damage occurs continuously upon any light exposure, increasing linearly with light intensity (Tyystjärvi and Aro, 1996). Plants and green algae combat this damage with a constantly operating repair cycle that involves phosphorylation of PSII subunits, D1 and D2, causing their monomerization. This is followed by migration of damaged PSII to the stroma lamella where damaged D1 removal and degradation occurs (Nath *et al.*, 2013). PSII monomers are then re-assembled with new D1.

Unlike excitation dependent quenching and state transitions, photoinhibition of PSII causes chlorophyll fluorescence quenching due to inactivation of PSII reaction centers (Baker, 2008). The D1 subunit is the main location of PSII damage and is proposed to act as a "suicide protein" that is sacrificed to protect the rest of PSII protein subunits from damage (Aro *et al.*, 1993b). The damage of PSII and its repair has been shown to also protect PSI from damage (Tikkanen *et al.*, 2014). This suggests that NPQ by photoinhibition of PSII may protect the rest of the electron transport machinery from over-reduction and damage during excess light conditions. PSII activity is also regulated by the rate of its repair cycle, which is facilitated by PSII subunit phosphorylation (Tikkanen *et al.*, 2008) and inhibited by $^1O_2$ (Nishiyama *et al.*, 2004). These results together suggest that PSII photoinhibition may be regulated by its rate of repair and under excess light PSII may be sacrificed to protect the electron transport chain.

PSI in contrast to PSII is extremely efficient at dissipating excitation energy (Shubin *et al.*, 2008). Damage to PSI only occurs when electron transport to PSI exceeds the capacity of its electron acceptor, ferredoxin (Sonoike *et al.*, 1995). The dependence on this damage on both oxygen and linear electron transport from PSII indicates that this process is mediated by ROS

dependent damage of the PSI reaction center (Sonoike and Terashima, 1994). Unlike PSII, PSI damage has a slow recovery that involves the costly degradation of the entire PSI reaction center complex (Kudoh and Sonoike, 2002).

*qM – Chloroplast movement-dependent quenching*

Chloroplast movement-dependent quenching (qM) describes a form of NPQ in higher plants were PSII fluorescence quenching is driven by chloroplast movement to the periphery of cells and occurs on the time scales of qE and qZ (Dall'Osto *et al.*, 2014).

*qZ – Zeaxanthin dependent quenching*

In addition to its role in qE, zeaxanthin is proposed to function in a slowly relaxing form of NPQ that is ΔpH independent and referred to as qZ (Nilkens *et al.*, 2010). qZ was originally proposed by Horton *et al.* (1992) who observed that LHCII remained aggregated in the dark well after the collapse of the ΔpH due to saturating light exposure. Creation of a zeaxanthin epoxidase mutant, *npq2*, that constitutively accumulated zeaxanthin and consequently displayed a reduced PSII quantum yield in the dark – indicating that NPQ was induced in the absence of photoinhibition or a ΔpH to induce qE (Niyogi *et al.* 1992.). Later characterization of qZ in Arabidopsis mutants demonstrated qZ was independent of qE, qT or qI and reflects a proportion of NPQ generated after 10-15 minutes of saturating illumination and relaxes over 10-15 minutes after light removal (Nilkens *et al.*, 2010).

*qH – Sustained quenching*

Sustained quenching (qH) is a recently described, slowly relaxing form of NPQ that may mediate NPQ during conditions were sustained downregulation of photosynthesis is advantageous. Likely first described in wintering evergreens, were sustained NPQ is proposed to facilitate maintenance of leaves during harsh winters, qH reflects a ΔpH independent quenching

mechanism that takes greater than 3 hours to relax (Malnoë, 2018; Verhoeven, 2014). Characterization of a negative regulator of qH, SOQ1, has suggested that this form of NPQ operates in wild type *Arabidopsis* under cold stress and high light (Malnoe *et al.*, 2018). Suppressor screens in the *soq1* mutant identified LCNP as a putative effector of qH quenching and is hypothesized to regulate NPQ like the plant qE effector protein PsbS by inducing aggregation and a conformational transition to a quenching state in PSII LHCs (Malnoë, 2018; Malnoe *et al.*, 2018).

Alternative electron transport

*PSI associated water-water cycles*

Dissipative alternate electron transport occurs in the stroma through futile water-water cycles that consume excess reductant generated by water splitting by PSII through $O_2$ reduction to water. Two pathways are proposed to operate in photosynthetic organisms downstream of PSI. The Mehler reaction, often called the water-water cycle, involves reduction of $O_2$ by PSI to form superoxide (Asada, 1999a). Superoxide is then rapidly detoxified by superoxide dismutase to hydrogen peroxide. Ascorbate peroxidase completes the water-water cycle by conversion of hydrogen peroxide to water, consuming extra reductant in the process (Asada, 1999a).

The flavodiiron (FLV) proteins regulate the second mode for light dependent $O_2$ reduction to water and are found across most microalgae families and gymnosperms (Ilik *et al.*, 2017; Peltier *et al.*, 2010). FLVs role were originally described in cyanobacteria where its proposed to protect PSII by dissipating between 20-60% of electrons generated during photosynthesis (Allahverdiyeva *et al.*, 2011). In the green algae *Chlamydomonas reinhardtii* FLVs are proposed to play an important role in photoprotection under fluctuating light conditions and during photosynthetic induction upon dark to light transition (Chaux *et al.*, 2017a;

Jokel *et al.*, 2018). Like green algae, characterization of FLV proteins in the non-vascular plants *pyscomitrella patens* and *Marchantia polymorpha* primarily proposed to act as a safety valve for photosystem I during fluctuating light exposure (Gerotto *et al.*, 2016; Jokel *et al.*, 2018; Mustila *et al.*, 2016; Shimakawa *et al.*, 2017).

*Chlororespiration*

Reductant can be recycled to generate additional ATP through plastid terminal oxidase (PTOX) (Houille-vernes *et al.*, 2011a). Two plastid terminal oxidase (PTOX) isoforms (PTOX1 and 2) are located in the thylakoid membranes downstream of PSII and dissipate extra reductant by oxidizing the plastoquinone and reducing $O_2$ (Houille-vernes *et al.*, 2011a). *Chlamydomonas ptox2* mutants exhibit reduced fitness in moderate light levels (Houille-vernes *et al.*, 2011a). This is proposed to stem from their inability to undergo state transitions due to overreduction of the plastoquinone pool. In addition to dissipating electrons from linear electron transport in the light, PTOX also functions in a chlororespiratory pathway operating in conjunction with NAD(P)H dehydrogenase (Cournac *et al.*, 2000). This pathway facilitates the translocation of protons to the lumen through a respiratory like, electron transport pathway from NADPH to $O_2$ in higher plants and adjustment of the NADPH/ATP in green algae (Cournac *et al.*, 2000; Saroussi *et al.*, 2016). Recent work on the *ptox2* mutant in C*hlamydomonas* has demonstrated that chlororespiration is required during growth in intermittent light by mediating plastoquinone oxidation during dark periods. In the absence of chlororespiration cyclic electron transport increases at the expense of linear electron transport during light exposure, which is interpreted as the cause for growth reduction in the *ptox2* mutant (Nawrocki *et al.*, 2019). In addition to direct role in regulating photosynthesis, PTOX has been ascribed roles in carotenoid biosynthesis, plastid development,

and abiotic stress outside of high light (For review see Krieger-Liszkay and Kathleen Feilke 2015).

*Cyclic electron transport*

Cyclic electron transport around photosystem I involves reduction of the plastoquinone pool by ferredoxin through a ferredoxin plastoquinone reductase (Hertle *et al.*, 2013b). The proton gradient regulator (PGR5) and proton gradient regulator like (PGRL1) proteins are proposed to be the primary proteins directing this process in plants and some algae (DalCorso *et al.*, 2008a; Iwai *et al.*, 2010; Johnson *et al.*, 2014). Previous work in C*hlamydomonas* has shown that CEF operates under steady state conditions (Alric *et al.*, 2010) and is stimulated when stromal electron carriers (ferredoxin and NADPH) are reduced (Alric *et al.*, 2010; Takahashi *et al.*, 2013a). This stimulation of CEF is hypothesized to be regulated by adjusting the ratio of PSI engaged in LEF with those associated with the CEF supercomplex containing the $b_6$/f complex, PGRL1 and ferredoxin $NADP^+$ reductase (FNR) (DalCorso *et al.*, 2008b; Joliot and Johnson, 2011). Adjustment of the ratio LEF to CEF is proposed to adjust the ATP /NADPH ratio to meet cellular demand under a variety of conditions in algae and plants: photosynthetic induction upon light exposure (Joliot and Joliot, 2002, 2005), temperature stress acclimation (Bukhov *et al.*, 1999; Clarke and Johnson, 2001; Havaux, 1996; Yamori *et al.*, 2016), low $CO_2$ conditions (Dang *et al.*, 2014b; Harbinson and Foyer, 1991; Miyake *et al.*, 2005), under anaerobiosis(Joet *et al.*, 2001), during fluctuating light exposure (Jokel *et al.*, 2018; Lucker and Kramer, 2013b; Suorsa *et al.*, 2012; Yamori *et al.*, 2016), and during drought (Golding *et al.*, 2004). In addition to ATP/NADPH ratio adjustment, CEF was also shown to regulate qE induction by luminal acidification in *Arabidopsis* and *Chlamydomonas* evidencing its duel role in photoprotection and metabolism (Johnson *et al.*, 2014; Miyake *et al.*, 2004; Takahashi *et al.*, 2009).

*Mitochondrial cooperation*

Mitochondrial cooperation is proposed to function in both reductant dissipation and adjustment of the ATP/NADPH ratio through the export of reductant from the chloroplast to the mitochondria (Scheibe, 2004). Reductant is exported by NADPH oxidization during the reduction of oxaloacetate to malate (Lemaire *et al.*, 2005). Malate is then exported from the chloroplast to the mitochondria where it is converted back to oxaloacetate – generating NADH for use in ATP synthesis during respiration (Scheibe, 2004b). This ATP may than be transferred back to the chloroplast by direct (ATP translocators) or indirect routes (DHAP/3-PGA shuttle; Hoefnagel *et al.*, 1998). Alternately reductant exported from chloroplast to the mitochondria can by dissipated by the alternative oxidase (AOX), which oxidizes the mitochondrial electron transport chain by the reduction of oxygen to water (Juszczuk and Rychter, 2003). Photosynthetic derived reductant dissipation by the AOX is proposed to provide a safety valve under high light (Kaye *et al.*, 2019; Vishwakarma *et al.*, 2014; Yoshida *et al.*, 2007), heat stress (Kaye *et al.*, 2019; Vishwakarma *et al.*, 2014; Yoshida *et al.*, 2007) cold stress (Molen *et al.*, 2006) and in mutants defective in cyclic electron transport (Dang *et al.*, 2014b).

**Mechanisms coordinating nuclear and chloroplast genome expression of photosynthetic proteins**

Chloroplasts are not only responsible for photosynthesis and the biosynthesis of many essential plant and algal compounds, but also for the perception of and acclimation to various environmental stresses such as high irradiance (Dietz, 2015; Neuhaus and Emes, 2000). The chloroplast organelle of Archaeplastidae (including plants) is the remnant of an ancient endosymbiosis between a cyanobacterium and a heterotrophic eukaryote. Plastids of other algae found in the eukaryotic tree of life are the result of independent and different endosymbiosis

events where separate heterotrophs enslaved a phototrophic eukaryote (Keeling, 2013). This complex evolutionary history has led to a diverse set of signals that functionally coordinate the chloroplast and extra-chloroplast metabolism. This is complicated by the chloroplasts' dependence on the nucleus for, on average, over 95% of their proteins including key factors involved in the regulation of the chloroplast genome (Barbrook *et al.*, 2006). In plants and algae, this coordination is achieved by intracellular signaling from the chloroplast to the nucleus, so-called retrograde signaling and by nucleus to chloroplast, so-called anterograde signaling (Chi *et al.*, 2013; Dietz, 2015; Pogson *et al.*, 2008).

Retrograde signals from the plastid to the nucleus[1]

*Plastoquinone pool dependent signaling*

The redox state of the PQ pool, the electron acceptor of PSII, has historically been considered a major initiation point in transcriptional regulation of photoacclimation. It is easily manipulated experimentally by adding the inhibitors DCMU (3-(3,4-dichlorophenyl)-1,1-dimethylurea) to induce an oxidized PQ pool and DBMIB (2,5-dibromo-3-methyl-6-isopropyl-p-benzoquinone) to reduce the PQ pool. The application of these inhibitors has been instrumental in unequivocally linking the expression of *petE, lhcb,* and *apx* to the redox state of the PQ pool (Escoubas *et al.*, 1995; Fey *et al.*, 2005). Manipulation of PQ pool has demonstrated that some LHCs required for qE, LHCSR3 from *Chlamydomonas* and LHCX1 and LHCX2 from *Phaeodactylum*, are induced in response to PQ reduction (Lepetit *et al.*, 2013; Maruyama *et al.*, 2014).

The PQ redox signal controls more than just genes involved directly in photosynthesis. Alternative splicing is a form of post-transcriptional regulation that involves processing a single pre-mRNA into multiple mRNAs, which can either encode a different protein isoform or lead degradation of mRNA through nonsense mediated decay (McGlincy and Smith, 2008). Petrillo *et al.* (2014) used DCMU/DBMIB to illustrate that the Arabidopsis nuclear serine arginine rich splicing factor, *AtRS31,* undergoes alternative splicing in response to a reduced PQ pool. *AtRS31* belongs to a large family of serine arginine splicing factors involved in constitutive and alternative splicing (Reddy *et al.*, 2013) and the mRNA encoding this gene was already known to

[1] Retrograde signaling from the plastid to the nucleus reflect a reprint of sections I wrote with minor edits from Jallet, D., Cantrell, M., and Peers, G. (2016). Chloroplasts: Current research and future trends with permission from Caister Academic Press.

be alternatively spliced in response to temperature stress. Several other light-dependent splicing events were observed under a light/dark treatment. These spliced transcripts mainly encoded proteins involved in RNA-binding and processing as well as DNA binding proteins (Petrillo *et al.*, 2014). Interestingly, RuBisCO activase was the only photosynthetic protein shown to undergo alternative splicing in response to a light/dark regime. Surprisingly, light dependent *AtRS31* splicing was observed in both leaves and roots, with roots showing at least a 2-hour time delay response (Petrillo *et al.*, 2014). This suggests that an uncharacterized signal reporting the plastoquinone pool redox state can be transmitted across plant tissues. These observations highlight the complexity and critical importance of alternative splicing in light response within the whole plant. Future studies focused on the impact of these splicing events on the re-structuring of the chloroplast proteome under different light regimes could reveal their overall importance to metabolism.

Systems-level responses to PQ manipulation, measured by RNAseq and proteomics focused on posttranslational modification, will undoubtedly lead to the identification of genes under the control of the PQ pool, and possibly even some of the transcription factors that control gene expression.

*Reactive Oxygen Species*

The buildup of excitation pressure on PSII by the over reduction of the electron transport chain increases the probability of $^1O_2$ production by excited chlorophyll at PSII (Krieger-Liszkay, 2005) and superoxide and subsequent hydrogen peroxide production through oxygen reduction by PSI (Asada, 2006). $^1O_2$ is proposed to be the major ROS generated in excess light (Gonzalez-Perez *et al.*, 2011), but both $^1O_2$ and $H_2O_2$ act as potent signals for retrograde signaling. This mediates acclimation to light stress through the expression of genes controlling

the production of ROS scavenging pigments, proteins, and metabolites or by instigating programmed cell death (Chi *et al.*, 2015).

New components of the excess light stress-sensing pathway have been isolated from mutants that show unusual responses to exogenous $^1O_2$ exposure. The singlet oxygen resistant 1 (*sor1)* mutant was isolated from a UV-mutagenized population of *Chlamydomonas* that was screened for constitutive tolerance to the $^1O_2$-photosensitizer Rose Bengal (Fischer *et al.*, 2012). The *SOR1* gene encodes a putative basic leucine zipper domain transcription factor. In the *sor1* line, a gain of function mutation led to constitutively higher expression of both *SOR1* and oxidative stress response genes. Intriguingly, an 8-bp palindromic sequence element was enriched in many of these genes. This element was shown to be required for the transcriptional induction of the σ-class glutathione-S-transferase gene *GSTS1* in response to increased levels of reactive electrophile species such as oxylipins (Fischer *et al.*, 2012). These findings implicate SOR1 in regulating genes associated with detoxification of $^1O_2$ – induced lipid peroxidation and that these genes may also play a part in acclimation to $^1O_2$ (see discussion of oxylipins in 7.6).

SAK1 is another putative basic leucine zipper domain transcription factor involved in the $^1O_2$ response in *Chlamydomonas (Wakao et al., 2014).* In WT cells, the SAK1 protein is accumulated 6-10 fold in the cytosol and is phosphorylated in response to $^1O_2$. *sak1* mutants show increased sensitivity to $^1O_2$ exposure (Wakao *et al.*, 2014). *sak1* mutants showed a reduction in transcript accumulation of two important high light stress related proteins; glutathione peroxidase (GPX5), which responds specifically to $^1O_2$ –challenges (and LHCSR1, which is involved in qE response (Truong *et al.* unpublished). All these pieces together point towards SAK1 acting as an intermediary in the $^1O_2$ dependent retrograde signal.

Methylene blue sensitivity (MBS) is a conserved zinc finger protein that is also required for singlet oxygen-dependent retrograde signaling (Shao *et al.*, 2013). *mbs* mutants in *Chlamydomonas* and Arabidopsis are hypersensitive to photooxidative stress while overexpression in plants leads to increased tolerance. MBS accumulates in distinct RNA granules in the cytosol during exposure to oxidative stress. Perhaps MBS affects mRNA stability, translation of a specific mRNA or another intermediary factor controlling $^1O_2$ acclimation (Shao *et al.*, 2013).

Brzezowski *et al.* (2012) isolated a GPX5 regulation mutant of *Chlamydomonas* that had increased sensitivity to exogenously generated $^1O_2$. This mutant was missing a paralog of the PSBP1 protein (PSBP2; Brzezowski *et al.*, 2014). PSBP1 is involved in the water-splitting reactions of the oxygen-evolving complex (Ifuku *et al.*, 2008). The PSPB2 peptide may be targeted to the chloroplast but its role in $^1O_2$ detection or signal transduction remains unclear at this time.

Unlike $^1O_2$, $H_2O_2$ generated in the chloroplast can diffuse to the cytosol (Mubarakshina *et al.*, 2010). While no responsive element has been identified in the $H_2O_2$ retrograde signaling cascade, $H_2O_2$ accumulation in the cytosol also appears to regulate excess light stress responses. Work in *Chlamydomonas* has shown that $H_2O_2$ transiently accumulates during the first 10 minutes following a shift from dark to high light and this accumulation occurs concurrently with a decrease in catalase activity (Michelet *et al.*, 2013a). This transient rise in $H_2O_2$ was shown to activate the expression of the nuclear encoded genes for the antioxidant enzymes ascorbate peroxidase (APX) and GPX, enzymes involved in chloroplast $H_2O_2$ defense response (Michelet *et al.*, 2013a).

*Pigment-related metabolites participating in retrograde signaling*

Contemporary studies of retrograde signaling have also highlighted the importance of ROS-dependent oxidative products, chlorophyll biosynthetic intermediates, and chloroplast metabolites as potential signaling molecules.

Carotenoids have received extensive study for their role in quenching $^1O_2$ generated by PSII (Telfer, 2014). The reaction of $^1O_2$ with β-carotene results in the generation of a number of volatile short-chain compounds, including β-cyclocitral, and these are accumulated in light stressed Arabidopsis (Ramel *et al.*, 2012). Five different $^1O_2$ stress marker transcripts were upregulated in Arabidopsis leaves after exposure to exogenous β-cyclocitral. Specific markers for $H_2O_2$ stress were not affected by exogenous β-cyclocitral (Ramel *et al.*, 2012). These results suggest that oxidative damage products derived from carotenoids can also serve as a retrograde signal.

Metabolic intermediates involved in tetrapyrrole biosynthesis exert control over the transcription of photosynthetic nuclear genes during dark to light transitions. Four classes of tetrapyrroles- chlorophyll, heme, siroheme, and phytochromobilin- are generated in the chloroplast from a common biosynthetic pathway (Tanaka and Tanaka, 2007). The Genome Uncoupled 4 (GUN4) mutants have been instrumental for the characterization of tetrapyrroles in retrograde signaling. Lately, Brzezowski *et al.* (2014) proposed a modified model for the role of GUN4 in retrograde signaling in *Chlamydomonas* whereby it is the protein itself, and not a metabolite alone, that senses the accumulation of chlorophyll biosynthesis intermediates and mediates the singlet oxygen signal to the retrograde pathway.

Heme has also been shown to be a retrograde signal in *Chlamydomonas* and Arabidopsis (von Gromoff *et al.*, 2008; Woodson *et al.*, 2011). Heme can be converted to linear bilins through the action of two enzymes, a heme oxygenase (HMOX1) and a ferredoxin-dependent

bilin reductase (PCYA). These bilins are then integrated into phytochromes in plants (Quail, 2007). Phytochromes are absent in *Chlamydomonas,* but the production of bilins occurs nonetheless. They are required for efficient growth in the light and are proposed to be a retrograde signal (Duanmu *et al.*, 2013). A multi-factor RNAseq experiment found a set of genes that were induced during a dark to light shift were also repressed by exogenously added bilins. These included high light stress response genes such as *LHCSR1*, *PSBS1*, *ELI3*, *GPX*, *HSP70* and others (Duanmu *et al.*, 2013). Bilins clearly play some role in dampening the excess light response, but it is not clear how.

*Other chloroplast metabolites involved in retrograde signaling*

Finally, recent studies have suggested a series of unexpected chloroplastic metabolites may also serve as signals for retrograde gene regulation in the nucleus. The first is dihydroxyacetone phosphate (DHAP), an intermediate of the Calvin Benson Bassham cycle that is exported to the cytosol by the triose phosphate /phosphate translocators. Vogel *et al.* (2014) proposed a model where Mitogen-Activated Protein Kinase 6 is activated by the exported DHAP in excess light. Within 10-45 minutes, the kinase influences the transcription of high light stress acclimation APETALA2/ETHYLENE RESPONSE FACTORs (Dietz, 2015; Lata and Prasad, 2011; Vogel *et al.*, 2014)

The second signal appears to be an isoprenoid precursor (MEcPP, methylerythritol cyclodiphosphate) produced in the chloroplast. This, and other isoprenoids, accumulate in leaves during light and heat stress (Xiao *et al.*, 2012). A *ceh1* mutant that accumulates MEcPP along with pharmacological manipulations of MEcPP levels convincingly demonstrated that the molecule increases nuclear transciption of a high light stress reponse gene encoding a plastid

localized hydroperoxide lyase. Interstingly, MEcPP did not affect any of the gun responsive genes, indicating independent signalling pathways (Xiao *et al.*, 2012).

Finally, the nucleotide precursor metabolite, 3'-phosphoadenosine 5'-phosphate (PAP), regulates retrograde signaling in high light and drought stress through the likely inhibition of a nuclear 5' to 3' exoribonuclease (XRNs), (Estavillo *et al.*, 2013). PAP is produced by sulphation reactions in the chloroplast and high light induces a 20-fold accumulation of PAP, which can move out of the chloroplast (Estavillo *et al.*, 2013). This accumulation correlated with the increased expression of the high light responsive gene ELIP2 and drought tolerance. PAP in yeast is known to inhibit XRNs (Dichtl *et al.*, 1997) and Estavillo *et al.* (2011) showed that mutants lacking XRNs showed similar nuclear gene expression to mutants with altered PAP levels. Clearly, these three examples, along with the examples provided above, reveal an incredible complexity in the signals that influence light acclimation state.

*Calcium*

Calcium is an essential nutrient that plays structural roles in photosynthetic proteins and cell walls as well as signaling functions in both development and environmental stress response (Gilroy *et al.*, 2014; Hochmal *et al.*, 2015). Calcium binding proteins like calmodulin are important actors in the calcium-dependent signaling cascades involved in activating transcriptional regulation. Recent work in *Chlamydomonas* on the chloroplast localized, calcium sensor (CAS), demonstrated that both CAS and $Ca^{2+}$ are involved in the nuclear regulation of LHCSR3 during acclimation to high light (Petroutsos *et al.*, 2011). CAS-RNAi knockdown lines displayed reduced LHCSR3 protein accumulation, which was rescued by a 10-fold increase in $Ca^{2+}$ concentration. This together with the repression of LHCSR3 protein accumulation and gene expression by calmodulin inhibitors indicates that $Ca^{2+}$ play a central role in the light-dependent

retrograde regulation of LHCSR3 (Maruyama *et al.*, 2014). The role of this possible retrograde signaling pathway in other photoacclimation responses remains uncharacterized.

*Integrating complex retrograde signals*

Efficient high light acclimation requires a range of temporally separated responses that occur across multiple signaling pathways (Dietz, 2015). Systems wide characterization of retrograde signals responding to high light stress observed some of the metabolites described above in addition to the oxylipins oxophytodeinoic acid and jasmonic acid, and redox cues as critical components in light dependent retrograde signaling (Alsharafa *et al.*, 2014; Oelze *et al.*, 2012). Their accumulation and effects are temporally separated. The overlap of these retrograde signaling pathways agrees with the "cross tolerance hypothesis" where multiple retrograde signals lead to synergistic co-activation of non-specific and specific stress responsive pathways enabling tolerance to both biotic and abiotic stresses (Bartoli *et al.*, 2013). This hypothesis is supported by a meta-analysis of retrograde signaling research on *Arabidopsis* that found a core response module consisting of 36 transcripts (Glasser *et al.*, 2014). This core module consists of a variety of pathways including genes involved in transcriptional regulation, biotic defense response, cell wall establishment and cell wall synthesis. There was a distinct lack of chloroplast generated signals in regulating general plant physiology. Contrary to the findings of Alsharafa *et al.* (2014) this analysis found auxin based signaling and not oxylipins, act as key secondary components integrating plastidial signals in the response cascade. This contradiction highlights the complexity of determining the specific signaling mechanisms involved in high light acclimation.

Chloroplast genome expression and anterograde signaling

*Chloroplast genome organization*

The majority of chloroplasts contain a circular genome of between 120-160 kb in size that encodes between 100-150 genes (Barbrook *et al.*, 2006; Palmer, 1985). For example, the *Chlamydomonas reinhardtii* genome contains 73 protein coding genes, 5 rRNA genes, 30 tRNA genes and 1 small RNA-coding gene. Of these protein coding regions, 37 encode subunits or assembly factors for key photosynthetic proteins (PSII, PSI, Cytochrome $b_6f$, Rubisco, ATP synthase, and Chlorophyll synthesis, 8 encode proteins associated the 70S ribosome, 5 encode the chloroplast RNA polymerase, and 17 remain as uncharacterized open reading frames (Maul *et al.*, 2002). These genes organization resemble bacterial operons, with many genes encoded as polycistronic units. Unlike bacteria though these the polycistronic units in the chloroplast do not contain function units of associated proteins (except for ribosomal encoding genes). Instead expression polycistronic genes undergo post-translational cleavage with protein synthesis occurring from the subsequent monocistronic units generated (Barkan *et al.*, 1994; Hirose and Sugiura, 1997; Sturm *et al.*, 1994).

*Chloroplast Transcription*

Chloroplast transcription is mediated by a bacterial-like polymerase encoded by the plastid genome (PEP) in most algae and additionally in some linages of higher plants and algae two or more nucleus-encoded RNA polymerase (Lyska *et al.*, 2013). NEP is a monomeric phage-type enzyme that was originally proposed to regulate housekeeping genes (Ribosomal proteins and rRNA) during plastid development (Lerbs-Mache, 1993; Mullet, 1993). NEP, which evolved from duplication of the mitochondrial phage-type polymerase, is still active in mature chloroplasts and is proposed to have overlapping function with PEP (Azevedo *et al.*, 2006; Bligny *et al.*, 2000; Cahoon *et al.*, 2004; Hedtke *et al.*, 1997, 2000). PEP is a eubacterial-type polymerase that recognizes transcriptional initiation sites by a consensus sequence of TTGACA

and TATAAT centered at 35 and 10 bp respectively. PEP transcription is regulated by interactions with nuclear encoded sigma factors that bind the PEP complex forming a holoenzyme that is required for transcriptional initiation site binding (Harley and Reynolds, 1987; Ishihama, 1988).

The number of sigma factor in photosynthetic linages range from 1 to 12 across. Extant cyanobacteria species today contain between 9-12 sigma factors that are functionally separated into three groups (Imamura *et al.*, 2003). Group I is comprised by a single sigma factor, *SigA*, and represents the primary sigma factor in cyanobacteria – transcribing most genes. Group II and III, while structurally similar to Group I control specific cellular gene suites associated with circadian rhythm and environmental stress (Huckauf *et al.*, 2000; Khudyakov and Golden, 2001; Nair *et al.*, 2002). In contrast, most higher plants contain 5-6 sigma factors that are orthologous to *SigA* with some exceptions. In contrast, algal linages contain between 1-3 sigma factors and are distantly diverged from group 1 and group II sigma factors (Lerbs-Mache, 2011; Lysenko, 2006).

Sigma factors in higher plants display a divergence of function. Sigma factors SIG2 and SIG6 are essential for photoautotrophic growth (Ishizaki *et al.*, 2005; Loschelder *et al.*, 2006; Shirano *et al.*, 2000). SIG 1 under goes redox dependent phosphorylation, which leads to its differential regulation of *psaA* transcript and appears to weakly bind *rbcL* and *psbA promoters* (Shimizu *et al.*, 2010; Tozawa *et al.*, 2007).. SIG 2 acts as an essential sigma factor in plants with direct activation for several tRNAs and PSII subunits *psbA, psbD,* and *psbJ* (Hanaoka *et al.*, 2003; Kanamaru *et al.*, 2001). SIG 3 regulates the PSII subunit *psbN* and the ATP synthase subunit *atpH* and is also proposed to regulate *psbB* by an antisense RNA generated during *psbN* transcription (Zghidi *et al.*, 2007). SIG 4 appears to regulate *ndh*F, a plastid encoded subunit of

the NADH dehydrogenase-complex (Zghidi *et al.*, 2007). SIG 5 appears to play a role in regulation plastid transcription in response to circadian oscillations and also regulates PSII subunit *psbD* in response to blue light and appears to be regulated by cytochromes and phyochrome A, but the transmission of the signal to the chloroplast remains unknown(Nagashima *et al.*, 2004; Onda *et al.*, 2008; Tsunoyama *et al.*, 2004). SIG 6, like SIG 2, displays a chlorophyll deficient phenotype and is proposed to be the main sigma factor involved in early plant development and regulates a number of plastid operons (*atpB/E, ndhC/psbG/ndhJ*) (Bock *et al.*, 2014; Ishizaki *et al.*, 2005; Kubota *et al.*, 2007).

*Chloroplast translation*

Chloroplast translational machinery is highly conserved and displays high homology with its evolutionary counterparts in cyanobacteria and *Escherichia coli*. Chloroplasts use a prokaryotic-type 70S ribose consisting of a small 30S and large 50S subunit in conjunction with orthologs of bacterial rRNAs (Yamaguchi and Subramanian, 2000; Yamaguchi *et al.*, 2000). Like bacteria, the chloroplast encoded 30S ribosomal forms a pre-initiation complex with the initiator tRNA (for *N*-formlymethionine) and require paralogous initiation factors (Sibjen 1986, Campos 2001, Miura 2007). Two-thirds of chloroplast open reading frames are proceeded by a purine-rich Shine-Dalgarno sequence, and those without appear to facilitate SD-independent translation initiation by mRNA secondary structure in the 5'UTR (Nakagawa *et al.*, 2017; Scharff *et al.*, 2011; Scharff *et al.*, 2017). After formation of the pre-initiation complex the 50S subunit can bind which generates the functional 70S ribosomal initiating translation. Homologs of bacterial elongation factors (EF-Tu, EF-G, and EF-T) are also present in the chloroplast, and based on their regulation by light and abiotic and biotic stimuli, likely play a role in control chloroplast translation in response to development and environmental conditions (Akkaya and

Breitenberger, 1992; Albrecht *et al.*, 2006; Bhadula *et al.*, 2001; Schroter *et al.*, 2010; Singh *et al.*, 2004).

*Anterograde signaling*

Anterograde regulation is believed to occur primarily through translational regulation (Lerb-Mache 2011; Lyska *et al.*, 2013; Rea *et al.*, 2018; Zoschke and Bock, 2018) through a collection of proteins referred to as "regulators of organelle gene expression" (ROGEs) and are comprised of proteins in an organelle specific helical repeat superfamily (Delannoy *et al.*, 2007; Hammani *et al.*, 2014). Members of this helical repeat protein super family are characterized by containing successively repeated modules of 2-3 α-helices that form a super helix and facilitate sequence specific binding to their cognate mRNA. Helical repeat protein families are believed to be evolutionarily independent despite similar protein structure. They are classified based on the length of their helical motif: tetratricopeptide proteins (TPR) containing a 34 aa module length, pentatricopepdite proteins (PPR; 35 aa per helix), and octotricopeptide proteins (OPR, 38 aa per helix). There are also closely related mitochondrial transcription termination factors (mTERF. 30 aa per helix). Members of this helical repeat family are involved in RNA editing, RNA splicing, RNA cleavage, RNA stability and translational control in chloroplast and mitochondrial genome regulation (Delannoy *et al.*, 2007; Hammani *et al.*, 2014). Post-transcriptional regulation of chloroplast encoded photosynthetic protein abundance by helical repeat proteins have been demonstrated for ATP synthase (*atpA and atpH*) (Pfalz*et al.*, 2009), Cytochrome $b_6f$ (*petA)* (Boulouis *et al.*, 2011)), PS I (*psaA, psaB and psaC)*(Del Campo *et al.*, 2002; Lefebvre-Legendre *et al.*, 2015; Schmitz-Linneweber *et al.*, 2005) and PS II (*psbB* and *psbC)*(Boudreau *et al.*, 2000; Mulo *et al.*, 2012).

**Research preface**

The research documented in this dissertation set out to characterize the physiological responses to growth in constant and variable saturating light and to identify regulatory factors mediating photosynthetic acclimation.

Chapters 2 and 3 primarily focused on the role of qE in this acclimation response in the physiological response of the green algae *Chlamydomonas reinhardtii* grown under constant saturating light and a sinusoidal light regime mimicking natural, diurnal oscillations in irradiance and. Chapter 2 assessed this through characterization of the qE mutant, *npq4lhcsr1*, which lacks all known qE effector proteins (LHCSR3.1, LHCSR3.2 and LHCSR1) found in this *Chlamydomonas*. A limited reduction in growth observed in chapter 2 suggested that *Chlamydomonas* was effectively compensating for the absence of LHCSR-dependent quenching. In chapter 3 we investigated AET as a potential compensatory mechanism and characterize the roles of light dependent oxygen consumption during acclimation to the aforementioned light conditions.

Chapter 4, in contrast with 2 and 3, focused on genetic identification of factors involved in light acclimation – specifically regulation of the chloroplast encoded photosystem I subunit *psaA*. This study generated a mutant library using a forward genetic screen and chapter 4 presents preliminary characterization of these mutants.

# CHAPTER 2: A MUTANT OF *CHLAMYDOMONAS* WITHOUT LHCSR MAINTAINS HIGH RATES OF PHOTOSYNTHESIS, BUT HAS REDUCED CELL DIVISION RATES IN SINUSOIDAL LIGHT CONDITIONS [2]


**Summary**

The LHCSR protein belongs to the light harvesting complex family of pigment-binding proteins found in oxygenic photoautotrophs. Previous studies have shown that this complex is required for the rapid induction and relaxation of excess light energy dissipation in a wide range of eukaryotic algae and moss. The ability of cells to rapidly regulate light harvesting between this dissipation state and one favoring photochemistry is believed to be important for reducing oxidative stress and maintaining high photosynthetic efficiency in a rapidly changing light environment. We found that a mutant of *Chlamydomonas reinhardtii* lacking LHCSR, *npq4lhcsr1*, displays minimal photoinhibition of photosystem II and minimal inhibition of short-term oxygen evolution when grown in constant excess light compared to a wild type strain. We also investigated the impact of no LHCSR during growth in a sinusoidal light regime, which mimics daily changes in photosynthetically active radiation. The absence of LHCSR correlated with a slight reduction in the quantum efficiency of photosystem II and a stimulation of the maximal rates of photosynthesis compared to wild type. However, there was no reduction in carbon accumulation during the day. Another novel finding was that *npq4lhcsr1* cultures underwent fewer divisions at night, reducing the overall growth rate compared to the wild type. Our results show that the rapid regulation of light harvesting mediated by LHCSR is required for


[2] Reprinted from *PlosONE,* Cantrell, M., Peers, G. A mutant of Chlamydomonas without LHCSR maintains high rates of photosynthesis, but has reduced cell division rates in sinusoidal light conditions.12(6), Copyright 2017, with permission from *PlosONE*. Figures and tables have been adjusted for formatting specific to this chapter.

high growth rates, but it is not required for efficient carbon accumulation during the day in a sinusoidal light environment. This finding has direct implications for engineering strategies directed at increasing photosynthetic productivity in mass cultures.

**Introduction**

The natural aquatic light environment fluctuates across space and time. Light intensity follows a sinusoidal oscillation across the day with superimposed rapid fluctuations due to changes in cloud cover, wave focusing, turbidity and vertical mixing (Falkowski and Raven, 2013; Jallet *et al.*, 2016a). These short-term changes can cause light absorption to exceed the capacity of utilization leading to the generation of reactive oxygen species (ROS) such as singlet oxygen ($^1O_2$), hydrogen peroxide ($H_2O_2$), superoxide anions ($O_2^-$) and hydroxyl radicals ($OH^-$). These ROS then damage surrounding proteins, pigments and lipids – impairing photosynthetic function and growth (Krieger-Liszkay *et al.*, 2008; Triantaphylides and Havaux, 2009). Algae, plants and cyanobacteria dynamically regulate a process termed non-photochemical quenching of light energy (NPQ) to avoid excess damage while maintaining efficient photosynthesis in lower light fluxes. This balance between energy dissipation and light harvesting capacity allows photosynthetic organisms to maintain optimal fitness in diverse environmental niches.

NPQ is comprised of four components that contribute to light energy dissipation as heat (Derks *et al.*, 2015; Erickson *et al.*, 2015; Ruban, 2015; Wobbe *et al.*, 2016). The components are physiologically distinguished based on their time of induction and relaxation. The slowest component is photoinhibition (qI). qI occurs when the rate of damage to the PSII D1 protein exceeds the rate of its repair and is caused by absorption of light energy in excess of its utilization and NPQ capacity (Aro *et al.*, 1993; Takahashi and Murata, 2005; Tyystjarvi and Aro, 1996). Faster forms of NPQ limit the amount of qI that occurs by protecting PSII reaction centers

from over excitation. Zeaxanthin-dependent quenching (qZ) occurs on the time scale of tens of minutes and involves the pH dependent accumulation of zeaxanthin in the thylakoid membranes. Zeaxanthin is then hypothesized to enhance the probability of quenching chlorophyll excited states as heat in PSII minor antenna (Dall'Osto *et al.*, 2005; Nilkens *et al.*, 2010; Wehner *et al.*, 2006). State transitions (qT) occur on the time scale of minutes and involves phosphorylation of PSII associated light harvesting complexes (LHCII) (Depege *et al.*, 2003; Lemeille *et al.*, 2009b). Phosphorylated LHCII can then either aggregate and enter a quenched state or migrate and associate with PSI reaction centers enhancing PSI functional antenna size (Nagy *et al.*, 2014a; Unlu *et al.*, 2014). The fastest component of NPQ is energy-dependent quenching (qE). qE is induced by luminal acidification and can be rapidly induced and relaxed in seconds to minutes (Horton *et al.*, 1994; Niyogi *et al.*, 1997a). Each component of NPQ is thought to regulate photosynthetic function in response to different forms and lengths of environmental stress.

qE is the major component of NPQ involved in responding to dynamic increases in light intensity (Allorent *et al.*, 2013b; Berteotti *et al.*, 2016; Peers *et al.*, 2009). *Chlamydomonas* has been instrumental for the characterization of qE in algae. In *Chlamydomonas* three stress related light harvesting complexes (LHCSR1, 3.1 and 3.2) are required for induction of qE (Peers *et al.*, 2009). LHCSR mediated qE requires luminal acidification (Tokutsu and Minagawa, 2013) and the xanthophylls zeaxanthin and lutein (Niyogi *et al.*, 1997b). *Chlamydomonas* has an atypical violaxanthin de-poxidase which catalyzes the conversion of violaxanthin to zeaxanthin through the xanthophyll cycle (Li *et al.*, 2016). LHCSR, unlike its functional analog in plants − PSBS, can bind chlorophylls and has limited quenching activity *in vitro* that is enhanced upon protonation in excess light (Bonente *et al.*, 2011; Liguori *et al.*, 2013).

LHCSRs accumulate in response to excess light (Ledford *et al.*, 2004; Peers *et al.*, 2009) and the deprivation of $CO_2$ (Brueggeman *et al.*, 2012; Yamano *et al.*, 2008), sulphur (Zhang *et al.*, 2004), and iron (Naumann *et al.*, 2007). Characterization of the qE-deficient *npq4* (Lacks LHCSR3.1 and LHCSR3.2) mutant in *Chlamydomonas* has demonstrated the importance of qE in limiting photoinhibition, ROS generation and cell death during a shift from low light to high light (Allorent *et al.*, 2013b; Berteotti *et al.*, 2016; Peers *et al.*, 2009), but little is known about the impact that complete loss of qE has on cell growth and photophysiology under excess light conditions or in natural day/night cycles.

Here we report on our observations of the complete LHCSR knockout, *npq4lhcsr1* (Ballottari *et al.*, 2016; Truong, 2011). We sought to investigate the impact of no LHCSR, and hence no qE, on photophysiology and cell growth in constant excess light and in a sinusoidal light regime that mimics natural changes in light, specifically as photosynthetically active radiation. We observed the expected reductions in photosynthetic capacity and cell physiology associated with growth in constant excess light for the mutant vs. wild type. Surprisingly, *npq4lhcsr1* did not display significant photoinhibition of photosynthesis in conditions that mimic natural light conditions and reduced daily growth rates were due to reduced cell divisions at night. We discuss the implications of these results for strategies to increase biofuel yields in industrial cultures of algae.

## Materials and Methods

### Strains

The *Chlamydomonas reinhardtii* 4A+ strain (137c genetic background) was used as wild type strain. The *npq4lhcsr1* mutant was made in the 4A+ genetic background and does not

produce any detectable LHCSR protein (Truong, 2011). Both strains were obtained from Krishna Niyogi, University of California, Berkeley.

Growth rates

Exponential growth rates were determined from tracking cell density for 2-3 days. Growth rates, μ, were calculated by linear regression using the exponential growth equation $\mu = \frac{\ln(F)-\ln(I)}{\Delta t}$ where $F$ is the final cell concentration, $I$ the initial cell concentration, $\mu$ is the specific growth rate ($d^{-1}$) and $t$ time in days (McDuff and Chisholm, 1982). Cell densities were determined using the Accuri C6 flow cytometer (BD). Samples were passed through a 30 μm pre-filter (MACS Miltenyi, 130-041-407) prior to each run to remove debris. Each count was performed for 60 seconds using a flow rate of 35 μl $min^{-1}$ and a core size of 14 μm. *Chlamydomonas* cells were identified as chlorophyll autofluorescence particles via excitation and emission at 640 and 675 ± 25 nm, respectively.

Culture conditions

All experiments were performed on axenic, photoautotrophically grown cultures using TP media at 25 °C (Kropat *et al.*, 2011). Each experiment started with an inoculation of between 10,000 – 50,000 cells $ml^{-1}$ from a stock culture acclimated for at least 10 generations in their respective light environment. Cells for the continuous light experiments were grown in 250 ml glass Erlenmeyer flask containing 100 mL of media and shaken at 150 RPM. Continuous light cultures were grown under 50, 400 or 860 μmol photons $m^{-2}$ $s^{-1}$ of Photosynthetically Active Radiation (PAR light supplied by cool white fluorescent bulbs (Phillips, F17T8/TL841). Light fluxes were measured using a 2pi, LICOR LI-250A light sensor.Growth and physiology in sinusoidal light conditions were characterized using a Phenometrics ePBR with a custom, autoclavable glass culture vessel (Jallet *et al.*, 2016a; Lucker *et al.*, 2014). Cells were grown in

500 mL of TP mixed by a stir bar running at 500 RPM and sparged with 0.45 µm filtered air supplied at 1 L $min^{-1}$. Cultures were illuminated with a white LED light programmed to follow a 12:12 light: dark cycle. Light intensity followed a sinusoidal light pattern peaking at 2134 µmol photons $m^{-2}$ $s^{-1}$ of PAR at the top of a 24 cm water column and 370 µmol photons $m^{-2}$ $s^{-1}$ at the bottom of the culture 6 hours after dawn (4pi Walz ULM-500 light meter, Fig 1B). The light intensity for either position can be approximated for *t* hours after dawn as follows:

$$Lightflux\ (t) = A_{max} \cdot \sin(\pi \cdot t \cdot \frac{1}{12})$$

$$where\ A_{max} = 2134\ or\ 370\ \mu mol\ photons\ m^{-2}\ s^{-1}, and\ t\ =\ hours\ after\ dawn.$$

See Jallet *et al.* (2016) for a full description and diagram of the ePBR culturing set up and Lucker *et al.* (2014) for the light spectra associated with these LEDs vs cool white fluorescent bulbs (Jallet *et al.*, 2016a; Lucker *et al.*, 2014).

Analyses of chlorophyll fluorescence parameters in steady state

Chlorophyll fluorescence measurements of *Chlamydomonas* were performed using a Dual-PAM (Walz). All measurements were made using a blue measuring light (460 nm, intensity setting 4) and red actinic light (620 nm). 5 ml of culture in exponential growth phase (ranging from 450,000 cells $ml^{-1}$ to 750,000 cells $ml^{-1}$) was agitated in a 50 mL beaker for 20 minutes prior to each measurement. Cells were then collected by gently filtering onto a 13 mm diameter glass fiber filter (Millipore, AP2501300) that was then placed in the Dual-PAM's leaf clip (Peers *et al.*, 2009). PSII quantum efficiency was measured as $\frac{F_m - F_o}{F_m}$, where $F_m$ is the maximum PSII fluorescence obtained with a red saturating pulse (620 nm, 600 ms duration, 10,000 µmol photons $m^{-2}$ $s^{-1}$) and $F_o$, the minimum fluorescence obtained after 10 minutes of far red light (intensity setting 10) to ensure a state 1 transition (Peers *et al.*, 2009). Cells were then

illuminated with either 600 µmol photons $m^{-2}$ $s^{-1}$ or 2005 µmol photons $m^{-2}$ $s^{-1}$ for 10 minutes. Saturating pulses were applied every minute during illumination. The actinic light was turned off, and the cells were re-illuminated with far red light and saturating pulses were applied every 2 minutes for 10 minutes. NPQ was calculated as $NPQ = \frac{F_m' - F_m}{F_m'}$ where $F_m'$ is the maximum fluorescence measured in the light-adapted state (during or after actinic light illumination). Closed PSII reaction centers were calculated as 1-qL , assuming the lake model (Kramer *et al.*, 2004; Oxborough and Baker, 1997). $qL = \frac{(F_m'/F)}{(F_m - F_o)} \cdot \frac{F_o'}{F}$ with $F$ representing fluorescence in the illuminated state and $Fo'$ , representing an approximation of the minimum fluorescence obtainable in an illuminated state, is calculated as $Fo' = \frac{F_o}{((F_m' - F_m / F_m) + F_o/F_m)}$ (Kramer *et al.*, 2004; Oxborough and Baker, 1997).

Simultaneous measurements of chlorophyll fluorescence and oxygen evolution

Cultures in late exponential (450,000 cells $ml^{-1}$ to 750,000 cells $ml^{-1}$) were collected by centrifugation at 1500 x g for 5 minutes at 25 °C. The supernatant was discarded. The pellet was then re-suspended in TP media supplemented with freshly prepared $NaHCO_3$ to final concentration of 5 mM. Cell density was adjusted to 4 ± 1 µM chlorophyll. One ml of these cells was transferred into a homemade 1 cm diameter cylindrical quartz cuvette with a magnetic stir bar. Cells were dark acclimated for 15 minutes then sealed in the cuvette using a custom 3D-printed plastic stopper fitted with a FireSting dark-coated robust probe (OXROB10) (Jallet *et al.*, 2016a). Dark respiration rates were recorded for 5 minutes before turning on the Dual-PAM far red light (intensity setting 20) for 10 minutes to induce a state 1 transition (Peers *et al.*, 2009). An initial red saturating pulse (620 nm, 600 ms, 10,000 µmol photons $m^{-2}$ $s^{-1}$) was used to measure maximum PSII quantum efficiency (as described above) followed by a rapid light curve

(RLC) of increasing 60-second actinic red light steps punctuated by saturating pulses. The assayed actinic light steps included 8, 19, 33, 56, 80, 106, 143, 191, 250, 323, 407, 505, 635, 783, 1203, 1850 µmol photons $m^{-2}$ $s^{-1}$ (measured with a 4pi Walz ULM-500 light meter). Gross oxygen evolution rates were determined based on the sum of the net oxygen evolution rates over the last 45 seconds of each light step and the absolute value of the dark respiration rates. The maximum oxygen evolution rate ($P_{max}$), the light limited slope (α) and the irradiance at saturation ($I_K$) was determined by fitting oxygen evolution rates (nmol $O_2$ $cell^{-1}$ $min^{-1}$) vs irradiance to the exponential difference equation described by Platt *et al.* (1980) using the curve fitting tool described in Ritchie (2008) (Platt *et al.*, 1980; Ritchie, 2008).

Dark respiration rates at night in sinusoidal light cultures

Dark respiration rates we measured ex-situ, using the apparatus described above, on late exponential cultures (ranging from 450,000 cells $ml^{-1}$ to 1,500,000 cells $ml^{-1}$). Respiration rates were measured immediately after sampling at 20 minutes before and after the dark period and 0.5, 1.5, 3, 6, 9, 10.5 and 11.5 hour after dusk.

Chlorophyll fluorescence parameters during growth in sinusoidal conditions

PSII fluorescence induction profiles across the sinusoidal light period were measured using a Fluorescence Induction and Relaxation Fluorometer (FIRe, Satlantic) using a blue (450 nm with a 30 nm band-width) LED to excite chlorophyll *a.* A saturating ($5 \times 10^4$ µmol photons $m^{-2}$ $s^{-1}$) single turnover flash (80 µs) and multiple turnover flash (20 ms) were used to calculate the effective quantum yield of PSII ($F_v/F_m$), the relative functional antenna size of PSII ($\sigma_{PSII}$) and the re-oxidation kinetics of the quinone $Q_B$ (τ) as described in Kolber *et al.* 1998 (Kolber *et al.*, 1998). *Chlamydomonas* cells (600,000 cells $ml^{-1}$ to 1,000,000 cells $ml^{-1}$) were collected from the ePBR photobioreactors and measured within 1 minute using a FIRe fluorometer (Satlantic).

We used the MATLAB software and the FIReWORX script (Audrey Barnett, http://sourceforge.net/project/fireworx/) with instrument specific light calibrations factors to extract fluorescence parameters, $F_o$ and $F_m$, and fit the fluorescence induction and relaxation curves generated.

Lipid peroxides

Lipid peroxidation was estimated by measuring the formation of thiobarbituric acid-reactive substances (TBARS) (Baroli *et al.*, 2004; Hodges *et al.*, 1999). 1 x $10^7$ cells were harvested during exponential growth phase (600,000 cells $ml^{-1}$ to 1,000,000 cells $ml^{-1}$). We added 0.01 % (w/v) butylated hydroxytoluene (BHT, Sigma-Aldrich) to each sample prior to freezing at -80 °C to arrest lipid peroxidation. Thawed cell samples were pelleted at 3220 x g for 5 minutes at 4 °C after the addition of 0.01 %, final concentration, TWEEN 20 (Sigma-Aldrich). Cell pellets were re-suspended in 1 ml ice-cold 80:20 (v/v) ethanol: water and lysed using sonication for 10 seconds (Q55 QSonica probe sonicator, 50 % duty cycle). After sonication, 750 µL of homogenate was added to a 9 ml glass screw top test tube with 750 µL of either a +TBA solution (20.0 % trichloracetic acid, 0.01 % butylated hydroxytoluene, and 0.65 % 2-thiobarbituric acid, all w/v, Sigma-Aldrich) or a -TBA solution. Samples were then heated to 95 °C in a water bath for 25 minutes and then cooled to room temperature. One mL of this solution was transferred to a centrifuge tube and clarified by centrifugation at 10,000 x g for 5 minutes at room temperature. TBARS in the supernatant was determined by absorbance at 532 nm with a correction for nonspecific absorbance at 440 nm and 600 nm and normalized per 1 x $10^7$ cells (Hodges *et al.*, 1999).

Pigment concentration

Cells were initially harvested as described in the simultaneous measurements of chlorophyll fluorescence and oxygen evolution. TWEEN 20 (0.01 % final concentration, Sigma-Aldrich, p7949) was added to 1 mL of culture and the cells were centrifuged at 10,000 x g for 10 minutes at 4 °C. The supernatant was removed. Chlorophylls were then extracted for 10 minutes in 80 % buffered acetone with 50 mM HEPES, pH 7.5 and then cell debris was removed by centrifugation at 10,000 x g for 5 minutes (Porra, 2002). Chlorophyll *a* and *b* concentrations were determined by spectrophotometry using established extinction coefficients (Porra, 2002).

Cell volumes

*Chlamydomonas* cell volumes were determined assuming a prolate spheroid shape (Sun and Liu, 2003). Cell dimensions were determined from at least 100 size-calibrated cell images from a Leica DM5500 B microscope using imageJ (Shriwastav *et al.*, 2014).

Total Organic Carbon

Total organic carbon (TOC) per cell were determined using a Shimadzu TOC-L Laboratory Total Organic Carbon analyzer**.** 9.5 x $10^6$ to 15 x $10^6$ cells were harvested from low density cultures (ranging from 450,000 cells $ml^{-1}$ to 1,600,000 cells $ml^{-1}$) by centrifugation (at 3,220 x g for 5 minutes at 25 °C) in acid washed (10 % HCl) 50 ml conical centrifuge tubes. Cell pellets were rinsed twice with an isotonic (0.523 mM NaCl) solution, re-suspended in 20 ml of 0.523 mM NaCl and then stored at -80 °C. Samples were thawed on the day of analysis and 5 x $10^6$ cells were diluted with water (18.2 MΩ) to a final volume of 40 ml in TOC glass vials (Sigma-Aldrich). Sample blanks were prepared using an equal volume of isotonic salt solution and water. Measurements and a calibration curves were made for Total Carbon (TC), and Inorganic Carbon (IC). Blank and internal controls with known TC or IC were tested throughout an individual set as a control. Each sample was measured sequentially in technical duplicate

using a 100 µl injection volume for TC and IC measurements. TOC per cell were calculated based on the manufacturer's instructions (Shimadzu Application News no. 049) as follows:

$$TC_{cells} = \frac{TC_{\ sample} - TC_{blank}}{Cells\ in\ diluted\ sample}$$

$$IC_{cells} = \frac{IC_{\ sample} - IC_{blank}}{Cells\ in\ diluted\ sample}$$

$$TOC_{cells} = IC_{\ sample} - IC_{blank}$$

Carbon accumulation across the day was calculated by subtracting TOC per cell at dawn from TOC per cell at dusk within each biological replicate.

Cell division frequency measurements

Division frequency and average division number under sinusoidal conditions was determined as previously described (Umen and Goodenough, 2001), but with some modifications. 300 µl of each culture were harvested at the start of the dark period and plated on TP agar plates (1.5 %). Plates were incubated for 24-30 hours in the dark and scored by counting 300-400 cell clusters with each cluster representing the progeny from one mother cell after dark incubation. The number of cells per cluster was used to determine the division number, n, for the multiple-fission events occuring during the night (Cross and Umen, 2015).

Immunoblot analysis

Cells were harvested in exponential growth phase (ranging from 450,000 cells $ml^{-1}$ to 750,000 cells $ml^{-1}$) by centrifugation (1,800 x g for 4 minutes at 25 °C). Samples were then prepared and ran on pre-cast Novex 10-20 % tris-glycine gels (EC6135BOX) as described in Peers *et al.* 2009 with the following modifications (Peers *et al.*, 2009). Membranes were blocked overnight with 3 % milk in TBS with 1 % TWEEN 20 (Sigma-Aldrich, P7949) and then incubated with anti-LHCSR polyclonal antibody (Richard *et al.*, 2000), anti-D2 antibody (PsbD,

Agrisera #AS06146), anti-PsaC antibody (Agrisera #AS10939), anti-Lhcb2 (Agrisera #AS01003) diluted 1:2,000, or anti-ATP-B (Agrisera #AS05085) diluted 1:5,000, in a 0.5 % milk TBS solution. Membranes were incubated with each respective antibody for one hour and then rinsed four times for 5 minutes. Band detection was performed using SuperSignal West Femto Maximum Sensitivity Substrate (Thermo Scientific, #34095) according to the manufacturer's protocol. 0.77 nmol total chlorophyll was loaded for immunoblots of LHCSR. 0.075 nmol total chlorophyll was loaded for immunoblots of D2 and PsaC. 0.2 nmol total chlorophyll was loaded for Lhcb2 immunoblots. Protein abundance was determined by the band intensity using the imageJ software, version 1.48 (http://imagej.nih.gov/ij/). Relative abundances for D2, PsaC and Lhcb2 are based on an in gel dilution series (25, 50, 100, 150 % of WT). Relative abundance was normalized within samples to ATP-B.

Statistics

Measurements were made on at least three independent cultures except for cell division frequency measurements. An un-paired Student's t-test was performed to compare *npq4lhcsr1* to wild type (SigmaStat).

**Results**

Growth rates of wild type and the *npq4lhcsr1* mutant under continuous and sinusoidal light regimes

*Chlamydomonas* cultures were acclimated for at least 10 generations to constant light conditions before physiological characterization. The *npq4lhcsr1* mutant obtained did not have any detectable LHCSR protein expression (Figure 2.1A) and no rapidly inducible NPQ when acclimated to 400 µmol photons $m^{-2}$ $s^{-1}$ (Figure 2.1C). There was also no rapidly inducible NPQ observed in either wild type and *npq4lhcsr1* cells acclimated to 50 µmol photons $m^{-2}$ $s^{-1}$.

We tested the effects of qE loss on cell physiology using five light regimes. To test if qE is required for rapid growth in continuous excess light, cultures were grown under continuous irradiance of 50, 400 and 860 µmol photons $m^{-2}$ $s^{-1}$. Under continuous irradiances wild type growth rate was highest at 400 and 860 µmol photons $m^{-2}$ $s^{-1}$ (Figure 2.2A). However, the measured growth rates were reduced by 11 % in *npq4lhcsr1* relative to wild type at the highest irradiance ($p<0.05$). To test the requirement of qE for growth in a sinusoidal light regime, we grew cells in a simulated "natural" light regime with a 12:12 light: dark cycle and a peak light intensity of 2134 µmol photons $m^{-2}$ $s^{-1}$ at the top of the water column (Figure 2.2B). We note that the light gradient found in the ePBR system resulted in light environments that rapidly changed (<10s) between the measured surface and bottom irradiances (Fig 2.2B). Growth in this sinusoidal light regime reduced the daily growth rate of *npq4lhcsr1* to 23 % relative to wild type (Fig 2.1A). However, strains grown in 12 hours 2134 µmol photons $m^{-2}$ $s^{-1}$ constant light, 12 hours dark in a ePBR grew at the same rate (Supplemental figure 2.4).

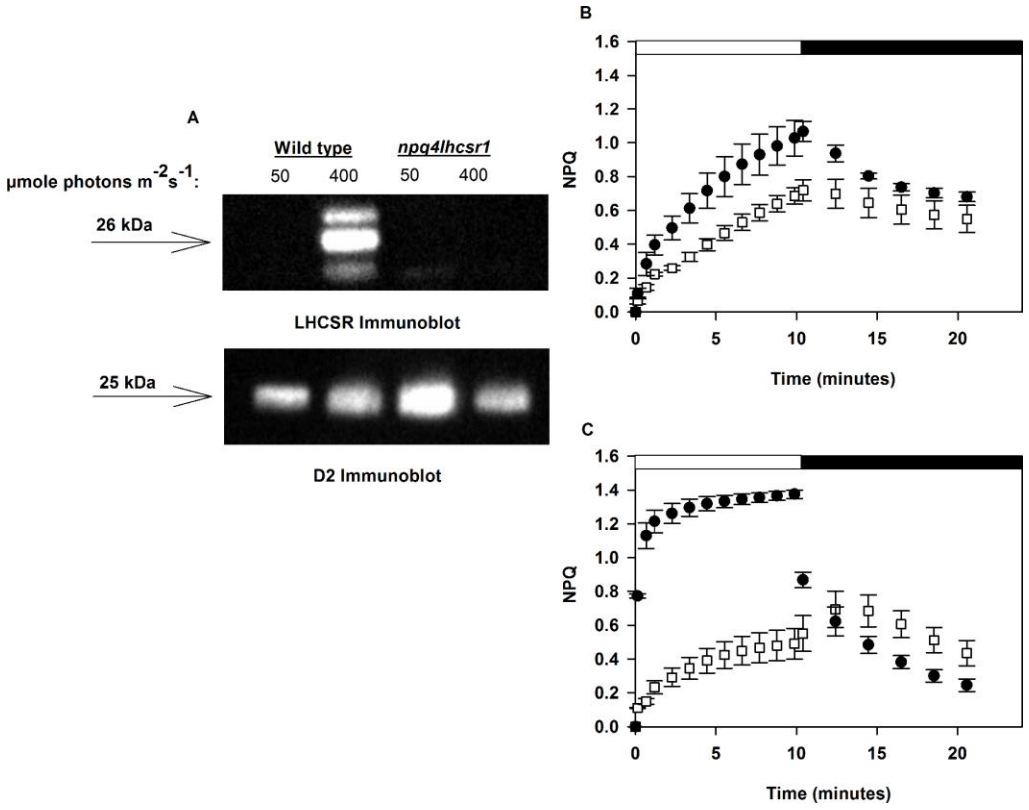


**Figure 2.1 *npq4lhcsr1* lacks detectable LHCSR and rapidly reversible NPQ.**
(A) Immunoblot analysis of LHCSR and D2 protein of the photosystem II reaction center from cultures acclimated to a continuous irradiance of 50 µmol photons $m^{-2}$ $s^{-1}$ and 400 µmol photons $m^{-2}$ $s^{-1}$. 0.77 nmol of chlorophyll was loaded in each lane. (B-C) Wild type (black circles) and the *npq4lhcsr1* (white squares) mutant cultures acclimated to 50 µmol photons $m^{-2}$ $s^{-1}$ (B) and 400 µmol photons $m^{-2}$ $s^{-1}$ (C) when exposed to a red actinic light level of 2005 µmol photons $m^{-2}$ $s^{-1}$ (white bar) followed by 10 minutes darkness (black bar) and far red light illumination to re-associate LHCII with PSII (state 1 transition) by preferentially driving PSI charge separation. Data represents means ± s.d. (n = 3).

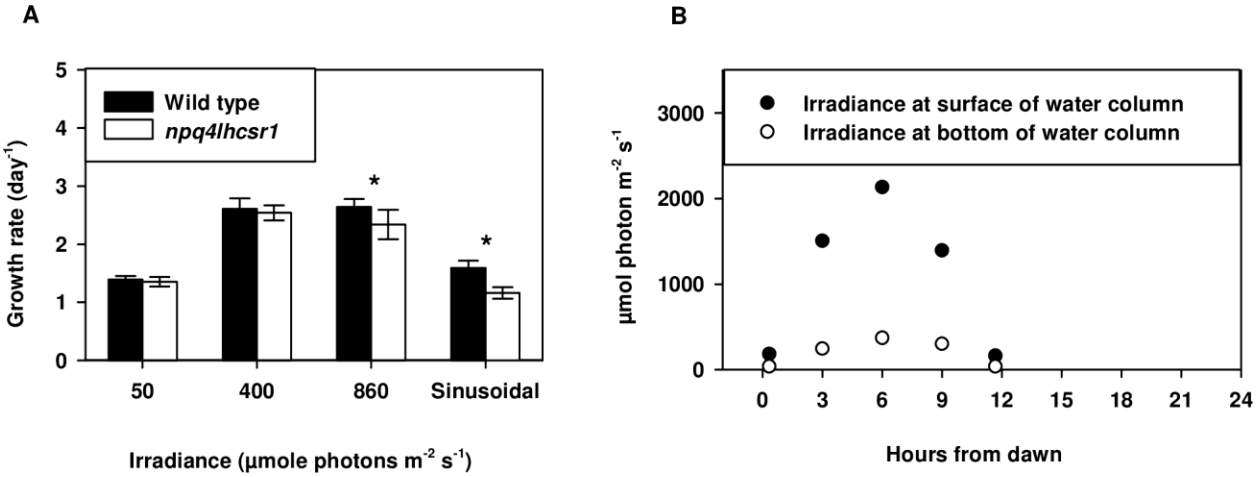


**Figure 2.2 *npq4lhcsr1* growth rate under continuous and sinusoidal conditions.**
(A) Chlamydomonas exponential growth rates determined by cell counts collected over 2-3 days of growth. Symbols (*) represent significant differences from wild type within light acclimated states based on an un-paired t-test ($p < 0.05$). Data represents means + s.d. (n=7-9) (B) Light levels measured across the 12:12 light dark cycle used for the sinusoidal light regime.

Chlorophyll content of wild type and *npq4lhcsr1* under continuous and sinusoidal light regimes

Wild type cultures reduced their total chlorophyll content with increasing irradiances under continuous light acclimated conditions (Table 2.1). This ranged from 1.25 ± 0.09 fmol chlorophyll cell$^{-1}$ at 50 µmol photons m$^{-2}$ s$^{-1}$ to 0.27 ± 0.05 fmol chlorophyll cell$^{-1}$ under 850 µmol photons m$^{-2}$ s$^{-1}$ representing a 78% reduction. Wild type cells grown in the sinusoidal regime and harvested 6 hours after dawn contained 1.15 fmol chlorophyll cell$^{-1}$.

The chlorophyll *a*:*b* ratio can be used to assess *Chlamydomonas's* photoacclimation response. Chlorophyll *b* is only found in the photosynthetic antenna proteins and thus higher ratios of chlorophyll *a*:*b* indicate a reduction in antenna size (Falkowski and Raven, 2013). At 50 µmol photons m$^{-2}$ s$^{-1}$ the chlorophyll *a:b* ratio was statistically identical between wild type and *npq4lhcsr1* ($p > 0.05$). We observed some reductions in the ratio between the mutant and wild type at higher light levels, but this was only statistically significant in cultures acclimated to 400 µmol photons m$^{-2}$ s$^{-1}$ (Table 2.1). 6 hours after dawn in the sinusoidal light regime, the *npq4lhcsr1* chlorophyll *a*:*b* ratio was significantly reduced compared to wild type cells.

**Table 2.1 Effects of acclimation state on *npq4lhcsr1* physiology.**
Data represents the mean ± s.d. (n = 3). Symbols (*) represent significant differences from wild type within light acclimated states based on an un-paired t-test ($p < 0.05$).

| | Units | 50 µmol photons $m^{-2}$ $s^{-1}$ | |
|---|---|---|---|
| | | wild type | *npq4lhcsr1* |
| Chlorophyll *a* + *b* | fmol $cell^{-1}$ | 1.25 ± 0.09 | 1.09 ± 0.15 |
| Chlorophyll *a* | fmol $cell^{-1}$ | 0.92 ± 0.06 | 0.79 ± 0.10 |
| Chlorophyll *a*:*b* | mol:mol | 2.76 ± 0.04 | 2.66 ± 0.21 |
| | Units | 400 µmol photons $m^{-2}$ $s^{-1}$ | |
| | | wild type | *npq4lhcsr1* |
| Chlorophyll *a* + *b* | fmol $cell^{-1}$ | 0.57 ± 0.03 | 0.64 ± 0.09 |
| Chlorophyll *a* | fmol $cell^{-1}$ | 0.43 ± 0.03 | 0.47 ± 0.07 |
| Chlorophyll *a*:*b* | mol:mol | 3.02 ± 0.09 | 2.69 ± 0.07 * |
| | Units | 860 µmol photons $m^{-2}$ $s^{-1}$ | |
| | | wild type | *npq4lhcsr1* |
| Chlorophyll *a* + *b* | fmol $cell^{-1}$ | 0.27 ± 0.05 | 0.31 ± 0.05 |
| Chlorophyll *a* | fmol $cell^{-1}$ | 0.20 ± 0.04 | 0.22 ± 0.03 |
| Chlorophyll *a*:*b* | mol:mol | 2.89 ± 0.28 | 2.51 ± 0.10 |
| | Units | Sinusoidal light regime | |
| | | wild type | *npq4lhcsr1* |
| Chlorophyll *a* + *b* | fmol $cell^{-1}$ | 1.15 ± 0.19 | 1.30 ± 0.18 |
| Chlorophyll *a* | fmol $cell^{-1}$ | 0.89 ± 0.15 | 0.98 ± 0.13 |
| Chlorophyll *a*:*b* | mol:mol | 3.49 ± 0.08 | 3.07 ± 0.05* |

Photosynthetic responses of wild type and *npq4lhcsr1*

Significant reductions in maximum PSII quantum yield ($F_v/F_m$) for *npq4lhcsr1* cells grown under 400 and 860 µmol photons $m^{-2}$ $s^{-1}$ correlated with a significant reduction in the maximum oxygen evolution rate per cell ($P_{max}$) only under 860 µmol photons $m^{-2}$ $s^{-1}$ (Table 2.2). $I_K$ and $\alpha$ remained the same between each strain in our excess light conditions. NPQ capacity in wild type increased between high and low light grown cells with similar levels of maximum NPQ observed between cultures acclimated to continuous irradiances of 400 and 860 µmol

photons $m^{-2}$ $s^{-1}$ (Figure 2.3E-G). NPQ capacity was reduced in *npq4lhcsr1* compared to wild type in all conditions. NPQ capacity was found to be rapidly reversible in the dark for wild type cells, suggesting most of the NPQ was due to qE. In the *npq4lhcsr1* strain little of the observed NPQ was reversible in the dark, suggesting photoinhibition (qI). These results are shown in Supplementary Figure 1.

**Table 2.2. Effects of acclimation state on *npq4lhcsr1* photophysiology.**

[a]Pmax (nmole $O_2$ evolved $min^{-1}$ $cell^{-1}$), [b]α ((nmole $O_2$ evolved $min^{-1}$ $cell^{-1}$)/(µmol photons per $m^2$)), [c]$I_K$ (µmol photons per $m^2$) and [e]Dark respiration (nmol $O_2$ consumed $cell^{-1}$ $min^{-1}$) were collected as described in the materials and methods. Low light acclimated samples had insufficient points for the accurate calculation of Pmax , α and $I_K$ (not determined - ND). Values determined for sinusoidal light regime reflect samples measured 6 hours after dawn. Data represents the mean ± s.d. (n = 3-6). Symbols (*) represent significant differences from wild type within light acclimated states based on an un-paired t-test ($p < 0.05$).

| Parameters | 50 µmol photons $m^{-2}$ $s^{-1}$ | |
|---|---|---|
| | wild type | *npq4lhcsr1* |
| Photosystem II efficiency ($F_v/F_m$) | 0.61 ± 0.02 | 0.59 ± 0.01 |
| Pmax[a] | ND | ND |
| α[b] | ND | ND |
| $I_K$[c] | ND | ND |
| Dark Respiration | $8.4 \times 10^{-7} \pm 3.1 \times 10^{-7}$ * | $1.1 \times 10^{-6} \pm 1.3 \times 10^{-7}$ * |
| Parameters | 400 µmol photons $m^{-2}$ $s^{-1}$ | |
| | wild type | *npq4lhcsr1* |
| Photosystem II efficiency ($F_v/F_m$) | 0.54 ± 0.01 | 0.47 ± 0.03 * |
| Pmax[a] | $7.9 \times 10^{-7} \pm 1.5 \times 10^{-7}$ | $6.5 \times 10^{-7} \pm 1.5 \times 10^{-7}$ |
| α[b] | $3.2 \times 10^{-2} \pm 0.3 \times 10^{-2}$ | $2.2 \times 10^{-2} \pm 0.8 \times 10^{-2}$ |
| $I_K$[c] | 299 ±35 | 313 ± 84 |
| Dark Respiration | $4.3 \times 10^{-7} \pm 1.2 \times 10^{-7}$ | $4.6. \times 10^{-7} \pm 6.5 \times 10^{-8}$ |
| Parameters | 860 µmol photons $m^{-2}$ $s^{-1}$ | |
| | wild type | *npq4lhcsr1* |
| Photosystem II efficiency ($F_v/F_m$) | 0.46 ± 0.03 | 0.31 ± 0.14 * |
| Pmax[a] | $1.3 \times 10^{-6} \pm 1.3 \times 10^{-7}$ | $9.0 \times 10^{-7} \pm 1.7 \times 10^{-7}$ * |
| α[b] | $3.1 \times 10^{-2} \pm 1.0 \times 10^{-2}$ | $2.1 \times 10^{-2} \pm 0.5 \times 10^{-2}$ |
| $I_K$[c] | 513 ± 143 | 439 ± 120 |
| Dark Respiration | $6.9 \times 10^{-7} \pm 5.1 \times 10^{-8}$ | $5.1 \times 10^{-7} \pm 1.3 \times 10^{-7}$ |
| Parameters | Sinusoidal light regime | |
| | wild type | *npq4lhcsr1* |
| Photosystem II efficiency ($F_v/F_m$) | 0.66 ± 0.01 | 0.62 ± 0.02 * |
| Pmax[a] | $2.7 \times 10^{-6} \pm 3.0 \times 10^{-7}$ | $5.7 \times 10^{-6} \pm 3.8 \times 10^{-7}$ * |
| α[b] | $3.4 \times 10^{-2} \pm 0.5 \times 10^{-2}$ | $2.4 \times 10^{-2} \pm 0.3 \times 10^{-2}$ * |
| $I_K$[c] | 380± 102 | 711 ± 60 * |
| Dark Respiration | $5.4 \times 10^{-7} \pm 1.2 \times 10^{-7}$ | $9.16 \times 10^{-7} \pm 1.7 \times 10^{-7}$ * |

There was no statistically significant change in the 1-qL parameter between the two strains (Figure 2.3I-L). 1-qL appeared to saturate at lower light intensities for cells grown at 50 vs 400 and 860 µmol photons $m^{-2}$ $s^{-1}$. Unfortunately, the small number of data points collected at low light fluxes did not permit the calculation of $P_{max}$, $I_k$ or α parameters for cells grown at 50 µmol photons $m^{-2}$ $s^{-1}$.

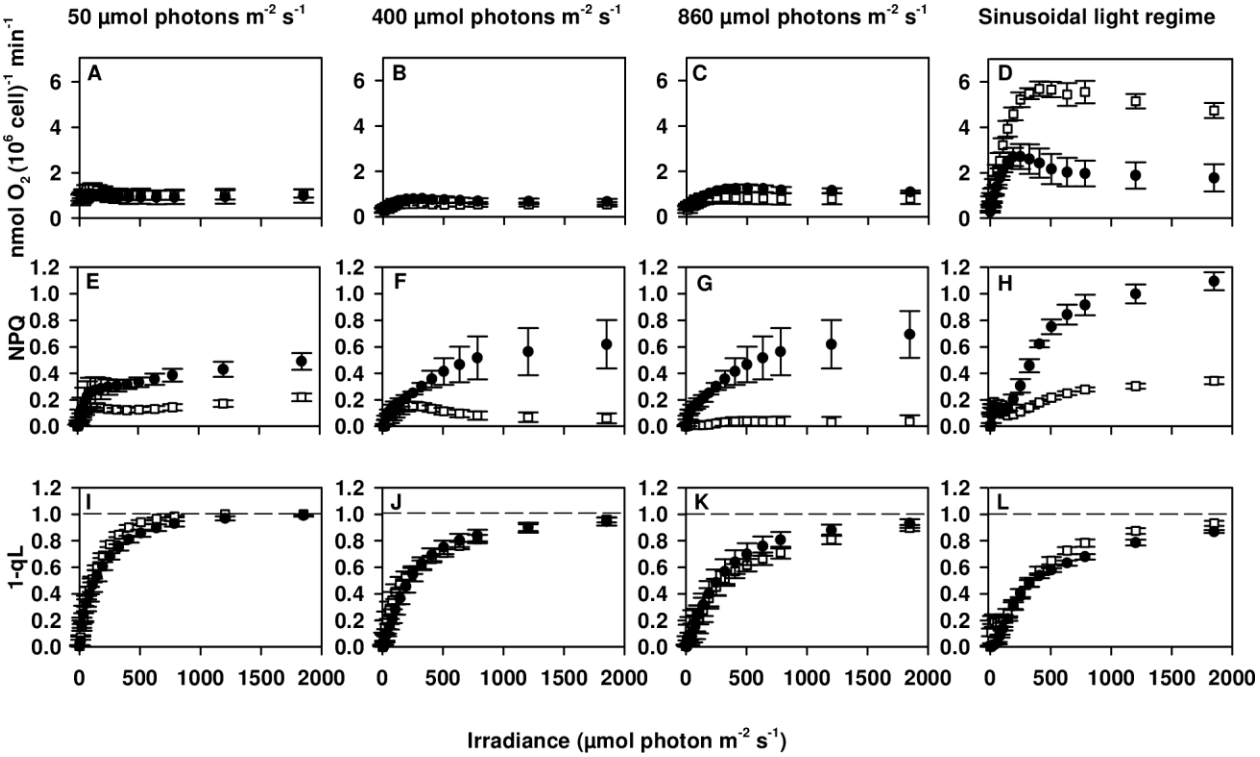


**Figure 2.3. Photosynthesis vs Irradiance (P vs I) curves for wild type and *npq4lhcsr1* acclimated to different light regimes.**

Wild type (black circles) and the *npq4lhcsr1* mutant (white squares) acclimated to either 50, 400, 860 µmol photons $m^{-2}$ $s^{-1}$ or a sinusoidal light regime (data collected 6 hours after dawn) were exposed to consecutive, increasing intensities of red light. Oxygen concentrations and PAM fluorescence were measured simultaneously. Data represent means ± s.d. (n = 3-6).

We characterized the photophysiology of cells grown in sinusoidal light conditions as well. Measurements taken 6 hours into the light period indicated only small reductions in the maximum PSII quantum yield ($F_v/F_m$, Table 2.2) in the mutant compared to the wild type. *npq4lhcsr1* displayed a significant increase in $P_{max}$ and $I_K$ and a decreased α compared to wild

type (Table 2.2). NPQ capacity was reduced in *npq4lhcsr1* compared to wild type and there was no change in the 1-qL parameter between the two strains (Figure 2.3).

Immunoblot based quantification of the PSII subunit D2, the PSI subunit PsaC and the PSII associated light harvesting complex Lhcb2 was also used to assess differences in photosynthetic architecture during growth in sinusoidal light. Relative protein content was normalized to the abundance of the beta subunit of ATP synthase (ATP-B). *npq4lhcsr1* displayed significantly more D2 subunit relative to wild type, suggesting an increase in the overall PSII:PSI ratio (Figure 2.4B). The relative abundance of Lhcb2 did not differ between the mutant and wild type.

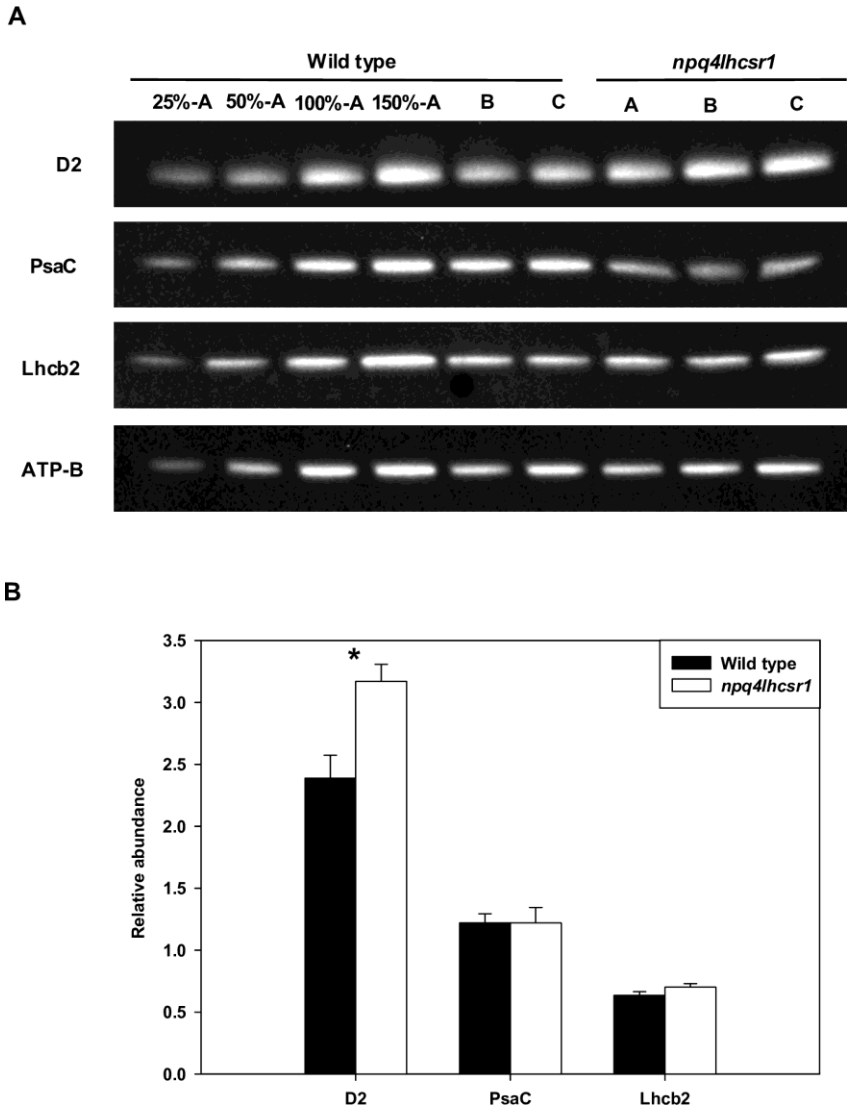


**Figure 2.4 Protein abundance of D2, PsaC and Lhcb2 6 hours after dawn in sinusoidal cultures.**

(A) Immunoblot detection of D2, PsaC, and Lhcb2 for wild type and *npq4lhcsr1*. Lanes were loaded on an equal chlorophyll basis with biological replicates for wild type and *npq4lhcsr1* shown as A, B, and C. (B) Results from comparative densitometry of relative protein abundance normalized to ATP-B content. Data represent means ± s.d. (n = 3). Symbols (*) represent significant differences between mutant and wild type based on an un-paired t-test ($p < 0.05$).

We also observed changes in PSII chlorophyll *a* fluorescence parameter using a FIRe fluorometer in cultures grown in sinusoidal light conditions. These were determined *ex situ* immediately after removal from their light environment. There was a significant reduction in the effective quantum yield of PSII in *npq4lhcsr1* compared to wild type after dawn (Figure 2.5A).

Functional antenna size ($\sigma_{PSII}$, $A^2$ $quantum^{-1}$) changed very little across the light period, with *npq4lhcsr1* having a significantly reduced functional antenna size at the beginning of the light period only (Figure 2.5B). The rate of $Q_B$ re-oxidation were also determined from the kinetics of fluorescence relaxation following a multiple turnover flash (MTF). Wild type and *npq4lhcsr1* cultures showed identical rates of $Q_B$ re-oxidation throughout the day but oxidation times were longer at dawn and dusk than throughout the rest of the illumination period (Figure 2.5C). In contrast with sinusoidal light conditions, cultures grown in 12 hours 2134 µmol photons $m^{-2}$ $s^{-1}$ constant light, 12 hours dark in a ePBR displayed no differences in the effective quantum yield and functional antenna size of PSII, and a significant increase in $Q_B$ re-oxidation 3 hours after dawn (Supplemental figure 2.5).

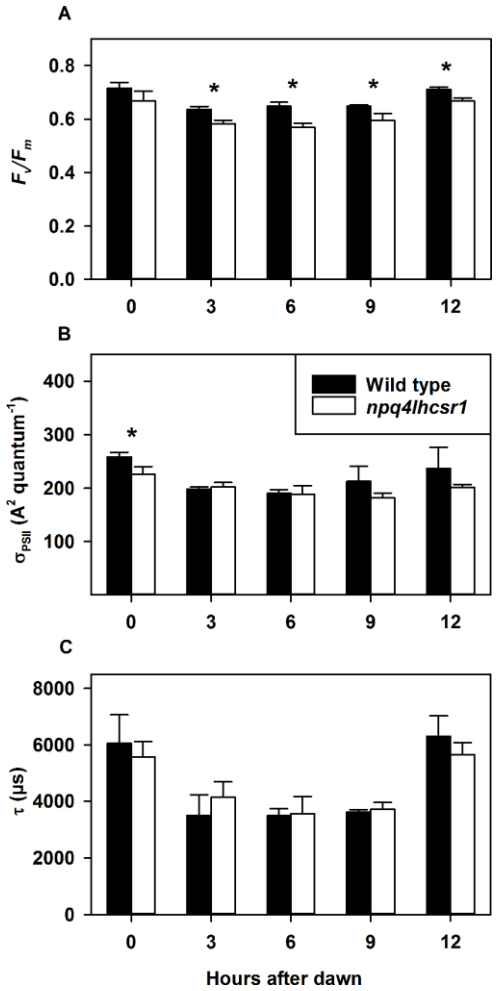


**Figure 2.5 Photophysiology of Photosystem II during growth in a sinusoidal light regime.** (A) Effective quantum yield ($F_v/F_m$). (B) Functional antenna size ($\sigma_{PSII}$, $A^2$ quantum$^{-1}$). (C) $Q_B$ re-oxidation kinetics ($\tau$, μs). Data represents the mean ± SD (n = 3-4). Symbols (*) represent significant differences from wild type within light acclimated states based on an un-paired t-test ($p < 0.05$).

Quantification of lipid peroxidation of wild type and *npq4lhcsr1* under continuous and sinusoidal light regimes

Thiobarbituric reactive substances (TBARS) were used to quantify the extent of lipid peroxidation in cultures acclimated to continuous and sinusoidal light regimes. Lipid peroxidation occurs predominantly through a reaction between $^1O_2$ and membrane lipids and has been used previously as a marker for reactive oxygen species (ROS) mediated stress in *Chlamydomonas* (Baroli *et al.*, 2004). TBARS normalized per cell increased from 50 μmol

photons $m^{-2}$ $s^{-1}$ to the higher light levels, including sinusoidal light (Figure 2.6). *npq4lhcsr1* had significantly higher TBARS than wild type only when grown at 50 µmol photons $m^{-2}$ $s^{-1}$ (Figure 6).

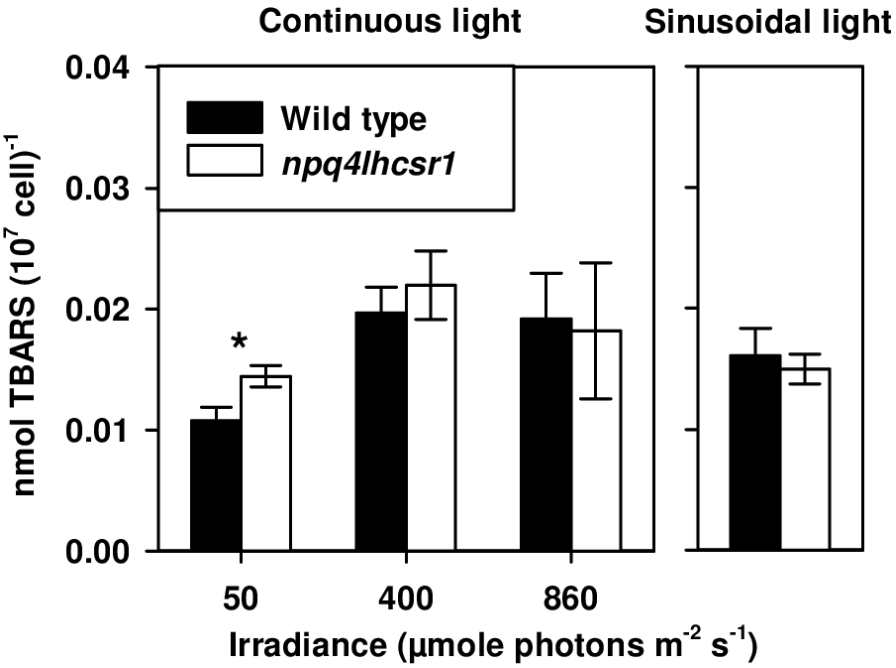


**Figure 2.6 Thiobarbituric acid reactive substance (TBARS) concentrations per $10^7$ cell for wild type and *npq4lhcsr1* acclimated to different light regimes.**
Data represents the mean ± SD (n = 3-6). Symbols (*) represent significant differences from wild type within light acclimated states based on an un-paired t-test ($p < 0.05$).

Total organic carbon accumulation of wild type and *npq4lhcsr1* under a sinusoidal light regime

We measured total organic carbon (TOC) content and cell size during the light period to determine if the loss of qE impacted carbon accumulation. Wild type cultures had 8.6 ± 0.6 pg TOC $cell^{-1}$ and an average cell volume of 118 ± 16 $\mu m^3$ at dawn and ended the light period at 25.5 ± 2.8 pg TOC $cell^{-1}$ and an average cell volume of 438 ± 45 $\mu m^3$ (Figure 2.7A-B). *npq4lhcsr1* cultures had significantly more TOC (12.8 ± 2.5 pg TOC $cell^{-1}$) and a similar cell volume to wild type cultures (149 ± 37$\mu m^3$) at dawn but ended the light period at approximately the same pg TOC $cell^{-1}$ (26.1 ± 5.9 pg TOC $cell^{-1}$) and cell volume (420 ± 87

μm$^3$) as wild type (Figure 2.7A-B). However, there was no statistical difference in total carbon accumulated over the course of the day between the two strains (16.8 ± 2.3, and 13.3 ± 4.6 pg TOC cell$^{-1}$, for wild type and *npqlhcsr1*, respectively; $p > 0.05$).

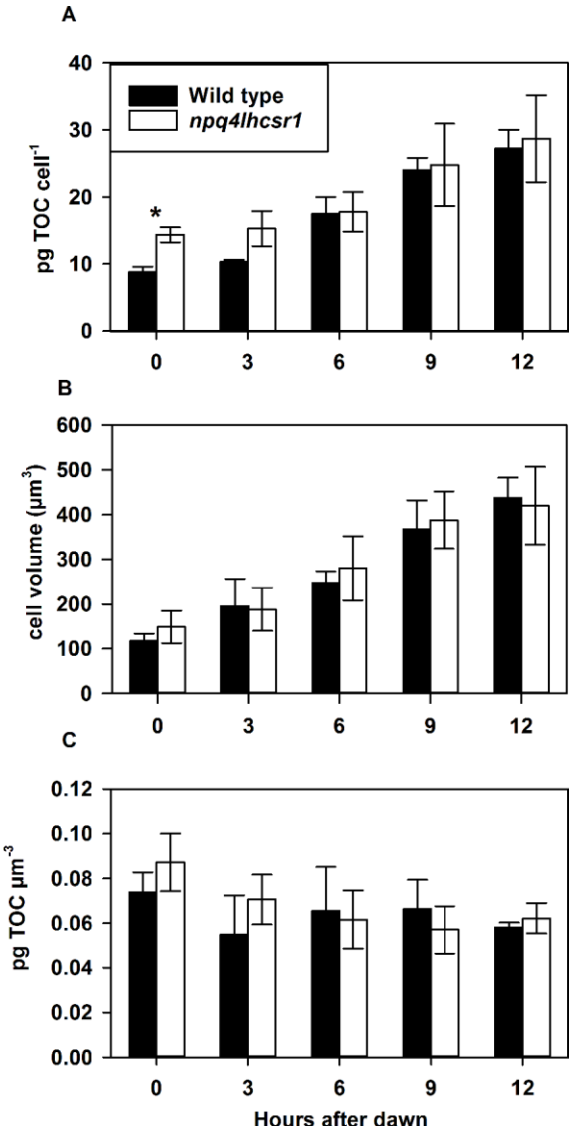


**Figure 2.7 Total organic carbon (TOC) accumulation across a 12 hour sinusoidal light regime.**

(A) shows pg TOC cell$^{-1}$, (B) shows Cell volume (μm$^3$) of cells measured and (C) shows pg TOC normalized to cell volume. Data represents the mean ± SD (n = 5). Symbols (*) represent significant differences between wild type and *npq4lhcsr1* for each time point based on an un-paired t-test ($p < 0.05$).

Patterns of cell division

We did not observe any significant cell divisions for either strain during the light period in our sinusoidal cultures (Supplemental figure 2.2). We assayed the number of cell fission events during three consecutive nights in wild type and *npq4lhcsr1* and observed that wild type underwent a greater number of multiple fission events per cell than *npq4lhcsr1* (Figure 2.8). This indicates that the reduced growth phenotype observed is due to a reduction in division number per cell at night.

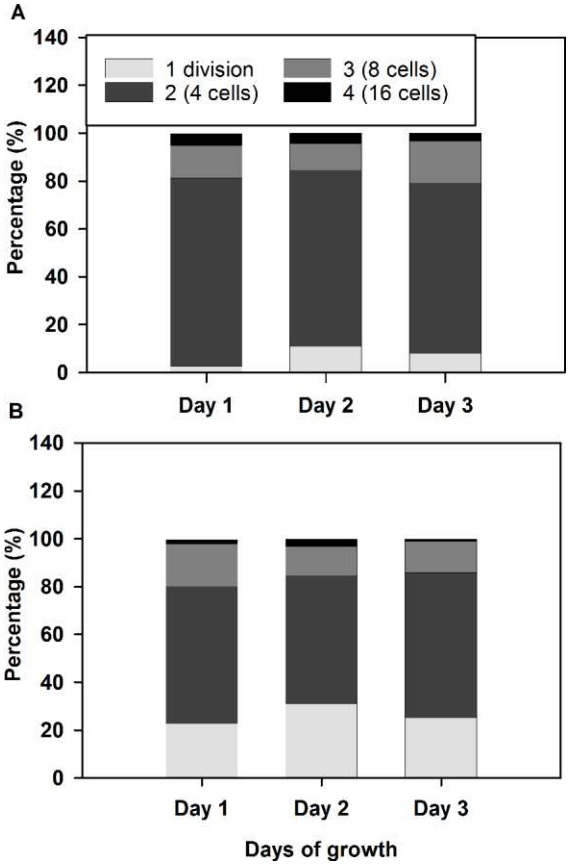


**Figure 2.8. Distribution of cell divisions per progenitor cell during growth in sinusoidal light conditions.**

Cell division number was quantified for 3 consecutive days in single replicate wild type (A) and *npq4lhcr1* (B) cultures. Wild type cells averaged 2.2 divisions per night and *npq4lhcsr1* averaged 1.9 divisions per night across the three nights measured.

**Discussion**

LHCSR is required for qE in green algae, diatoms and presumably all algae with an LHC-based light harvesting antenna (Bailleul *et al.*, 2010; Niyogi and Truong, 2013; Peers *et al.*, 2009). Previous work on the qE deficient mutant, *npq4*, showed that absence of LHCSR3 leads to a 50% reduction in NPQ capacity and this capacity could be recovered by complementation (Peers *et al.*, 2009). This lead to the hypothesis that LHCSR3 and LHCSR1 both could mediate qE in *Chlamydomonas.* Characterization of the *npq4lhcsr1* mutant indicates that complete loss of all of the LHCSR proteins (Figure 2.1A) correlated with a lack of rapidly inducible and reversible NPQ (Figure 2.1B). This indicates that LHCSR3 and LHCSR1 proteins both contribute to qE and this result is corroborated in other recently published studies (Berteotti *et al.*, 2016; Correa-Galvis *et al.*, 2016b; Dinc *et al.*, 2016).

Previous studies in *Chlamydomonas* have dissected the sensitivity of NPQ deficient mutants to light stress (Allorent *et al.*, 2013b; Baroli *et al.*, 2004; Berteotti *et al.*, 2016; Correa-Galvis *et al.*, 2016b; Niyogi *et al.*, 1997b; Peers *et al.*, 2009). Observations of *npq4* have shown that qE is important for maintaining fitness during a single step increase in light intensity (Allorent *et al.*, 2013; Peers *et al.*, 2009). However, *npq4* displayed no significant reduction in exponential growth under continuous irradiances of 325 µmole photons $m^{-2}$ $s^{-1}$ (Peers *et al.*, 2009). We found that an absence of qE was associated with a small, but significant reduction (11 %) in exponential growth rates only when acclimated to a continuous irradiance of 860 µmole photons $m^{-2}$ $s^{-1}$ (Figure 2.2A). Analogous experiments on a qE-deficient, PsbS mutant of *Arabidopsis thaliana, npq4,* observed similarly weak phenotypes under high light acclimated laboratory conditions (Golan *et al.*, 2006). Interestingly, photoprotective pigment mutants of *Chlamydomonas* lacking lutein or zeaxanthin and lutein show reduced growth rates compared to

wild type cells at moderate light intensities of 350 µmole photons $m^{-2}$ $s^{-1}$ (Niyogi *et al.*, 1997b). This may be due to their dual role in directly quenching excitation energy (Bonente *et al.*, 2011) and also their ability to quench $^1O_2$ in the thylakoid membrane and reduce oxidative stress (Triantaphylides and Havaux, 2009).

Photoacclimation to steady-state excess light with and without qE

Our wild type light acclimation phenotype mirrored previous observations in *Chlamydomonas* whereby total chlorophyll content per cell decreases with increasing irradiance and maximal capacity for photosynthesis increases as do growth rates (Tables 2.1 & 2.2) (Bonente *et al.*, 2012; Peers *et al.*, 2009). Previous studies performed at 400 µmol photons $m^{-2}$ $s^{-1}$ constant light revealed a decrease in the PSI:PSII ratio and a change in the ratio of LHCs relative to low light (Bonente *et al.*, 2012). We also acclimated our cultures to continuous light at 860 µmol photons $m^{-2}$ $s^{-1}$, which is more than the two aforementioned studies. In this condition, the chlorophyll *a*:*b* ratio of wild type cells was significantly increased relative to low light acclimated cultures. Chlorophyll *a* is only present in reaction centers and LHC proteins contain both chlorophylls *a* and *b* (Falkowski and Raven, 2013). These results contribute to the suggestion that *Chlamydomonas* acclimates to excess light conditions by reducing the number of LHC proteins associated with each reaction center at very high light intensities. We did not directly investigate changes in protein composition during steady state growth.

The *npq4lhcsr1* produces more singlet oxygen compared to wild type cells, following a shift from 400 to 1600 µmol photons $m^{-2}$ $s^{-1}$ (Berteotti *et al.*, 2016). This increase in reactive oxygen species generation explains the observed decrease in $F_v/F_m$ over several days growth in excess light reported in the same study. We found that $F_v/F_m$ was also lower in *npq4lhcsr1* compared to the wild type in cells grown in 400 and 860 µmol photons $m^{-2}$ $s^{-1}$, suggesting that

even fully acclimated cells experience photodamage due to a lack of qE. Despite this clear inhibition of PSII, we did not observe major changes in the photosynthetic capacity at low light ($\alpha$) and irradiance at photosynthetic saturation ($I_k$), regardless of growth irradiance. We did observe a slight, but statistically significant reduction in $P_{max}$ at 860 µmol photons $m^{-2}$ $s^{-1}$ during short term assays (Figure 2.3 and Table 2.2). Additionally, we found no difference in the ability of cells to maintain open reaction centers during the *ex situ* assay of photosynthetic capability (1-qL, Figure 2.3). The sum of these results suggest that, while a lack of qE certainly affects light harvesting at the level of PSII, there is minimal detriment to the overall process of photosynthesis during growth in constant light.

The rest of our discussion relates to our novel observations of photophysiology in a changing light environment.

Lack of qE results in distinct responses to sinusoidal light

The absence of LHCSR appears to alter the photosynthetic apparatus when cells are grown in a changing, sinusoidal light regime. The following observations were all made 6 hours into the light period, corresponding to the highest light intensity of the day. *npq4lhcsr1* displayed a large increase in $P_{max}$ and $\alpha$ was 71 % relative to wild type when normalized by cell. The mutant appeared to have an increase in the PSII:PSI ratio relative to wild type, as estimated by changes in the relative abundance of the D2 and PsaC proteins, respectively.

Decreases in the chlorophyll *a*:*b* ratio suggested an increase in the relative content of antenna relative to the photosystems if LHCSR was absent. However, this is a bulk measurement that could be associated with either photosystem. We also observed an increase in the relative abundance of D2 in *npq4lhcsr1*. This in conjunction with no differences observed in PSII antenna protein Lhcb2, suggests a decrease in the antenna size of PSII in the mutant. But we note

the Lhcb2 antibody was designed for use in *Arabidopsis* and while it recognizes LHCs in *Chlamydomonas*, it may recognize LHCs other than those associated with PSII. Estimations of the functional antenna size measurements using FIRe fluorescence techniques found no significant difference between wild type and *npq4lhcsr1* at midday (Figure 2.5B). Cumulatively, these observations indicate that absence of LHCSR impacts photoacclimation and likely alters the architecture of the light harvesting apparatus.

Alternate energy dissipation strategies may compensate for the loss of qE in sinusoidal light

If excess light energy is unable to be dissipated as heat when light fluxes increase, then the plastoquinone pool may become more reduced at lower light fluxes in *npq4lhcsr1* compared to the wild type strain. To estimate the redox state of the PQ pool, we looked at the proportion of closed PSII reaction centers during rapid light curves (1-qL; Kramer *et al.*, 2004). We found that *npq4lhcsr1* cells maintained a PQ pool with a redox state comparable to wild type cells during a rapid light curve protocol. This could be due to an increased flux of electrons through alternate electron transport pathways mediated by the plastid terminal oxidase (PTOX; Houille-Vernes *et al.*, 2011), the mitochondrial Alternative Oxidase (AOX; Mathy *et al.*, 2010), or the Mehler reaction (Asada, 1999). These mechanisms are known to be important for reducing the occurrence of oxidative damage during stress.

Alternately, *npq4lhcsr1* may maintain an equivalent PQ redox state to wild type by altering its LHCSR independent NPQ. qT capacity, which can quench excess energy by facilitating LHCII aggregation (Nagy *et al.*, 2014a; Unlu *et al.*, 2014), may be increased in *npq4lhcsr1*, but the lack of NPQ relaxation observed on filtered samples exposed to far red light does not support this hypothesis (Supplemental figure 2.1). qZ or qI may also compensate for loss of qE in *npq4lhcsr1*. qZ takes tens of minutes to relax and occurs through the pH dependent

accumulation of zeaxanthin in the thylakoid membranes antenna (Dall'Osto *et al.*, 2005). qI reflects quenching due to photodamage to the PSII D1 protein and can take greater than 30 minutes for full recovery (Takahashi and Murata, 2005). In our sinusoidal light experiment, we observed minor reductions in $F_v/F_m$ (~0.6 after 6 hours in the light, vs. ~0.7 at dawn), so we cannot rule out that qZ or qI plays a role in quenching excess light energy in the mutant (Figure 2.5A). Neither zeaxanthin accumulation nor D1 damage and repair rates were measured in this study.

Photosynthetic cells can also utilize energy that is in excess of that used for growth by funneling reduced carbon to storage metabolites like starch or triacylglycerol (Juergens *et al.*, 2016; Lucker and Kramer, 2013a). Reducing the capacity to make or utilize these energy storage compounds can result in increased photoinhibition in plants, suggesting a strong interaction between light harvesting and central metabolism (Adams *et al.*, 2013). We observed no change in the accumulation of organic carbon over the course of the day (16.8 ± 2.3, and 13.3 ± 4.6 pg TOC $cell^{-1}$, for wild type and *npqlhcsr1*, respectively; $p > 0.05$). This shows that the relatively high $P_{max}$ observed in the *npq4lhcsr1* mutant in the short term rapid light curve assay does not translate to more biomass. However, we only tested photosynthetic capacity at solar noon, so there may be other changes in photosynthetic efficiency that occur throughout the day that are not captured in our observations. It also suggests that relatively low levels of PSII photoinhibition observed by fluorescence techniques did not impact overall biomass accumulation during the day. This may not be surprising because the Rubisco activity of cells, and not light harvesting capacity, likely sets the maximal rates of carbon fixation during excess light (Vandenhecke *et al.*, 2015).

Potential costs associated with no qE

Based on the reduced $F_v/F_m$ observed in *npq4lhcsr1* relative to wild type, we conclude that damage to PSII reaction centers occurred (Table 2.2, Figure 2.5A). Degradation and re-synthesis of photo damaged D1 protein is an ATP dependent process (Malnoe *et al.*, 2014; Nixon *et al.*, 2010; Raven, 1989, 2011). Energetic costs associated with photoinhibition may be further increased due to the maintenance of a larger pool of amino acids and ribosomes for elongating the D1 polypeptides for insertion to PSII reaction centers (Raven, 2011). To compensate for increased ATP demand associated with photoinhibition, *npq4lhcsr1* mutants may have higher relative rates of cyclic electron transport and mitochondrial respiration (Alric *et al.*, 2010; Lucker and Kramer, 2013; Takahashi *et al.*, 2013). While cyclic electron transport was not measured in this study, dark respiration rates measured 6 hours after dawn were increased in the mutant compared to WT. This suggests that the absence of qE may increase the metabolic burden associated with repair to damaged cellular components.

We investigated if the reduction in the growth rates of *npq4lhscsr1* relative to wild type in sinusoidal conditions was due to changes in cell divisions at night. *Chlamydomonas* cells grown under day:night cycles display synchronous cell division, whereby organic carbon stores and cell size increases during the day (Figure 2.5) (Bisova and Zachleder, 2014; Craigie and Cavaliersmith, 1982; Zones *et al.*, 2015). Cells then divide at night by multiple fission events ($2^n$), where n is the number of cell divisions that occurs in each progenitor cell (Bisova and Zachleder, 2014; Craigie and Cavaliersmith, 1982). We examined wild type and *npq4lhcsr1* cell division number across 3 days by assaying cell division number from an individual mother cell after dark incubation on plates (Umen and Goodenough, 2001). Using this technique, we observed a higher proportion of *npq4lhcsr1* cells undergo single divisions relative to wild type

(Figure 2.8). This observation, coupled with our biomass accumulation results, indicates that the reduced growth rate phenotype observed is not due to a reduced capacity to fix carbon, but instead because of a reduction in cell divisions at night. This suggests that there is a metabolic penalty associated with an inability to perform qE under sinusoidal light conditions. Our measurements of respiration at noon suggest that there is a higher metabolic rate per cell in the mutant compared to the wild type (Table 2.2), but this increase in respiration was not consistently observed at night (Supplemental figure 2.3). More energy could be required to repair macromolecules damaged by oxidative stress, but our measurements of TBARS suggest that there is no increase in peroxidated macromolecules at noon (Figure 2.6). However, this measurement of steady state damage products does not take into account active repair processes or the production of additional defenses against oxidative stress such as antioxidant enzymes and small molecules (Apel and Hirt, 2004). Maintaining these enzymes, antioxidants and the affiliated machinery to produce them (as discussed above for D1 replacement) may also reduce the amount of carbon and energy available for cell divisions at night.

In summary, the results from our sinusoidal light experiments show that a lack of qE capacity in *Chlamydomonas* leads to a reduction in daily growth rates, but this is not due to a decrease in carbon accumulation during the day. However, there is some metabolic penalty associated with no qE which leads to reduced cell division rates at night. The *Arabidopsis thaliana* qE-less *npq4* mutant grown in the field had a lower seed production compared to wild type, but similar vegetative biomass production. These results highlight the importance for assaying the physiology of photosynthetic mutants in more realistic environments to determine the true impact of a given process on growth and survival.

Engineering NPQ to increase photosynthetic productivites in mass culture

Algae growing in dense culture experience rapid changes in the light environment that are superimposed on the daily sinusoidal light cycle (Peers, 2014). The amount of time spent in the dark or sub-saturating light levels relative to the amount of time spent in excess light influences the photoacclimation process and NPQ induction. Improving photosynthetic efficiency in response to their growth conditions has been a major goal of algal bioengineering (Murchie and Niyogi, 2011; Perrine *et al.*, 2012). *Chlamydomonas* cells spending more time in the dark show signs of low light photoacclimation and accumulate less LHCSR3 relative to those grown in scenarios with longer periods of excess light or in constant light (Yarnold *et al.*, 2016). Cells acclimated to high density and fluctuating light conditions also exhibited lower biomass productivities, which was presumed to be due to the increase in energy required to repair photodamage (Yarnold *et al.*, 2016). These results suggested that high light photo-acclimation responses such as the induction of qE capacity are required to maintain high productivities in industrial situations.

However, the down regulation or absence of light energy dissipation pathways in algae and cyanobacteria may result in higher biomass productivities overall. It has been hypothesized that the slow reversal of NPQ during the transition to low light conditions may reduce the conversion efficiency of photons to biomass. So, it may be that reducing NPQ capacity may result in more biomass accumulation (Peers, 2014). Indeed, Peers (2015) found that the deletion of the OCP protein, responsible for NPQ in the phycobillisome of many cyanobacteria, resulted in a 30 % increase of biomass accumulation in dense cultures of *Synechocystis* vs. wild type cells in conditions that mimicked outdoor light environments (Peers, 2015). Furthermore, it appeared that the *npq4* strain of *Chlamydomonas* also accumulated more biomass not only in constant

moderate light (200-800 µmol photons $m^{-2}$ $s^{-1}$) but also in rapidly oscillating light relative to wild type cells (Berteotti *et al.*, 2016). This difference was not observed in the mutant *npq4lhcsr1* strain grown at 200-400 µmol photons $m^{-2}$ $s^{-1}$ constant light (Berteotti *et al.*, 2016). We highlight that these experiments on *Chlamydomonas* were carried out without a night cycle and therefore reduction in growth associated with nighttime divisions would not have been observed.

We observed no significant differences in biomass accumulation during the day between wild type and *npq4lhcsr1* cells in our sinusoidal light conditions (Figure 2.7A), but an overall reduced growth rate across days due to fewer nightly cell divisions (Figure 2.2A and 2.8). We note that our conditions resemble a low biomass photobioreactor as significant amounts of light still penetrated the entire culture (Figure 2B, (Jallet *et al.*, 2016a; Lucker *et al.*, 2014)). The relative productivities could change with increasing cell density, mixing rates or nutrient status, which can affect cell physiology or light distribution. Our observations suggest that manipulating the kinetics or capacity of NPQ may be a promising strategy for improving photosynthetic efficiency in algae and plants (Horton, 2012; Murchie and Niyogi, 2011; Wobbe and Remacle, 2015). But the complex environment associated with production conditions may negate promising predictions based off of experiments done in simple lab environments (Peers, 2014).

# CHAPTER 3: COMPENSATORY MECHANISMS INVOLVED IN *CHLAMYDOMONAS* ACCLIMATION TO SINUSOIDAL LIGHT CONDITIONS IN THE ABSENCE OF LHCSR-DEPENDENT NPQ


## Summary

Photosynthetic organisms in nature experience frequent periods where the light absorbed exceeds the capacity for photosynthetic capture and conversion to stable chemical energy. Under these conditions, where light saturates photosynthesis, excess absorbed energy can drive the production of reaction oxygen species. To avoid death by photooxidative damage, photosynthetic organisms have evolved a suite of photoprotective mechanisms involved in both quenching excess absorbed light and balancing the ratio of ATP and NADPH generated during light dependent reactions with the metabolic needs of the cell. In the green alga *Chlamydomonas reinhardtii,* the stress related light harvesting complex (LHCSR) is responsible for the rapid non-photochemical quenching of light energy in photosynthetic antenna. Two LHCSR proteins, LHCSR3 and LHCSR1, have previously been shown to be required for fitness in *Chlamydomonas* grown in a sinusoidal light regime. Here, we use chlorophyll fluorescence and oxygen exchange measurements using $^{18}O_2$ and a membrane inlet mass spectrometer to characterize possible compensatory mechanism involved in the acclimation of the *Chlamydomonas* LHCSR-less mutant *npq4lhcsr1* to sinusoidal light. Absence of LHCSR dependent quenching in *npq4lhcsr1*was found to have no significant impact on light dependent oxygen consumption in cultures acclimated to 50, 400 µmol photons $m^{-2}$ $s^{-1}$ or under a sinusoidal light regime. The relative contribution of mitochondrial respiration and the plastid terminal oxidase activity were assessed using specific inhibitors. In cells acclimated to continuous illumination by 400 µmol photons $m^{-2}$ $s^{-1}$ and found small reductions in sensitivity in *npq4lhcsr1*

cells to each inhibitor relative to wild type – further supporting the conclusion that *Chlamydomonas* does not compensate for absence of LHCSR dependent NPQ by light dependent oxygen reduction. We then assessed PSI p700 capacity during sequential increasing irradiance and found that under sinusoidal light conditions, *npq4lhcsr1* exhibited less PSI closure due to reduced acceptor side limitation. This, in conjunction with the absence of increased light dependent oxygen consumption suggests that the *npq4lhcsr1* mutant compensates for loss of LHCSR dependent quenching by increasing cyclic electron transport. This is further supported by an increased capacity for state transition under sinusoidal conditions in *npq4lhcsr1* cells relative to wild type. We conclude that the absence of LHCSR dependent NPQ in *Chlamydomonas*, leads to compensation through mechanisms associated with sink capacity downstream of PSI likely mediated by cyclic electron transport and state transitions.

**Introduction**

Oxygenic photosynthesis in nature acts as the main entry point of carbon into earth's ecosystem by converting solar energy into chemical energy. Light energy harvesting during photosynthesis couples the extraction of electrons from water to the reduction of NADPH while generating a proton gradient that drives ATP synthesis. ATP and NADPH are then used to fuel $CO_2$ fixation in the chloroplast, among other metabolic processes. In both terrestrial and aquatic conditions, photosynthetic organisms face environmental variability that effect both the formation rate of ATP and NADPH (illumination and temperature) and demand (availability of nutrients, water and seasonality). This ultimately results in imbalances between the harvesting of light energy and its utilization (Demmig-Adams *et al.*, 2012; Demmig-Adams *et al.*, 2014). Harmful reactive oxygen species (ROS) are produced when the rates of formation of activated intermediates is greater than their utilization. Algae, cyanobacteria and plants have evolved a

suite of photoprotective mechanisms that relieve excitation pressure on the photosystems by non-photochemical quenching (NPQ) of fluorescence at the level of light absorption, cyclic electron transport around PSI and reductant dissipation downstream of light harvesting through light dependent oxygen consumption (Alric and Johnson, 2017; Finazzi and Minagawa, 2014; Magdaong and Blankenship, 2018). Together three mechanisms dynamically manage both light absorption and the ratio of ATP and NADPH generated by photochemistry to optimize chloroplast metabolism in response to environmental conditions.

NPQ is comprised of 4 main components that functionally act together to limit excess generation of ROS during light capture. Each component was originally defined by the time scales of their induction and relaxation (Erickson *et al.*, 2015). The fastest component – energy dependent quenching (qE)– occurs on the time scale of seconds and reflects chlorophyll excited state dissipation facilitated by affecter proteins and pigments (Giovagnetti and Ruban, 2018). NPQ can be induced on the time scale of minutes by either state transitions (qT) or zeaxanthin dependent quenching (qZ). State transitions involve the dissociation of PSII associated antenna followed by either their aggregation into quenching centers or by their migration and association with PSI (Nagy *et al.*, 2014; Unlu *et al.*, 2014). Zeaxanthin dependent quenching (qZ) which in plants involves the accumulation of zeaxanthin and subsequent increase in energy decay (Holzwarth *et al.*, 2009; Nilkens *et al.*, 2010). The last mechanism for NPQ is the unregulated damage of PSII reaction centers, termed photoinhibition (qI) (Nishiyama *et al.*, 2011). This occurs continuously regardless of light intensity and takes 10s of minutes for relaxation by repair mechanisms which replace the preferentially damaged D1 subunit of PSII (Tyystjarvi and Aro, 1996).

Energy dependent quenching (qE) is often considered to be the main sink for excess energy within NPQ based photoprotection and it is regulated by the stress related light harvesting complex (LHCSR) and its homologs in most eukaryotic algae (Bailleul *et al.*, 2010; Peers *et al.*, 2009). In the model green algae *Chlamydomonas reinhardtii* qE depends on the light induced expression of two LHCSR proteins – LHCSR3( encoded by *LHCSR3.1* and *LHCSR3.*2 genes) and LHCSR1 which shares 87% protein sequence identity (Dinc *et al.*, 2016; Peers *et al.*, 2009). Upon luminal acidification both LHCSR3 and LHCSR1 become protonated and undergo a conformational shift to a quenching state – increasing the probability of energy transfer to associated carotenoids (Ballottari *et al.*, 2016; Dinc *et al.*, 2016). *Chlamydomonas reinhartii* also expresses the 4 transmembrane helix protein PsbS transiently under high light, low $CO_2$ availability and UV-B exposure (Allorent *et al.*, 2016; Correa-Galvis *et al.*, 2016; Tibiletti *et al.*, 2016). Unlike plants, PsbS alone is insufficient to induce qE and instead appears to influence NPQ capacity and LHCSR3 accumulation (Correa-Galvis *et al.*, 2016).

Cyclic electron transport around photosystem I (CET) facilitates both the balancing of the ATP/NADPH production ratio in response to sink demand and luminal acidification for NPQ by recycling reductant to generate a proton motive force (*pmf* )(Wang *et al.*, 2015). Mutants and inhibitor studies have revealed the necessity of CET for induction of NPQ (Johnson *et al.*, 2014), low $CO_2$ conditions (Dang *et al.*, 2014; Lucker and Kramer, 2013), during fluctuating light exposure (Jokel *et al.*, 2018), nitrogen starvation (Saroussi *et al.*, 2016) and iron starvation (Petroutsos *et al.*, 2009). CET is proposed to relieve PSI acceptor side limitation – limiting PSI inhibition (Chaux *et al.*, 2015; Jokel *et al.*, 2018). This is achieved by altering the ATP/NADPH ratio to alleviate imbalances in sink consumption (Yamori and Shikanai, 2016) and conditionally acidifying the lumen, which regulates electron transport through the cytochrome $b_6f$ complex

(Finazzi *et al.*, 2016; Tikkanen *et al.*, 2015) and qE induction (Dang *et al.*, 2014; Hertle *et al.*, 2013a; Miyake *et al.*, 2004). The two main pathways for CET around PSI are either NADPH dependent or ferredoxin dependent. During NADPH- dependent CET, NADPH reduces plastoquinone by the non-electrogenic type II NAD(P)H dehydrogenase complex (NDA) in *Chlamydomonas* and other algae (Jans *et al.*, 2008). CET also occurs by a ferredoxin dependent pathway regulated by the PROTON GRADIENT REGULATION 5 (PGR5) and PGR5-LIKE PHOTOSYNTHETIC PHENOTYPE 1 (PGRL1) protein in *Chlamydomonas* and higher plants (Chaux *et al.*, 2017b; DalCorso *et al.*, 2008; Hertle *et al.*, 2013a; Johnson *et al.*, 2014). PGR5 and PGRL1 are proposed to function synergistically in the oxidation of ferredoxin and reduction of quinones. Together CET pathways in parallel with NPQ functionally constrain the rate and products generated during light harvesting to meet sink demand.

Light dependent oxygen consumption downstream of light harvesting provides an additional alternate sink for excess energy and has been proposed to optimize ATP/NADPH ratio during environmental stress. Light dependent oxygen consumption can occur in several cellular locations. Excess reductant generated during light harvesting can be consumed in the chloroplast by the plastid terminal oxidase (PTOX; Houille-Vernes *et al.*, 2011), the Mehler reaction downstream of photosystem I (Roberty *et al.*, 2014) and Flavodiiron proteins (Allahverdiyeva *et al.*, 2013; Chaux *et al.*, 2017a). Two plastid terminal oxidase (PTOX) isoforms (PTOX1 and 2) are located in the thylakoid membranes downstream of PSII and dissipate extra reductant by oxidizing plastoquinone and reducing $O_2$ to $H_2O$ (Houille-Vernes *et al.*, 2011b). The Mehler reaction describes the production of superoxide at the PSI acceptor side. This superoxide is then rapidly converted to $H_2O_2$ by the activity of the superoxide dismutase (SOD) enzyme which is subsequently scavenged by the chloroplast-associated ascorbate peroxidase (APX)(Miyake and

Asada 1992). Flavodiiron proteins have also been shown to dissipate reductant downstream of photosystem I by the paired oxidation of NADPH and reduction of $O_2$ to $H_2O$ (Allahverdiyeva *et al.*, 2013; Chaux *et al.*, 2017). FLV proteins have been shown to be important for energy dissipation downstream of Photosystem I during fluctuating light, during ATP/NADPH imbalance, NPQ induction during initial exposure to light (Chaux *et al.*, 2017; Dang *et al.*, 2014; Ilik *et al.*, 2017).

Mitochondrial cooperation involves the export of reductant from the chloroplast to the mitochondria (Scheibe, 2004). The malate valve is proposed to facilitate this cooperation by NADPH oxidization and the reduction of oxaloacetate to malate (Lemaire *et al.*, 2005). Malate is then exported from the chloroplast to the mitochondria where it is converted back to oxaloacetate – generating NADH for use in ATP synthesis during respiration (Scheibe, 2004). This ATP may than be transferred back to the chloroplast by direct (ATP translocators) or indirect routes (DHAP/3-PGA shuttle; (Hoefnagel *et al.*, 1998). Mitochondrial cooperation is required for ATP/NADPH adjustment in the cyclic electron transport mutants *pgrl1* and *pgr5*. In the absence of cyclic electron transport, light dependent oxygen consumption increases, with much of this consumption inhibited by pre-incubation with mitochondrial inhibitors (Dang *et al.*, 2014a; Johnson *et al.*, 2014; Larosa *et al.*, 2018). Each of these pathways provides a route for excess reductant to be either dissipated or converted to ATP and may act in parallel to adjust the ATP/NADPH ratio to meet chloroplast.

Complete loss of LHCSR based NPQ in the *npq4lhcsr1* mutant has been associated with increased photoinhibition under excess light, and decreased growth in cultures grown under light conditions simulating a natural sinusoidal light regime (Cantrell and Peers, 2017). Despite these impacts, little difference was observed in oxygen evolution during rapid light curves under

continuous light and an increase in oxygen evolution was observed under sinusoidal light conditions on a per cell basis. An absence of significant over reduction of the PQ pool in the study by Cantrell and Peers (2017) suggested that dissipative mechanisms downstream of light harvesting could compensate for the absence of LHCSR dependent NPQ. Work on the *npq4pgrl1* mutant, deficient in NPQ and cyclic electron transport, indicates that cyclic electron transport may facilitate photosynthetic control of PSII in the absence of LHCSR dependent NPQ (Chaux *et al.*, 2017b).

In this paper we focused on testing the hypothesis that compensatory mechanisms in the LHCSR-less mutant *npq4lhcsr1* limit photoinhibition and growth inhibition continuous saturating light and under a more natural sinusoidal light regime. We investigated possible compensation by increasing light dependent oxygen capacity, altering partitioning of light dependent consumption, altered PSI photochemistry and state transition capacity. *npq4lhcsr1* exhibited less PSI closure due to reduced acceptor side limitation. In the absence of increased light dependent oxygen consumption this suggests *npq4lhcsr1* mutant compensates for loss of LHCSR dependent quenching by increasing cyclic electron transport. This is further supported by an increased capacity for state transition under sinusoidal conditions.

**Methods**

Strains and culture conditions

All experiments were performed on axenic, photoautotrophically grown cultures using TP media at 25 °C as described previously in Cantrell *et al.* 2017 (Cantrell and Peers, 2017). The *Chlamydomonas reinhardtii* 4A+ strain (137c genetic background) was used as wild type strain, and the *npq4lhcsr1* mutant was made in the 4A+ genetic background and does not produce any detectable LHCSR protein. Both strains were obtained from Krishna Niyogi, University of

California, Berkeley. Each experiment started with an inoculation of between 10,000 – 100,000 cells $ml^{-1}$ from a stock culture acclimated for at least 10 generations in their respective light environment. Continuous light cultures were grown in 500 ml glass Erlenmeyer flasks containing 200 mL of media and shaken at 150 RPM under 50 or 400 µmol photons $m^{-2}$ $s^{-1}$ of Photosynthetically Active Radiation (PAR, light supplied by cool white fluorescent bulbs (Phillips, F17T8/TL841)). Light fluxes were measured using a 2pi light sensor (LICOR LI-250A). Physiology under a 12:12 light:dark sinusoidal light cycle (Peaking at 2134 µmol photons $m^{-2}$ $s^{-1}$) were characterized in 500 ml ePBR photobioreactors (Phenotmetrics) sparged with air at 1 L $min^{-1}$ as previously described in Cantrell *et al.* 2017.

Membrane inlet mass spectrometry (MIMS) quantification of oxygen production and consumption ex situ

Oxygen production and consumption were measured in parallel with chlorophyll fluoresence using a custom cuvette and cuvette holder which pairs measurement of $^{16}O_2$ and $^{18}O_2$ by MIMS and chlorophyll fluorescence by the Walz Dual PAM. A quad mass spectrometer (Pfieffer PrismaPlus QMS200; PTM28612) fitted with a 1/8 inch diameter steal tubing and swagelock adapter connected to a custom quartz sample cuvette. Cells were removed from their growth flasks and prepared by centrifugation at 1500 x g at 25°C for 5 minutes. Samples were then resuspended in TP + 5 mM sodium bicarbonate to a chlorophyll concentration of 4-8 µg chlorophyll per ml and incubated in the dark for 15 minutes unless otherwise noted. 2 mls of culture were than purged with $N_2$ to approximately 75% atmospheric oxygen and then placed in the cuvette and loosely capped with a custom cuvette stopper milled from a PolyEtherEtherKetone (PEEK) rod (McMaster Cat # 7707T21). Samples were maintained at 25°C by recirculating water through a custom aluminum cuvette holder (Supplementary figure

#1). $^{18}O_2$ (Sigma Aldrich Cat# 490474) was bubbled into the top of the cuvette and allowed to equilibrate for 10 minutes until $^{18}O_2$ replaced purged $^{16}O_2$. Far red light was also applied during this time to oxidize the plastoquinone pool. The residual gas bubble was then removed, and actinic light regimes was then applied as described in the following sections.

After data collection ion current for $^{16}O_2$ and $^{18}O_2$ were normalized to Ar, a biologically inert gas with similar solubility properties as $O_2$, to account for drift associated with abiotic factors associated with variation in atmospheric pressure and gas consumption by the MIMS system (Kana *et al.*, 2002). Ion currents were calibrated to atmospheric oxygen (256 nmol $O_2$/L) using the ion currents for $^{16}O_2$ for air saturated media generated by shaking 10 mls in a 250 ml flask for 5 minutes. Oxygen depleted media (0 nmol $O_2$/L) was generated by addition of sodium dithionite. Rates of $^{16}O_2$ and $^{18}O_2$ consumption ($O_u$) and evolution ($O_p$) were determined as described in Bailleul *et al.* (2017) using the following equations:

**Oxygen consumption**

$$([\Delta^{18}O_2]/\Delta t - k[^{18}O_2]) \times (1 + [^{16}O_2])/ [^{18}O_2])$$

**Oxygen evolution**

$$([\Delta\ ^{16}O_2]/\Delta t - k[^{16}O_2]) - \Delta\ ^{18}O_2([^{16}O_2]/ [^{18}O_2])$$

Where the rates of change, $^{16}O_2$ and $^{18}O_2$, were determined over discrete 2 minute segments unless noted otherwise ($\Delta t$), $k[^{18}O_2]$ and $k[^{16}O_2]$ reflect consumption rates of $^{16}O_2$ and $^{18}O_2$ in a media blank control, and the ratio of $[^{16}O_2]$ to $[^{18}O_2]$ determined at the beginning of each segment. These values are then normalized to the cell concentration in the sample or chlorophyll concentrations.

MIMS Photosynthesis vs irradiance curves.

The impact of increasing irradiance on light dependent oxygen consumption was assessed during photosynthesis vs irradiance curves. Samples were capped and dark respiration rates were recorded for 5 minutes. Then the Dual-PAM far red light (intensity setting 20) was turned on for 5 minutes to induce a state 1 transition (Peers *et al.*, 2009). An initial red saturating pulse (620 nm, 600 ms, 10,000 µmol photons $m^{-2}$ $s^{-1}$) was used to measure maximum PSII quantum efficiency followed by a rapid light curve (RLC) of sequential increasing 3 minute actinic red light steps punctuated by saturating pulses. PSII fluorescence and changes in $^{16}O_2$ and $^{18}O_2$ concentration were assesed during red illumination at 27, 47, 116, 209, 366, 473, 739, 1144, 1754, 2177, and 2712 µmol photons $m^{-2}$ $s^{-1}$ (measured with a 4pi Walz ULM-500 light meter).

Light shift experiment with inhibitor injections

Several different oxidase and mitochondrial inhibitors were used to investigate the roles of different light dependent oxygen consumption pathways during excess light. These experiments were carried out in the apparatus described above. Dark respiration rates were recorded for 5 minutes followed by 5 minutes of far red light (intensity setting 20 on the Dual PAM) to induce a state 1 transition (Peers *et al.*, 2009). Then, 3 µL of 100% ethanol (control), or inhibitor was injected into samples after 4 minutes and during a 10 minute 50 µmol photons $m^{-2}$ $s^{-1}$ treatment to activate photosynthesis. Light intensity was then increased to 2000 µmol photons $m^{-2}$ $s^{-1}$ to quantify the impact of inhibitors under saturating irradiance. Inhibitor treatments included propyll gallate (stock concentration 500 mM in ethanol ; final concentration 1 mM; Sigma Aldrich Cat# P3130), Salicylhdroxamic acid (stock concentration 200 mM in ethanol ; final concentration 0.4 mM; Sigma Aldrich Cat# S607), and Myxothiazol (stock concentration 1 mM in ethanol; final concentration 2 µM; Sigma Aldrich Cat# T5580).

PSI activity

Oxidizable P700 and donor and acceptor side limitation were assessed using the artificial leaf technique and walz Dual-PAM (Qiao *et al.*, 2015). ~ 50 µg of chlorophyll was gently filtered onto a glass fiber filter (MilliporeSigma, AP2001300) and the placed in the Dual-PAM's leaf clip. 5 minutes of FR (Intensity setting 20) was applied to induce a state 1 transition, after which Y(I), Y(NA) and Y(ND) was determined during sequential increasing 3 minute actinic red light steps by the saturating pulse method (Klughammer, 2008). P700 parameters were determined during illumination at 44, 77, 195, 354, 645, 833, 1296, 2005, 2476, 3073, and 3811 µmol photons $m^{-2}$ $s^{-1}$ (measured with a 4pi Walz ULM-500 light meter).

Pigment concentration

1 ml of residual cells were harvested Eppendorf tubes and the cells were centrifuged at 10,000 x g for 10 minutes at 4 °C after the photophysiology measurements described above. The supernatant was removed. Chlorophylls were then extracted for 10 minutes in 80 % buffered acetone with 50 mM HEPES, pH 7.5 and cell debris was removed by centrifugation at 10,000 x g for 5 minutes. Chlorophyll *a* and *b* concentrations were determined by spectrophotometry using a Cary 60 spectrophotometer (Agilent technologies) as previously described (Porra, 2002).

Low temperature (77k) Fluorescence

Low temperature fluorescence was determined using a Horiba Jobin-Yvon Fluorolog-3 spectrofluorometer equipped with a Horiba Liquid nitrogen Dewar Assembly (FL-1013). *In situ* sampling took less than 30 seconds - samples were harvested, immediately transferred into the Horiba dewar flask and frozen in liquid nitrogen. State 1 was induced in samples by aerating 25 ml of sample in a 50 ml flask for 1 hour under far red light illumination (Build my LED; Cat# LUC-025S035DT). State 2 was induced in samples by incubating 5 ml of cells in a 25 ml flask

for 25 minutes with 5 µM FCCP in the dark. Emission spectra were performed by exciting the sample at 435 nm and recording emissions from 650 to 750 nm. The emission spectral resolution was 1 nm with excitation and emission bandwidths of 1 and 5 nm, respectively. 5 spectral measurements were averaged and the processed by subtracting the baseline at 750 nm and normalizing emission values to the PSII peak at 685 nm in each sample (Allorent *et al.*, 2013b).

Statistics

All data presented represent independent experimental replicates and statistical analysis was performed using Sigma Plot (V13, Systat Software Inc.). Two-way repeated measurement analysis of variance (RM-ANOVA), was used to assess statistical differences between genotype for photosynthetic measurements collected for photosynthesis vs irradiance. Samples with a $p<0.5$ were considered statistically significant. Summary tables of statistical analysis are presented in the supplemental section of this chapter.

**Results**

Photosynthesis and light dependent oxygen consumption in wild type and the *npq4lhcsr1* mutant under continuous and sinusoidal light regimes

A custom measurement vessel was constructed for paired membrane inlet mass spectrometry (MIMS) and Dual-PAM fluorometry to investigate dynamics of NPQ and light dependent oxygen consumption (Supplemental Figure 3.1). Light dependent oxygen consumption was discriminated from light dependent oxygen evolution by the addition of [$^{18}$O]-labeled $O_2$. Change in the lighter isotope ($^{16}O_2$) are associated primarily with water oxidation by PSII and oxygen photoreduction of $^{16}O_2$ and $^{18}O_2$ are light dependent oxygen consumption pathways (Beckmann *et al.*, 2009). Initial investigations during a 10 minute exposure to excess light (2000 µmol photon $m^{-2}$ $s^{-1}$) found that light dependent oxygen consumption initially spiked

to 2.5 times the dark respiration rate during the first 2 minutes of light exposure in cultures acclimated to 400 µmol photon $m^{-2}$ $s^{-1}$ continuous light (Figure 3.1A). A consumption/evolution ratio of 1 during this first 2 minutes indicates that this initial spike drove the majority of electrons generated though oxygen evolution by PSII into oxygen consuming pathways over utilization in the Calvin Benson cycle (Figure 3.1B). The consumption/evolution ratio dropped off after the first two minutes leveling off at ~ 0.5 during the last 6 minutes of the 10-minute light treatment (Figure 3.1B). This correlated inversely with a rise in NPQ and net photosynthesis. This suggests that light dependent oxygen consumption is important during the initial activation of photosynthesis and that photochemical quenching and NPQ facilitate maximal net photosynthesis.

To investigate whether light dependent oxygen consumption increases in the absence of LHCSR dependent NPQ – we quantified the rate of light dependent oxygen consumption during sequential 3 minute red actinic light steps. Under continuous light, net photosynthesis increased on per chlorophyll bases with light intensity (Figure 3.2A and 3.2E) – with the highest rates on a per chlorophyll basis observed in sinusoidal light conditions. The greatest rates of light dependent oxygen consumption were observed under sinusoidal light conditions (Figure 3.2J). This light dependent oxygen consumption was completely reduced by inhibition of PSII by DCMU (Supplementary figure 3.2B). The ratio of oxygen consumption to oxygen evolution at 2124 µmol photon $m^{-2}$ $s^{-1}$ was 77 ± 9% in wild type cultures acclimated to continuous illumination at 50 µmol photon $m^{-2}$ $s^{-1}$ and decreased to 60 ± 9% and 61 ± 9% in cultures acclimated to 400 µmol photon $m^{-2}$ $s^{-1}$ and sinusoidal light regimes respectively (Supplemental figure 3.3, all values = mean +/- stdev, n=3). No significant differences in net photosynthetic rate for *npq4lhcsr1* relative to wild type under continuous light conditions but had significantly

reduced net photosynthetic rates under sinusoidal light conditions on a per chlorophyll basis compared to wild type (Figure 3.2A, 3.2E, and 3.2I). Wild type displayed significantly higher light dependent oxygen consumption relative *npq4lhcsr1* under sinusoidal light condition (Figure 3.2J). Differences between wild type and *npq4lhcsr1* under sinusoidal conditions don't reflect increased flux of linear electron transport towards oxygen consumption pathways based on an equivalent consumption to evolution ratio suggesting that reductions in net photosynthesis in *npq4lhcsr1* relative to wild type reflect a decrease in overall electron transport rate (Supplemental Figure 3.3C). NPQ induction was significantly higher in wild type in cultures acclimated to 400 µmol photon $m^{-2}$ $s^{-1}$ and sinusoidal light and no small, but statistically significant differences were observed in PSII closure based on the fluorescence parameter 1-qLbetween wild type and *npq4lhcsr1* cells acclimated to 400 µmol photon $m^{-2}$ $s^{-1}$ and sinusoidal light (Figures 3.2).

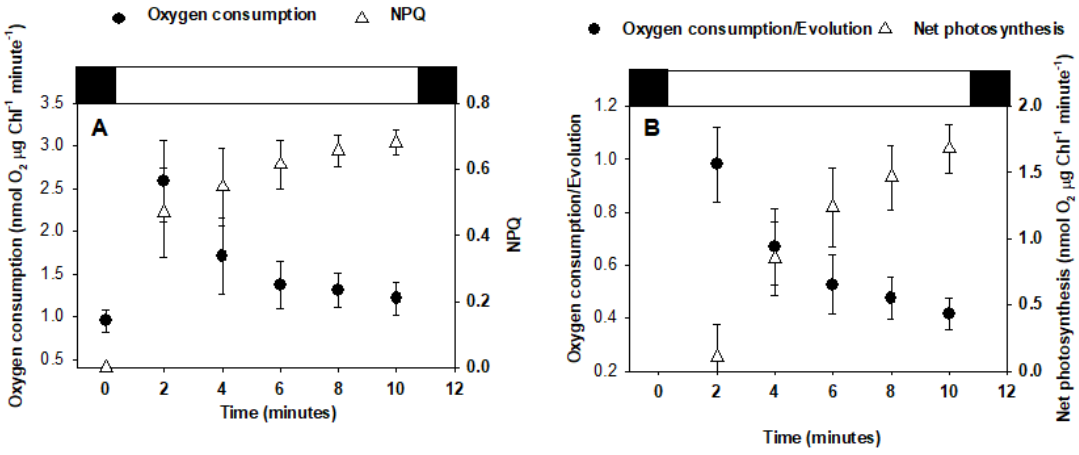


**Figure 3.1 Dynamics of light dependent consumption and NPQ in culture acclimated to 400 µmol photon $m^{-2}$ $s^{-1}$ continuous light.**

Light dependent oxygen consumption and evolution were determined in parallel with NPQ during a 10 minute 2000 µmol photon $m^{-2}$ $s^{-1}$ exposure to red light (white block). Data represents means ± s.d. (n = 3).

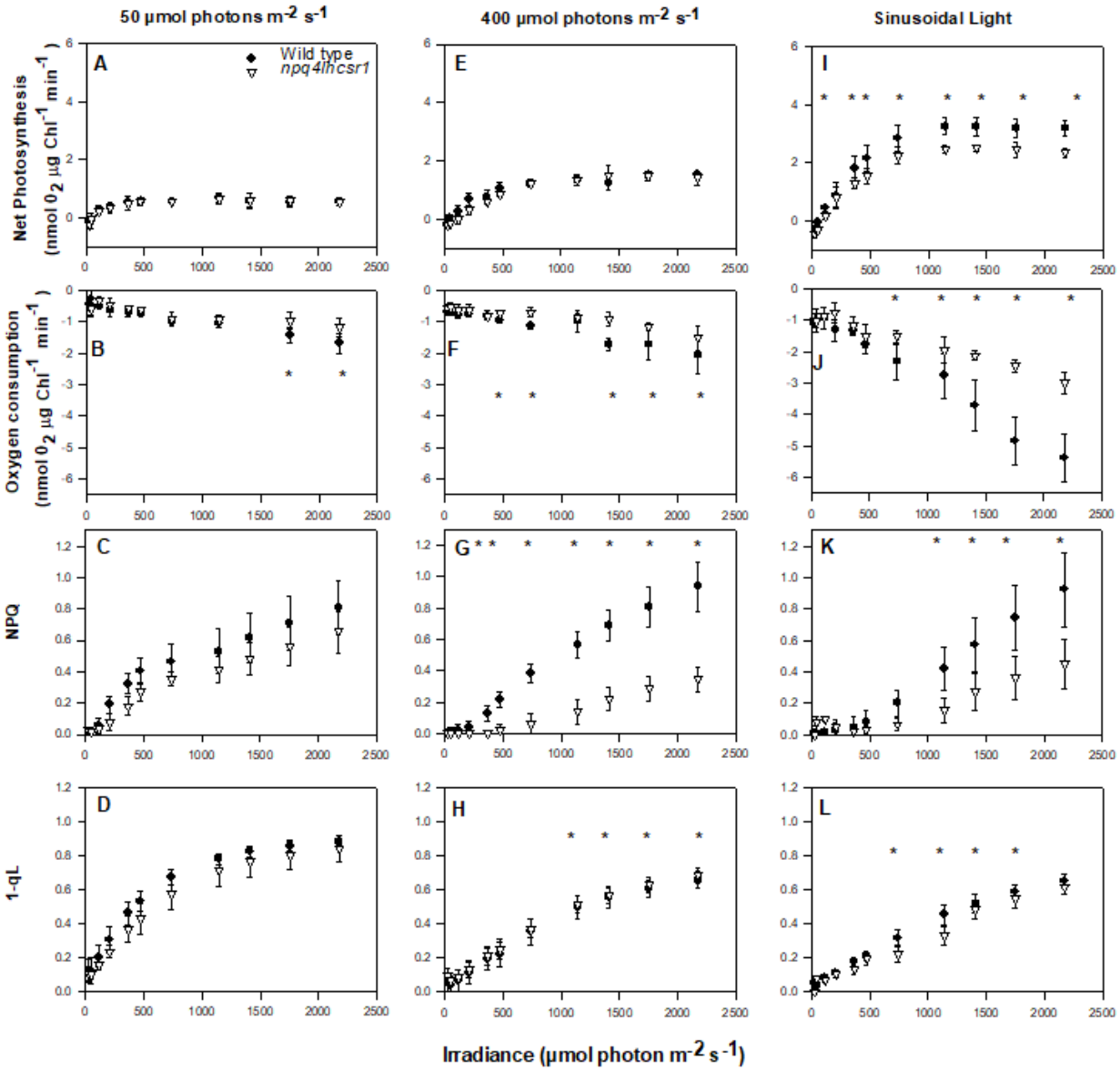


**Figure 3.2 Light dependent oxygen consumption capacity vs Irradiance for wild type and *npq4lhcsr1* acclimated to different light regimes.**

Wild type (black circles) and the *npq4lhcsr1* mutant (White triangles) acclimated to either 50 (a-d), 400 (e-h) µmol photon $m^{-2}$ $s^{-1}$ or a sinusoidal light regime (I-L, data collected 6 hours after dawn) were exposed to consecutive, increasing intensities of red light for a 3-minute duration. Net photosynthesis, oxygen consumption, NPQ and 1-qL were measured simultaneously. Symbols (*) represent significant differences between wild type and *npq4lhcsr1* within light measurement based on a two-way repeated measures ANOVA ($p < 0.05$). Data represents means ± s.d. (n = 3).

Light dependent oxygen consumption did not increase in *npq4lhcsr1* during our P vs I curves suggesting that *Chlamydomonas* does not compensate for the absence of LHCSR dependent NPQ by increasing light dependent oxygen consumption. To test the hypothesis that *npq4lhcsr1* has altered partitioning of excess reductant among the possible oxygen consumption pathways, we characterized light dependent oxygen consumption under our continuous 400 µmol photon $m^{-2}$ $s^{-1}$ using inhibitors of mitochondrial and the plastid terminal oxidase. Previous work characterizing photosynthesis by MIMS during mitochondrial inhibition used dark incubation with myxothiazol, an inhibitor of the cytochrome $bc_1$ complex, and salicylhydromoxamic acid (SHAM), an inhibitor of the mitochondrial Alternative Oxidase (AOX; Dang *et al.*, 2014; Johnson *et al.*, 2014). These studies found dark incubation with mitochondrial inhibitors leads to a 40-50% reduction in net photosynthesis during excess light exposure (Dang *et al.*, 2014b; Johnson *et al.*, 2014). We observed similar reductions during a 2000 µmol photon $m^{-2}$ $s^{-1}$ in wild type after 8 minutes of dark incubation with each inhibitor (Supplemental figure 3.6). This inhibition of net photosynthesis was not observed where inhibitors when inhibitors were injected during a 10 minute 50 µmol photon $m^{-2}$ $s^{-1}$ pre-treatment (Supplemental figure 3.3C). This suggested that the large reductions observed from dark inhibitor treatment reflect a consequence of the pre-treatment and not its direct effect on photosynthesis. The following paragraphs focus on the impact of inhibitors when injected during a 10-minute low light pre-treatment prior to a 10 minute exposure to 2000 µmol photon $m^{-2}$ $s^{-1}$. First, we discuss the results for wild type cells and follow this with contrasting observations for *npq4lhcsr1* versus wild type.

Wild type cells treated with myxothiazol/SHAM had higher NPQ and a slower activation of photosynthesis relative to the ethanol treated control (Figure 3.3). Immediately after injection, wild type and the *npq4lhcsr1* mutant experienced a significant increase in 1-qL and NPQ –

indicating that mitochondrial inhibition leads to a reduction of the plastoquinone pool within minutes in low light ($p$ <0.004; Figure 3.3B and 3.3F). NPQ after transition to 2000 µmol photon $m^{-2}$ $s^{-1}$ was significantly higher in mitochondrial inhibited wild type cells compared to the ethanol control ($p$<0.004; Figure 3.3A). Absence of any increase in NPQ in *npq4lhcsr1* after inhibitor treatment (Figure 3.3E) suggests increased NPQ in wild type is due to LHCSR dependent quenching. The increased NPQ observed in wild type was not correlated with increased PSII closure, inferred from a higher 1-qL, during saturating light illumination (Figure 3.3B). Myxothiazol/SHAM treated wild type cells required 6 minutes to reach equivalent rates of net photosynthesis, relative to the ethanol control which reached its maximum net photosynthetic rate within one minute (Figure 3.3C). Interestingly, the initial spike in oxygen consumption lasted for 1 minute longer in myxothiazol/SHAM treated wild type relative to the ethanol control. Also, the later rise in oxygen consumption observed in the ethanol control was significantly reduced relative to myxothiazol/SHAM treated cells (Figure 3.3D). Mitochondrial inhibition also appears to lead to significant LHCSR dependent NPQ induction during post FR treatment ($p$ <0.001; Figure 3.3A and 3.3E).

Plastid terminal oxidase by propyl gallate (PG) inhibition in wild type increased NPQ and reduced the maximum net photosynthetic rate obtained relative to the ethanol control during exposure to 2000 µmol photon $m^{-2}$ $s^{-1}$. In contrast to mitochondrial inhibition, PG does not induce significant NPQ during the initial 10 minute 50 µmol photon $m^{-2}$ $s^{-1}$ treatment but does lead to significant PSII closure based on an increased 1-qL after injection ($p$<0.002; Figure 3.3A and 3.3B). PG treated samples exhibited similar levels of LHCSR dependent NPQ as Myxothiazol/SHAM treated samples after transition to 2000 µmol photon $m^{-2}$ $s^{-1}$ (Figure 3.3D). PG treated wild type cells reached a maximum net photosynthetic rate of 0.72 ± 0.25 nmol $O_2$ µg

$Chl^{-1}$ $minute^{-1}$ after one-minute relative to our 1.54 ± 0.12 nmol $O_2$ µg $Chl^{-1}$ $minute^{-1}$ in our ethanol control – a 53% reduction ($p<0.043$; Figure 3.3C). Oxygen consumption in PG treated wild type samples displayed equivalent levels to the ethanol control during the first 6 minutes of saturating illumination but was significantly reduced during the last 4 minutes when oxygen consumption rises in ethanol treated samples ($p<0.014$; Figure 3.3D). Unlike myxothiazol/SHAM treatment though, post FR light treatment did not induce NPQ in wild type treated with PG (Figure 3A).

We observed numerous differences in the photosynthetic behavior of the *npq4lhcsr1* compared to the wild type post inhibitor injection. Like wild type, myxothiazol/SHAM treatment induced NPQ immediately after addition in the *npq4lhcsr1* mutant during the 50 µmol photon $m^{-2}$ $s^{-1}$ pretreatment ($p<0.02$; Figure3.3E). This was correlated with significantly increased PSII closure based on 1-qL ($p<0.001$; Figure3.3F). Upon transition to saturating light neither myxothiazol/SHAM nor PG treatment lead to more NPQ in the *npq4lhcsr1* mutant relative to wild type and little difference was observed in the pattern of PSII closure based on 1-qL (Figure 3.3E and 3.3F). The lag observed in the rise of net photosynthesis in myxothiazol/SHAM treated wild type samples was absent after the 1st minute ($p<0.001$) in the *npq4lhcr1* mutant (Figure 3G). This appears to be reflected by a more dramatic increase in oxygen consumption during the first 2 minutes of light exposure in wild type treated with myxothiazol/SHAM relative to *npq4lhcsr1* (Figure 3.3H). After the first 2 minutes, oxygen consumption in *npq4lhcsr1* follows the same pattern observed in wild type treated with myxothiazol/SHAM (Figure 3.3H). PG treatment lead to a significant reduction in net photosynthesis after 4 minutes and was less severe in *npq4lhcsr1* cells compared to wild type. Maximum net photosynthesis in *npq4lhcsr1* was reduced significantly by 31% from 1.71 ± 0.17 nmol $O_2$ µg $Chl^{-1}$ $minute^{-1}$ in ethanol treated

samples to 1.17 ± 0.14 nmol $O_2$ µg $Chl^{-1}$ $minute^{-1}$ in those treated with PG relative to the 53% reduction observed in wild type (*p=0.02;* Figure 3.3G). Oxygen consumption after PG treatment was significantly reduced relative to the ethanol control during the first 2 minutes and last 4 minutes (*p*=0.01; Figure 3.3H). Together these observations suggest that *npq4lhcsr1* acclimated to continuous 400 µmol photon $m^{-2}$ $s^{-1}$ does not does not compensate for absence of LHCSR dependent NPQ by up-regulating mitochondrial cooperation or plastid terminal oxidase capacity.

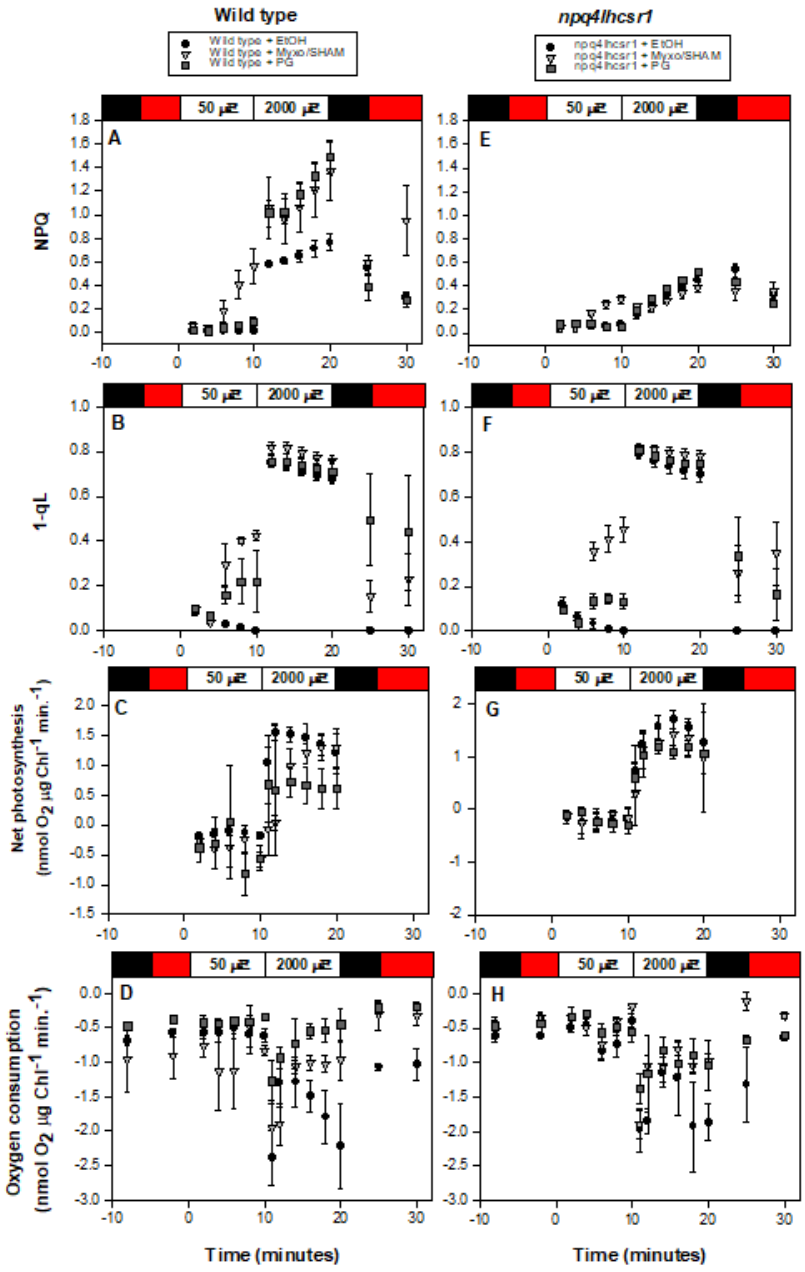


**Figure 3.3 Impact of the mitochondrial inhibitors (Myxothiazol and SHAM) and PTOX inhibitors (Propyll gallate) on light dependent oxygen consumption in wild type and *npq4lhcsr1* acclimated to 400 µmol photon $m^{-2}$ $s^{-1}$ continuous light.**

Wild type (black symbols) and *npq4lhcsr1* (white symbols) samples were dark incubated for 30 minutes prior to 5 minutes of FR light to induce a state I transition. Time 0 reflects when the actinic light is turned on. 3 µl 100% ethanol (circles), 2 µM myxothiazol and 0.4 mM SHAM (upside down triangles), or 1 mM propyll gallate (squares) were injected into the sample cuvette 4 minutes into a 10 minute 50 µmol photon $m^{-2}$ $s^{-1}$ (µE) light treatment. After 10 minutes the light was shifted for 10 minutes to 2000 µmol photon $m^{-2}$ $s^{-1}$. Net photosynthesis, oxygen consumption, NPQ and 1-qL were collected simultaneously. Significant difference based on a two-way repeated measures ANOVA are reported in supplementary information. Data represents means ± s.d. (n = 3-4).

PSI quantum yields of wild type and the *npq4lhcsr1* mutant under continuous and sinusoidal light regimes

An artificial leaf technique was used to assess PSI photochemistry during increasing light intensities for wild type and *npq4lhcsr1* cultures under each acclimated condition (Qiao *et al.*, 2015). The saturating pulse method was used to determine the proportion of PSI reaction centers that were open to photochemistry (Y(I)) and the proportion closed due to either donor side limitation (Y(ND)) or acceptor side limitation (Y(NA); Klughammer, 2008).

Wild type PSI photochemistry varied across light acclimated conditions (Figure 3.4). The highest proportion of open PSI reaction centers (Y(I)) after dark recovery were observed in cultures acclimated to 400 µmol photon $m^{-2}$ $s^{-1}$ (Figure 3.4D). Cells acclimated to each light condition showed a decrease in the proportion of open reaction centers with increasing light intensity. The minimal values for Y(I) were approximately 0.4 in excess light, regardless of acclimation state (Figure 3.4A, 3.4D and 3.4G). PSI closure at light intensities above 1000 µmol photon $m^{-2}$ $s^{-}$ in sinusoidal conditions reflect closure primarily to acceptor side limitation (Figure 3.4H) while under continuous light acclimated conditions PSI closure is primarily due to increases in the proportion of PSI with donor side limitation (Figure 3.4C and 3.4F).

The *npq4lhcsr1* strain differed from the wild type in its PSI photochemistry under light limiting conditions (continuous 50 µmol photon $m^{-2}$ $s^{-1}$) and the sinusoidal light regime used. Under LL acclimated conditions *npq4lhcsr1* has a significant reduction in the proportion of PSI reactions in an open state at intensities under 1405 µmol photon $m^{-2}$ $s^{-1}$ relative to wild type (Y(I); Figure 3.4A). This is significantly greater proportion of closed reaction centers undergoing acceptor side limitation in wild type relative to the *npq4lhcsr1* mutant (Figure 3.4B). *npq4lhcsr1* grown in sinusoidal light displays a greater number of PSI reaction centers open to

photochemistry between light intensities of 350 – 2000 µmol photon $m^{-2}$ $s^{-1}$ compared to Wild type (Figure 3.2G). This is primarily due to a significant reduction in the fraction of PSI reaction centers experiencing acceptor side limitation (Figure 3.2H) in combination with small, but significant increase in the proportion of PSI reaction centers experiencing donor side limitation (Figure 3.2I).

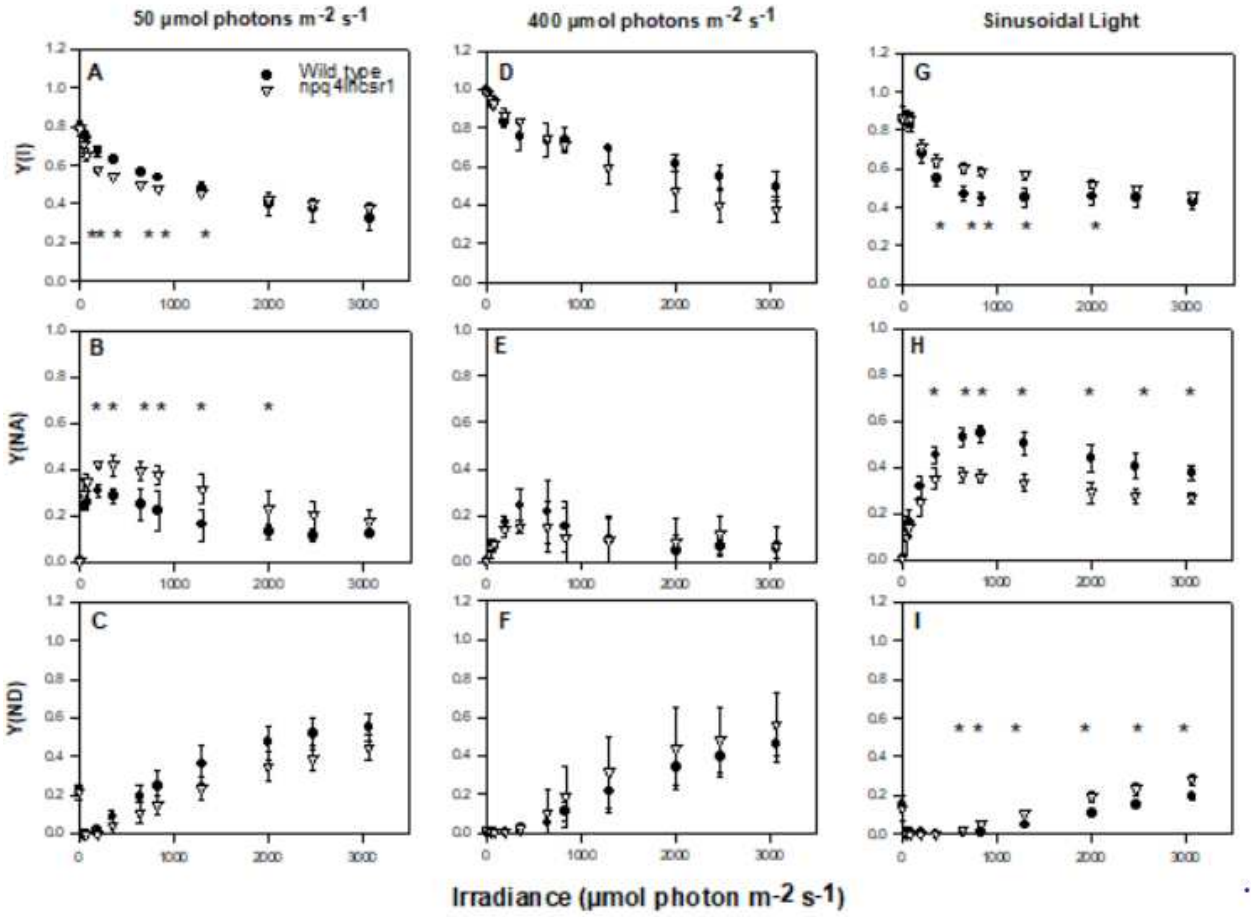


**Figure 3.4 Light irradiances impact on PSI quantum yields using an artificial leaf.** Wild type (black circles) and the *npq4lhcsr1* mutant (White triangles) acclimated to either 50 (A-C), 400 (D-F) µmol photon $m^{-2}$ $s^{-1}$ or a sinusoidal light regime (G-I, data collected 6 hours after dawn) were exposed to consecutive, increasing intensities of red light for a 3-minute duration. Symbols (*) represent significant differences between wild type and *npq4lhcsr1* within light measurement based on a two-way repeated measures ANOVA ($p < 0.05$). Data represents means ± s.d. (n = 3-4).

State transition phenotype of wild type and the *npq4lhcsr1* mutants under continuous and sinusoidal light regimes

The relative state transition capacity under each light acclimated condition and the *in situ* state transition phenotype was assessed by low temperature (77k) fluorescence (Figure 3.5). At low temperatures *Chlamydomonas* exhibits fluorescence emission bands at 715 nm, reflecting PSI associated fluorescence, and at 685 nm, reflecting PSII associated fluorescence. A high ratio of PSI emission (715 nm) to PSII emission (685 nm) is indicative of state 2 transition where PSI has enhanced energy collection due to the migration of LHCII from PSII reaction centers while a low ratio of PSI emission to PSII emission is indicative of a state 1 transition (Allorent *et al.*, 2013b).

Under excess light conditions, the ratio of PSI and PSII emissions increase during state II transitions (Figure 3.5). In wild type the ratio of PSI:PSII emissions during a state 2 transition is 0.83 in cultures acclimated to 50 µmol photon $m^{-2}$ $s^{-1}$ (Figure 3.5A), 1.06 under 400 µmol photon $m^{-2}$ $s^{-1}$ (Figure 3.4B) and 1.00 under sinusoidal light regimes (Figure 3.5C). In contrast, *npq4lhcsr1* displays a greater state 2 transition under light limited and sinusoidal light conditions with a PSI: PSII emission of 0.99 in cultures acclimated to 50 µmol photon $m^{-2}$ $s^{-1}$ (Figure 3.5D), 0.96 under 400 µmol photon $m^{-2}$ $s^{-1}$ (Figure 3.5E) and 1.12 under sinusoidal light regimes (Figure 3.5F). *In situ* measurements suggest that cultures in continuous light maintain state 2 while under sinusoidal conditions both WT and *npq4lhcsr1* display an intermediate phenotype.

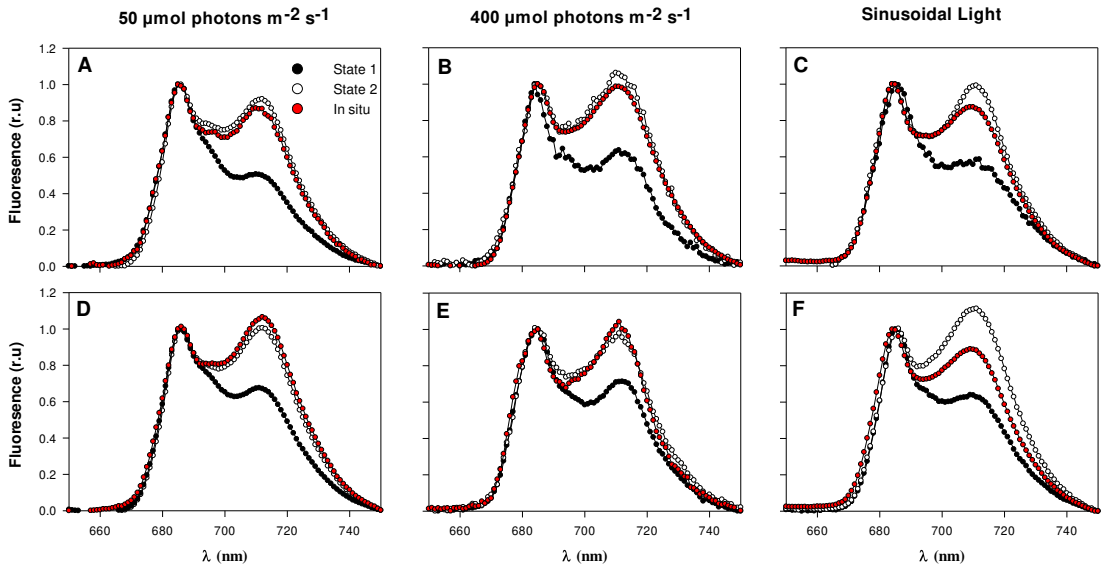


**Figure 3.5. State transition phenotype under different light acclimated conditions.** Low-temperature (77 K) fluorescence emission spectra of cells under state 1 (closed circles), state 2 (open circles) or in situ (red circles) for wild type (A-C) or *npq4lhcsr1* (D-F) for each culture condition. State 1 (closed squares) and State 2 (open circles) were induced by placing samples in darkness under strong aeration with far red light illumination for an hour (for state 1) or by incubating them with 5 µM FCCP in the dark for 25 minutes (for state 2). In situ measurements were quenched in liquid nitrogen within 30 seconds are harvesting samples from culture conditions.

## Discussion

Excitation dependent quenching is proposed to be the dominant photoprotective component in plants and some algae (Ruban, 2017). In this study we sought to evaluate mechanisms that may compensate for the loss of LHCSR dependent NPQ in the *npq4lhcsr1* mutant in the model green algae *Chlamydomonas reinhardtii.* Previously, we observed increased photoinhibition in *npq4lhcsr1* under continuous 400 µmol photon $m^{-2}$ $s^{-1}$and sinusoidal light conditions, but little to no increase in PSII closure based on 1-qL during photosynthesis irradiance curves (Cantrell and Peers, 2017). We interpreted this as an indication that *Chlamydomonas* in the absence of LHCSR dependent NPQ acclimates to saturating light intensity by increasing sinks downstream of light harvesting. In this paper we tested the

hypothesis that this was due to increased light dependent oxygen consumption and characterized its role in acclimation to saturating light.

Compensation by light dependent oxygen consumption

In this study we characterized light dependent oxygen consumption and NPQ in parallel using a custom cuvette system for paired membrane inlet mass spectrometry (MIMS) and Dual-PAM fluorometery. To our knowledge this is the first of its kind (Supplementary figure 3.1). The spike in light dependent $O_2$ consumption observed during a dark to light transition in *Chlamydomonas* was first observed 40+ years by Radmer and Kok (1967) using MIMS. They observed ratio of oxygen consumption to evolution of 1 and interpreted this and as suggesting that light dependent oxygen consumption could effectively compete for reductant consumption by $CO_2$ fixation during the first minute of photosynthetic induction (Radmer and Kok, 1976). Chaux *et al.* 2017 later showed that this spike reflected the action of photoreduction by chloroplast localized FLV proteins. This spike in oxygen consumption facilitated the generation of the *pmf* needed for ATP synthesis and rapid NPQ establishment during the minutes just after a dark to light transition (Chaux *et al.*, 2017a). Our initial investigation, like Chaux *et al.* 2017, observed a similar spike in oxygen consumption during a 10-minute exposure to excess light (2000 µmol photon $m^{-2}$ $s^{-1}$). We found that light dependent oxygen consumption is highest during the time frame involved in induction of LHCSR-dependent NPQ during the first minutes of light exposure (Figure 3.1A, 3.3A, 3.3D, and supplemental figures 3.7C and 3.7F).

We demonstrate that steady state oxygen evolution takes multiple minutes to reach a maximum after dark incubation as previously observed in other algae and plants (Figure 3.1B). Upon initial light to dark transition the majority of reductant generated by photosynthesis is directed towards oxygen consumption pathways which is followed by a slow rise in net

photosynthetic rates and NPQ as flux towards consumption pathways decrease (Figure 3.1). This slow rise in net photosynthesis is proposed to reflect the time required to build up the necessary concentration of ATP needed to match its consumption in $CO_2$ fixation (Forti, 2008). Furthermore, Forti *et al.* (2008) observed that it can take between 6 to 10 minutes for low light acclimated, mixotrophically grown *Chlamydomonas* cells to reach a maximum rate of photosynthesis during sub-saturating light illumination. We observed a similar lag in the activation of photosynthesis, in our saturating light conditions shown in Figure 3.1, with wild type cells taking 10 minutes to reach equivalent rates of photosynthesis observed during our photosynthesis vs irradiance curves. In contrast, a maximum photosynthetic rate is observed within 1 minute of our saturating light treatment when primed with 10 minutes of sub-saturating illumination. This indicates that priming with sub-saturating light can effectively activate photosynthesis for maximum photosynthetic rates under saturating light. Interestingly, we observed that cells primed with sub-saturating light display an increase in light dependent oxygen consumption in both wild type and *npq4lhcsr1* during the last 4 minutes of illumination. This to our knowledge is this first time this observation been made and it is discussed below.

Previous work investigating the dependence of photosynthesis on the mitochondria using MIMS have used dark addition of inhibitors to characterize its impact on photosynthesis, which we propose slows the activation of photosynthesis upon illumination (Dang *et al.*, 2014; Johnson *et al.*, 2014). These previous studies found dark incubation with mitochondrial inhibitors leads to a 40-60% reduction in net photosynthesis during excess light exposure depending on the condition and mutants tested (Dang *et al.*, 2014; Johnson *et al.*, 2014). This was interpreted as metabolic cooperation between the chloroplast and mitochondria, with mutants impaired in CEF (*pgrl1 and* pgr5) and $CO_2$ fixation (*RbcL and pgr5rbcL*) displaying an increased dependence

light dependent oxygen consumption (Dang *et al.*, 2014; Johnson *et al.*, 2014). In contrast, we found in our study that dark addition of mitochondrial inhibitors leads to a 90% inhibition of net photosynthesis after 10 minutes in wild type cells acclimated to 400 µmol photon $m^{-2}$ $s^{-1}$ (Supplemental figure 3.6). These levels of inhibition are similar to those observed previously for Rubisco mutants (*RbcL and pgr5rbcL*) where carbon fixation is inhibited and, based of mitochondrial inhibition, the majority of reductant generated in photosynthesis is consumed in the mitochondria (Johnson *et al.*, 2014). We observed in wild type *Chlamydomonas* cells that this large reduction in net photosynthesis was dependent on treatment timing. When inhibitors were injected during a sub-saturating light treatment, there was no significant differences observed in net photosynthesis obtained after 6 minutes of illumination in mitochondrial inhibited samples relative to the ethanol control (Figure 3.3C). Consequently, the impact that mitochondrial inhibition on net photosynthesis is likely explained by how dark inhibition of respiration impacts ATP levels in the chloroplast, and subsequently the time it takes to activate $CO_2$ fixation. In the dark, chloroplasts are proposed to avoid futile metabolic reactions associated with low ATP levels by import of ATP generated by the mitochondria (for review see Alric *et al.,*2013). In its absence, ATP levels drop in the chloroplast activating glycolysis, were starch and glucose catabolism is proposed to generate ATP and NADPH in phenomena known as the "Pasteur effect" (Gans and Rebeille, 1990; Rebeille and Gans, 1988). NADPH generated by glycolysis in the dark is then consumed by chlororespiration generating $NADP^+$ and facilitating continued glycolytic production of ATP (Atteia *et al.*, 2013). This process has been shown to induce a state transition and cyclic electron transport (Allorent *et al.*, 2013b; Alric, 2014; Cardol *et al.*, 2009)– indicating that general loss of mitochondrial respiration reduces electron carriers in the stroma and thylakoids of the chloroplast. Both reductant and ATP are needed for activation

of the Calvin-Benson-Bassham cycle. Thioredoxin, which is dependent on linear electron transport for reductant, mediates the activation of key enzymes involved in the Calvin-Benson-Bassham cycle (Gutle *et al.*, 2016). Redox poise in addition to pH, also tunes the activity of ATP synthase (Mills *et al.*, 1980). ATP is also required for the activation of Rubisco by Rubisco activase (Seemann *et al.*, 1985). Upon illumination, Rubisco activity is low due to absence of ATP and electron carriers are over reduced. ATP production subsequently must overcome the deficit generated in the dark and activate Rubisco. Consequently, observations of an increased dependence of photosynthesis on mitochondrial respiration shown here (Supplemental figure 3.S6) and previously more accurately reflect its role on chloroplast metabolism in the dark and in activation of photosynthesis (Dang *et al.*, 2014; Johnson *et al.*, 2014). This conclusion is supported by similar observations by Forti *et al.* (2008) that demonstrated that mitochondrial inhibition slows the activation of photosynthesis in sub-saturating light conditions. Furthermore, this also appears to be the case even when cells are primed with sub-saturating light, based on the slow rise in net photosynthesis observed in mitochondrial inhibited cells relative to the control (Figure 3.3D) – indicating the importance of the mitochondria in photosynthetic metabolism during changing light conditions.

Inhibition of mitochondrial $O_2$ consumption provides unique evidence for its role in photosynthesis in saturating light conditions in wild type *Chlamydomonas.* Previous work on the interactions between mitochondria and chloroplast in *Chlamydomonas* has suggested that mitochondrial cooperation reflects a valve to dissipate excess reducing power when the chloroplast's capacity for ATP production is genetically disrupted (Cardol *et al.*, 2009; Dang *et al.*, 2014; Johnson *et al.*, 2014). Recently, Kayes *et al.* demonstrated that the mitochondrial alternative oxidase is required for *Chlamydomonas* survival during a shift from light limited to

saturating light conditions using the *aox1* mutant (Kaye *et al.*, 2019). Evidence previously presented for this claim has primarily relied on mutants or inhibitor studies and assessment based on fluorescence, growth rate, or as we describe above, dark inhibitor addition which inhibits activation of photosynthesis. Here we primed photosynthesis, which allowed rapid attainment of the maximum net photosynthetic rate – allowing the evaluation of mitochondrial inhibition on steady state photosynthesis in saturating light. Inhibition of the mitochondria leads to a slower rise in net photosynthesis during a saturating light treatment in cultures acclimated to continuous illumination by 400 µmol photon $m^{-2}$ $s^{-1}$ (Figure 3.3C). This further supports its putative role in acting as an energy buffer for the chloroplast during transitions from dark to light, or in this case sub-saturating to saturating light intensities.

We also observed that mitochondrial inhibition correlated with a higher NPQ induction in wild type, and this increased during the same time frame as the late rise in oxygen consumption observed (Figure 3.3A and 3.3D). This increase in NPQ is LHCSR dependent based on its absence in *npq4lhcsr1* and likely reflects increased luminal acidification in wild type treated with mitochondrial inhibitors over the ethanol control. This reflects feedback inhibition on photosynthesis – suggesting cooperation between the chloroplast and mitochondria in dealing with saturating light intensities in the absence of any mutation. This observation, in conjunction with the immediate reduction of the plastoquinone pool (based on 1-qL, Figure 3.3C), suggests a tight coupling between chloroplast and mitochondrial metabolism even in sub saturating light conditions – which also occurs in diatoms where cyclic electron transport is a minor pathway for ATP/NADPH adjustment (Bailleul *et al.*, 2015). Mitochondrial inhibition also suppresses the late rise in oxygen consumption observed in Figure 3.3D and 3.3H for wild type cells. This suggests that mitochondrial respiration may be required for either reductant dissipation or

adjustment of the ATP/NADPH ratio in saturating light conditions (Figure 3.3D). These observations together demonstrate unique aspects of the tight metabolic coupling between the chloroplast and mitochondria in *Chlamydomonas* cells and isolate them from the affects on photosynthetic activation observed when inhibitors are applied in the dark.

Inhibition of PTOX leads to reductions in net photosynthesis and light dependent oxygen consumption. This provides evidence for its photoprotective role in photosynthesis during saturating light conditions in wild type *Chlamydomonas* acclimated to continuous 400 µmol photon $m^{-2}$ $s^{-1}$. Previous work on PTOX in *Chlamydomonas* has suggested that it plays a role in dissipating excess reductant generating during growth in saturating light or during nitrogen stress (Houille-Vernes *et al.*, 2011b; Saroussi *et al.*, 2016). Furthermore, characterization of a *Chlamydomonas* PTOX mutant, *ptox2,* has demonstrated that PTOX activity is required for maximum growth during frequent dark to light transitions (Nawrocki *et al.*, 2019). In this study, we investigated the impact of PTOX inhibition after priming photosynthesis with sub-saturating light. PTOX inhibition by PG leads to the immediate closure of plastoquinone pool (based on 1-qL, Figure 3C). This suggests that PTOX mediated light dependent oxygen consumption occurs even under light-limiting conditions, as previously proposed by the low, constant photoreduction determined by Houille-Vernes *et al.* (2011). PTOX inhibition reduced net photosynthetic rates in wild type cells exposed to saturating light while suppressing oxygen consumption - including the late rise in oxygen consumption observed in Figure 3.3D. Like myxothiazol/SHAM treatment, PG treatment lead to increased NPQ during the same time frame as the late rise in oxygen consumption – indicating a downregulation of photosynthesis (Figure 3.3A and 3.3D). These observations together suggest a critical role for PTOX in regulating electron transport in saturating light, which in its absence leads to the down regulation of photosynthesis.

Inhibitor treatment of *npq4lhcsr1* cells acclimated to 400 µmol photon $m^{-2}$ $s^{-1}$ lead to small reductions in the sensitivity of *npq4lhcsr1* to the inhibitors tested. *npq4lhcr1* treated with ethanol displayed a slower rise in net photosynthesis relative to wild type, which was not significantly impacted by inhibition mitochondrial respiration (Figure 3.3G). PG treatment significantly reduced the maximum rate of net photosynthesis relative to the ethanol control in *npq4lhcsr1* cells by 31% relative to the 53% reduction observed in wild type (Figure 3.3C and 3.3G). These two observations taken together suggest less sensitivity to mitochondrial and PTOX inhibitors – indicating that *npq4lhcsr1* does not compensate for absence of LHCSR dependent quenching by increasing dependence on PTOX or mitochondrial associated reductant consumption. This decrease in sensitivity could reflect increased partitioning to FLV dependent oxygen consumption (not measured here due to an absence of inhibitors), or to increased dependence on CEF discussed below.

The proportion of electrons directed towards light dependent oxygen consumption pathways, measured as the ratio of $O_2$ consumed to $O_2$ evolved, decreased in cultures acclimated to 400 µmol photon $m^{-2}$ $s^{-1}$ and sinusoidal light regimes relative to low-light acclimated conditions (Figure 3.3). This suggests decreased reliance on light dependent oxygen consumption in *Chlamydomonas* during acclimation to saturating light conditions. Previous work characterizing light dependent oxygen consumption has suggested that it plays a role during acclimation to fluctuating light (Chaux *et al.*, 2017a; Jokel *et al.*, 2018) and in compensating for mutations that impact reductant consumption downstream of photosystem I by preventing acceptor side limitation at PSI (Dang *et al.*, 2014; Johnson *et al.*, 2014). Thus, it is surprising that we don't observe an increase in the proportion of electrons going to oxygen consumption during

our photosynthesis vs irradiance curves in samples of wild type harvested from our sinusoidal light regime at solar noon (Supplemental figure 3.3).

Previous work quantifying oxygen consumption rates have focused on light dependent oxygen consumption during the first 24 hours of exposure to fluctuating light or $CO_2$ limitation in *Chlamydomonas*. Chaux *et al.* (2017) demonstrated that the proportion of photosynthesis diverted to light dependent oxygen consumption increased during the initial 4 hours of acclimation to fluctuating light exposure (1 minute at 50 µmol photon $m^{-2}$ $s^{-1}$ and 5 minute at 500 µmol photon $m^{-2}$ $s^{-1}$) (Chaux *et al.*, 2017). Dang *et al.* 2014 observed similar increases in oxygen consumption during the first 24 hour in high light (500 µmol photon $m^{-2}$ $s^{-1}$) acclimated *Chlamydomonas* cells after a shift from aeration with high $CO_2$ (air + 2% $CO_2$) to ambient (air; 0.04%), which was exacerbated in the cyclic electron transport mutant *pgrl1* (Dang *et al.*, 2014). These observations indicate a role for light dependent oxygen consumption during short-term acclimation to environments when light absorption and subsequent generation of ATP and NADPH exceeds the capacity for its utilization in carbon fixation. Observations in this study, where cultures were acclimated to light conditions for greater than 5 days, indicate that the proportion of electron consumed by light dependent oxygen consumption pathways decreases in *Chlamydomonas* cells acclimated to saturating light. This indicates that light dependent oxygen consumption, may only be involved during short-term acclimation and in cells with mutations that perturb energy homeostasis.

The proportion of electrons directed towards light dependent oxygen consumption pathways was the same between wild type and the *npq4lhcsr1* mutant – indicating that *Chlamydomonas* does not acclimate to the absence of LHCSR-dependent NPQ by upregulating light dependent oxygen consumption (Supplemental figure 3.3). This further supports the claim

that *npq4lhcsr1* does not acclimate to saturating light by upregulation of its light dependent oxygen capacity.

We observed a reduction in the net photosynthetic rate in *npq4lhcsr1* relative to wild type using our MIMS conditions, which contradicts previous observations found in our sinusoidal light acclimated cultures (Cantrell and Peers, 2017). This difference is explained by the longer light steps used in this studies measurement (3 minutes vs 1 minute) and normalization by chlorophyll in this steady versus a per cell basis used previously. Chlorophyll content is in the *npq4lhcsr1* mutant is 13% higher than wild type (Cantrell and Peers, 2017). Consequently, normalization by cell would overestimate photosynthetic rates relative to a per chlorophyll basis, which provides a more accurate representation of photosynthetic electron transport. Additionally, the short light steps and longer dark incubation used previously likely lead to the increased NPQ observed in wild type due to a slower activation of photosynthesis, and consequently greater feedback inhibition (Cantrell and Peers, 2017). These two factors ultimately lead to less NPQ induced in wild type and consequently a higher net photosynthetic rate observed in this study.

Compensation by cyclic electron transport and state transitions

Our data suggests that *Chlamydomonas* acclimates to saturating light in the absence of LHCSR dependent NPQ by increasing sink capacity downstream of PSI. *npq4lhcsr1* cells acclimated to sinusoidal light conditions displayed reduced PSI closure due to acceptor side limitation at light intensities between 350 – 1290 µmol photon $m^{-2}$ $s^{-1}$ (Figure 3.4G and 3.4H). A reduced fraction of acceptor side limited PSI in *npq4lhcsr1*, in the absence of increased oxygen photoreduction indicates either an increased capacity for carbon assimilation or increased capacity for cyclic electron transport. A decrease in net photosynthesis in the present study and decreased growth rates in the absence of any significant difference in organic carbon

accumulation observed previously suggests that this is a result of increased cyclic electron transport (Cantrell and Peers, 2017). Previously, cyclic electron transport has been shown to be regulated by stromal redox state (Alric, 2014; Alric *et al.*, 2010a; Takahashi *et al.*, 2013). Loss of photosynthetic control of PSII by LHCSR dependent NPQ in the *npq4lhcsr1* mutant is expected to lead to increased stromal reduction and consequently may increase the proportion of electrons recycled through cyclic electron transport associated pathways. Increased cyclic electron transport may then facilitate photosynthetic control by limiting electron transport through the cytochrome $b_6f$ complex as previously suggested in the *npq4* mutant and the *rbcL* mutant (Chaux *et al.*, 2017; Finazzi *et al.*, 2016; Johnson *et al.*, 2014). Indeed, cyclic electron transport mediated by the PGRL1 complex is proposed to compensate for reduction in LHCSR dependent NPQ, as *npq4pgrl1* mutants exhibited drastic reduction in growth and $CO_2$ fixation relative to individual mutants (Chaux *et al.*, 2017).

We, and others, have previously reported a reduction of $F_v/F_m$ in LHCSR mutants during both short- (<24 hours) and long-term (>24 hours) acclimation to saturating light intensities. Cyclic electron transport may adjust the ATP/NADPH ratio to meet increased ATP demand. The reduced $F_v/F_m$ observed in LHCSR mutants is interpreted as reflecting an increase in PSII damage (Allorent *et al.*, 2013; Cantrell and Peers, 2017). This necessitates the degradation and re-synthesis of photo damaged D1 proteins – an ATP dependent process (Malnoe *et al.*, 2014; Raven, 2011). Furthermore, we previously observed an increase in D2 protein in *npq4lhcsr1* cells relative to wild type acclimated to sinusoidal light – suggesting that they maintain a larger pool of PSII reaction centers likely to facilitate higher PSII turnover rates. In the absence of evidence for increased light dependent oxygen consumption, this suggests that cyclic electron transport or some previously undiscovered pathway can alleviate PSI acceptor side limitation in

*npq4lhcsr1* mutants. In higher plants, cyclic electron transport has been proposed to be the main constituent of PSI photoprotection based on its role in relieving both acceptor side limitation and reducing linear electron transport (Suorsa *et al.*, 2012; Suorsa *et al.*, 2016; Tikkanen *et al.*, 2015). This may explain the relatively limited impact loss of excitation dependent quenching has on fitness in algae and plants relative to the fitness defects observed in cyclic electron transport mutants (Dang *et al.*, 2014; Johnson *et al.*, 2014; Kulheim *et al.*, 2002; Munekage *et al.*, 2002; Yamori *et al.*, 2016). Interestingly, in *Chlamydomonas,* the *pgrl1* mutant displayed higher FLV protein abundance when acclimated to even low light intensities (Dang *et al.*, 2014b). Additionally, exogenous expression of FLV proteins in higher plant cyclic electron mutants has been shown to complement the mutant phenotype (Wada *et al.*, 2018; Yamamoto *et al.*, 2016). These observations suggest that CEF may be more central to photosynthetic regulation than qE under nutrient replete conditions, with upregulation of reductant consumption downstream of PSI compensating in mutants perturbing CEF function.

The *npq4lhcsr1* mutant displayed a greater capacity for state transitions under light limited and the sinusoidal light condition tested – indicating altered antenna architecture or state transition capacity (Figure 3.5). Under light limiting and sinusoidal light condition the capacity for state II transition is increased in the *npq4lhcsr1* mutant relative to wild type (Figure 3.5) and is congruent with previous observations in the *npq4* mutant during a shift from light limited to saturating light and under state II inducing conditions (Allorent *et al.*, 2013b). A lower chlorophyll a:b ratio and higher total chlorophyll content under sinusoidal light conditions suggests that this capacity may reflect an increase in antenna proteins, though no increase in LHCB2 protein level was previously observed under sinusoidal conditions at solar noon (Cantrell and Peers, 2017). This may represent an increase in LHCII dissociation, aggregation

and quenching by an LHCSR independent process in the *npq4lhcsr1* or their migration to PSI reaction centers (Nagy *et al.*, 2014a; Unlu *et al.*, 2014). Compensation by state transitions via the dissociation of LHCII from PSII and subsequent quenching is supported by a faster increase in NPQ in *npq4lhcsr1* relative to wild type across light intensities where *npq4lhcsr1* experiences less PSI closure (Figure 3.4G and 3.S4H). Alternately, a small increase in cyclic electron transport has been show to occur under state II but the impact of state transitions on light harvesting in cells acclimated to saturating light conditions has not been measured (Alric, 2014; Takahashi *et al.*, 2013). Together these observations suggest an overlap in compensation by state transitions and cyclic electron transport in the *npq4lhcsr1* mutant under sinusoidal light conditions.

Alternative compensatory mechanisms

NPQ mechanisms previously uncharacterized in algae could also be compensating for the absence of LHCSR dependent NPQ. Zeaxanthin dependent quenching qZ or slow antenna quenching qH, previously characterized in *Arabidopsis*, could represent one possible avenue for compensation. Zeaxanthin dependent quenching occurs by the pH dependent accumulation of zeaxanthin in the thylakoid membranes and is proposed to reflect a slowly reversable form of NPQ independent of qE (Nilkens *et al.*, 2010). Sustained antenna quenching (qH) was recently described in *Arabidopsis* and depends on the luminal accumulation of plastidial lipocain protein (LCNP; Malnoe *et al.*, 2018). LCNP is proposed to function by modifying a molecule in the vicinity or with antenna proteins that triggers a conformational change in antenna from a harvesting to a dissipative state (Malnoë, 2018). While components of qH exist in algae, it's unclear whether a LCNP homolog exists in *Chlamydomonas* due to the lipocalin superfamily having poor sequence identity while maintain high structural and functional similarity (Lakshmi

*et al.*, 2015; Malnoë, 2018). Neither zeaxanthin concentrations nor LCNP were measured in this study, but previous measurements of $F_v/F_m$ taken immediately after harvesting on cells across the sinusoidal light regime and in cells acclimated to continuous 400 µmol photon $m^{-2}$ $s^{-1}$ in this study (Supplemental figure 3.5A) indicate that only small differences exist in *in situ* NPQ between wild type and *npq4lhcsr1*. This suggests that mechanisms outside of NPQ are likely compensating for its absence in the *npq4lhcsr1* mutant.

**Conclusions**

Fine tuning photosynthesis for industrial cultivation remains a driving objective of photosynthesis research and many challenges remain in unraveling the redundancy, regulation and dynamic activation of the numerous pathways underlying photosynthetic control. There is a growing body of evidence to suggest that qE may be dispensable under nutrient replete conditions and may even limit growth due to the kinetics of its induction and relaxation and high energy quenching capacity (Berteotti *et al.*, 2016; Kromdijk *et al.*, 2016; Perozeni *et al.*, 2018). Here we provide further evidence supporting the claim that cyclic electron transport can provide photosynthetic control in the absence of LHCSR dependent quenching. We also demonstrate direct evidence for the role of mitochondria in activation of photosynthesis and it's role during steady state photosynthesis (Figure 3.3A and 3.3D). Additional characterization of PTOX inhibition directly links it to maintenance of maximum photosynthesis, which previously has been under dispute due to the low oxidation rates estimated by fluorescence techniques (Houille-Vernes *et al.*, 2011; Nawrocki *et al.*, 2015). This work, and recent characterization of photoprotection has suggested a complex web of dissipation mechanisms which functionally overlap, have evolved specific roles for energy dissipation during abiotic stress and synergistically function together to maintain energetic homeostasis in natural environments

where abiotic stress rarely occurs by just one factor. In this study we show that *Chlamydomonas* during long-term acclimation to saturating light, like short-term, compensates primarily by cyclic electron transport mechanisms. Additionally, we provide direct evidence for the roles of mitochondrial cooperation and PTOX activity in induction and maintenance of steady state photosynthesis in saturating light. A challenge moving forward will be fine tuning each photoprotective mechanism for optimal synergy in industrially relevant conditions.

# *CHAPTER 4:* A NEGATIVE SELECTABLE MARKER AND MUTAGENESIS STRATEGY USED TO IDENTIFY NUCLEAR ENCODED FACTORS REGULATING CHLOROPLAST GENE EXPRESSION IN THE GREEN ALGAE *CHLAMYDOMONAS REINHARDTII*


## Summary

Algae and higher plants originated from a primary endosymbiotic event when a non-photosynthetic protist engulfed and enslaved a cyanobacterium. Evolutionary enslavement occurred through horizontal gene transfer from the engulfed cyanobacterium to the nuclear genome in parallel with gene loss in the proto-chloroplast. Subunits for photosynthetic machinery became split between two genomes – necessitating the evolution of a complex regulatory system for proper photosynthetic function. Coordination of genome expression in response to biotic and abiotic stimuli requires both chloroplast to nucleus signaling (retrograde) and nucleus to chloroplast signaling (anterograde). Expression of chloroplast genes in plants and algae requires nuclear-encoded factors that are primarily believed to act at the post-transcriptional level through interactions with the 5'UTR of mRNA. We aimed to identify new factors involved in nuclear control of chloroplast gene expression. We used the previously described negative selectable marker cytosine deaminase (*CodA*) in conjunction with nuclear insertional mutagenesis to identify novel mutations effecting promoter and 5' UTR elements for the chloroplast encoded genes *chlB* (light independent chlorophyll synthase) and *psaA* (Photosystem I (PSI) subunit A). Weak expression of cytosine deaminase by a 1 kb *ChlB* promoter lead to limited selection pressure with a 60% reduction in colony forming units (CFU) on selection plates relative to mutagenesis controls. Additionally, we observed no mutants with the expected yellow in the dark phenotype under our selection conditions. In contrast, mutagenized lines expressing *CodA* under the regulation of the *psaA* promoter resulted in a 97%

reduction in CFU on selection plates relative to a mutagenesis control. A mutant library of 700 independent strains was generated. This chapter focuses on an ongoing characterization of these mutants and provides a report on 29 putative *psaA* expression mutants with nuclear loci identified. It also describes their potential role in in regulating chloroplast genome expression. One notable mutant is in a previously characterized protein, TBA1. It has previously been shown to regulate the translation of the photosystem II (PSII) subunit *psbA* in response to the chloroplast redox state. It may also regulate *psaA* translation - providing a mechanism for adjustment of the ratio of PSII to PSI in *Chlamydomonas* analogous to mechanism mediated by the Chloroplast sensor kinase in higher plants and other algae. Further characterization of this and other mutants will provide insights into the evolutionary history of chloroplast genome regulation and potential targets for improving photosynthetic efficiency.

**Introduction**

Chloroplast function is generated from a mosaic of proteins encoded in both the nuclear and chloroplast genomes, necessitating coordination of expression in response to environmental ques. Despite a large reduction in the chloroplast genome size in every photosynthetic linage, several genes encoding subunits for key components of light harvesting (PSII, PS I, Cytochrome $b_6f$ , light independent chlorophyll synthesis) and core biochemistry (large rubisco subunit ) have been maintained with the chloroplast genome (Ku *et al.*, 2015). This maintenance is hypothesized to result from the necessity for colocalization of redox regulation and gene expression (Allen, 2015). The presence of photosynthetic genes in two different genomes has necessitated a complex system of communication between organelles. This coordination is mediated by metabolites and other factors that facilitate signal transduction from the chloroplast to the nuclear genome in response to environmental conditions and during chloroplast

development. Chloroplasts regulate nuclear encoded chloroplast proteins by transmitting their functional state through retrograde signals that include chloroplast gene expression (Woodson *et al.*, 2013), pigment biosynthesis intermediates (e.g. tetrapyroles - *lhcsr1*, *psbs1*,eli*3*, *gpx*, *hsp70*; Duanmu *et al.*, 2013; von Gromoff *et al.*, 2008; Woodson *et al.*, 2011), reactive oxygen species (ROS; *gst1, gpx5, lhcsr1*and *apx*; Chi *et al.*, 2015; Fischer *et al.*, 2012; Wakao *et al.*, 2014)), oxidized lipids (Fischer *et al.*, 2012), redox state of the electron transport chain (*petE, lhcB* and *apx* (Escoubas *et al.*, 1995; Fey *et al.*, 2005), and metabolite pools (*gpx5, elip2 and gst1*; Dietz, 2015; Estavillo *et al.*, 2013; Lata and Prasad, 2011; Ramel *et al.*, 2012; Vogel *et al.*, 2014; Xiao *et al.*, 2012)) . In contrast, the nuclear genome controls chloroplast genome regulation by providing the proteins required for transcriptional regulation (Sigma factors; for review see Lysenko *et al.* 2007 ), translational regulation (RNA-processing , -editing, -stability, and translation), protein maturation and protein import and are collectively termed anterograde signals (Barkan, 2011; Dietz, 2015; Lyska *et al.*, 2013; Zoschke and Bock, 2018).

Transcriptional regulation of the plastid genome is primarily attributed to a set of evolutionarily conserved sigma factors derived from a single cyanobacterial lineage (Lysenko, 2007; Ponce-Toledo *et al.*, 2017). Sigma factors are DNA binding proteins that control transcription by first binding to RNA polymerase to form a haloenzyme, which than facilitates binding to specific promoters to initiate transcription (Bohne *et al.*, 2006; Carter *et al.*, 2004). Extant cyanobacteria species today contain between 9-12 sigma factors that are functionally separated into three groups (Imamura *et al.*, 2003). Group I is comprised by a single sigma factor, *SigA*, and represents the primary sigma factor in cyanobacteria – transcribing most genes. Group II and IIII, while structurally similar to Group I control specific cellular gene suites associated with circadian rhythm and environmental stress (Huckauf *et al.*, 2000; Khudyakov

and Golden, 2001; Nair *et al.*, 2002). There is clearly less sigma factor diversity in plastids compared to cyanobacteria. Higher plants contain 5-6 sigma factors that are orthologous to *SigA*. In contrast, algal linages contain between 1-3 sigma factors and are distantly diverged from Group 1 and Group II sigma factors (Lysenko, 2006).

While sigma factors appear to be the main driver for transcriptional regulation in the plastid, post transcriptional regulation of mRNA stability and translation has been demonstrated for chloroplast encoded photosynthetic subunits and is widely proposed to be the main factor driving differential accumulation of proteins encoded in the chloroplast genome (Lyska *et al.*, 2013; Manavski *et al.*, 2018; Marin-Navarro *et al.*, 2007; Zoschke and Bock, 2018). This claim is based on two observations. In *Chlamydomonas* protein abundance in the chloroplast encoded photosynthetic subunits (PSII: *psbA* and *psbD;* Cytochrome $b_6f$: *petA* and *petD;* PSI: *psaA* and *psaB;* ATP synthase: *atpA* and *atpB*) is independent of transcript abundance. This was eloquently demonstrated by reducing transcript abundance through the reduction of the chloroplast genome copy number using 5-fluoro-2'deoxyuridine – a DNA replication inhibitor. This led to a 90% reduction in transcript for some subunits, but had no significant impact on protein abundance (Eberhard *et al.*, 2002).

Only two of the six sigma factors (*Sig1* and *Sig6*) are essential for photoautotrophic growth in *Arabidopsis* with mutants of the remaining sigma factors showing no discernable phenotype (Loschelder *et al.*, 2006; Shirano *et al.*, 2000). Despite this, each plant encoded sigma factor is specific for one or more chloroplast genes (Hanaoka *et al.*, 2003; Ishizaki *et al.*, 2005; Lerbs-Mache, 2011; Oikawa *et al.*, 2000; Privat *et al.*, 2003; Schweer *et al.*, 2010a; Schweer *et al.*, 2010b). Redundancy though between sigma factors, and the transcription of plastid genes from multiple independent promoters by either the plastid encoded polymerase (PEP) or the

nuclear encoded polymerase (NEP; Not found in green algae) has suggested though that this may serve an evolutionary rather than regulatory function. This is proposed by Lerbs-Mache *et al.* (2011), who suggested that the expansion of nuclear encoded regulatory factors in higher plants occurred in order to suppress point mutations occurring in chloroplast promoter regions – insuring constant genome transcription by facilitating the evolution of new promoter-polymerase pairs (Lerbs-Mache, 2011). One exception to this hypothesis appears to be the *Arabidopsis Sig1* transcription factor. *Sig1* has been demonstrated to regulate the transcript abundance of *psaA* in response to the redox state of the chloroplast electron transport chain. This redox regulation is proposed to provide photosynthetic control by balancing the ratio of PSII and PSI in response to light conditions (Shimizu *et al.*, 2010). *Sig1* becomes phosphorylated when the instersystem electron transport chain is oxidized and subsequently inhibits transcription of *psaA* and based on work in rice subsequent PsaA protein abundance (Shimizu *et al.*, 2010; Tozawa *et al.*, 2007). SIG1 phosphorylation is proposed to occur through the direct or indirect actions of the chloroplast sensor kinase (CSK). CSK like *Sig1*, is phosphorylated when the electron transport chain is oxidized and has been shown to mediate changes in PSI to PSII (Puthiyaveetil *et al.*, 2012; Puthiyaveetil *et al.*, 2008). Currently an analogous study to Eberhard *et al.* (2002) has not been completed for higher plants, but abundance of most proteins in the chloroplast are proposed to be regulated post-transcriptionally (Barkan, 2011; Lyska *et al.*, 2013; Zoschke and Bock, 2018).

Anterograde translation regulation is believed to occur primarily through a collection of proteins referred to as “regulators of organelle gene expression” (ROGEs) and are comprised of proteins in an organelle specific helical repeat superfamily (Delannoy *et al.*, 2007; Hammani *et al.*, 2014). Members of this helical repeat protein super family are characterized by containing

successively repeated modules of 2-3 α-helices that form a super helix and facilitate sequence specific binding to their cognate mRNA. Helical repeat protein families are believed to be evolutionarily independent despite similar protein structure. They are classified based on the length of their helical motif: tetratricopeptide proteins (TPR) containing a 34 aa module length, pentatricopepdite proteins (PPR; 35 aa per helix), and octotricopeptide proteins (OPR, 38 aa per helix). There are also closely related mitochondrial transcription termination factors (mTERF. 30 aa per helix). Members of this helical repeat family are involved in RNA editing, RNA splicing, RNA cleavage, RNA stability and translational control in chloroplast and mitochondrial genome regulation (Delannoy *et al.*, 2007; Hammani *et al.*, 2014). Post-transcriptional regulation of chloroplast encoded photosynthetic protein abundance by helical repeat proteins have been demonstrated for ATP synthase (*atpA and atpH*; Pfalz*et al.*, 2009), Cytochrome *f* (*petA;* (Boulouis *et al.*, 2011), PS I (*psaA, psaB and psaC;* Del Campo *et al.*, 2002; Lefebvre-Legendre *et al.*, 2015; Schmitz-Linneweber *et al.*, 2005) and PS II (*psbB* and *psbC;* Boudreau *et al.*, 2000; Mulo *et al.*, 2012). Among these, differential regulation in response to environmental queues has only been demonstrated for the PSII subunit D1 in response to light (Mulo *et al.*, 2012), and in the PSI subunit PsaA in response to iron limitation (Lefebvre-Legendre *et al.*, 2015).

Previous work identifying trans-acting regulatory factors involved in chloroplast gene expression have been limited in *Chlamydomonas* by time consuming screens based on identification of color mutants and altered chlorophyll fluorescence phenotypes underlying mis-regulation of chloroplast genes (Kuck *et al.*, 1987; Yohn *et al.*, 1998). These approaches were further limited by methods of mutagenesis, which often required labor intensive mutation mapping approaches (Gumpel *et al.*, 1995). To address the former challenge, the negative selectable marker cytosine deaminase from *Escherichia coli* has been codon optimized for

chloroplast expression in *Chlamydomonas reinhartii* (Young and Purton, 2014). Cytosine deaminase converts 5-fluorocytosine (5-FC) to 5-fluorouracil (5-FU), which inhibits DNA synthesis and subsequent cell divisions and ultimately leads to cell death (Dai *et al.*, 2001). Using this marker, Young and Purton demonstrated that UV mutagenesis of strains expressing cytosine deaminase from either the 5' UTR of chloroplast expressed *psaA* (Photosystem I) or *petA* (Cytochrome $b_6f$) allowed selection of mutants insensitive to 5- Fluorocytosine. This led to the identification of two trans-acting factors. TAA1 was hypothesized to regulate *PsaA* mRNA translation in response to iron availability (Lefebvre-Legendre *et al.*, 2015), and MCA1 stabilizes *PetA* mRNA (Boulouis *et al.*, 2011; Lefebvre-Legendre *et al.*, 2016). Recent advances made in insertional mutagenesis now make identifying gene disruption relatively simple. Pollock *et al.* (2017) demonstrated flanking sequence amplification with a 74% success rate using a strategy that involves genome digestion and subsequent adaptor and ligation mediated PCR amplification (Pollock *et al.*, 2017). This technique alleviates the second challenge.

In this study, we use the negative selectable marker cytosine deaminase regulated by the *psaA* and the light independent chlorophyll synthase gene *chlB* promoters to identify novel chloroplast regulatory factors using insertional mutagenesis. The promoter of *chlB* was chosen because its transcript abundance has previously been shown to decrease in response to increases in light intensity and mutants display a yellow phenotype when grown under dark conditions (Fujita *et al.*, 1996; Mettler *et al.*, 2014). The promoter of *psaA-exon1* was chosen because it has previously shown to drive high chloroplast gene expression (Michelet *et al.*, 2011) and there is evidence to suggest that PSI undergoes dynamic regulation in response to light quality (Bonente *et al.*, 2012; Matsui, 2002; Murakami, 1997; Murakami *et al.*, 1997). We have generated 400 putative *psaA* and 317 putative *chlB* regulatory mutants using this approach. We have focused

our characterization on mutants effecting expression from the *psaA* mutant and have currently identified 29 putative mutations impacting expression of the *psaA* promoter based on loss of cytosine deaminase expression.

**Methods**

*C. reinhardtii* strains and growth media

The recipient line used to create transformant lines for *psaA* and *chlB* screens was the TN72 line. This is a cell wall-less deficient strain of *C. reinhardtii (cw15.13a (mt+))* with a deletion in the chloroplast *psbH* gene and it was obtained from Chlamycollection.org (Young and Purton, 2014). Cell lines generated were maintained on Tris acetate phosphate (TAP) plates containing 2 % agar. For transformations, genomic and protein preparation liquid culture was grown in TAP medium in 50-250 ml Erlenmeyer flasks using 2-4 colonies from axenic plate cultures as inoculum. Growth for complemented lines and the base TN72 strains was performed at 25˚C with shaking at 150 rpm under continuous light fluxes of 25 µmol photon $m^{-2}$ $s^{-1}$ unless otherwise noted.

*C. reinhardtii* Chloroplast Transformation Vector construction

Chloroplast transformation vectors were constructed using the pRY127D vector constructed by Young *et al.* 2014 and obtained from Chlamycollection.org. Generation of *Chlamydomonas* lines expressing *codA* under regulation of the *psaA* promoter and 5'UTR were generated using the pRY127D base vector without modification. The *chlB* promoter was amplified with primers from the start codon to1 kb upstream from the coding region. Primers were designed using the CC-125 *Chlamydomonas* chloroplast genome sequence and are supplied in the supplementary information with vector maps (Supplemental table 4.5). Vector backbones for cloning were generated by Phusion polymerase amplification. Assembly of *chlB* synthase

promoter – cytosine deaminase – *rbcL*3'UTR cassettes and empty vector control were constructed by blunt ligation and sequence verified.

*C. reinhardtii* Chloroplast Transformation

Plasmids containing the *psaA::codA, chlB::codA* and no insert cassette were transformed into the *psbH-trnE2* intergenic region of the chloroplast genome of *C. reinhardtii* line TN72 by homologous recombination as previously described with some modifications (Young and Purton, 2014). 300-500 ml of cells were grown in TAP medium to a density of 2 x $10^6$ cells $ml^{-1}$ were harvested by centrifugation (3444 x g, 5 min at 25˚C) and resuspended in TP medium at 2 x $10^8$ cells $ml^{-1}$. We found that resuspension in TAP prior to transformation lead to a significant increase in false positives not previously reported (Economou *et al.*, 2014). After resuspension, 300 ul of cells, 10 µg of circular plasmid DNA and 0.3 g of glass beads (Sigma-Aldrich, diameter 0.4-0.6 mm) were vortexed in 2 ml Eppendorf tubes for 15 s. 1 ml of TP containing 0.5% agar was then added to the mixture and subsequently poured on to TP plates. Transformation plates were incubated for 2-3 weeks at 25˚C under 50 µmol photon $m^{-2}$ $s^{-1}$. Putative chloroplast transformations were then re-streaked on TP twice and screened by PCR for homoplasmy (Supplementary table 4.3).

Nuclear mutagenesis by electroporation

Nuclear transformation was performed as described in Pollock *et al.* 2017 (Pollock *et al.*, 2017). The pSL18 plasmid (Chlamycollection.org) was digested with high fidelity KpnI and XhoI (Thermoscientific) to generate a 1.8 kb cassette, isolated by agarose gel electrophoresis and gel extracted (Qiagen Cat# 28704). *Chlamydomonas* cells were prepared for transformation by growth in liquid TAP medium for 2-3 days at 25˚C under 25 µmol photon $m^{-2}$ $s^{-1}$. Cells were harvested at a density of 1-5 x $10^6$ cells $ml^{-1}$ and resuspended in TAP + 60 mM sorbitol at a

concentration of 1 x $10^8$ cells $ml^{-1}$. 250 µL of cells was than mixed with 180 ng of the paromomycin resistance cassette and added to electroporation cuvettes (Bio-Rad #165-2091) with a gap width of 0.4 cm and incubated on ice for 10-20 minutes prior to electroporation. Electroporation was carried out using the Bio-Rad Gene Pulser II system with a voltage setting of 0.8 kV and a capacitance of 25 µF. Following electroporation, cells were transferred to 10 ml of TAP medium containing 60 mM sorbitol in a 15 ml conical tube. Samples were then allowed to recover overnight at 25˚C under low light (10-20 µmol photon $m^{-2}$ $s^{-1}$) with gentle shaking. Cells were than centrifuged for 10 minutes at 1500 g, resuspended in 100 µL TAP + 2 mg $ml^{-1}$ 5-FC (Chem-Impex Int'l Cat# 01260) and plated on petri dishes with solid TAP medium containing 1.5% agar (w/v), 20 µg $ml^{-1}$ paromomycin sulfate (Sigma,# p5057; stock of 100 mg $ml^{-1}$ dissolved in $H_2O$ and filtered via a 0.2 micron syringe filter; stored at 4 ˚C) and either 2 or 9 mg $ml^{-1}$ 5-FC. This initial selection on TAP +20 µg $ml^{-1}$ paromomycin + 2 or 9 mg $ml^{-1}$ constituted our primary selection for mutants defective in chloroplast expression regulation. Colonies insensitive to 5-FC were picked for isolation on the same primary selection media to verify insensitivity. Three transformation efficiency controls were included with each mutagenesis run by plating on TAP + 20 µg $ml^{-1}$ paromomycin sulfate. Mutagenesis plates were incubated in the dark at 23˚C for 2-4 weeks.

Secondary selection and mutant line maintenance

Colonies were picked after primary selection and streaked for isolation on TAP +20 µg $ml^{-1}$ paromomycin sulfate and either 2 or 9 mg $ml^{-1}$5-FC. Colonies that displayed growth under selection were than maintained under selection conditions for later characterization.

Flanking sequence identification and characterization

Flanking sequences were identified as previously described in Pollock *et al.* (2017) with the following modifications. Strains were prepared by inoculating 50 ml of TAP medium in a 125 ml shake flask. Cells were pelleted during late exponential phase (ranging from 5x106–1x107cells ml-1) and DNA was extracted using the Qiagen DNeasy Plant Mini kit. 200 ng of genomic DNA was digested with a mixture of AleI (10 units), NaeI (10 units), PmlI (10 units), and PvuII (1 unit) restriction endonucleases (New England Biolabs). For amplification of flanking sequences, digested DNA was ligated to adaptors and flanking sequences amplified in a two-step process (Primers provided in supplemental table 4.4). Amplified sequences of greater than 300 bp were isolated by electrophoresis in a 1% agarose gel, gel extracted (Qiagen Cat# 28704) and sanger sequenced. The resulting sequences obtained were processed by trimming the insert cassette and adaptor sequences from putative flanking sequences and assembling 5' and 3' flanking sequences together, when possible. Putative mutation sites were then identified using this processed sequence by BLAST against the JGI Phytozome genome portal and the Chlamydomonas reinhardtii v5.5 genome assembly (Boratyn *et al.*, 2012). The presence of a putative chloroplast transit peptide was determined using the TargetP v1.1 web portal (Emanuelsson *et al.*, 2007). Protein domains were determined initially by the Phytozome functional annotation search and then compared with results from NCBI Conserved Domains web portal (Marchler-Bauer *et al.*, 2017).

Immunoblot Blot Analysis

Cells were harvested in late exponential growth phase (ranging from $5x10^{-6}$ – $1.0x10^{-7}$ cells $ml^{-1}$) by centrifugation (3000 x g for 5 minutes at 25°C). Protein was quantified using either the Quibit™ protein assay kit or Pierce™ BCA protein assay kit. Proteins were resolved and detected as described in Cantrell and Peers (2017) with the following modifications. Membranes

were blocked overnight with 3% milk in TBS with 1% TWEEN 20 (Sigma-Aldrich, P7949) and then incubated with anti-HA peroxidase monoclonal antibody (Sigma Aldrich Cat# 12013819001 Roche) diluted to 50 mU $ml^{-1}$ in a 0.5% milk TBS solution. Membranes were incubated with antibody for one hour and then rinsed four times for 5 minutes. Band detection was performed using SuperSignal West Femto Maximum Sensitivity Substrate (Thermo Scientific, #34095) according to the manufacturer's protocol. A loading control was generated by staining a replica gel with Imperial™ protein stain according to the manufacture's protocol (Thermo Scientific, #24615).

*C. reinhardtii* 5-fluorocytosine (5-FC) sensitivity examination

5-Fluorocytosine (Chem Impext International VWR Cat # 102588-128) stocks were prepared at 15 mg $ml^{-1}$ in TAP medium by heating to 50 ˚C and subsequently filtered through 0.2 micron filter). 2 and 9 mg $ml^{-1}$ plates were made by mixing 866.6 ml or 600 ml of autoclaved TAP media (1.5% agar) with either 133.3 ml or 400 ml of 15 mg $ml^{-1}$ 5-FC stock respectively. Sensitivity to 5-Fluorocytosine was assessed on TAP plates under heterotrophic (dark) conditions at concentrations of either 2 or 9 mg $ml^{-1}$ 5-FC. For sensitivity tests, cultures were harvested during late exponential mixotrophic growth (ranging from $5x10^{-6}$ – $1.0x10^{-7}$ cells $ml^{-1}$) and densities adjusted to equal cell densities of $2.0x10^{-6}$ cells $ml^{-1}$. Sensitivity was than tested TAP + 2 and 9 mg $ml^{-1}$ 5-FC by the spotting 10 µl of a serial dilution of the $2x10^{-6}$ cells $ml^{-1}$ stock. After spotting 4 dilutions ($2x10^{-4}$, $2x10^{-3}$, $2x10^{-2}$ and $2x10^{-1}$ cells) plates were incubated at 23 ˚C in the dark.

**Results**

Construction of CodA expressing Chlamydomonas lines under the regulation of the *psaA* and *chlB* promoter region

*Chlamydomonas* lines with a human influenza hemagglutinin (HA) tagged *codA* under the regulation of either the *psaA* or 1 kb *chlB* promoter regions and *rbcL* 3' UTR were generated by homologous recombination in the TN72 background (Figure 4.1). The *psaA::codA* or *chlB::codA* cassettes were inserted into a intergenic region using homologous recombination with flanking sequences that complemented a mutation in the photosystem II gene *psbH*. Without *psbH,* TN72 is an obligate heterotroph (Economou *et al.*, 2014). Thus, complementation and selection on autotrophic media facilitated selection of homeoplasmic lines containing each transformation cassette – including an empty vector control based on the loss of the TN72 background PCR product (Figure 4.1A). Proper insertion was confirmed by amplicons of the expected size for each cassette (Figure 4.1B).

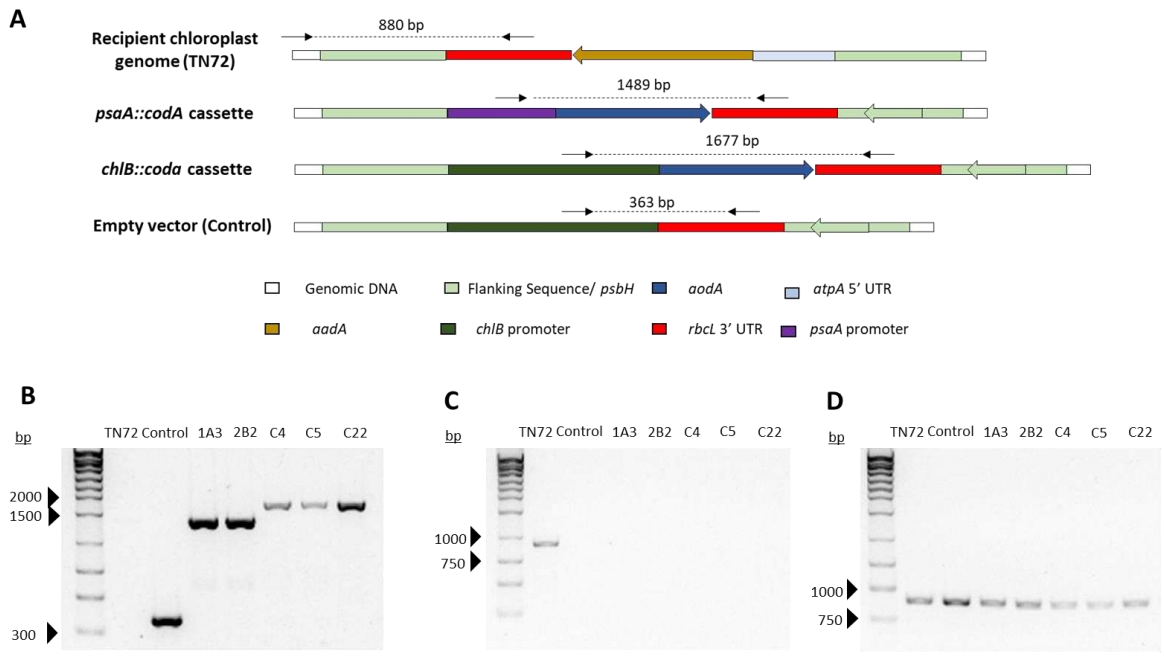


**Figure 4.1 Genotyping by PCR of *Chlamydomonas* chloroplast transformants for presence of cytosine deaminase cassette and homeoplasmy.**
(A) Representation of recipient and transformed chloroplast genomes with primer binding sites. (B) Agarose gel electrophoresis of verification PCRs for cassette insertion for TN72 (tested with *psaA* primers), empty vector control and the expression cassettes for *psaA::codA* (1A3 and 2B2) and *chlB::codA* lines (C4, C5 and C22). (C) PCR verification of homeoplasmy using primers specific to the recipient chloroplast sequence (TN72). (D) Positive control for amplification of chloroplast genomic DNA.

Expression of cytosine deaminase in each line was confirmed by immunoblot and by sensitivity to 5-FC on plates under heterotrophic growth conditions (Figure 4.2). Expression from the *psaA* promoter displayed high expression levels of CodA protein and lead to similar levels of sensitivity to 2 mg $ml^{-1}$5-FC as previously described by Young and Purton (2014; Figure 4.2A and 4.2B). Expression of CodA from the *chlB* 5'promoter was reduced relative to the *psaA* promoter, required loading of 60 µg of protein for detection, and varied between chloroplast transformation lines (Figure 4.2A). This lower expression required selection on 9 mg $ml^{-1}$ 5-FC, the maximum tested, and still resulted in minimal growth inhibition (Figure 4.2B).

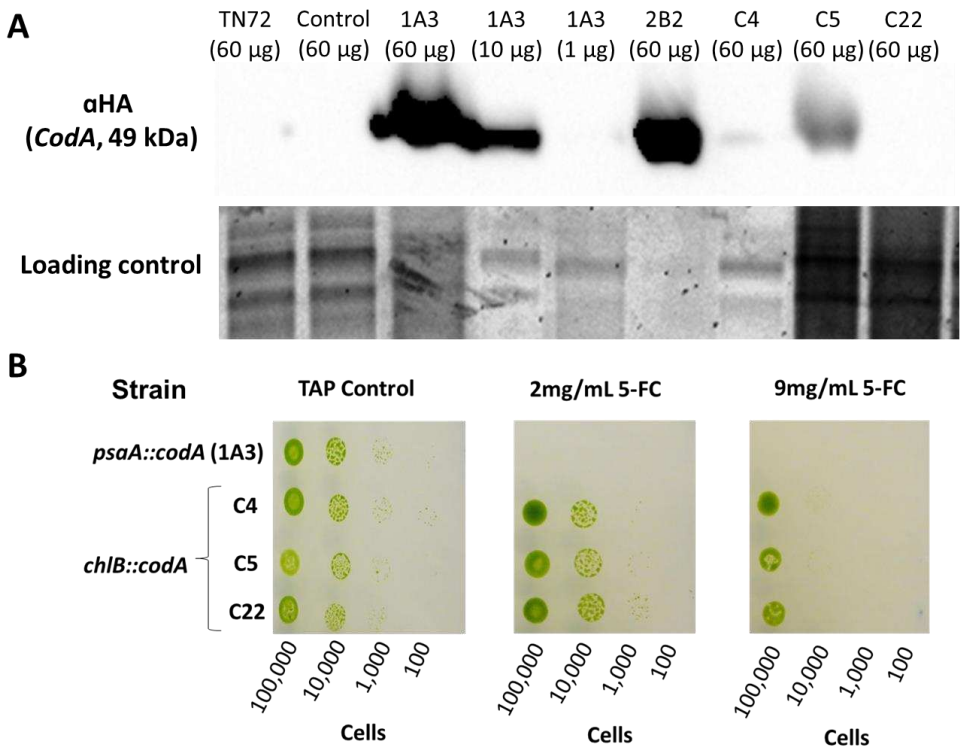


**Figure 4.2 Expression of Cytosine Deaminase from *psaA* promoter and 1 kb *chlB* promoter confers sensitivity to 5' Fluorocytosine.**
(A) Immunoblot analysis of CodA tagged with a human influenza hemagglutinin (HA) for *Chlamydomonas* recipient background strain (TN72), empty vector control (Control), lines transformed with the *psaA::codA* cassette (1A3 and 2B2) and lines transformed with the *chlB:codA* cassette (C4, C5 and C22). (C) Heterotrophic sensitivity of *CodA* expressing lines to 5-FC.

Mutagenesis and selection of mutants deficient in *psaA* and *chlB* regulation

The mutants in this study were generated over 23 rounds of mutagenesis using lines of cytosine expressing cells with verified cytosine deaminase production and sensitivity to 5-FC. Mutagenesis was performed using a 1.8 kb paromomycin selection cassette that facilitates flanking sequence amplification and sequencing (Pollock *et al.*, 2017). Transformation control plates (TAP + 20 µg $ml^{-1}$ paromomycin) provided estimates of our transformation efficiency and values obtained were congruent with previous observed efficiencies for analogous conditions (Table 1; Shimogawara *et al.*, 1998). The average percent selection determined by colony

forming units (CFU) on selection plates divided by control transformation plates using the *psaA* and *chlB* promoter was 3% and 40 % respectively (Table 4.1). 717 total mutants were picked for isolation over 23 mutagenesis runs. 317 of these were putative mutations affecting expression from the *chlB* promoter and 400 were putative mutants effecting expression from the *psaA* 5' UTR. Mutants generated using the *chlB::codA* expression cassette were discarded due to the low selection efficiency (Table 4.1) and high false positive rate based on the absence of yellow in the dark mutants on our mutant selection plates (TAP + 20 µg $ml^{-1}$ paromomycin + 9 mg $ml^{-1}$ 5-FC). In contrast, mutants generated using the *psaA::codA* cassette had a 34% false positive rate for the maintenance of insensitivity during a 2nd exposure to 5-FC during isolation on TAP + 20 µg $ml^{-1}$ paromomycin + 2 mg $ml^{-1}$.

**Table 4.1 Summary of cumulative mutagenesis runs for each *CodA* expressing background.** Average transformation efficiency based on colony forming units (CFU) per µg of insertional DNA cassette. Average percent selection across mutagenesis runs based on the colonies obtained on selection plates (TAP +20 µg $ml^{-1}$ paromomycin + 2 or 9 mg $ml^{-1}$) divided by control transformation plates (TAP + 20 µg $ml^{-1}$ paromomycin). Total number of mutants generated calculated from average transformation efficiency observed during mutagenesis runs multiplied by the number of transformation events.

| Promoter | Average transformation efficiency (CFU/µg DNA) | Average percent selection | Total mutations generated |
|---|---|---|---|
| *psaA::codA* | 6999 | 3% | 217311 |
| *chlB::codA* | 8577 | 40% | 230113 |

Characterization of putative mutants effecting expression from *PsaA* 5' UTR

At this point, we have verified changes in *CodA* protein accumulation in 75 of the of the 400 putative mutants effecting expression from the *PsaA* 5'UTR. 59 of the 75 tested by immunoblot displayed a decrease in cytosine deaminase protein expression (Table 4.2). This represents a 21% false positive rate. We verified the presence of *codA* expression cassette to rule out the possibility that loss of sensitivity to 5-FC resulted from unexpected mutagenesis or

deletion of the *psaA::codA* expression cassette (Figure 4.4B). 10% of lines tested thus far show loss of the *psaA::codA* cassette based on the absence of a PCR band (Figure 4.4B). The 29 mutants summarized in Table 4.2 reflect flanking sequence amplifications that received a low e-value when blasted against the *Chlamydomonas* genome and were found in coding regions. 12 of these putative mutation sites contain putative chloroplast targeting peptide sequences and 2 were identified in previously described proteins: TBA1 in the mutant AM12 and HSP70 in the mutant AM56. 15 of the 29 contain conserved protein domains and 11 mutations are in proteins with unknown function (No conserved protein domains).

**Table 4.2 Summary of putative *psaA* expression mutant characterization with putative mutation sites identified.**

All mutants presented in the table display loss of sensitivity to 5-FC on plates. 0 indicates no expression, L indicates lowered expression and N represents no change in expression levels in the CodA western blot column. A "–" in any column indicates absence of a measurement.

| Label | CodA Western Blot | Putative Mutation Loci | Putative Gene Description | cTP | Insertion type | PCR verified *CodA* | Light sensitivity |
|---|---|---|---|---|---|---|---|
| AM106 | 0 | Cre11.g467692, Cre11.g467693 | DUF1517, DUF1517 | Yes, Yes | Multiple | Yes | Yes |
| AM14 | 0 | Cre11.g467590 | Unknown | Yes | Multiple | No | No |
| AM43 | 0 | Cre03.g185950 | Zinc Finger Domain Related | Yes | Multiple (deletion) | Yes | Yes |
| AM12 | 0 | Cre13.g578750 | TBA1 | Yes | Single | Yes | Yes |
| AM130 | 0 | Cre01.g013100 | Predicted extracellular protein | Yes | Single | Yes | - |
| BM13 | N | Cre14.g628600 | Leucine Rich Repeat protein | Yes | Single | Yes | - |
| BM15 | N | Cre14.g628600 | Leucine Rich Repeat protein | Yes | Single | Yes | - |
| AM177 | - | Cre02.g120150 | Ribulose-1,5-bisphosphate carboxylase/oxygenase small subunit 2 | Yes | Single | Yes | Yes |
| AM78 | 0 | Cre17.g737702, Cre17.g737650 | Leucine-rich repeat protein, Putative methyltransferase | No, Yes | Multiple | Yes | Yes |
| AM100 | 0 | Cre12.g516100, Cre12.g516050 | ORMDL PROTEINS, CENTROSOMAL PROTEIN OF 170 KDA | No, No | Single | Yes | Yes |
| AM26 | 0 | Cre02.g110050 | Fbox and WD40 with signaling peptide domain | No | Single | Yes | - |
| AM56 | 0 | Cre08.g372100 | HSP70A | No | Single | Yes | - |
| AM61 | 0 | Cre13.g562250 | Flagellar Associated Protein | No | Single | Yes | No |
| AM66 | 0 | Cre02.g094700 | Unknown | No | Single | Yes | Yes |
| AM73 | 0 | Cre06.g274400 | Protein N-terminal methyltransferase | No | Single | Yes | No |
| AM87 | 0 | Cre09.g391986 | Phospholipase A(1) | No | Single | Yes | No |
| AM08 | 0 | Cre01.g028550 | OUT-like cysteine protease | No | Single | Yes | No |
| BM07 | 0 | Cre13.g562300 | Histone 1 | No | Single | Yes | - |
| AM24 | 0 | Cre08.g381075 | Unknown | No | Single | Yes | - |
| AM113 | 0 | Cre11.g467579 | Unknown | No | Single | Yes | No |
| AM131 | 0 | Cre02.g094700 | Unknown | No | Multiple (deletion) | Yes | - |
| AM102 | 0 | Cre01.g036700 | Ser/Theronine Kinase | No | Single | Yes | - |
| AM107 | L | Cre17.g737463 | Leucine Rich Repeat Protein | No | Multiple | Yes | Yes |
| AM119 | 0 | Cre08.g368226 | Unknown | Yes | Multiple | Yes | - |
| AM158 | L | Cre06.g278107 | Unknown | No | Single | Yes | Yes |
| AM162 | 0 | Cre06.g302500, Cre06.g302551, Cre06.g302600, Cre06.g302450 | Unkown, Unknown, VHS Domain, Unknown | No | Multiple | Yes | - |
| AM165 | N | Cre01.g036700 | Ser/Theronine Kinase | No | Single | Yes | Bleach |
| AM183 | - | Cre03.g169350 | Unknown | No | Single | Yes | Bleach |

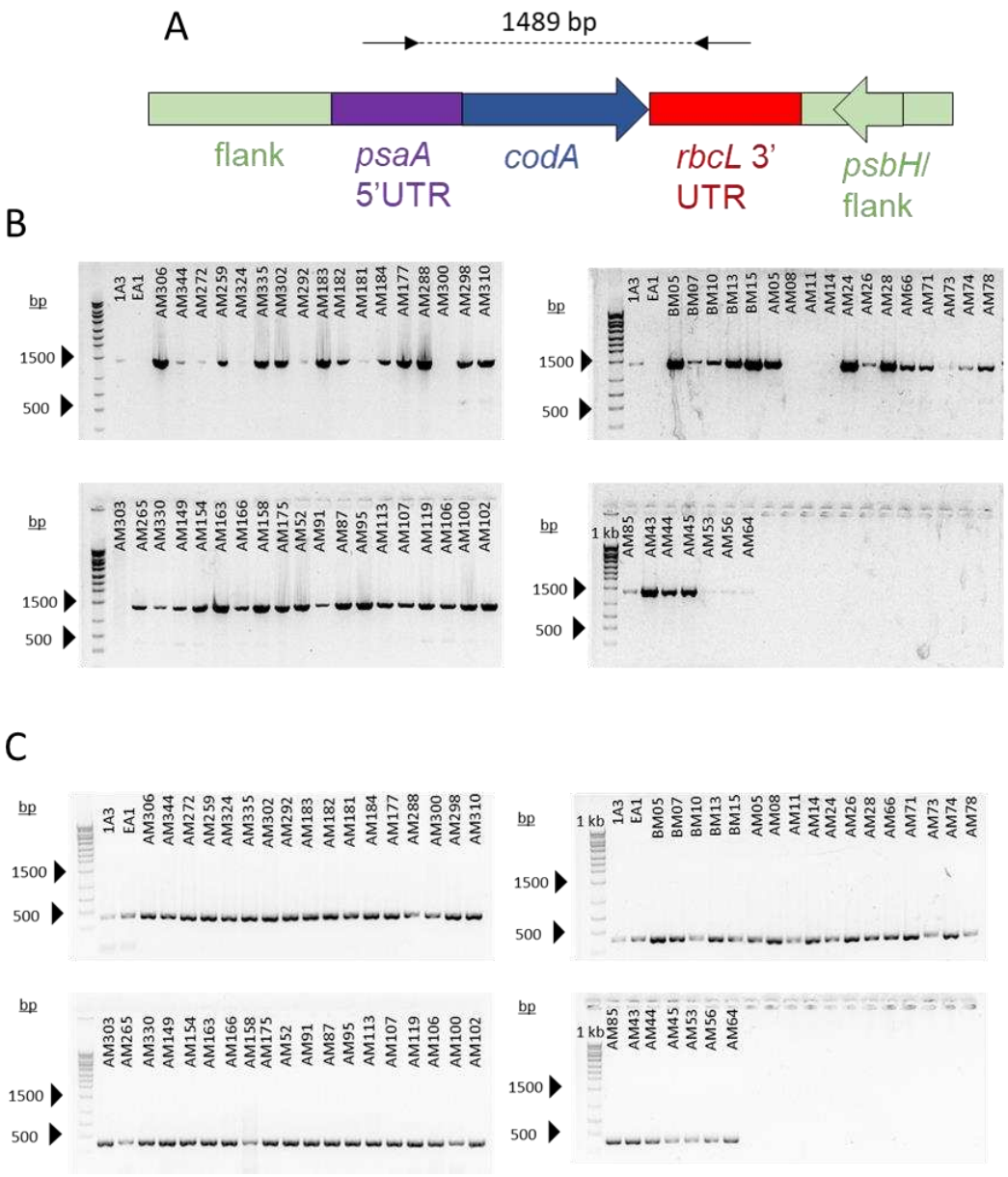


**Figure 4.4 Agarose gel electrophoresis of PCRs verifying the chloroplast localized *psaA::codA* in putative *psaA* regulatory mutants.**

(A) Diagram of *psaA::coda* cassette insertion site and location of primers used to screen for insert. (B) Screening agarose gel electrophoresis of diagnostic PCR amplifications for presence of *psaA::codA* in putative *psaA* mutant lines. (C) 23s rRNA template positive control. Lanes labeled 1A3 reflect base strain expression psaA::codA cassette. EA1 is our empty vector control and AM and BM lines are mutants generated in this study.

**Discussion**

This chapter aimed to identify novel nuclear encoded factors involved in regulating chloroplast gene expression in the model green alga *Chlamydomonas*. A mutant library was generated using a cytosine deaminase negative selectable marker under the regulation of the chloroplast encoded promoter and 5'UTR from *psaA* or *chlB* in conjunction with random, insertional mutagenesis of the nuclear genome. In total, 400 putative mutants effecting expression from the *psaA* promoter and 317 putative mutants effecting expression from the *chlB* promoter were generated.

Generation of *Chlamydomonas* lines expressing *codA* under the control of the *psaA* or *chlB* promoter was successful but lead to variability in cytosine deaminase protein abundance. Reduced expression of cytosine deaminase protein under the regulation of the *chlB* promoter relative to the *psaA* promoter resulted in reduced sensitivity to 5-FC and consequently a 60% reduction in CFU per plate under selection relative to the 3% observed in *psaA* lines(Figure 4.2, Table 1). This led to a high false positive rate based on the absence of yellow in the dark mutants among the 317 selected colonies displaying insensitivity to 5-FC. Consequently, the remainder of this discussion will focus on putative *psaA* mutants due to the low selection and high false positive rate observed in lines expressing the *chlB::codA* cassette.

In contrast to lines expressing the *chlB::codA* cassette, mutagenesis of lines expressing *psaA::codA* cassette resulted in a 34% false positive rate based on maintenance of 5-FC sensitivity and 20 % false positive rate based on loss of cytosine deaminase expression. The remainder of the discussion will focus on predicted mutations and a discussion of possible roles that identified putative mutations may be playing in the regulation of the *psaA* promoter.

<u>Known and expected mutations effecting expression from the *psaA* promoter</u>

*Chlamydomonas* chloroplast protein abundance is proposed to be regulated primarily by post-transcriptional processes (Barkan, 2011; Lyska *et al.*, 2013). This is based on the absence of a correlation between transcript abundance and associated protein synthesis (Eberhard *et al.*, 2002) and by the presence of a single sigma factor proposed to by the primary regulator of chloroplast transcription (Bohne *et al.*, 2006; Carter *et al.*, 2004). Eberhard *et al.* (2002) observed that protein abundance wasn't affected even when transcript abundance dropped by 90% during transcriptional inhibition. Additionally, sigma factors are believed to be the only DNA-binding factor involved in the recruitment of the plastid encoded RNA polymerase based on its bacterial origin (Feklistov *et al.*, 2014; Lysenko, 2007). A single sigma factor in *Chlamydomonas* further supports the claim that the chloroplast genome in this alga is primarily regulated by translational regulation. Additionally, the absence of the CSK or evidence for *Chlamydomonas* sigma factor phosphorylation indicates that *psaA* regulation likely occurs post-transcriptionally (Kawazoe *et al.*, 2012; Puthiyaveetil *et al.*, 2008). Consequently, we expected that mutants identified in this screen would consist of plastid targeted RNA binding proteins specific to the *psaA* promoter, non-RNA binding factors that indirectly regulate mRNA stability or translation, and cytosolic/nuclear localized factors that regulate the ladder proteins expression or activity.

We expected, but failed to identify, mutants from the helical repeat superfamily primarily associated with organellular RNA maturation, stability and translation (Hammani *et al.*, 2014). Previous work characterizing PSI-deficient mutants have identified several factors involved in accumulation of functional PSI. Among these, 14 were associated with trans splicing of the three separate *psaA* exons encoded in isolated loci in the chloroplast genome (Kuck *et al.*, 1987). This process appears to be primarily mediated by intron sequence and it is unlikely to be affected by the promoter of the *psaA* used in this study (Balczun *et al.*, 2005; Glanz *et al.*, 2006; Merendino

*et al.*, 2006; Perron *et al.*, 1999; Rivier *et al.*, 2001). Among the remaining mutants, only one other factor has been identified as regulating *psaA* expression. Lefebre-Legendre *et al.* (2015) identified a nuclear encoded factor required for translation of the *PsaA* mRNA called TRANSLATION OF *PsaA1* (TAA1) (Lefebvre-Legendre *et al.*, 2015). TAA1 is a chloroplast localized RNA binding protein that binds to the *psaA* exon 1 5' UTR and protects the *PsaA* mRNA from degradation by 5' to 3' RNA exonucleases. TAA1 also appears to be directly or indirectly required for translation with absence of TAA1 leading to translational inhibition *psaA* transcripts even when *psaA* mRNA degradation is inhibited. PsaA protein concentrations are down-regulated during Fe-starvation (Lefebvre-Legendre *et al.*, 2015). TAA1 protein concentrations also decreased during Fe-starvation in the absence of any change in transcript abundance – suggesting regulation by an uncharacterized post-transcriptional mechanism affects protein turn over (Lefebvre-Legendre *et al.*, 2015). Based on characterization of TAA1, we expect to identify nuclear encoded factors that regulate TAA1 protein abundance post-transcriptionally and additional factors associated with the 5'UTR or chloroplast translational machinery that regulate PSI abundance in response to light quality and quantity (Bonente *et al.*, 2012; Matsui, 2002; Murakami, 1997; Murakami *et al.*, 1997).

We also expected to identify mutants which indirectly inhibit translation from the *psaA* promoter by disrupting PSI biogenesis. Assembling most photosynthetic proteins is a complex process - requiring the sequential assembly of subunits and incorporation of co-factors and pigments. To ensure stoichiometric production for smooth assembly of each photosynthetic complex, unassembled subunits appear to provide negative feedback regulation on their associated mRNAs (Choquet and Wollman, 2002). These negative feedback loops, called control of epistasy of synthesis (CES), regulate the assembly of all photosynthetic complexes in

*Chlamydomonas* and appear to also function in regulating Rubisco subunit stoichiometry in tabacco plastids (Choquet and Wollman, 2002; Lyska *et al.*, 2013; Wostrikoff and Stern, 2007). Feedback inhibition appears to primarily be regulated by interactions between the 5' UTR and domain in its associated unassembled subunit based on work in each photosynthetic component: Photosystem I (Girardbascou *et al.*, 1987; Stampacchia *et al.*, 1997; Takahashi *et al.*, 1991), Photosystem II (Bennoun *et al.*, 1986; de Vitry, 1989; Erickson *et al.*, 1986; Jensen *et al.*, 1986), Cytochrome $b_6f$ (Kuras and Wollman, 1994; Kuras *et al.*, 1995), ATPase (Drapier *et al.*, 1992; Drapier *et al.*, 2007), and Rubisco (Khrebtukova and Spreitzer, 1996). In the case of photosystem I, chloroplast encoded PsaA and PsaB assemble in the early steps of PSI biogenesis forming the chlorophyll a-protein complex I (CP1), which then acts as a template for the assembly of extrinsic PsaC (Yu *et al.*, 1995). CES interactions consequently follow assembly with *psaA* translation requiring *psaB* protein and the 5' UTR of *psaA* (Girardbascou *et al.*, 1987; Stampacchia *et al.*, 1997). *psaA* expression is then required for *psaC* expression (Takahashi *et al.*, 1991). Thus, CES regulation of PSI assembly ensures stoichiometric synthesis of each subunit in its order of assembly. While it is unclear whether other factors are involved in *psaA* CES outside of unassembled PsaA, this processes dependence on the 5'UTR suggests that mutations generated in nuclear proteins involved in regulating *psaB* expression or CES of *psaA* could subsequently lead to translation inhibition of the *psaA* 5' UTR used in this study. We note no mutants identified thus far appear to be candidates for regulating this process.

Currently there are no cytosolic factors implicated in anterograde signaling transduction or mediation. In the following sections we present putative mutants and speculate on their possible function in regulating expression of the *psaA* promoter based on their putative localization and conserved functional domains.

Putative mutants generated in previously characterized genes

Mutant AM56 contains a putative mutation in the 5' UTR of the nuclear encoded *hsp70A*. This heat shock protein does not contain a chloroplast transit peptide sequence and it is unlikely to play a direct role in regulating the *psaA* promoter (Table 4.2). Members of the Hsp70 protein family are proposed to function at every stage of a protein's life cycle – from preventing aggregation during synthesis to recruiting proteins for ubiquitylation and subsequent degradation (Mayer, 2013). Interestingly, the *hsp70A* promoter has shown to be responsive to high light in addition to temperature stress and shows induction in response to magnesium-protoporphyrin IX accumulation (Kropat *et al.*, 2000; von Gromoff *et al.*, 2006; Voss *et al.*, 2011). Magnesium proporphyrin IX is a precursor in chlorophyll biosynthesis that has previously been implicated in retrograde signaling from the chloroplast to the nucleus in *Chlamydomonas* during chloroplast development and in response to dark to light transitions (Kropat *et al.*, 1997; Kropat *et al.*, 2000; Larkin, 2016). Altogether, this suggests a role for *hsp70* in light dependent photoacclimation – but currently its direct function in this process remains uncharacterized. Its identification in this mutant screen suggests that it may play a indirect role in regulating chloroplast gene expression

Mutant AM12 contains a putative mutation in the 3' UTR of a previously characterized oxidoreductase, TBA1, which was previously proposed to influence the accumulation of the PSII protein, PsbA (D1), in response to the chloroplast redox state (Somanchi *et al.*, 2005). It was originally identified in a screen for PSII mutants deficient in *psbA* translation based on a high fluorescence phenotype associated with PSII loss of function mutations (Yohn *et al.*, 1998). Somanchi *et al.* (2005) showed that TBA1 plays a role in regulating the accumulation of the *psbA* associated Poly(A) binding protein (cPAB1) and its association with polyribosomes in the chloroplast. This is proposed to functionally regulate PsbA protein abundance by increasing

translation when the stroma is reduced (Somanchi *et al.*, 2005). Its identification in this study suggests that it may regulate translation of both *psaA and psbA*. This may reflect an analogous regulatory mechanism to that seen in plants where a CSK and SIG1 balance PSII and PSI abundance in response to the reduction state of the thylakoid plastoquinone pool (Khudyakov and Golden, 2001; Puthiyaveetil *et al.*, 2012; Puthiyaveetil *et al.*, 2008; Shimizu *et al.*, 2010).

Uncharacterized mutants with chloroplast transit peptide sequences

We identified 13 uncharacterized proteins with chloroplast transit peptide sequences suggesting that they likely function in regulating *psaA* by directly or indirectly interacting with its associated transcriptional or translation machinery. Below we discuss their possible roles.

AM43 contains a putative deletion in exons 3-5 of a protein (Cre03.g185950) containing 5 zinc finger domains displaying homology to the $Cys_2His_2$ (C2H2) zinc-finger family. C2H2 zinc fingers are among the largest family of zinc-finger proteins and they function most often as transcription factors in eukaryotic organisms, but examples of RNA binding due exist (Fedotova *et al.*, 2017; Kielbowicz-Matuk, 2012). While a number of chloroplast-localized zinc finger proteins have been identified in higher plants, none contain zinc-finger domain associated with nucleotide binding and are all proposed to function as chaperones based on the presence of a DnaJ domain (Fristedt *et al.*, 2014; Munoz-Nortes *et al.*, 2017; Sun *et al.*, 2016; Wang *et al.*, 2016). Cre03.g185950 may act directly on the promoter or 5'UTR of *psaA* gene as either a DNA or RNA binding protein and consequently reflect a new class of RNA or DNA regulator in the chloroplast.

AM78 and AM107 both contain the same putative deletion of an unknown protein containing serine/threonine protein kinase and a leucine rich repeat domain (Cre17.g737463). Leucine-rich repeat receptor like kinases in plants are involved in signaling cascades regulating

response to both biotic and biotic stress (Padmarasu *et al.*, 2018; Thapa *et al.*, 2018; Wang *et al.*, 2016). This suggests that it may be functioning in either a anterograde signaling cascade regulating *psaA* promoter expression directly, or an retrograde signaling cascade that indirectly impacts *psaA* promoter expression by nuclear genome regulation. Alternately, Cre17.g737463 could be facilitating an analogous role to the chloroplast sensor kinase. Kawozoe *et al.* (2012) claimed that the *Chlamydomonas* sigma factor did not undergo phosphorylation based on the absence of changes in electrophoretic mobility observed during diurnal protein abundance characterization. However, this does not rule out phosphorylation and may not have been detected due to only a few phosphorylation sites present in this sigma factor.

AM130 contains a putative deletion in the 3' UTR of a small protein containing a conserved cysteine-rich secretory protein (SCP, Cre01.g013100). The SCP super family has been ascribed a wide range of functions depending on the domain of life. In plants, the SCP-like protein, pathogenesis-related protein 1, accumulates after pathogen infection and is believed to function in pathogen recognition by a sterol binding site and signaling (Breen *et al.*, 2017). In the related chlorophyte, *Volvox carteri, a* member of the same SCP family was identified to be in involved in induction of sexual reproduction and proposed to function as a signal and transducer molecule, an extracellular second messenger, or an unknown role within the stress response (Hallmann, 2007). This suggests, in conjunction with the putative chloroplast transit peptide sequence in Cre01.g013100, that this mutation may be impacting signal reception and transduction of either a known or unknown factor involved in chloroplast genome regulation.

AM106 and AM14 contain insertions in coding regions with no conserved protein domain (unknown function), making their possible role in *psaA* regulation hard to interpret. It may be that the presence of a second mutation site or a genome deletion generated adjacent to

the insertion site could be causing the phenotype. Multiple insertions and deletions were previously shown to occur in 6% and 25% of the time in the analogous mutant library generated by Pollock *et al.* (2017). Consequently, some of the mutants characterized may reflect mutations that are not specific to *psaA* regulation.

Putative mutants without a chloroplast transit peptide sequence

We identified 16 putative target genes without chloroplast transit peptide sequences suggesting that they play a role anterograde signaling associated with *psaA* regulation. Below we discuss the possible roles of putative mutants in regulating the *psaA* promoter.

AM08 contains a putative mutation in the first exon of OTU1 (Cre01.g028550), a protein containing an Ovarian tumor (OTU) -like cysteine protease domain (Messick *et al.*, 2008). OTU-like cysteine proteases function in protein de-ubiquitinase and a distant homolog in plants have been shown to regulate gene expression through epigenetic regulatory mechanisms (Keren and Citovsky, 2017). Keren and Citovsky (2017) showed that *Arabidopsis* OTDL1, a member of the OTU deubiquitinase family, can act as both a transcriptional repressor and transcriptional activator. OTDL1 is proposed to deubiquitylate histones causing depletion of histone modification in euchromatic regions and subsequent repression of gene expression (Keren and Citovsky, 2016). As a transcriptional activator, OTDL1 is proposed to occupy a region of chomatin, deubiquitinating proximal histones causing acetylation and methylation of adjacent regions. This apparent contradiction in regulation was discerned by comparing histone modifications in gain-of-function and loss-of-function alleles that alter OTDL1 transcript abundance, but the exact mechanism of dual action remains unclear. Thus, OTU1 could be performing a similar function to repress or activate expression of a nuclear encoded proteins associated with a anterograde regulation of *psaA*.

AM87 contains a putative mutation in the 3' UTR of a phospholipase A(1) protein(Cre09.g391986). In plants, phospholipase (PLA) is proposed to regulate the abundance of free fatty acids and inositol phosphate lysophosophlipids, which act as signaling compounds and have roles in mediating cellular signaling pathways in plant development and in response to abiotic and biotic stimuli. Type I PLAs can catalyze the hydrolysis of membrane glycerophospholipids (Kim and Ryu, 2014). In plants hydrolyses of phasphatidylcholine Type I PLAs releases linolenic acid for Jasmonic acid biosynthesis and plays a large role in regulation development and stress response in plants (Creelman and Mullet, 1995; shiguro *et al.*, 2001). In *Chlamydomonas,* knock out of type II PLAs leads to an increase in free fatty acid during nitrogen starvation (FFAs)– suggesting that it regulates FFAs storage by catabolism (Shin *et al.*, 2019). Interestingly, in *Chlamydomonas* FFAs accumulate under iron starvation and both iron and nitrogen starvation leads to downregulation of photosynthesis- including PSI (Devadasu *et al.*, 2019; Juergens *et al.*, 2015; Park *et al.*, 2015). While Type I PLAs have not been characterized in algae, one possible hypothesis for its role in regulating *psaA* function is by generating a signal through reduction of FFA catabolism that either directly or indirectly mediates regulation of nuclear expression of *psaA* anterograde factors responsive to iron or nitrogen starvation – like TAA1. However, we note this is highly speculative linkage.

Several proteins without chloroplast transit peptide have annotated domains that suggest a function in a signaling cascade. AM102 (Cre01.g03670) and AM165 (Cre01.g036700) both contain Ser/Threonine protein kinases domains and likely reside in the cytosol. These, in conjunction with putative chloroplast localized Ser/Threonine protein kinase, suggest that there may be a kinase cascade involved in regulation of the *psaA* promoter. The mutant AM26 (Cre02.g110050) contains an Fbox/WD40 domain with a predicted signaling peptide domain.

Fbox/WD40 protein domains commonly function as scaffolds to mediate protein interactions and can mediate a variety of functions from signal transduction to transcriptional regulation-suggesting many possible avenues for this mutation to affect *psaA* expression (Xu and Min, 2011).

Conclusion and future directions

In this study we utilize a new combination of techniques for the identification of nuclear mutations effecting the regulation of chloroplast promoters and use it to identify 29 putative mutants that lead to a decrease in translation of *codA* under the regulation of a *psaA* promoter/5'UTR. Among the mutants with putative mutation sites identified, many reflect mutations in proteins of unknown function with protein domains suggesting either direct effects on *psaA* transcription or translation – as is the case with TBA1 and the putative $Cys_2His_2$ (C2H2) zinc finger identified – or may play a role in cytosolic signaling involved in regulating anterograde signaling to the chloroplast. The TBA1 mutation may represent an analogous mechanism for redox regulation of PSI to PSII ratios to that observed in plants where CSK and SIG1 functionally mediate signaling between the intersystem electron transport chain and the chloroplast genome. Alternately, the uncharacterized ORF Cre17.g737463 may mediate this function based on its kinase domain. Future characterization of these proteins and other interesting candidates will further elucidate differences observed between plants and green algae.

Of the 29 putative mutations characterized thus far, we did not identify a mutation in *taa1* nor proteins containing helical repeats characteristic of ROGEs. This may reflect the small sampling size of mutants characterized thus far, or a high false positive rate among our putative mutants. Future work will focus on verifying the role of putative mutants in regulating the *psaA* promoter/5'UTR by protein quantification of endogenous PsaA protein accumulation,

confirming putative mutation sites by PCR and molecular and biochemical characterization of the role of promising candidates in *psaA* promoter regulation.

Further characterization of the mutant library generated in this study will provide insight into chloroplast genome regulation and as a result – a better understanding of the evolutionary history and divergence in chloroplast genome regulation between algal linages and higher plants.

# CHAPTER 5: SYNOPSIS

The research documented in the previous chapters set out to characterize the physiological responses to growth in variable light and to identify regulatory factors mediating photosynthetic acclimation.

Chapter 2 primarily focused on characterizing the physiological impact that absence of qE has on *Chlamydomonas* during long-term acclimation to saturating or sinusoidal light regimes. This work began by investigating the interactions between qE with qT by using the qE mutant *npq4lhcs1*, qT mutant *stt7-9*, and qE and qT mutant *npq4lhcsr1stt7-9. Stt7-9,* despite use in 13 publications previously had never had its mutation site verified and characterized. I found that this mutation contained background mutations in Rubisco that could potentially impact its physiological response to light. Consequently chapter 2 has focused on the qE mutant *npq4lhcsr1* and early research associated with the *stt7-9* mutant is briefly summarized in Appendix A. Previous work characterizing qE in *Chlamydomonas* had used the LHCSR deficient mutant, *npq4* to look at short-term acclimation to saturating light (Allorent *et al.*, 2013b; Peers *et al.*, 2009). Consequently, work in chapter 2 focused on characterizing the complete LHCSR knockout mutant, *npq4lhcsr1*, which had not yet been characterized. Chapter 2 demonstrated that the absence of LHCSR-dependent NPQ lead to decreased PSII efficiency and had significant, but minimal impacts on growth and carbon accumulation under sinusoidal light conditions. Based on relatively small reduction in growth rates observed in *npq4lhcsr1* when acclimated to sinusoidal light (23%) relative to the high mortality rate (40%) in the *npq4* mutant observed during a short, 4-hour shift from sub-saturating light to high light – I can conclude that LHCSR-dependent NPQ is more important to fitness during short-term acclimation relative to long-term acclimation. This

work provides insight for engineering NPQ capacity and kinetics, a topic of increasing interest for algal cultivation for biofuels, by clarifying the role of qE in long-term acclimation to light regimes mimicking natural, diurnal changes in irradiance (Berteotti *et al.*, 2016; Kromdijk *et al.*, 2016; Perozeni *et al.*, 2018).

In Chapter 3 we sought to characterize the potential compensatory mechanisms involved in limiting the fitness defects observed in *npq4lhcsr1* cells during chapter 2. The absence of any apparent reduction in the electron transport chain in *npq4lhcsr1* cells relative to wild type indicated that this was due to an increase in sink capacity (Cantrell and Peers, 2017). This did not appear to be due to increased carbon accumulation based on the absence of any increase in total organic carbon per cell in *npq4lhcsr1* relative to wild type grown in sinusoidal light. Thus, we hypothesized initially that this was due to an increase in reductant dissipation by light dependent photoreduction, which at the time was gaining growing literary support as an avenue for energy dissipation in algae. This required the development of a membrane inlet mass spectrometry (MIMS) measurement system for delineation of oxygen consumption in the light by isotopic oxygen consumption rates ($^{18}O_2$) in the Peers lab. I designed and constructed this system to be paired with a Dual-PAM fluorometer, allowing measurement of oxygen evolution, oxygen consumption and PSII fluorescence in parallel. To my knowledge, this is the first of its kind and currently is the only instrument for parallel measurement of NPQ and reductant consumption downstream of light harvesting. Surprisingly, I found no evidence to support our initial hypothesis. During the course of this investigation though I made novel observations regarding the roles of mitochondrial respiration and the plastid terminal oxidase during steady state photosynthesis. I later found that *npq4lhscr1* appears to undergo less acceptor side limitation at PSI. This, in the absence of increase light dependent oxygen consumption, and in conjunction

with increased state transition capacity indicated that *Chlamydomonas* primarily acclimates to saturating light in the absence of LHCSR-dependent NPQ by increasing the proportion of linear electron transport through cyclic electron transport pathways. This also appears to also be the case during short-term acclimation experiments based on severe reductions in growth and $CO_2$ fixation observed in the LHCSR-deficient, cyclic electron transport mutant *npq4pgrl1* (Chaux *et al.*, 2017b). Collectively these observations have expanded our understanding of the role of NPQ, AET and CEF in light acclimation and stead-state photosynthesis. In particular, our observations made using our MIMS system have provided the most direct evidence to date for the roles of Mitochondrial and PTOX mediated reductant consumption during light saturated photosynthesis and will provide a jumping off point for future studies.

In chapter 4 I report a study on the identification of nuclear encoded factors regulating chloroplast genome expression. I show using a *psaA* promoter that we can effectively select for loss of expression of a chloroplast encoded positive selectable marker and generated a library of 400 putative *psaA* mutants. Current characterization of the mutant library generated in this study has identified many novel mutants previously unassociated with *psaA* regulation and are now targets for further study. Among these, TBA1 has previously be characterized as a redox dependent regulator of the PSII subunit *psbA* (Somanchi *et al.*, 2005). This suggests that TBA1 may represents a possible novel redox-dependent regulator of the ratio of PSI to PSII. Additionally, we found numerous putative cytosolic and chloroplast kinases that may be involved in a previously un-identified kinase cascade mediating anterograde signaling. Future characterization of this library will provide insights into chloroplast regulation and reveal evolutionary differences between algal and plant linages.

This dissertation expands our understanding of the role of LHCSR-dependent NPQ on long-term acclimation in green algae and compensatory mechanisms that occur in its absence, identified new aspects of the role and function of light dependent oxygen consumption in photosynthesis, and established a new strategy for investigation into chloroplast promoter regulation – resulting in a mutant library with novel regulatory candidates. These contributions will directly advance efforts aimed at both understanding photoprotection and optimizing algal cultivation for outdoor growth.

# REFERENCES


Adams Iii, W.W., Demmig-Adams, B., Rosenstiel, T.N., Brightwell, A.K., and Ebbert, V. (2002). Photosynthesis and Photoprotection in Overwintering Plants. Plant Biology *4*, 545-557.

Adams, M.S., Adams, R.B., Wessman, C.A., and Demmig-Adams, B. (2016). Nutritional Cues Tie Living Organisms to Their Environment and Its Sustainability. Front Nutr *3*, 28.

Adams, W.W., 3rd, Muller, O., Cohu, C.M., and Demmig-Adams, B. (2013). May photoinhibition be a consequence, rather than a cause, of limited plant productivity? Photosynth Res *117*, 31-44.

Akkaya, M.S., and Breitenberger, C.A. (1992). Light regulation of protein-synthesis of factor EF-G in Pear Chloroplasts. Plant Molecular Biology *20*, 791-800.

Albrecht, V., Ingenfeld, A., and Apel, K. (2006). Characterization of the Snowy cotyledon 1 mutant of Arabidopsis thaliana: The impact of chloroplast elongation factor G on chloroplast development and plant vitality. Plant Molecular Biology *60*, 507-518.

Allahverdiyeva, Y., Ermakova, M., Eisenhut, M., Zhang, P., Richaud, P., Hagemann, M., Cournac, L., and Aro, E.-M. (2011). Interplay between flavodiiron proteins and photorespiration in Synechocystis sp. PCC 6803. The Journal of biological chemistry *286*, 24007-24014.

Allahverdiyeva, Y., Mustila, H., Ermakova, M., Bersanini, L., Richaud, P., Ajlani, G., Battchikova, N., Cournac, L., and Aro, E.M. (2013). Flavodiiron proteins Flv1 and Flv3 enable cyanobacterial growth and photosynthesis under fluctuating light. Proc Natl Acad Sci U S A *110*, 4111-4116.

Allen, J.F. (2003). Cyclic, pseudocyclic and noncyclic photophosphorylation: New links in the chain. Trends in plant science *8*, 15-19.

Allen, J.F. (2015). Why chloroplasts and mitochondria retain their own genomes and genetic systems: Colocation for redox regulation of gene expression. Proc Natl Acad Sci U S A *112*, 10231-10238.

Allorent, G., Lefebvre-Legendre, L., Chappuis, R., Kuntz, M., Truong, T.B., Niyogi, K.K., Ulm, R., and Goldschmidt-Clermont, M. (2016). UV-B photoreceptor-mediated protection of the photosynthetic machinery in Chlamydomonas reinhardtii. Proc Natl Acad Sci U S A *113*, 14864-14869.

Allorent, G., Tokutsu, R., Roach, T., Peers, G., Cardol, P., Girard-bascou, J., Petroutsos, D., Kuntz, M., Franck, F., Niyogi, K.K.*, et al.* (2013). A Dual Strategy to Cope with High Light in Chlamydomonas reinhardtii. *25*, 545-557.

Alric, J. (2014). Redox and ATP control of photosynthetic cyclic electron flow in Chlamydomonas reinhardtii: (II) involvement of the PGR5-PGRL1 pathway under anaerobic conditions. Biochim Biophys Acta *1837*, 825-834.

Alric, J., and Johnson, X. (2017). Alternative electron transport pathways in photosynthesis: a confluence of regulation. Curr Opin Plant Biol *37*, 78-86.

Alric, J., Lavergne, J., and Rappaport, F. (2010). Redox and ATP control of photosynthetic cyclic electron flow in Chlamydomonas reinhardtii (I) aerobic conditions. Biochim Biophys Acta *1797*, 44-51.

Alsharafa, K., Vogel, M.O., Oelze, M.L., Moore, M., Stingl, N., Konig, K., Friedman, H., Mueller, M.J., and Dietz, K.J. (2014). Kinetics of retrograde signalling initiation in the high light response of Arabidopsis thaliana. Philosophical transactions of the Royal Society of London Series B, Biological sciences *369*, 20130424.

Anderson, J.M., Chow, W.S., and De Las Rivas, J. (2008). Dynamic flexibility in the structure and function of photosystem II in higher plant thylakoid membranes: the grana enigma. Photosynth Res *98*, 575-587.

Anderson, J.M., Chow, W.S., and Goodchild, D.J. (1988). Thylakoid Membrane Organisation in Sun/Shade Acclimation. Functional Plant Biology *15*, 11-26.

Apel, K., and Hirt, H. (2004). Reactive oxygen species: metabolism, oxidative stress, and signal transduction. Annu Rev Plant Biol *55*, 373-399.

Aro, E.M., Virgin, I., and Andersson, B. (1993a). Photoinhibition of Photosystem II. Inactivation, protein damage and turnover. Biochim Biophys Acta *1143*, 113-134.

Aro, E.M., Virgin, I., and Andersson, B. (1993b). Photoinhibition of Photosystem II. Inactivation, protein damage and turnover. Biochimica et biophysica acta *1143*, 113-134.

Asada, K. (1999a). THE WATER-WATER CYCLE IN CHLOROPLASTS : Scavenging of Active Oxygens and Dissipation of Excess Photons. Annu Rev Plant Physiol Plant Mol Biol *50*, 601-639.

Asada, K. (1999b). THE WATER-WATER CYCLE IN CHLOROPLASTS: Scavenging of Active Oxygens and Dissipation of Excess Photons. Annu Rev Plant Physiol Plant Mol Biol *50*, 601-639.

Asada, K. (2006). Production and scavenging of reactive oxygen species in chloroplasts and their functions. Plant Physiol *141*, 391-396.

Atteia, A., van Lis, R., Tielens, A.G., and Martin, W.F. (2013). Anaerobic energy metabolism in unicellular photosynthetic eukaryotes. Biochim Biophys Acta *1827*, 210-223.

Azevedo, J., Courtois, F., and Lerbs-Mache, S. (2006). Sub-plastidial localization of two different phage-type RNA polymerases in spinach chloroplasts. Nucleic Acids Res *34*, 436-444.

Bailleul, B., Berne, N., Murik, O., Petroutsos, D., Prihoda, J., Tanaka, A., Villanova, V., Bligny, R., Flori, S., Falconet, D.*, et al.* (2015). Energetic coupling between plastids and mitochondria drives CO2 assimilation in diatoms. Nature *524*, 366-369.

Bailleul, B., Rogato, A., de Martino, A., Coesel, S., Cardol, P., Bowler, C., Falciatore, A., and Finazzi, G. (2010). An atypical member of the light-harvesting complex stress-related protein family modulates diatom responses to light. Proc Natl Acad Sci U S A *107*, 18214-18219.

Baker, N.R. (2008). Chlorophyll fluorescence: a probe of photosynthesis in vivo. Annu Rev Plant Biol *59*, 89-113.

Balczun, C., Bunse, A., Hahn, D., Bennoun, P., Nickelsen, J., and Kuck, U. (2005). Two adjacent nuclear genes are required for functional complementation of a chloroplast trans-splicing mutant from Chlamydomonas reinhardtii. Plant Journal *43*, 636-648.

Ballottari, M., Truong, T.B., De Re, E., Erickson, E., Stella, G.R., Fleming, G.R., Bassi, R., and Niyogi, K.K. (2016). Identification of pH-sensing Sites in the Light Harvesting Complex Stress-related 3 Protein Essential for Triggering Non-photochemical Quenching in Chlamydomonas reinhardtii. J Biol Chem *291*, 7334-7346.

Barbrook, A.C., Howe, C.J., and Purton, S. (2006). Why are plastid genomes retained in non-photosynthetic organisms? Trends Plant Sci *11*, 101-108.

Barkan, A. (2011). Expression of plastid genes: organelle-specific elaborations on a prokaryotic scaffold. Plant Physiol *155*, 1520-1532.

Barkan, A., Walker, M., Nolasco, M., and Johnson, D. (1994). A nuclear mutation in maize blocks the processing and translation of several chloroplast mRNAs and provides evidence for the differential translation of alternative mRNA forms. The EMBO Journal *13*, 3170-3181.

Baroli, I., Gutman, B.L., Ledford, H.K., Shin, J.W., Chin, B.L., Havaux, M., and Niyogi, K.K. (2004). Photo-oxidative stress in a xanthophyll-deficient mutant of Chlamydomonas. J Biol Chem *279*, 6337-6344.

Bartoli, C.G., Casalongué, C.A., Simontacchi, M., Marquez-Garcia, B., and Foyer, C.H. (2013). Interactions between hormone and redox signalling pathways in the control of growth and cross tolerance to stress. Environmental and Experimental Botany *94*, 73-88.

Beckmann, K., Messinger, J., Badger, M.R., Wydrzynski, T., and Hillier, W. (2009). On-line mass spectrometry: membrane inlet sampling. Photosynth Res *102*, 511-522.

Bennoun, P., Spiererherz, M., Erickson, J., Girardbascou, J., Pierre, Y., Delosme, M., and Rochaix, J.D. (1986). Characterization of the Photosystem II mutants of chalmydomonas lacking the PsbA gene. Plant Molecular Biology *6*, 151-160.

Bergantino, E., Segalla, A., Brunetta, A., Teardo, E., Rigoni, F., Giacometti, G.M., and Szabo, I. (2003). Light- and pH-dependent structural changes in the PsbS subunit of photosystem II. Proc Natl Acad Sci U S A *100*, 15265-15270.

Bergner, S.V., Scholz, M., Trompelt, K., Barth, J., Gabelein, P., Steinbeck, J., Xue, H., Clowez, S., Fucile, G., Goldschmidt-Clermont, M.*, et al.* (2015). STATE TRANSITION7-Dependent Phosphorylation Is Modulated by Changing Environmental Conditions, and Its Absence Triggers Remodeling of Photosynthetic Protein Complexes. Plant Physiol *168*, 615-634.

Berteotti, S., Ballottari, M., and Bassi, R. (2016). Increased biomass productivity in green algae by tuning non-photochemical quenching. Sci Rep *6*, 21339.

Betterle, N., Ballottari, M., Zorzan, S., de Bianchi, S., Cazzaniga, S., Dall'osto, L., Morosinotto, T., and Bassi, R. (2009). Light-induced dissociation of an antenna hetero-oligomer is needed for non-photochemical quenching induction. J Biol Chem *284*, 15255-15266.

Bhadula, S.K., Elthon, T.E., Habben, J.E., Helentjaris, T.G., Jiao, S.P., and Ristic, Z. (2001). Heat-stress induced synthesis of chloroplast protein synthesis elongation factor (EF-Tu) in a heat-tolerant maize line. Planta *212*, 359-366.

Bisova, K., and Zachleder, V. (2014). Cell-cycle regulation in green algae dividing by multiple fission. J Exp Bot *65*, 2585-2602.

Blankenship, R.E. (2002a). Molecular Mechanisms of Photosynthesis (Osney Mead, Oxford: Blackwell Science LTD).

Blankenship, R.E. (2002b). Molecular Mechanisms of Photosynthesis Vol 1, 1 edn (Oxford, London: Blackwell Science LTD).

Bligny, M., Courtois, F., Thaminy, S., Chang, C.C., Lagrange, T., Baruah-Wolff, J., Stern, D., and Lerbs-Mache, S. (2000). Regulation of plastid rDNA transcription by interaction of CDF2 with two different RNA polymerases. EMBO J *19*, 1851-1860.

Bock, S., Ortelt, J., and Link, G. (2014). AtSIG6 and other members of the sigma gene family jointly but differentially determine plastid target gene expression in Arabidopsis thaliana. Front Plant Sci *5*, 667.

Bohne, A.V., Irihimovitch, V., Weihe, A., and Stern, D.B. (2006). Chlamydomonas reinhardtii encodes a single sigma70-like factor which likely functions in chloroplast transcription. Curr Genet *49*, 333-340.

Bonente, G., Ballottari, M., Truong, T.B., Morosinotto, T., Ahn, T.K., Fleming, G.R., Niyogi, K.K., and Bassi, R. (2011). Analysis of LhcSR3, a protein essential for feedback de-excitation in the green alga Chlamydomonas reinhardtii. PLoS Biol *9*, e1000577.

Bonente, G., Pippa, S., Castellano, S., Bassi, R., and Ballottari, M. (2012). Acclimation of Chlamydomonas reinhardtii to different growth irradiances. J Biol Chem *287*, 5833-5847.

Boratyn, G.M., Schaffer, A.A., Agarwala, R., Altschul, S.F., Lipman, D.J., and Madden, T.L. (2012). Domain enhanced lookup time accelerated BLAST. Biol Direct *7*, 12.

Boudreau, E., Nickelsen, J., Lemaire, S.D., Ossenbuhl, F., and Rochaix, J.D. (2000). The Nac2 gene of Chlamydomonas encodes a chloroplast TPR-like protein involved in psbD mRNA stability. EMBO J *19*, 3366-3376.

Boulouis, A., Raynaud, C., Bujaldon, S., Aznar, A., Wollman, F.A., and Choquet, Y. (2011). The nucleus-encoded trans-acting factor MCA1 plays a critical role in the regulation of cytochrome f synthesis in Chlamydomonas chloroplasts. Plant Cell *23*, 333-349.

Breen, S., Williams, S.J., Outram, M., Kobe, B., and Solomon, P.S. (2017). Emerging Insights into the Functions of Pathogenesis-Related Protein 1. Trends Plant Sci *22*, 871-879.

Brueggeman, A.J., Gangadharaiah, D.S., Cserhati, M.F., Casero, D., Weeks, D.P., and Ladunga, I. (2012). Activation of the carbon concentrating mechanism by CO2 deprivation coincides with massive transcriptional restructuring in Chlamydomonas reinhardtii. Plant Cell *24*, 1860-1875.

Brzezowski, P., Schlicke, H., Richter, A., Dent, R.M., Niyogi, K.K., and Grimm, B. (2014). The GUN4 protein plays a regulatory role in tetrapyrrole biosynthesis and chloroplast-to-nucleus signalling in Chlamydomonas reinhardtii. Plant J *79*, 285-298.

Bukhov, N.G., Wiese, C., Neimanis, S., and Heber, U. (1999). Heat sensitivity of chloroplasts and leaves: Leakage of protons from thylakoids and reversible activation of cyclic electron transport. Photosynthesis Research *59*, 81-93.

Cahoon, A.B., Harris, F.M., and Stern, D.B. (2004). Analysis of developing maize plastids reveals two mRNA stability classes correlating with RNA polymerase type. EMBO Rep *5*, 801-806.

Cantrell, M., and Peers, G. (2017). A mutant of Chlamydomonas without LHCSR maintains high rates of photosynthesis, but has reduced cell division rates in sinusoidal light conditions. PLoS One *12*, e0179395.

Cardol, P., Alric, J., Girard-Bascou, J., Franck, F., Wollman, F.-A., and Finazzi, G. (2009). Impaired respiration discloses the physiological significance of state transitions in Chlamydomonas. Proceedings of the National Academy of Sciences of the United States of America *106*, 15979-15984.

Carter, M.L., Smith, A.C., Kobayashi, H., Purton, S., and Herrin, D.L. (2004). Structure, circadian regulation and bioinformatic analysis of the unique sigma factor gene in Chlamydomonas reinhardtii. Photosynth Res *82*, 339-349.

Chaux, F., Burlacot, A., Mekhalfi, M., Auroy, P., Blangy, S., Richaud, P., and Peltier, G. (2017a). Flavodiiron Proteins Promote Fast and Transient O2 Photoreduction in Chlamydomonas. Plant Physiol *174*, 1825-1836.

Chaux, F., Johnson, X., Auroy, P., Beyly-Adriano, A., Te, I., Cuine, S., and Peltier, G. (2017b). PGRL1 and LHCSR3 Compensate for Each Other in Controlling Photosynthesis and Avoiding Photosystem I Photoinhibition during High Light Acclimation of Chlamydomonas Cells. Mol Plant *10*, 216-218.

Chaux, F., Peltier, G., and Johnson, X. (2015). A security network in PSI photoprotection: regulation of photosynthetic control, NPQ and O2 photoreduction by cyclic electron flow. Front Plant Sci *6*, 875.

Chi, W., Feng, P., Ma, J., and Zhang, L. (2015). Metabolites and chloroplast retrograde signaling. Curr Opin Plant Biol *25*, 32-38.

Chi, W., Sun, X., and Zhang, L. (2013). Intracellular signaling from plastid to nucleus. Annu Rev Plant Biol *64*, 559-582.

Choquet, Y., and Wollman, F.-A. (2002). Translational regulations as specific traits of chloroplast gene expression. FEBS Letters *529*, 39-42.

Clarke, J.E., and Johnson, G.N. (2001). In vivo temperature dependence of cyclic and pseudocyclic electron transport in barley. Planta *212*, 808-816.

Correa-Galvis, V., Poschmann, G., Melzer, M., Stuhler, K., and Jahns, P. (2016a). PsbS interactions involved in the activation of energy dissipation in Arabidopsis. Nat Plants *2*, 15225.

Correa-Galvis, V., Redekop, P., Guan, K., Griess, A., Truong, T.B., Wakao, S., Niyogi, K.K., and Jahns, P. (2016b). Photosystem II Subunit PsbS Is Involved in the Induction of LHCSR Protein-dependent Energy Dissipation in Chlamydomonas reinhardtii. J Biol Chem *291*, 17478-17487.

Cournac, L., Redding, K., Ravenel, J., Rumeau, D., Josse, E.M., Kuntz, M., and Peltier, G. (2000). Electron flow between photosystem II and oxygen in chloroplasts of photosystem I-deficient algae is mediated by a quinol oxidase involved in chlororespiration. The Journal of biological chemistry *275*, 17256-17262.

Craigie, R.A., and Cavaliersmith, T. (1982). Cell-Volume and the Control of the Chlamydomonas Cell-Cycle. J Cell Sci *54*, 173-191.

Creelman, R.A., and Mullet, J.E. (1995). Jasmonic acid distribution and action in plants: regulation during development and response to biotic and abiotic stress. Proceedings of the National Academy of Sciences *92*, 4114-4119.

Cross, F.R., and Umen, J.G. (2015). The Chlamydomonas cell cycle. Plant J *82*, 370-392.

Dai, S., Carcamo, R., Zhang, Z., Chen, S., and Beachy, R.N. (2001). The bacterial cytosine deaminase gene used as a conditional negative selection marker in transgenic rice plants. Plant Cell Reports *20*, 738-743.

DalCorso, G., Pesaresi, P., Masiero, S., Aseeva, E., Schunemann, D., Finazzi, G., Joliot, P., Barbato, R., and Leister, D. (2008). A complex containing PGRL1 and PGR5 is involved in the switch between linear and cyclic electron flow in Arabidopsis. Cell *132*, 273-285.

Dall'Osto, L., Caffarri, S., and Bassi, R. (2005). A mechanism of nonphotochemical energy dissipation, independent from PsbS, revealed by a conformational change in the antenna protein CP26. Plant Cell *17*, 1217-1232.

Dall'Osto, L., Cazzaniga, S., Wada, M., and Bassi, R. (2014). On the origin of a slowly reversible fluorescence decay component in the Arabidopsis npq4 mutant. Philos Trans R Soc Lond B Biol Sci *369*, 20130221.

Dang, K.-v., Plet, J., Tolleter, D., Jokel, M., Carrier, P., Auroy, P., Richaud, P., Johnson, X., Alric, J., Allahverdiyeva, Y.*, et al.* (2014a). Combined Increases in Mitochondrial Cooperation and Oxygen Photoreduction Compensate for Deficiency in Cyclic Electron Flow in Chlamydomonas reinhardtii. 1-16.

de Vitry, C. (1989). Posttranslational events leading to the assembly of photosystem II protein complex: a study using photosynthesis mutants from Chlamydomonas reinhardtii. The Journal of Cell Biology *109*, 991-1006.

Del Campo, E.M., Sabater, B., and Martin, M. (2002). Post-transcriptional control of chloroplast gene expression. Accumulation of stable psaC mRNA is due to downstream RNA cleavages in the ndhD gene. J Biol Chem *277*, 36457-36464.

Delannoy, E., Stanley, W.A., Bond, C.S., and Small, I.D. (2007). Pentatricopeptide repeat (PPR) proteins as sequence-specificity factors in post-transcriptional processes in organelles. Biochem Soc Trans *35*, 1643-1647.

Delsome, R., Olive, Jacqueline, Wollman, Francis-Andre (1996). Changes in light energy distribution upon state transitions: an in vivo photoacoustic study of the wild type and photosynthesis mutants from Chlamydomonas reinhardtii. Biochimica et Biophysica Acta (BBA) - Bioenergetics *150-158*.

Demmig-Adams, B., Cohu, C.M., Muller, O., and Adams, W.W., 3rd (2012). Modulation of photosynthetic energy conversion efficiency in nature: from seconds to seasons. Photosynth Res *113*, 75-88.

Demmig-Adams, B., Stewart, J.J., and Adams, W.W., 3rd (2014). Multiple feedbacks between chloroplast and whole plant in the context of plant adaptation and acclimation to the environment. Philos Trans R Soc Lond B Biol Sci *369*, 20130244.

Depège, N., Bellafiore, S., and Rochaix, J.-D. (2003). Role of chloroplast protein kinase Stt7 in LHCII phosphorylation and state transition in Chlamydomonas. Science (New York, NY) *299*, 1572-1575.

Depege, N., Bellafiore, S., and Rochaix, J.D. (2003). Role of chloroplast protein kinase Stt7 in LHCII phosphorylation and state transition in Chlamydomonas. Science *299*, 1572-1575.

Dera, J., Sagan, S.. Stramski, D (1992). Focusing of sunlight by sea-surface waves: new measurement results from the Black Sea. Proc EPIE.

Derks, A., Schaven, K., and Bruce, D. (2015). Diverse mechanisms for photoprotection in photosynthesis. Dynamic regulation of photosystem II excitation in response to rapid environmental change. Biochim Biophys Acta *1847*, 468-485.

Devadasu, E., Chinthapalli, D.K., Chouhan, N., Madireddi, S.K., Rasineni, G.K., Sripadi, P., and Subramanyam, R. (2019). Changes in the photosynthetic apparatus and lipid droplet formation in Chlamydomonas reinhardtii under iron deficiency. Photosynthesis Research *139*, 253-266.

Dichtl, B., Stevens, A., and Tollervey, D. (1997). Lithium toxicity in yeast is due to the inhibition of RNA processing enzymes. The EMBO Journal *16*, 7184-7195.

Dietz, K.J. (2015). Efficient high light acclimation involves rapid processes at multiple mechanistic levels. Journal of experimental botany.

Dinc, E., Tian, L., Roy, L.M., Roth, R., Goodenough, U., and Croce, R. (2016). LHCSR1 induces a fast and reversible pH-dependent fluorescence quenching in LHCII in Chlamydomonas reinhardtii cells. Proc Natl Acad Sci U S A *113*, 7673-7678.

Drapier, D., Girardbascou, J., and Wollman, F.A. (1992). Evidence for nuclear control of expression of the atpA and atpB chloroplast genes of *Chlamydomonas*. Plant Cell *4*, 283-295.

Drapier, D., Rimbault, B., Vallon, O., Wollman, F.A., and Choquet, Y. (2007). Intertwined translational regulations set uneven stoichiometry of chloroplast ATP synthase subunits. EMBO J *26*, 3581-3591.

Drop, B., Yadav K N, S., Boekema, E.J., and Croce, R. (2014). Consequences of state transitions on the structural and functional organization of Photosystem I in the green alga Chlamydomonas reinhardtii. The Plant journal : for cell and molecular biology.

Duanmu, D., Casero, D., Dent, R.M., Gallaher, S., Yang, W., Rockwell, N.C., Martin, S.S., Pellegrini, M., Niyogi, K.K., Merchant, S.S.*, et al.* (2013). Retrograde bilin signaling enables Chlamydomonas greening and phototrophic survival. Proc Natl Acad Sci U S A *110*, 3621-3626.

Eberhard, S., Drapier, D., and Wollman, F.-A. (2002). Searching limiting steps in the expression of chloroplast-encoded proteins: relations between gene copy number, transcription, transcript abundance and translation rate in the chloroplast of Chlamydomonas reinhardtii. The Plant Journal *31*, 149-160.

Economou, C., Wannathong, T., Szaub, J., and Purton, S. (2014). A Simple, Low-Cost Method for Chloroplast Transformation of the Green Alga Chlamydomonas reinhardtii. In Chloroplast Biotechnology: Methods and Protocols, P. Maliga, ed., pp. 401-411.

Emanuelsson, O., Brunak, S., von Heijne, G., and Nielsen, H. (2007). Locating proteins in the cell using TargetP, SignalP and related tools. Nat Protoc *2*, 953-971.

Erickson, E., Wakao, S., and Niyogi, K.K. (2015). Light stress and photoprotection in Chlamydomonas reinhardtii. Plant J *82*, 449-465.

Erickson, J.M., Rahire, M., Malnoe, P., Girardbascou, J., Pierre, Y., Bennoun, P., and Rochaix, J.D. (1986). Lack of the D2 protein in *Chlamydomonas reinhardtii* psbD mutant affects Photosystem II stability and D1 expression. Embo Journal *5*, 1745-1754.

Escoubas, J.M., Lomas, M., LaRoche, J., and Falkowski, P.G. (1995). Light intensity regulation of cab gene transcription is signaled by the redox state of the plastoquinone pool. Proceedings of the National Academy of Sciences *92*, 10237-10241.

Estavillo, G.M., Chan, K.X., Phua, S.Y., and Pogson, B.J. (2013). Reconsidering the nature and mode of action of metabolite retrograde signals from the chloroplast. Frontiers in Plant Science *3*.

Falkowski, P.G., and Raven, J.A. (2007). Aqautic photosynthesis (Princeton, New Jersey: Princeton University Press ).

Falkowski, P.G., and Raven, J.A. (2013). Aquatic Photosynthesis. Princeton University Press

Fedotova, A.A., Bonchuk, A.N., Mogila, V.A., and Georgiev, P.G. (2017). C2H2 Zinc Finger Proteins: The Largest but Poorly Explored Family of Higher Eukaryotic Transcription Factors. Acta Naturae *9*, 47-58.

Feklistov, A., Sharon, B.D., Darst, S.A., and Gross, C.A. (2014). Bacterial Sigma Factors: A Historical, Structural, and Genomic Perspective. In Annual Review of Microbiology, Vol 68, S. Gottesman, ed., pp. 357-376.

Fey, V., Wagner, R., Brautigam, K., Wirtz, M., Hell, R., Dietzmann, A., Leister, D., Oelmuller, R., and Pfannschmidt, T. (2005). Retrograde plastid redox signals in the expression of nuclear genes for chloroplast proteins of Arabidopsis thaliana. J Biol Chem *280*, 5318-5328.

Finazzi, G., and Minagawa, J. (2014). High Light Acclimation in Green Microalgae. In Non-Photochemical Quenching and Energy Dissipation in Plants, Algae and Cyanobacteria, B. DemmigAdams, G. Garab, W. Adams, and Govindjee, eds., pp. 445-469.

Finazzi, G., Minagawa, J., and Johnson, G.N. (2016). The Cytochrome b 6 f Complex: A Regulatory Hub Controlling Electron Flow and the Dynamics of Photosynthesis? In Cytochrome Complexes: Evolution, Structures, Energy Transduction, and Signaling, W.A. Cramer, and T. Kallas, eds. (Dordrecht: Springer Netherlands), pp. 437-452.

Fischer, B.B., Ledford, H.K., Wakao, S., Huang, S.G., Casero, D., Pellegrini, M., Merchant, S.S., Koller, A., Eggen, R.I., and Niyogi, K.K. (2012). SINGLET OXYGEN RESISTANT 1 links reactive electrophile signaling to singlet oxygen acclimation in Chlamydomonas reinhardtii. Proc Natl Acad Sci U S A *109*, E1302-1311.

Fleischmann, M.M., Ravanel, S., Delosme, R., Olive, J., Zito, F., Wollman, F.a., and Rochaix, J.D. (1999). Isolation and characterization of photoautotrophic mutants of Chlamydomonas reinhardtii deficient in state transition. The Journal of biological chemistry *274*, 30987-30994.

Forti, G. (2008). The role of respiration in the activation of photosynthesis upon illumination of dark adapted Chlamydomonas reinhardtii. Biochim Biophys Acta *1777*, 1449-1454.

Forti, G., and Fusi, P. (1990). Influence of thylakoid protein phosphorylation on Emerson enhancement and the quantum requirement of Photosystem I. Biochimica et Biophysica Acta (BBA) - Bioenergetics *1020*, 247-252.

Fristedt, R., Williams-Carrier, R., Merchant, S.S., and Barkan, A. (2014). A Thylakoid Membrane Protein Harboring a DnaJ-type Zinc Finger Domain Is Required for Photosystem I Accumulation in Plants. Journal of Biological Chemistry *289*, 30657-30667.

Fujita, Y., Takagi, H., and Hase, T. (1996). Identification of the chlB gene and the gene product essential for the light-independent chlorophyll biosynthesis in the cyanobacterium Plectonema boryanum. Plant Cell Physiol *37*, 313-323.

Funk, C., Schroder, W.P., Napiwotzki, A., Tjus, S.E., Renger, G., and Andersson, B. (1995). The PSII-S protein of higher plants: a new type of pigment-binding protein. Biochemistry-Us *34*, 11133-11141.

Gans, P., and Rebeille, F. (1990). Control in the Dark of the Plastoquinone Redox State by Mitochondrial Activity in Chlamydomonas-Reinhardtii. Biochimica Et Biophysica Acta *1015*, 150-155.

Gerotto, C., Alboresi, A., Giacometti, G.M., Bassi, R., and Morosinotto, T. (2011). Role of PSBS and LHCSR in Physcomitrella patens acclimation to high light and low temperature. Plant, cell & environment *34*, 922-932.

Gerotto, C., Alboresi, A., Giacometti, G.M., Bassi, R., and Morosinotto, T. (2012). Coexistence of plant and algal energy dissipation mechanisms in the moss Physcomitrella patens. New Phytol *196*, 763-773.

Gerotto, C., Alboresi, A., Meneghesso, A., Jokel, M., Suorsa, M., Aro, E.M., and Morosinotto, T. (2016). Flavodiiron proteins act as safety valve for electrons in Physcomitrella patens. Proc Natl Acad Sci U S A *113*, 12322-12327.

Gilroy, S., Suzuki, N., Miller, G., Choi, W.G., Toyota, M., Devireddy, A.R., and Mittler, R. (2014). A tidal wave of signals: calcium and ROS at the forefront of rapid systemic signaling. Trends in plant science *19*, 623-630.

Giovagnetti, V., and Ruban, A.V. (2018). The evolution of the photoprotective antenna proteins in oxygenic photosynthetic eukaryotes. Biochem Soc Trans *46*, 1263-1277.

Girardbascou, J., Choquet, Y., Schneider, M., Delosme, M., and Dron, M. (1987). Characterization of a chloroplast mutation in the *psaA2* gene of *Chlamydomonas rienhartii*. Current Genetics *12*, 489-495.

Girolomoni, L., Cazzaniga, S., Pinnola, A., Perozeni, F., Ballottari, M., and Bassi, R. (2019). LHCSR3 is a nonphotochemical quencher of both photosystems in Chlamydomonas reinhardtii. Proc Natl Acad Sci U S A.

Glanz, S., Bunse, A., Wimbert, A., Balczun, C., and Kuck, U. (2006). A nucleosome assembly protein-like polypeptide binds to chloroplast group II intron RNA in Chlamydomonas reinhardtii. Nucleic Acids Research *34*, 5337-5351.

Glasser, C., Haberer, G., Finkemeier, I., Pfannschmidt, T., Kleine, T., Leister, D., Dietz, K.J., Hausler, R.E., Grimm, B., and Mayer, K.F. (2014). Meta-analysis of retrograde signaling in Arabidopsis thaliana reveals a core module of genes embedded in complex cellular signaling networks. Mol Plant *7*, 1167-1190.

Golan, T., Muller-Moule, P., and Niyogi, K.K. (2006). Photoprotection mutants of Arabidopsis thaliana acclimate to high light by increasing photosynthesis and specific antioxidants. Plant Cell Environ *29*, 879-887.

Golding, A.J., Finazzi, G., and Johnson, G.N. (2004). Reduction of the thylakoid electron transport chain by stromal reductants--evidence for activation of cyclic electron transport upon dark adaptation or under drought. Planta *220*, 356-363.

Gonzalez-Perez, S., Gutierrez, J., Garcia-Garcia, F., Osuna, D., Dopazo, J., Lorenzo, O., Revuelta, J.L., and Arellano, J.B. (2011). Early transcriptional defense responses in Arabidopsis cell suspension culture under high-light conditions. Plant physiology *156*, 1439-1456.

Goss, R., and Lepetit, B. (2015). Biodiversity of NPQ. J Plant Physiol *172*, 13-32.

Gumpel, N.J., Ralley, L., Girard-Bascou, J., Wollman, F.A., Nugent, J.H., and Purton, S. (1995). Nuclear mutants of Chlamydomonas reinhardtii defective in the biogenesis of the cytochrome b6f complex. Plant Mol Biol *29*, 921-932.

Gutle, D.D., Roret, T., Muller, S.J., Couturier, J., Lemaire, S.D., Hecker, A., Dhalleine, T., Buchanan, B.B., Reski, R., Einsle, O.*, et al.* (2016). Chloroplast FBPase and SBPase are thioredoxin-linked enzymes with similar architecture but different evolutionary histories. Proc Natl Acad Sci U S A *113*, 6779-6784.

Hallmann, A. (2007). A small cysteine-rich extracellular protein, VCRP, is inducible by the sex-inducer of Volvox carteri and by wounding. Planta *226*, 719-727.

Hammani, K., Bonnard, G., Bouchoucha, A., Gobert, A., Pinker, F., Salinas, T., and Giege, P. (2014). Helical repeats modular proteins are major players for organelle gene expression. Biochimie *100*, 141-150.

Hanaoka, M., Kanamaru, K., Takahashi, H., and Tanaka, K. (2003). Molecular genetic analysis of chloroplast gene promoters dependent on SIG2, a nucleus-encoded sigma factor for the plastid-encoded RNA polymerase, in Arabidopsis thaliana. Nucleic Acids Res *31*, 7090-7098.

Harbinson, J., and Foyer, C.H. (1991). Relationships between the Efficiencies of Photosystems I and II and Stromal Redox State in CO2-Free Air : Evidence for Cyclic Electron Flow in Vivo. Plant Physiology *97*, 41-49.

Harley, C.B., and Reynolds, R.P. (1987). Analysis of E.Coli Pormoter sequences. Nucleic Acids Research *15*, 2343-2361.

Havaux, M. (1996). Short-term responses of Photosystem I to heat stress : Induction of a PS II-independent electron transport through PS I fed by stromal components. Photosynth Res *47*, 85-97.

Hedtke, B., Borner, T., and Weihe, A. (1997). Mitochondrial and chloroplast phage-type RNA polymerases in Arabidopsis. Science *277*, 809-811.

Hedtke, B., Borner, T., and Weihe, A. (2000). One RNA polymerase serving two genomes. EMBO Rep *1*, 435-440.

Hertle, A.P., Blunder, T., Wunder, T., Pesaresi, P., Pribil, M., Armbruster, U., and Leister, D. (2013a). PGRL1 is the elusive ferredoxin-plastoquinone reductase in photosynthetic cyclic electron flow. Mol Cell *49*, 511-523.

Hertle, A.P., Blunder, T., Wunder, T., Pesaresi, P., Pribil, M., Armbruster, U., and Leister, D. (2013b). PGRL1 is the elusive ferredoxin-plastoquinone reductase in photosynthetic cyclic electron flow. Molecular cell *49*, 511-523.

Hirose, T., and Sugiura, M. (1997). Both RNA editing and RNA cleavage are required for translation of tobacco chloroplast ndhD mRNA: a possible regulatory mechanism for the expression of a chloroplast operon consisting of functionally unrelated genes. EMBO J *16*, 6804-6811.

Hochmal, A.K., Schulze, S., Trompelt, K., and Hippler, M. (2015). Calcium-dependent regulation of photosynthesis. Biochim Biophys Acta.

Hodges, D.M., DeLong, J.M., Forney, C.F., and Prange, R.K. (1999). Improving the thiobarbituric acid-reactive-substances assay for estimating lipid peroxidation in plant tissues containing anthocyanin and other interfering compounds. Planta *207*, 604-611.

Hoefnagel, M.H.N., Atkin, O.K., and Wiskich, J.T. (1998). Interdependence between chloroplasts and mitochondria in the light and the dark. Biochimica et Biophysica Acta (BBA) - Bioenergetics *1366*, 235-255.

Holzwarth, A.R., Miloslavina, Y., Nilkens, M., and Jahns, P. (2009). Identification of two quenching sites active in the regulation of photosynthetic light-harvesting studied by time-resolved fluorescence. Chem Phys Lett *483*, 262-267.

Horton, P. (2012). Optimization of light harvesting and photoprotection: molecular mechanisms and physiological consequences. Philos Trans R Soc Lond B Biol Sci *367*, 3455-3465.

Horton, P., Ruban, A.V., and Walters, R.G. (1994). Regulation of Light Harvesting in Green Plants (Indication by Nonphotochemical Quenching of Chlorophyll Fluorescence). Plant Physiol *106*, 415-420.

Houille-vernes, L., Rappaport, F., Wollman, F.-a., Alric, J., and Johnson, X. (2011a). Plastid terminal oxidase 2 (PTOX2) is the major oxidase involved in chlororespiration in Chlamydomonas. *2*.

Huckauf, J., Nomura, C., Forchhammer, K., and Hagemann, M. (2000). Stress responses of Synechocystis sp. strain PCC 6803 mutants impaired in genes encoding putative alternative sigma factors. Microbiology *146 ( Pt 11)*, 2877-2889.

Ifuku, K., Ishihara, S., Shimamoto, R., Ido, K., and Sato, F. (2008). Structure, function, and evolution of the PsbP protein family in higher plants. Photosynthesis research *98*, 427-437.

Ilik, P., Pavlovic, A., Kouril, R., Alboresi, A., Morosinotto, T., Allahverdiyeva, Y., Aro, E.M., Yamamoto, H., and Shikanai, T. (2017). Alternative electron transport mediated by flavodiiron proteins is operational in organisms from cyanobacteria up to gymnosperms. New Phytol *214*, 967-972.

Imamura, S., Yoshihara, S., Nakano, S., Shiozaki, N., Yamada, A., Tanaka, K., Takahashi, H., Asayama, M., and Shirai, M. (2003). Purification, Characterization, and Gene Expression of All Sigma Factors of RNA Polymerase in a Cyanobacterium. Journal of Molecular Biology *325*, 857-872.

Ishihama, A. (1988). Promoter selectivity of prokaryotic RNA polymerases. Trends Genet *4*, 282-286.

Ishizaki, Y., Tsunoyama, Y., Hatano, K., Ando, K., Kato, K., Shinmyo, A., Kobori, M., Takeba, G., Nakahira, Y., and Shiina, T. (2005). A nuclear-encoded sigma factor, Arabidopsis SIG6, recognizes sigma-70 type chloroplast promoters and regulates early chloroplast development in cotyledons. Plant J *42*, 133-144.

Iwai, M., Takizawa, K., Tokutsu, R., Okamuro, A., Takahashi, Y., and Minagawa, J. (2010). Isolation of the elusive supercomplex that drives cyclic electron flow in photosynthesis. Nature *464*, 1210-1213.

Jallet, D., Caballero, M.A., Gallina, A.A., Youngblood, M., and Peers, G. (2016a). Photosynthetic physiology and biomass partitioning in the model diatom Phaeodactylum tricornutum grown in a sinusoidal light regime. Algal Res *18*, 51-60.

Jallet, D., Cantrell, M., and Peers, G. (2016b). Chloroplasts: Current research and future trends (Caister Academic Press).

Jans, F., Mignolet, E., Houyoux, P.A., Cardol, P., Ghysels, B., Cuine, S., Cournac, L., Peltier, G., Remacle, C., and Franck, F. (2008). A type II NAD(P)H dehydrogenase mediates light-independent plastoquinone reduction in the chloroplast of Chlamydomonas. Proc Natl Acad Sci U S A *105*, 20546-20551.

Jensen, K.H., Herrin, D.L., Plumley, F.G., and Schmidt, G.W. (1986). Biogenesis of photosystem II complexes – transcriptional, translational, and post-translational regulation. Journal of Cell Biology *103*, 1315-1325.

Jia, H., Liggins, J.R., and Chow, W.S. (2012). Acclimation of leaves to low light produces large grana: the origin of the predominant attractive force at work. Philos Trans R Soc Lond B Biol Sci *367*, 3494-3502.

Joet, T., Cournac, L., Horvath, E.M., Medgyesy, P., and Peltier, G. (2001). Increased sensitivity of photosynthesis to antimycin A induced by inactivation of the chloroplast ndhB gene. Evidence for a participation of the NADH-dehydrogenase complex to cyclic electron flow around photosystem I. Plant Physiol *125*, 1919-1929.

Johnson, M.P., Goral, T.K., Duffy, C.D., Brain, A.P., Mullineaux, C.W., and Ruban, A.V. (2011). Photoprotective energy dissipation involves the reorganization of photosystem II light-harvesting complexes in the grana membranes of spinach chloroplasts. Plant Cell *23*, 1468-1479.

Johnson, X., and Alric, J. (2012). Interaction between starch breakdown, acetate assimilation, and photosynthetic cyclic electron flow in Chlamydomonas reinhardtii. J Biol Chem *287*, 26445-26452.

Johnson, X., Steinbeck, J., Dent, R.M., Takahashi, H., Richaud, P., Ozawa, S., Houille-Vernes, L., Petroutsos, D., Rappaport, F., Grossman, A.R.*, et al.* (2014). Proton gradient regulation 5-mediated cyclic electron flow under ATP- or redox-limited conditions: a study of DeltaATpase pgr5 and DeltarbcL pgr5 mutants in the green alga Chlamydomonas reinhardtii. Plant Physiol *165*, 438-452.

Jokel, M., Johnson, X., Peltier, G., Aro, E.M., and Allahverdiyeva, Y. (2018). Hunting the main player enabling Chlamydomonas reinhardtii growth under fluctuating light. Plant J *94*, 822-835.

Joliot, P., and Johnson, G.N. (2011). Regulation of cyclic and linear electron flow in higher plants. Proceedings of the National Academy of Sciences of the United States of America *108*, 13317-13322.

Joliot, P., and Joliot, A. (2002). Cyclic electron transfer in plant leaf. Proc Natl Acad Sci U S A *99*, 10209-10214.

Joliot, P., and Joliot, A. (2005). Quantification of cyclic and linear flows in plants. Proc Natl Acad Sci U S A *102*, 4913-4918.

Juergens, M.T., Deshpande, R.R., Lucker, B.F., Park, J.-J., Wang, H., Gargouri, M., Holguin, F.O., Disbrow, B., Schaub, T., Skepper, J.N.*, et al.* (2015). The regulation of photosynthetic structure and function during nitrogen deprivation in Chlamydomonas reinhardtii. Plant physiology *167*, 558-573.

Juergens, M.T., Disbrow, B., and Shachar-Hill, Y. (2016). The Relationship of Triacylglycerol and Starch Accumulation to Carbon and Energy Flows during Nutrient Deprivation in Chlamydomonas reinhardtii. Plant Physiol *171*, 2445-2457.

Juszczuk, I.M., and Rychter, A.M. (2003). Alternative oxidase in higher plants. Acta Biochim Pol *50*, 1257-1271.

Kana, T.M., Darkangelo, C., Hunt, M.D., Oldham, J.B., Bennett, G.E., and Cornwell, J.C. (2002). Membrane Inlet Mass Spectrometer for Rapid High-Precision Determination of N2, O2, and Ar in Environmental Water Samples. Anal Chem *66*, 4166-4170.

Kanamaru, K., Nagashima, A., Fujiwara, M., Shimada, H., Shirano, Y., Nakabayashi, K., Shibata, D., Tanaka, K., and Takahashi, H. (2001). An Arabidopsis sigma factor (SIG2)-dependent expression of plastid-encoded tRNAs in chloroplasts. Plant Cell Physiol *42*, 1034-1043.

Kawazoe, R., Mahan, K.M., Venghaus, B.E., Carter, M.L., and Herrin, D.L. (2012). Circadian regulation of chloroplast transcription in Chlamydomonas is accompanied by little or no fluctuation in RPOD levels or core RNAP activity. Mol Biol Rep *39*, 10565-10571.

Kaye, Y., Huang, W., Clowez, S., Saroussi, S., Idoine, A., Sanz-Luque, E., and Grossman, A.R. (2019). The mitochondrial alternative oxidase from Chlamydomonas reinhardtii enables survival in high light. J Biol Chem *294*, 1380-1395.

Keeling, P.J. (2013). The Number, Speed, and Impact of Plastid Endosymbioses in Eukaryotic Evolution. In Annu Rev Plant Biol, S.S. Merchant, ed., pp. 583-607.

Keren, I., and Citovsky, V. (2016). The histone deubiquitinase OTLD1 targets euchromatin to regulate plant growth. Sci Signal *9*, ra125.

Keren, I., and Citovsky, V. (2017). Activation of gene expression by histone deubiquitinase OTLD1. Epigenetics *12*, 584-590.

Khrebtukova, I., and Spreitzer, R.J. (1996). Elimination of the Chlamydomonas gene family that encodes the small subunit of ribulose-1,5-bisphosphate carboxylase/oxygenase. Proceedings of the National Academy of Sciences *93*, 13689-13693.

Khudyakov, I.Y., and Golden, J.W. (2001). Identification and inactivation of three group 2 sigma factor genes in Anabaena sp. strain PCC 7120. J Bacteriol *183*, 6667-6675.

Kielbowicz-Matuk, A. (2012). Involvement of plant C(2)H(2)-type zinc finger transcription factors in stress responses. Plant Sci *185-186*, 78-85.

Kim, H.J., and Ryu, S.B. (2014). sPLA(2) and PLA(1): Secretory Phospholipase A(2) and Phospholipase A(1) in Plants. In Phospholipases in Plant Signaling, X. Wang, ed., pp. 109-118.

Klughammer, C.U.S. (2008). Saturation Pulse method for assessment of energy conversion in PS I PAM Application Notes *1*, 11-14.

Kolber, Z.S., Prasil, O., and Falkowski, P.G. (1998). Measurements of variable chlorophyll fluorescence using fast repetition rate techniques: defining methodology and experimental protocols. Bba-Bioenergetics *1367*, 88-106.

Kouril, R., Wientjes, E., Bultema, J.B., Croce, R., and Boekema, E.J. (2013). High-light vs. low-light: Effect of light acclimation on photosystem II composition and organization in Arabidopsis thaliana. Biochimica Et Biophysica Acta-Bioenergetics *1827*, 411-419.

Kramer, D.M., and Evans, J.R. (2011). The importance of energy balance in improving photosynthetic productivity. Plant physiology *155*, 70-78.

Kramer, D.M., Johnson, G., Kiirats, O., and Edwards, G.E. (2004). New Fluorescence Parameters for the Determination of QA Redox State and Excitation Energy Fluxes. Photosynth Res *79*, 209.

Krieger-Liszkay, A. (2005). Singlet oxygen production in photosynthesis. J Exp Bot *56*, 337-346.

Krieger-Liszkay, A., Fufezan, C., and Trebst, A. (2008). Singlet oxygen production in photosystem II and related protection mechanism. Photosynth Res *98*, 551-564.

Kromdijk, J., Glowacka, K., Leonelli, L., Gabilly, S.T., Iwai, M., Niyogi, K.K., and Long, S.P. (2016). Improving photosynthesis and crop productivity by accelerating recovery from photoprotection. Science *354*, 857-861.

Kropat, J., Hong-Hermesdorf, A., Casero, D., Ent, P., Castruita, M., Pellegrini, M., Merchant, S.S., and Malasarn, D. (2011). A revised mineral nutrient supplement increases biomass and growth rate in Chlamydomonas reinhardtii. Plant J *66*, 770-780.

Kropat, J., Oster, U., Rudiger, W., and Beck, C.F. (1997). Chlorophyll precursors are signals of chloroplast origin involved in light induction of nuclear heat-shock genes. Proc Natl Acad Sci U S A *94*, 14168-14172.

Kropat, J., Oster, U., Rudiger, W., and Beck, C.F. (2000). Chloroplast signalling in the light induction of nuclear HSP70 genes requires the accumulation of chlorophyll precursors and their accessibility to cytoplasm/nucleus. The Plant Journal *24*, 523-531.

Ku, C., Nelson-Sathi, S., Roettger, M., Sousa, F.L., Lockhart, P.J., Bryant, D., Hazkani-Covo, E., McInerney, J.O., Landan, G., and Martin, W.F. (2015). Endosymbiotic origin and differential loss of eukaryotic genes. Nature *524*, 427-432.

Kubota, Y., Miyao, A., Hirochika, H., Tozawa, Y., Yasuda, H., Tsunoyama, Y., Niwa, Y., Imamura, S., Shirai, M., and Asayama, M. (2007). Two novel nuclear genes, OsSIG5 and OsSIG6, encoding potential plastid sigma factors of RNA polymerase in rice: tissue-specific and light-responsive gene expression. Plant Cell Physiol *48*, 186-192.

Kuck, U., Choquet, Y., Schneider, M., Dron, M., and Bennoun, P. (1987). Structural and transcription analysis of 2 homologous genes for the p700 chlorophyll A-Apoproteins in *chlamydomonas reinhartii* – evidence for *in vivo* trans splicing. Embo Journal *6*, 2185-2195.

Kudoh, H., and Sonoike, K. (2002). Irreversible damage to photosystem I by chilling in the light: Cause of the degradation of chlorophyll after returning to normal growth temperature. Planta *215*, 541-548.

Kulheim, C., Agren, J., and Jansson, S. (2002). Rapid regulation of light harvesting and plant fitness in the field. Science *297*, 91-93.

Kuras, R., and Wollman, F.A. (1994). The assembly of cytochrome b6/f complexes: an approach using genetic transformation of the green alga Chlamydomonas reinhardtii. The EMBO Journal *13*, 1019-1027.

Kuras, R., Wollman, F.A., and Joliot, P. (1995). Conversion of cytochrom-f to a soluble form *in vivo* in *Chalmydomonas reinhartii*. Biochemistry *34*, 7468-7475.

Lakshmi, B., Mishra, M., Srinivasan, N., and Archunan, G. (2015). Structure-Based Phylogenetic Analysis of the Lipocalin Superfamily. PLoS One *10*, e0135507.

Larkin, R.M. (2016). Tetrapyrrole Signaling in Plants. Front Plant Sci *7*, 1586.

Larosa, V., Meneghesso, A., La Rocca, N., Steinbeck, J., Hippler, M., Szabo, I., and Morosinotto, T. (2018). Mitochondria Affect Photosynthetic Electron Transport and Photosensitivity in a Green Alga. Plant Physiol *176*, 2305-2314.

Lata, C., and Prasad, M. (2011). Role of DREBs in regulation of abiotic stress responses in plants. Journal of Experimental Botany *62*, 4731-4748.

Ledford, H.K., Baroli, I., Shin, J.W., Fischer, B.B., Eggen, R.I., and Niyogi, K.K. (2004). Comparative profiling of lipid-soluble antioxidants and transcripts reveals two phases of photo-oxidative stress in a xanthophyll-deficient mutant of Chlamydomonas reinhardtii. Mol Genet Genomics *272*, 470-479.

Lefebvre-Legendre, L., Choquet, Y., Kuras, R., Loubery, S., Douchi, D., and Goldschmidt-Clermont, M. (2015). A nucleus-encoded chloroplast protein regulated by iron availability governs expression of the photosystem I subunit PsaA in Chlamydomonas reinhardtii. Plant Physiol *167*, 1527-1540.

Lefebvre-Legendre, L., Reifschneider, O., Kollipara, L., Sickmann, A., Wolters, D., Kuck, U., and Goldschmidt-Clermont, M. (2016). A pioneer protein is part of a large complex involved in trans-splicing of a group II intron in the chloroplast of Chlamydomonas reinhardtii. Plant J *85*, 57-69.

Lemaire, D., Quesada, A., Merchan, F., Corral, J.M., and Igeno, M.I. (2005). NADP-Malate Dehydrogenase from Unicellular Green Alga Chlamydomonas reinhardtii . A First Step toward Redox Regulation ? 1. *137*, 514-521.

Lemeille, S., Willig, A., Depège-Fargeix, N., Delessert, C., Bassi, R., and Rochaix, J.-D. (2009a). Analysis of the chloroplast protein kinase Stt7 during state transitions. PLoS biology *7*, e45.

Lemeille, S., Willig, A., Depege-Fargeix, N., Delessert, C., Bassi, R., and Rochaix, J.D. (2009b). Analysis of the chloroplast protein kinase Stt7 during state transitions. PLoS Biol *7*, e45.

Lepetit, B., Sturm, S., Rogato, A., Gruber, A., Sachse, M., Falciatore, A., Kroth, P.G., and Lavaud, J. (2013). High light acclimation in the secondary plastids containing diatom Phaeodactylum tricornutum is triggered by the redox state of the plastoquinone pool. Plant Physiol *161*, 853-865.

Lerbs-Mache, S. (1993). The 110-kDa polypeptide of spinach plastid DNA-dependent RNA polymerase: single-subunit enzyme or catalytic core of multimeric enzyme complexes? Proceedings of the National Academy of Sciences *90*, 5509-5513.

Lerbs-Mache, S. (2011). Function of plastid sigma factors in higher plants: regulation of gene expression or just preservation of constitutive transcription? Plant Mol Biol *76*, 235-249.

Li, Z., Peers, G., Dent, R.M., Bai, Y., Yang, S.Y., Apel, W., Leonelli, L., and Niyogi, K.K. (2016). Evolution of an atypical de-epoxidase for photoprotection in the green lineage. Nat Plants *2*, 16140.

Liguori, N., Roy, L.M., Opacic, M., Durand, G., and Croce, R. (2013). Regulation of light harvesting in the green alga Chlamydomonas reinhardtii: the C-terminus of LHCSR is the knob of a dimmer switch. J Am Chem Soc *135*, 18339-18342.

Loschelder, H., Schweer, J., Link, B., and Link, G. (2006). Dual temporal role of plastid sigma factor 6 in Arabidopsis development. Plant Physiol *142*, 642-650.

Lucker, B., and Kramer, D.M. (2013a). Regulation of cyclic electron flow in Chlamydomonas reinhardtii under fluctuating carbon availability. Photosynth Res *117*, 449-459.

Lucker, B.F., Hall, C.C., Zegarac, R., and Kramer, D.M. (2014). The environmental photobioreactor (ePBR): An algal culturing platform for simulating dynamic natural environments. Algal Res *6*, 242-249.

Lysenko, E.A. (2006). Analysis of the evolution of the family of the Sig genes encoding plant sigma factors. Russian Journal of Plant Physiology *53*, 605-614.

Lysenko, E.A. (2007). Plant sigma factors and their role in plastid transcription. Plant Cell Rep *26*, 845-859.

Lyska, D., Meierhoff, K., and Westhoff, P. (2013). How to build functional thylakoid membranes: from plastid transcription to protein complex assembly. Planta *237*, 413-428.

Magdaong, N.C.M., and Blankenship, R.E. (2018). Photoprotective, excited-state quenching mechanisms in diverse photosynthetic organisms. J Biol Chem *293*, 5018-5025.

Malnoë, A. (2018). Photoinhibition or photoprotection of photosynthesis? Update on the (newly termed) sustained quenching component qH. Environmental and Experimental Botany *154*, 123-133.

Malnoe, A., Schultink, A., Shahrasbi, S., Rumeau, D., Havaux, M., and Niyogi, K.K. (2018). The Plastid Lipocalin LCNP Is Required for Sustained Photoprotective Energy Dissipation in Arabidopsis. Plant Cell *30*, 196-208.

Malnoe, A., Wang, F., Girard-Bascou, J., Wollman, F.A., and de Vitry, C. (2014). Thylakoid FtsH protease contributes to photosystem II and cytochrome b6f remodeling in Chlamydomonas reinhardtii under stress conditions. Plant Cell *26*, 373-390.

Manavski, N., Schmid, L.M., and Meirer, J. (2018). RNA-stabilization factors in chloroplasts of vascular plants. In Chloroplasts: The Capture and Production Modules of Plants, S. Gutteridge, ed., pp. 51-64.

Marchler-Bauer, A., Bo, Y., Han, L., He, J., Lanczycki, C.J., Lu, S., Chitsaz, F., Derbyshire, M.K., Geer, R.C., Gonzales, N.R.*, et al.* (2017). CDD/SPARCLE: functional classification of proteins via subfamily domain architectures. Nucleic Acids Res *45*, D200-D203.

Marin-Navarro, J., Manuell, A.L., Wu, J., and S, P.M. (2007). Chloroplast translation regulation. Photosynth Res *94*, 359-374.

Maruyama, S., Tokutsu, R., and Minagawa, J. (2014). Transcriptional regulation of the stress-responsive light harvesting complex genes in Chlamydomonas reinhardtii. Plant Cell Physiol *55*, 1304-1310.

Mathur, S., Jain, L., and Jajoo, A. (2018). Photosynthetic efficiency in sun and shade plants. Photosynthetica *56*, 354-365.

Mathy, G., Cardol, P., Dinant, M., Blomme, A., Gerin, S., Cloes, M., Ghysels, B., DePauw, E., Leprince, P., Remacle, C.*, et al.* (2010). Proteomic and functional characterization of a Chlamydomonas reinhardtii mutant lacking the mitochondrial alternative oxidase 1. J Proteome Res *9*, 2825-2838.

Matsui, M. (2002). Dual roles of photosynthetic electron transport in photosystem I biogenesis: light induction of mRNAs and chromatic regulation at post-mRNA level. Plant Cell Physiol.

Maul, J., Lilly, J., Cui, L., Miller, W., and Stern, D. (2002). The Chlamydomonas reinhardtii Plastid Chromosome: Islands of Genes in a Sea of Repeats. Plant Cell *14*, 2659-2679.

Mayer, M.P. (2013). Hsp70 chaperone dynamics and molecular mechanism. Trends Biochem Sci *38*, 507-514.

McDuff, R.E., and Chisholm, S.W. (1982). The calculation of in situ growth rates of phytoplankton populations from fractions of cells undergoing mitosis: A clarification. Limnology and Oceanography *27*, 783-788.

McGlincy, N.J., and Smith, C.W. (2008). Alternative splicing resulting in nonsense-mediated mRNA decay: what is the meaning of nonsense? Trends in biochemical sciences *33*, 385-393.

Merendino, L., Perron, K., Rahire, M., Howald, I., Rochaix, J.D., and Goldschmidt-Clermont, M. (2006). A novel multifunctional factor involved in trans-splicing of chloroplast introns in Chlamydomonas. Nucleic Acids Research *34*, 262-274.

Messick, T.E., Russell, N.S., Iwata, A.J., Sarachan, K.L., Shiekhattar, R., Shanks, J.R., Reyes-Turcu, F.E., Wilkinson, K.D., and Marmorstein, R. (2008). Structural basis for ubiquitin recognition by the Otu1 ovarian tumor domain protein. J Biol Chem *283*, 11038-11049.

Mettler, T., Muhlhaus, T., Hemme, D., Schottler, M.A., Rupprecht, J., Idoine, A., Veyel, D., Pal, S.K., Yaneva-Roder, L., Winck, F.V.*, et al.* (2014). Systems Analysis of the Response of Photosynthesis, Metabolism, and Growth to an Increase in Irradiance in the Photosynthetic Model Organism Chlamydomonas reinhardtii. Plant Cell *26*, 2310-2350.

Michelet, L., Lefebvre-Legendre, L., Burr, S.E., Rochaix, J.D., and Goldschmidt-Clermont, M. (2011). Enhanced chloroplast transgene expression in a nuclear mutant of Chlamydomonas. Plant Biotechnol J *9*, 565-574.

Michelet, L., Roach, T., Fischer, B.B., Bedhomme, M., Lemaire, S.D., and Krieger-Liszkay, A. (2013a). Down-regulation of catalase activity allows transient accumulation of a hydrogen peroxide signal in Chlamydomonas reinhardtii. Plant, cell & environment *36*, 1204-1213.

Michelet, L., Zaffagnini, M., Morisse, S., Sparla, F., Perez-Perez, M.E., Francia, F., Danon, A., Marchand, C.H., Fermani, S., Trost, P.*, et al.* (2013b). Redox regulation of the Calvin-Benson cycle: something old, something new. Front Plant Sci *4*, 470.

Mills, J.D., Mitchell, P., and Schürmann, P. (1980). Modulation of coupling factor ATPase activity in intact chloroplasts. FEBS Letters *112*, 173-177.

Mittler, R. (2002). Oxidative stress, antioxidants and stress tolerance. Trends in Plant Science *7*, 405-410.

Miyake, C., Miyata, M., Shinzaki, Y., and Tomizawa, K. (2005). CO2 response of cyclic electron flow around PSI (CEF-PSI) in tobacco leaves--relative electron fluxes through PSI and PSII determine the magnitude of non-photochemical quenching (NPQ) of Chl fluorescence. Plant Cell Physiol *46*, 629-637.

Miyake, C., Shinzaki, Y., Miyata, M., and Tomizawa, K. (2004). Enhancement of cyclic electron flow around PSI at high light and its contribution to the induction of non-photochemical quenching of chl fluorescence in intact leaves of tobacco plants. Plant Cell Physiol *45*, 1426-1433.

Miyata, K., Noguchi, K., and Terashima, I. (2012). Cost and benefit of the repair of photodamaged photosystem II in spinach leaves: roles of acclimation to growth light. Photosynthesis research *113*, 165-180.

Molen, T.A., Rosso, D., Piercy, S., and Maxwell, D.P. (2006). Characterization of the alternative oxidase of Chlamydomonas reinhardtii in response to oxidative stress and a shift in nitrogen source. Physiologia Plantarum *127*, 74-86.

Mubarakshina, M.M., Ivanov, B.N., Naydov, I.A., Hillier, W., Badger, M.R., and Krieger-Liszkay, A. (2010). Production and diffusion of chloroplastic H2O2 and its implication to signalling. J Exp Bot *61*, 3577-3587.

Mullet, J.E. (1993). Dynamic regulation of chloroplast transcription. Plant Physiol *103*, 309-313.

Mulo, P., Sakurai, I., and Aro, E.M. (2012). Strategies for psbA gene expression in cyanobacteria, green algae and higher plants: From transcription to PSII repair. Biochimica Et Biophysica Acta-Bioenergetics *1817*, 247-257.

Munekage, Y., Hojo, M., Meurer, J., Endo, T., Tasaka, M., and Shikanai, T. (2002). PGR5 Is Involved in Cyclic Electron Flow around Photosystem I and Is Essential for Photoprotection in Arabidopsis. Cell *110*, 361-371.

Munoz-Nortes, T., Perez-Perez, J.M., Ponce, M.R., Candela, H., and Micol, J.L. (2017). The ANGULATA7 gene encodes a DnaJ-like zinc finger-domain protein involved in chloroplast function and leaf development in Arabidopsis. Plant Journal *89*, 870-884.

Murakami, A. (1997). Quantitative analysis of 77K fluorescence emission spectra in Synechocystis sp. PCC 6714 and Chlamydomonas reinhardtii with variable PS I/PS II stoichiometries. Photosynthesis Research *53*, 141-148.

Murakami, A., Fujita, Y., Nemson, J.A., and Melis, A. (1997). Chromatic Regulation in Chlamydomonas reinhardtii: Time Course of Photosystem Stoichiometry Adjustment Following a Shift in Growth Light Quality. Plant and Cell Physiology *38*, 188-193.

Murchie, E.H., and Niyogi, K.K. (2011). Manipulation of photoprotection to improve plant photosynthesis. Plant Physiol *155*, 86-92.

Mustila, H., Paananen, P., Battchikova, N., Santana-Sanchez, A., Muth-Pawlak, D., Hagemann, M., Aro, E.M., and Allahverdiyeva, Y. (2016). The Flavodiiron Protein Flv3 Functions as a Homo-Oligomer During Stress Acclimation and is Distinct from the Flv1/Flv3 Hetero-Oligomer Specific to the O2 Photoreduction Pathway. Plant Cell Physiol *57*, 1468-1483.

Nagashima, A., Hanaoka, M., Shikanai, T., Fujiwara, M., Kanamaru, K., Takahashi, H., and Tanaka, K. (2004). The multiple-stress responsive plastid sigma factor, SIG5, directs activation of the psbD blue light-responsive promoter (BLRP) in Arabidopsis thaliana. Plant Cell Physiol *45*, 357-368.

Nagy, G., Unnep, R., Zsiros, O., Tokutsu, R., Takizawa, K., Porcar, L., Moyet, L., Petroutsos, D., Garab, G., Finazzi, G.*, et al.* (2014a). Chloroplast remodeling during state transitions in Chlamydomonas reinhardtii as revealed by noninvasive techniques in vivo. Proc Natl Acad Sci U S A *111*, 5042-5047.

Nair, U., Ditty, J.L., Min, H., and Golden, S.S. (2002). Roles for sigma factors in global circadian regulation of the cyanobacterial genome. J Bacteriol *184*, 3530-3538.

Nakagawa, S., Niimura, Y., and Gojobori, T. (2017). Comparative genomic analysis of translation initiation mechanisms for genes lacking the Shine-Dalgarno sequence in prokaryotes. Nucleic Acids Research *45*, 3922-3931.

Nath, K., Jajoo, A., Poudyal, R.S., Timilsina, R., Park, Y.S., Aro, E.-M., Nam, H.G., and Lee, C.-H. (2013). Towards a critical understanding of the photosystem II repair mechanism and its regulation during stress conditions. FEBS letters *587*, 3372-3381.

Naumann, B., Busch, A., Allmer, J., Ostendorf, E., Zeller, M., Kirchhoff, H., and Hippler, M. (2007). Comparative quantitative proteomics to investigate the remodeling of bioenergetic pathways under iron deficiency in Chlamydomonas reinhardtii. Proteomics *7*, 3964-3979.

Nawrocki, W.J., Buchert, F., Joliot, P., Rappaport, F., Bailleul, B., and Wollman, F.A. (2019). Chlororespiration Controls Growth Under Intermittent Light. Plant Physiol *179*, 630-639.

Nawrocki, W.J., Tourasse, N.J., Taly, A., Rappaport, F., and Ewollman, F.A. (2015). The Plastid Terminal Oxidase: Its Elusive Function Points to Multiple Contributions to Plastid Physiology. In Annual Review of Plant Biology, Vol 66, S.S. Merchant, ed., pp. 49-74.

Neuhaus, H.E., and Emes, M.J. (2000). Nonphotosynthetic Metabolism in Plastids. Annu Rev Plant Physiol Plant Mol Biol *51*, 111-140.

Nilkens, M., Kress, E., Lambrev, P., Miloslavina, Y., Muller, M., Holzwarth, A.R., and Jahns, P. (2010). Identification of a slowly inducible zeaxanthin-dependent component of non-photochemical quenching of chlorophyll fluorescence generated under steady-state conditions in Arabidopsis. Biochim Biophys Acta *1797*, 466-475.

Nishiyama, Y., Allakhverdiev, S.I., and Murata, N. (2006). A new paradigm for the action of reactive oxygen species in the photoinhibition of photosystem II. Biochimica et biophysica acta *1757*, 742-749.

Nishiyama, Y., Allakhverdiev, S.I., and Murata, N. (2011). Protein synthesis is the primary target of reactive oxygen species in the photoinhibition of photosystem II. Physiol Plantarum *142*, 35-46.

Nishiyama, Y., Allakhverdiev, S.I., Yamamoto, H., Hayashi, H., and Murata, N. (2004). Singlet oxygen inhibits the repair of photosystem II by suppressing the translation elongation of the D1 protein in Synechocystis sp. PCC 6803. Biochemistry *43*, 11321-11330.

Nixon, P.J., Michoux, F., Yu, J., Boehm, M., and Komenda, J. (2010). Recent advances in understanding the assembly and repair of photosystem II. Ann Bot *106*, 1-16.

Niyogi, K.K., Bjorkman, O., and Grossman, A.R. (1997a). Chlamydomonas Xanthophyll Cycle Mutants Identified by Video Imaging of Chlorophyll Fluorescence Quenching. Plant Cell *9*, 1369-1380.

Niyogi, K.K., Bjorkman, O., and Grossman, A.R. (1997b). The roles of specific xanthophylls in photoprotection. Proc Natl Acad Sci U S A *94*, 14162-14167.

Niyogi, K.K., and Truong, T.B. (2013). Evolution of flexible non-photochemical quenching mechanisms that regulate light harvesting in oxygenic photosynthesis. Curr Opin Plant Biol *16*, 307-314.

Oelze, M.L., Vogel, M.O., Alsharafa, K., Kahmann, U., Viehhauser, A., Maurino, V.G., and Dietz, K.J. (2012). Efficient acclimation of the chloroplast antioxidant defence of Arabidopsis thaliana leaves in response to a 10- or 100-fold light increment and the possible involvement of retrograde signals. J Exp Bot *63*, 1297-1313.

Ohnishi, N., Allakhverdiev, S.I., Takahashi, S., Higashi, S., Watanabe, M., Nishiyama, Y., and Murata, N. (2005). Two-step mechanism of photodamage to photosystem II: Step 1 occurs at the oxygen-evolving complex and step 2 occurs at the photochemical reaction center. Biochemistry *44*, 8494-8499.

Oikawa, K., Fujiwara, M., Nakazato, E., Tanaka, K., and Takahashi, H. (2000). Characterization of two plastid σ factors, SigA1 and SigA2, that mainly function in matured chloroplasts in Nicotiana tabacum. Gene *261*, 221-228.

Olaizola, M., La Roche, J., Kolber, Z., and Falkowski, P.G. (1994). Non-photochemical fluorescence quenching and the diadinoxanthin cycle in a marine diatom. Photosynth Res *41*, 357-370.

Onda, Y., Yagi, Y., Saito, Y., Takenaka, N., and Toyoshima, Y. (2008). Light induction of Arabidopsis SIG1 and SIG5 transcripts in mature leaves: differential roles of cryptochrome 1 and cryptochrome 2 and dual function of SIG5 in the recognition of plastid promoters. Plant J *55*, 968-978.

Oxborough, K., and Baker, N.R. (1997). Resolving chlorophyll a fluorescence images of photosynthetic efficiency into photochemical and non-photochemical components - calculation of qP and Fv '/Fm ' without measuring Fo '. Photosynthesis Research *54*, 135-142.

Padmarasu, S., Sargent, D.J., Patocchi, A., Troggio, M., Baldi, P., Linsmith, G., Poles, L., Jansch, M., Kellerhals, M., Tartarini, S.*, et al.* (2018). Identification of a leucine-rich repeat receptor-like serine/threonine-protein kinase as a candidate gene for Rvi12 (Vb)-based apple scab resistance. Molecular Breeding *38*.

Palmer, J.D. (1985). Comparative organization of chloroplast genomes. Annu Rev Genet *19*, 325-354.

Park, J.J., Wang, H., Gargouri, M., Deshpande, R.R., Skepper, J.N., Holguin, F.O., Juergens, M.T., Shachar-Hill, Y., Hicks, L.M., and Gang, D.R. (2015). The response of Chlamydomonas reinhardtii to nitrogen deprivation: a systems biology analysis. Plant J *81*, 611-624.

Peers, G. (2014). Increasing algal photosynthetic productivity by integrating ecophysiology with systems biology. Trends Biotechnol *32*, 551-555.

Peers, G. (2015). Enhancement of biomass production by disruption of light energy dissipation pathways, P.a.T. Office, ed. (United States of America).

Peers, G., Truong, T.B., Ostendorf, E., Busch, A., Elrad, D., Grossman, A.R., Hippler, M., and Niyogi, K.K. (2009). An ancient light-harvesting protein is critical for the regulation of algal photosynthesis. Nature *462*, 518-521.

Peltier, G., Tolleter, D., Billon, E., and Cournac, L. (2010). Auxiliary electron transport pathways in chloroplasts of microalgae. Photosynthesis research *106*, 19-31.

Perozeni, F., Stella, G.R., and Ballottari, M. (2018). LHCSR Expression under HSP70/RBCS2 Promoter as a Strategy to Increase Productivity in Microalgae. Int J Mol Sci *19*.

Perrine, Z., Negi, S., and Sayre, R.T. (2012). Optimization of photosynthetic light energy utilization by microalgae. Algal Res *1*, 134-142.

Perron, K., Goldschmidt-Clermont, M., and Rochaix, J.D. (1999). A factor related to pseudouridine synthases is required for chloroplast group II intron trans-splicing in Chlamydomonas reinhardtii. Embo Journal *18*, 6481-6490.

Petrillo, E., Godoy Herz, M.A., Fuchs, A., Reifer, D., Fuller, J., Yanovsky, M.J., Simpson, C., Brown, J.W., Barta, A., Kalyna, M.*, et al.* (2014). A chloroplast retrograde signal regulates nuclear alternative splicing. Science *344*, 427-430.

Petroutsos, D., Busch, A., Janssen, I., Trompelt, K., Bergner, S.V., Weinl, S., Holtkamp, M., Karst, U., Kudla, J., and Hippler, M. (2011). The chloroplast calcium sensor CAS is required for photoacclimation in Chlamydomonas reinhardtii. Plant Cell *23*, 2950-2963.

Petroutsos, D., Terauchi, A.M., Busch, A., Hirschmann, I., Merchant, S.S., Finazzi, G., and Hippler, M. (2009). PGRL1 participates in iron-induced remodeling of the photosynthetic apparatus and in energy metabolism in Chlamydomonas reinhardtii. J Biol Chem *284*, 32770-32781.

Platt, T., Gallegos, C.L., and Harrison, W.G. (1980). Photoinhibition of Photosynthesis in Natural Assemblages of Marine-Phytoplankton. J Mar Res *38*, 687-701.

Pogson, B.J., Woo, N.S., Forster, B., and Small, I.D. (2008). Plastid signalling to the nucleus and beyond. Trends Plant Sci *13*, 602-609.

Pollock, S.V., Mukherjee, B., Bajsa-Hirschel, J., Machingura, M.C., Mukherjee, A., Grossman, A.R., and Moroney, J.V. (2017). A robust protocol for efficient generation, and genomic characterization of insertional mutants of Chlamydomonas reinhardtii. Plant Methods *13*, 22.

Ponce-Toledo, R.I., Deschamps, P., Lopez-Garcia, P., Zivanovic, Y., Benzerara, K., and Moreira, D. (2017). An Early-Branching Freshwater Cyanobacterium at the Origin of Plastids. Curr Biol *27*, 386-391.

Porra, R.J. (2002). The chequered history of the development and use of simultaneous equations for the accurate determination of chlorophylls a and b. Photosynth Res *73*, 149-156.

Pospíšil, P. (2012). Molecular mechanisms of production and scavenging of reactive oxygen species by photosystem II. Biochimica et biophysica acta *1817*, 218-231.

Privat, I., Hakimi, M.A., Buhot, L., Favory, J.J., and Mache-Lerbs, S. (2003). Characterization of Arabidopsis plastid sigma-like transcription factors SIG1, SIG2 and SIG3. Plant Mol Biol *51*, 385-399.

Puthiyaveetil, S., Ibrahim, I.M., and Allen, J.F. (2012). Oxidation-reduction signalling components in regulatory pathways of state transitions and photosystem stoichiometry adjustment in chloroplasts. Plant, cell & environment *35*, 347-359.

Puthiyaveetil, S., Kavanagh, T.A., Cain, P., Sullivan, J.A., Newell, C.A., Gray, J.C., Robinson, C., van der Giezen, M., Rogers, M.B., and Allen, J.F. (2008). The ancestral symbiont sensor kinase CSK links photosynthesis with gene expression in chloroplasts. Proc Natl Acad Sci U S A *105*, 10061-10066.

Qiao, H., Fan, X., Xu, D., Ye, N., Wang, J., and Cao, S. (2015). Artificial leaf aids analysis of chlorophyll fluorescence and P700 absorbance in studies involving microalgae. Phycol Res *63*, 72-76.

Quail, P.H. (2007). Phytochrome-regulated Gene Expression. Journal of Integrative Plant Biology *49*, 11-20.

Radmer, R., and Kok, B. (1976). Photoreduction of O2 Primes and Replaces CO2 Assimilation. Plant Physiol *58*, 336-340.

Ramel, F., Birtic, S., Ginies, C., Soubigou-Taconnat, L., Triantaphylidès, C., and Havaux, M. (2012). Carotenoid oxidation products are stress signals that mediate gene responses to singlet oxygen in plants. Proceedings of the National Academy of Sciences *109*, 5535-5540.

Raven, J.A. (1989). Flight or flight: the Economics of Repair and Avoidance of Photoinhibition of Photosynthesis. Funct Ecol *3*, 5.

Raven, J.A. (2011). The cost of photoinhibition. Physiol Plantarum *142*, 87-104.

Rea, G., Antonacci, A., Lambreva, M.D., and Mattoo, A.K. (2018). Features of cues and processes during chloroplast-mediated retrograde signaling in the alga Chlamydomonas. Plant Sci *272*, 193-206.

Rebeille, F., and Gans, P. (1988). Interaction between Chloroplasts and Mitochondria in Microalgae - Role of Glycolysis. Plant Physiology *88*, 973-975.

Reddy, A.S., Marquez, Y., Kalyna, M., and Barta, A. (2013). Complexity of the alternative splicing landscape in plants. Plant Cell *25*, 3657-3683.

Rensing, S.A., Lang, D., Zimmer, A.D., Terry, A., Salamov, A., Shapiro, H., Nishiyama, T., Perroud, P.F., Lindquist, E.A., Kamisugi, Y.*, et al.* (2008). The Physcomitrella genome reveals evolutionary insights into the conquest of land by plants. Science *319*, 64-69.

Richard, C., Ouellet, H., and Guertin, M. (2000). Characterization of the LI818 polypeptide from the green unicellular alga Chlamydomonas reinhardtii. Plant Mol Biol *42*, 303-316.

Rinalducci, S., Pedersen, J.Z., and Zolla, L. (2004). Formation of radicals from singlet oxygen produced during photoinhibition of isolated light-harvesting proteins of photosystem II. Biochimica et Biophysica Acta - Bioenergetics *1608*, 63-73.

Ritchie, R.J. (2008). Fitting light saturation curves measured using modulated fluorometry. Photosynth Res *96*, 201-215.

Rivier, C., Goldschmidt-Clermont, M., and Rochaix, J.D. (2001). Identification of an RNA-protein complex involved in chloroplast group II intron trans-splicing in Chlamydomonas reinhardtii. Embo Journal *20*, 1765-1773.

Roach, T., and Krieger-Liszkay, A. (2012). The role of the PsbS protein in the protection of photosystems I and II against high light in Arabidopsis thaliana. Biochimica et biophysica acta *1817*, 2158-2165.

Roberty, S., Bailleul, B., Berne, N., Franck, F., and Cardol, P. (2014). PSI Mehler reaction is the main alternative photosynthetic electron pathway in Symbiodinium sp., symbiotic dinoflagellates of cnidarians. New Phytol *204*, 81-91.

Ruban, A.V. (2015). Evolution under the sun: optimizing light harvesting in photosynthesis. J Exp Bot *66*, 7-23.

Ruban, A.V. (2017). Quantifying the efficiency of photoprotection. Philos Trans R Soc Lond B Biol Sci *372*.

Sacharz, J., Giovagnetti, V., Ungerer, P., Mastroianni, G., and Ruban, A.V. (2017). The xanthophyll cycle affects reversible interactions between PsbS and light-harvesting complex II to control non-photochemical quenching. Nat Plants *3*, 16225.

Saroussi, S.I., Wittkopp, T.M., and Grossman, A.R. (2016). The Type II NADPH Dehydrogenase Facilitates Cyclic Electron Flow, Energy-Dependent Quenching, and Chlororespiratory Metabolism during Acclimation of Chlamydomonas reinhardtii to Nitrogen Deprivation. Plant Physiol *170*, 1975-1988.

Savard, F., Richard, C., and Guertin, M. (1996). The Chlamydomonas reinhardtii LI818 gene represents a distant relative of the cabI/II genes that is regulated during the cell cycle and in response to illumination. Plant molecular biology *32*, 461-473.

Scharff, L.B., Childs, L., Walther, D., and Bock, R. (2011). Local Absence of Secondary Structure Permits Translation of mRNAs that Lack Ribosome-Binding Sites. Plos Genetics *7*.

Scharff, L.B., Ehrnthaler, M., Janowski, M., Childs, L.H., Hasse, C., Gremmels, J., Ruf, S., Zoschke, R., and Bock, R. (2017). Shine-Dalgarno Sequences Play an Essential Role in the Translation of Plastid mRNAs in Tobacco. Plant Cell *29*, 3085-3101.

Scheibe, R. (2004). Malate valves to balance cellular energy supply. Physiologia plantarum *120*, 21-26.

Schmitz-Linneweber, C., Williams-Carrier, R., and Barkan, A. (2005). RNA immunoprecipitation and microarray analysis show a chloroplast Pentatricopeptide repeat protein to be associated with the 5' region of mRNAs whose translation it activates. Plant Cell *17*, 2791-2804.

Schroter, Y., Steiner, S., Matthai, K., and Pfannschmidt, T. (2010). Analysis of oligomeric protein complexes in the chloroplast sub-proteome of nucleic acid-binding proteins from mustard reveals potential redox regulators of plastid gene expression. Proteomics *10*, 2191-2204.

Schweer, J., Turkeri, H., Kolpack, A., and Link, G. (2010). Role and regulation of plastid sigma factors and their functional interactors during chloroplast transcription - recent lessons from Arabidopsis thaliana. Eur J Cell Biol *89*, 940-946.

Seemann, J.R., Berry, J.A., Freas, S.M., and Krump, M.A. (1985). Regulation of ribulose bisphosphate carboxylase activity in vivo by a light-modulated inhibitor of catalysis. Proceedings of the National Academy of Sciences *82*, 8024-8028.

Shao, N., Duan, G.Y., Bock, R., and Molekulare, M.-p.-i. (2013). A Mediator of Singlet Oxygen Responses in Chlamydomonas reinhardtii and Arabidopsis Identified by a Luciferase-Based Genetic Screen in Algal Cells. *25*, 4209-4226.

shiguro, S., Kawai-Oda, A., Ueda, J., Nishida, I., and Okada, K. (2001). The DEFECTIVE IN ANTHER DEHISCIENCE gene encodes a novel phospholipase A1 catalyzing the initial step of jasmonic acid biosynthesis, which synchronizes pollen maturation, anther dehiscence, and flower opening in Arabidopsis. Plant Cel *13*, 2191-2209.

Shimakawa, G., Ishizaki, K., Tsukamoto, S., Tanaka, M., Sejima, T., and Miyake, C. (2017). The Liverwort, Marchantia, Drives Alternative Electron Flow Using a Flavodiiron Protein to Protect PSI. Plant Physiol *173*, 1636-1647.

Shimizu, M., Kato, H., Ogawa, T., Kurachi, A., Nakagawa, Y., and Kobayashi, H. (2010). Sigma factor phosphorylation in the photosynthetic control of photosystem stoichiometry. Proc Natl Acad Sci U S A *107*, 10760-10764.

Shimogawara, K., Fujiwara, S., Grossman, A., and Usuda, H. (1998). High-efficiency transformation of Chlamydomonas reinhardtii by electroporation. Genetics *148*, 1821-1828.

Shin, Y.S., Jeong, J., Nguyen, T.H.T., Kim, J.Y.H., Jin, E., and Sim, S.J. (2019). Targeted knockout of phospholipase A2 to increase lipid productivity in Chlamydomonas reinhardtii for biodiesel production. Bioresour Technol *271*, 368-374.

Shirano, Y., Shimada, H., Kanamaru, K., Fujiwara, M., Tanaka, K., Takahashi, H., Unno, K., Sato, S., Tabata, S., Hayashi, H.*, et al.* (2000). Chloroplast development in Arabidopsis thaliana requires the nuclear-encoded transcription factor sigma B. FEBS Lett *485*, 178-182.

Shriwastav, A., Mohmed, J., Bose, P., and Shekhar, M. (2014). Deconvoluting algal and bacterial biomass concentrations in algal-bacterial suspensions. Journal of Applied Phycology *27*, 211-222.

Shubin, V.V., Terekhova, I.N., Kirillov, B.A., and Karapetyan, N.V. (2008). Quantum yield of P700+ photodestruction in isolated photosystem I complexes of the cyanobacteriumArthrospira platensis. Photochemical & Photobiological Sciences *7*, 956-962.

Singh, B.N., Mishra, R.N., Agarwal, P.K., Goswami, M., Nair, S., Sopory, S.K., and Reddy, M.K. (2004). A pea chloroplast translation elongation factor that is regulated by abiotic factors. Biochemical and Biophysical Research Communications *320*, 523-530.

Somanchi, A., Barnes, D., and Mayfield, S.P. (2005). A nuclear gene of Chlamydomonas reinhardtii, Tba1, encodes a putative oxidoreductase required for translation of the chloroplast psbA mRNA. Plant J *42*, 341-352.

Sonoike, K., and Terashima, I. (1994). Mechanism of photosystem-I photoinhibition in leaves of Cucumis sativus L. Planta *194*, 287-293.

Sonoike, K., Terashima, I., Iwaki, M., and Itoh, S. (1995). Destruction of photosystem I iron-sulfur centers in leaves of Cucumis sativus L. by weak illumination at chilling temperatures. FEBS letters *362*, 235-238.

Stampacchia, O., GirardBascou, J., Zanasco, J.L., Zerges, W., Bennoun, P., and Rochaix, J.D. (1997). A nuclear-encoded function essential for translation of the chloroplast psaB mRNA in Chlamydomonas. Plant Cell *9*, 773-782.

Sturm, N.R., Kuras, R., Büschlen, S., Sakamoto, W., Kindle, K.L., Stern, D.B., and Wollman, F.A. (1994). The petD gene is transcribed by functionally redundant promoters in Chlamydomonas reinhardtii chloroplasts. Molecular and Cellular Biology *14*, 6171-6179.

Sun, J., and Liu, D.Y. (2003). Geometric models for calculating cell biovolume and surface area for phytoplankton. Journal of Plankton Research *25*, 1331-1346.

Sun, T.H., Zhou, F., Liu, C.J., Zhuang, Z., and Lu, S. (2016). The DnaJ-like zinc finger domain protein ORANGE localizes to the nucleus in etiolated cotyledons of Arabidopsis thaliana. Protoplasma *253*, 1599-1604.

Suorsa, M., Jarvi, S., Grieco, M., Nurmi, M., Pietrzykowska, M., Rantala, M., Kangasjarvi, S., Paakkarinen, V., Tikkanen, M., Jansson, S.*, et al.* (2012). PROTON GRADIENT REGULATION5 is essential for proper acclimation of Arabidopsis photosystem I to naturally and artificially fluctuating light conditions. Plant Cell *24*, 2934-2948.

Suorsa, M., Rossi, F., Tadini, L., Labs, M., Colombo, M., Jahns, P., Kater, M.M., Leister, D., Finazzi, G., Aro, E.M.*, et al.* (2016). PGR5-PGRL1-Dependent Cyclic Electron Transport Modulates Linear Electron Transport Rate in Arabidopsis thaliana. Mol Plant *9*, 271-288.

Takahashi, H., Clowez, S., Wollman, F.-A., Vallon, O., and Rappaport, F. (2013). Cyclic electron flow is redox-controlled but independent of state transition. Nature communications *4*, 1954.

Takahashi, S., Milward, S.E., Fan, D.Y., Chow, W.S., and Badger, M.R. (2009). How does cyclic electron flow alleviate photoinhibition in Arabidopsis? Plant Physiol *149*, 1560-1567.

Takahashi, S., and Murata, N. (2005). Interruption of the Calvin cycle inhibits the repair of Photosystem II from photodamage. Biochim Biophys Acta *1708*, 352-361.

Takahashi, Y., Goldschmidtclermont, M., Soen, S.Y., Franzen, L.G., and Rochaix, J.D. (1991). Directed chloroplast transformation in *Chlamydomonas reinhartii* -insertional inactivation of the *psaC* gene encoding the iron sulfur proteni destabilised Photosystem. Embo Journal *10*, 2033-2040.

Tanaka, R., and Tanaka, A. (2007). Tetrapyrrole biosynthesis in higher plants. Annual review of plant biology *58*, 321-346.

Telfer, A. (2014). Singlet oxygen production by PSII under light stress: mechanism, detection and the protective role of beta-carotene. Plant & cell physiology *55*, 1216-1223.

Thapa, G., Gunupuru, L.R., Hehir, J.G., Kahla, A., Mullins, E., and Doohan, F.M. (2018). A Pathogen-Responsive Leucine Rich Receptor Like Kinase Contributes to Fusarium Resistance in Cereals. Frontiers in Plant Science *9*.

Tibiletti, T., Auroy, P., Peltier, G., and Caffarri, S. (2016). Chlamydomonas reinhardtii PsbS Protein Is Functional and Accumulates Rapidly and Transiently under High Light. Plant Physiol *171*, 2717-2730.

Tikkanen, M., Mekala, N.R., and Aro, E.-M. (2014). Photosystem II photoinhibition-repair cycle protects Photosystem I from irreversible damage. Biochimica et biophysica acta *1837*, 210-215.

Tikkanen, M., Nurmi, M., Kangasjärvi, S., and Aro, E.-M. (2008). Core protein phosphorylation facilitates the repair of photodamaged photosystem II at high light. Biochimica et biophysica acta *1777*, 1432-1437.

Tikkanen, M., Rantala, S., and Aro, E.M. (2015). Electron flow from PSII to PSI under high light is controlled by PGR5 but not by PSBS. Front Plant Sci *6*, 521.

Tokutsu, R., and Minagawa, J. (2013). Energy-dissipative supercomplex of photosystem II associated with LHCSR3 in Chlamydomonas reinhardtii. Proc Natl Acad Sci U S A *110*, 10016-10021.

Tozawa, Y., Teraishi, M., Sasaki, T., Sonoike, K., Nishiyama, Y., Itaya, M., Miyao, A., and Hirochika, H. (2007). The plastid sigma factor SIG1 maintains photosystem I activity via regulated expression of the psaA operon in rice chloroplasts. Plant J *52*, 124-132.

Triantaphylides, C., and Havaux, M. (2009). Singlet oxygen in plants: production, detoxification and signaling. Trends Plant Sci *14*, 219-228.

Truong, T.B. (2011). Investigating the Role(s) of LHCSRs in Chlamydomonas reinhardtii (eScholarship University of California: UC Berkeley).

Tsunoyama, Y., Ishizaki, Y., Morikawa, K., Kobori, M., Nakahira, Y., Takeba, G., Toyoshima, Y., and Shiina, T. (2004). Blue light-induced transcription of plastid-encoded psbD gene is mediated by a nuclear-encoded transcription initiation factor, AtSig5. Proc Natl Acad Sci U S A *101*, 3304-3309.

Tyystjarvi, E., and Aro, E.M. (1996). The rate constant of photoinhibition, measured in lincomycin-treated leaves, is directly proportional to light intensity. Proc Natl Acad Sci U S A *93*, 2213-2218.

Tyystjärvi, E., and Aro, E.M. (1996). The rate constant of photoinhibition, measured in lincomycin-treated leaves, is directly proportional to light intensity. Proceedings of the National Academy of Sciences of the United States of America *93*, 2213-2218.

Umen, J.G., and Goodenough, U.W. (2001). Control of cell division by a retinoblastoma protein homolog in Chlamydomonas. Genes Dev *15*, 1652-1661.

Unlu, C., Drop, B., Croce, R., and van Amerongen, H. (2014). State transitions in Chlamydomonas reinhardtii strongly modulate the functional size of photosystem II but not of photosystem I. Proc Natl Acad Sci U S A *111*, 3460-3465.

Vandenhecke, J.M., Bastedo, J., Cockshutt, A.M., Campbell, D.A., and Huot, Y. (2015). Changes in the Rubisco to photosystem ratio dominates photoacclimation across phytoplankton taxa. Photosynth Res *124*, 275-291.

Verhoeven, A. (2014). Sustained energy dissipation in winter evergreens. New Phytol *201*, 57-65.

Vishwakarma, A., Bashyam, L., Senthilkumaran, B., Scheibe, R., and Padmasree, K. (2014). Physiological role of AOX1a in photosynthesis and maintenance of cellular redox homeostasis under high light in Arabidopsis thaliana. Plant Physiol Biochem *81*, 44-53.

Vogel, M.O., Moore, M., Konig, K., Pecher, P., Alsharafa, K., Lee, J., and Dietz, K.J. (2014). Fast retrograde signaling in response to high light involves metabolite export, MITOGEN-ACTIVATED PROTEIN KINASE6, and AP2/ERF transcription factors in Arabidopsis. Plant Cell *26*, 1151-1165.

Vollmar, M., Schlieper, D., Winn, M., Büchner, C., and Groth, G. (2009). Structure of the c14 rotor ring of the proton translocating chloroplast ATP synthase. The Journal of biological chemistry *284*, 18228-18235.

von Gromoff, E.D., Alawady, A., Meinecke, L., Grimm, B., and Beck, C.F. (2008). Heme, a plastid-derived regulator of nuclear gene expression in Chlamydomonas. Plant Cell *20*, 552-567.

von Gromoff, E.D., Schroda, M., Oster, U., and Beck, C.F. (2006). Identification of a plastid response element that acts as an enhancer within the Chlamydomonas HSP70A promoter. Nucleic Acids Res *34*, 4767-4779.

Voss, B., Meinecke, L., Kurz, T., Al-Babili, S., Beck, C.F., and Hess, W.R. (2011). Hemin and magnesium-protoporphyrin IX induce global changes in gene expression in Chlamydomonas reinhardtii. Plant Physiol *155*, 892-905.

Wada, S., Yamamoto, H., Suzuki, Y., Yamori, W., Shikanai, T., and Makino, A. (2018). Flavodiiron Protein Substitutes for Cyclic Electron Flow without Competing CO2 Assimilation in Rice. Plant Physiol *176*, 1509-1518.

Wakao, S., Chin, B.L., Ledford, H.K., Dent, R.M., Casero, D., Pellegrini, M., Merchant, S.S., and Niyogi, K.K. (2014). Phosphoprotein SAK1 is a regulator of acclimation to singlet oxygen in Chlamydomonas reinhardtii. eLife *3*, e02286.

Wang, C., Yamamoto, H., and Shikanai, T. (2015). Role of cyclic electron transport around photosystem I in regulating proton motive force. Biochim Biophys Acta *1847*, 931-938.

Wang, J., Zhang, P.Y., Liu, S.H., Cong, B.L., and Chen, K.S. (2016). A Leucine-Rich Repeat Receptor-like Kinase from the Antarctic Moss Pohlia nutans Confers Salinity and ABA Stress Tolerance. Plant Molecular Biology Reporter *34*, 1136-1145.

Wehner, A., Grasses, T., and Jahns, P. (2006). De-epoxidation of violaxanthin in the minor antenna proteins of photosystem II, LHCB4, LHCB5, and LHCB6. J Biol Chem *281*, 21924-21933.

Wobbe, L., Bassi, R., and Kruse, O. (2016). Multi-Level Light Capture Control in Plants and Green Algae. Trends Plant Sci *21*, 55-68.

Wobbe, L., and Remacle, C. (2015). Improving the sunlight-to-biomass conversion efficiency in microalgal biofactories. J Biotechnol *201*, 28-42.

Woodson, J.D., Perez-Ruiz, J.M., and Chory, J. (2011). Heme synthesis by plastid ferrochelatase I regulates nuclear gene expression in plants. Current biology : CB *21*, 897-903.

Woodson, J.D., Perez-Ruiz, J.M., Schmitz, R.J., Ecker, J.R., and Chory, J. (2013). Sigma factor-mediated plastid retrograde signals control nuclear gene expression. Plant J *73*, 1-13.

Wostrikoff, K., and Stern, D. (2007). Rubisco large-subunit translation is autoregulated in response to its assembly state in tobacco chloroplasts. Proc Natl Acad Sci U S A *104*, 6466-6471.

Xiao, Y., Savchenko, T., Baidoo, E.E., Chehab, W.E., Hayden, D.M., Tolstikov, V., Corwin, J.A., Kliebenstein, D.J., Keasling, J.D., and Dehesh, K. (2012). Retrograde signaling by the plastidial metabolite MEcPP regulates expression of nuclear stress-response genes. Cell *149*, 1525-1535.

Xu, C., and Min, J. (2011). Structure and function of WD40 domain proteins. Protein Cell *2*, 202-214.

Yamaguchi, K., and Subramanian, A.R. (2000). The plastid ribosomal proteins - Identification of all the proteins in the 50 S subunit of an organelle ribosome (chloroplast). Journal of Biological Chemistry *275*, 28466-28482.

Yamaguchi, K., von Knoblauch, K., and Subramanian, A.R. (2000). The plastid ribosomal proteins - Identification of all the proteins in the 30 S subunit of an organelle ribosome (chloroplast). Journal of Biological Chemistry *275*, 28455-28465.

Yamamoto, H., Takahashi, S., Badger, M.R., and Shikanai, T. (2016). Artificial remodelling of alternative electron flow by flavodiiron proteins in Arabidopsis. Nat Plants *2*, 16012.

Yamamoto, H.Y., Nakayama, T.O., and Chichester, C.O. (1962). Studies on the light and dark interconversions of leaf xanthophylls. Arch Biochem Biophys *97*, 168-173.

Yamano, T., Miura, K., and Fukuzawa, H. (2008). Expression analysis of genes associated with the induction of the carbon-concentrating mechanism in Chlamydomonas reinhardtii. Plant Physiol *147*, 340-354.

Yamori, W., Makino, A., and Shikanai, T. (2016). A physiological role of cyclic electron transport around photosystem I in sustaining photosynthesis under fluctuating light in rice. Sci Rep *6*, 20147.

Yamori, W., and Shikanai, T. (2016). Physiological Functions of Cyclic Electron Transport Around Photosystem I in Sustaining Photosynthesis and Plant Growth. Annu Rev Plant Biol *67*, 81-106.

Yarnold, J., Ross, I.L., and Hankamer, B. (2016). Photoacclimation and productivity of Chlamydomonas reinhardtii grown in fluctuating light regimes which simulate outdoor algal culture conditions. Algal Res *13*, 182-194.

Yohn, C.B., Cohen, A., Rosch, C., Kuchka, M.R., and Mayfield, S.P. (1998). Translation of the chloroplast psbA mRNA requires the nuclear-encoded poly(A)-binding protein, RB47. J Cell Biol *142*, 435-442.

Yoshida, K., Terashima, I., and Noguchi, K. (2007). Up-regulation of mitochondrial alternative oxidase concomitant with chloroplast over-reduction by excess light. Plant Cell Physiol *48*, 606-614.

Young, R.E., and Purton, S. (2014). Cytosine deaminase as a negative selectable marker for the microalgal chloroplast: a strategy for the isolation of nuclear mutations that affect chloroplast gene expression. Plant J *80*, 915-925.

Yu, J., Smart, L.B., Jung, Y.S., Golbeck, J., and McIntosh, L. (1995). Absence of PsaC subunit allows assembly of photosystem I core but prevents the binding of PsaD and PsaE in Synechocystis sp. PCC6803. Plant Mol Biol *29*, 331-342.

Zghidi, W., Merendino, L., Cottet, A., Mache, R., and Lerbs-Mache, S. (2007). Nucleus-encoded plastid sigma factor SIG3 transcribes specifically the psbN gene in plastids. Nucleic Acids Res *35*, 455-464.

Zhang, Z., Shrager, J., Jain, M., Chang, C.W., Vallon, O., and Grossman, A.R. (2004). Insights into the survival of Chlamydomonas reinhardtii during sulfur starvation based on microarray analysis of gene expression. Eukaryot Cell *3*, 1331-1348.

Zones, J.M., Blaby, I.K., Merchant, S.S., and Umen, J.G. (2015). High-Resolution Profiling of a Synchronized Diurnal Transcriptome from Chlamydomonas reinhardtii Reveals Continuous Cell and Metabolic Differentiation. Plant Cell *27*, 2743-2769.

Zoschke, R., and Bock, R. (2018). Chloroplast Translation: Structural and Functional Organization, Operational Control, and Regulation. Plant Cell *30*, 745-770.

## Chapter 2 supplemental information

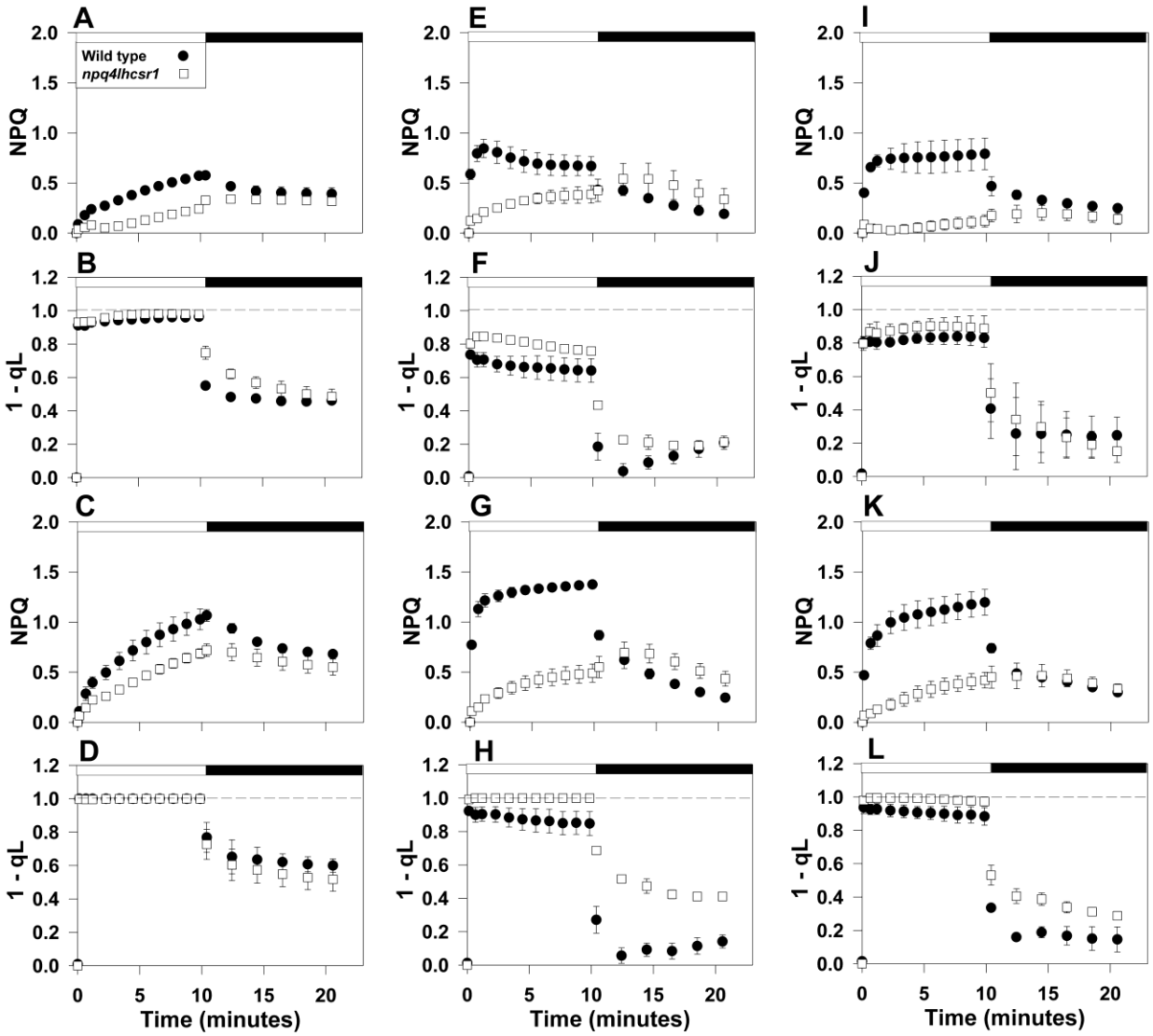


**Supplemental figure 2.1 NPQ of chlorophyll fluorescence and 1-qL for wild type and *npq4lhcsr1* acclimated to different light levels.**

Wild type (closed circles) and the *npq4lhcsr1* mutant (open squares) acclimated to either 50 (A-D), 400 (E-H) and 860 µmol photons $m^{-2}$ $s^{-1}$ (I-L) were exposed to an actinic light level of 600 (A, E, I, B, F, J) or 2005 (C, G, K, D, H, L) µmol photons $m^{-2}$ $s^{-1}$ (white bars) followed by 10 minutes darkness (black bar) and far red light illumination to re-associate LHCII with PSII (state 1 transition) by preferentially driving PSI charge separation. Data represent means ± s.d. (n = 3).

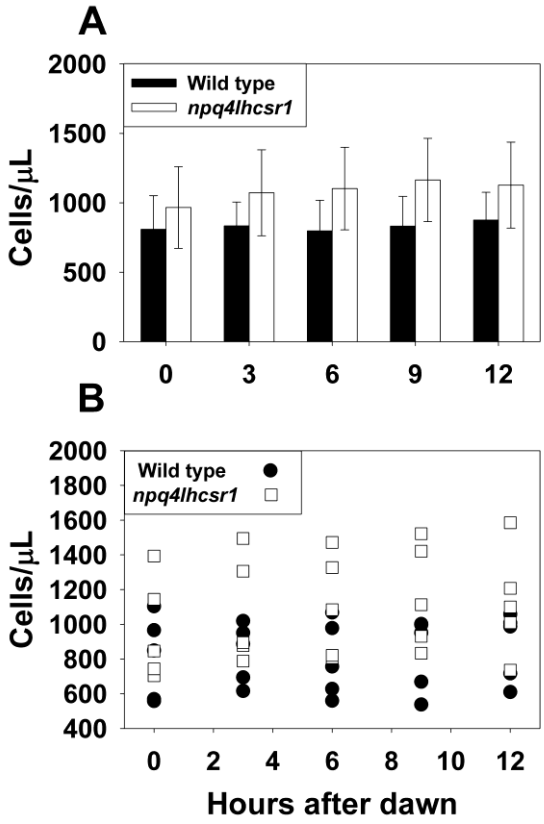


**Supplemental figure 2.2 Cell densities used for total organic carbon (TOC) measurements.** (A) Average cell densities for wild type and *npq4lhcsr1* across a single day (n = 5). (B) Individual measurements for wild type and *npq4lhcsr1*.

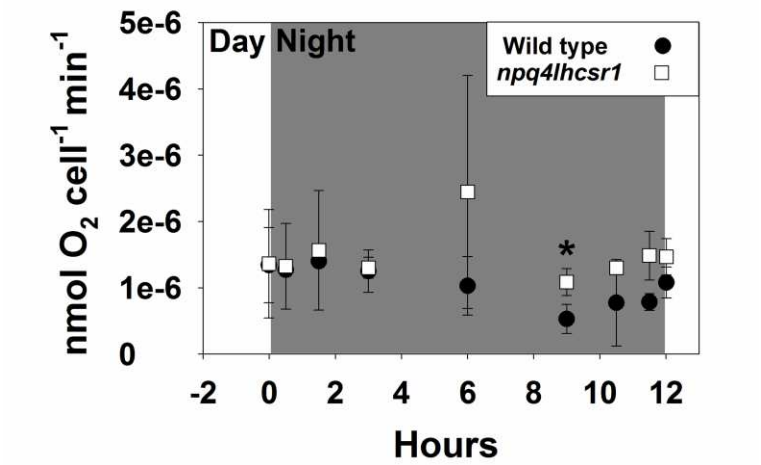


**Supplemental figure 2.3 Respiration rates at night in a sinusoidal light regime.** Respiration rates in wild type (black circles) and *npq4lhcsr1* (open squares) were measured immediately after sampling at 20 minutes before and after the night period and 0.5, 1.5, 3, 6, 9, 10.5 and 11.5 hour after dusk. Data represents the mean ± SD (n = 3). Symbols (*) represent

significant differences between wild type and *npq4lhcsr1* for each time point based on an un-paired t-test ($p < 0.05$).

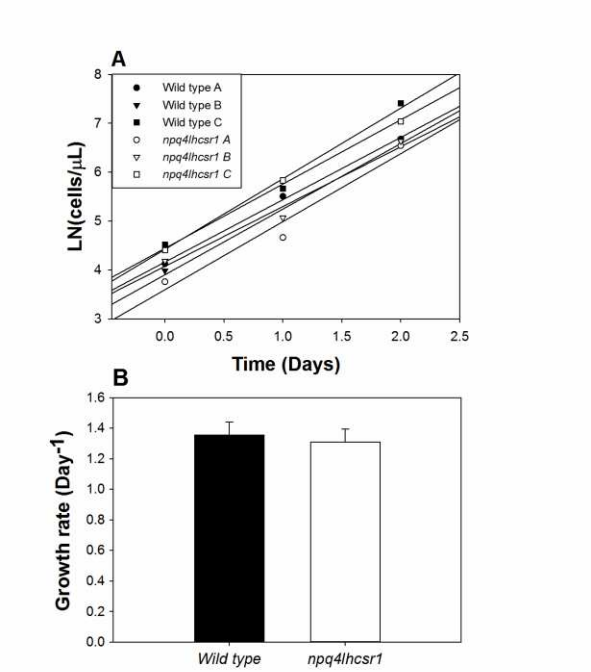


**Supplemental figure 2.4 Growth rates in ePBRs under a constant 2134 µmol photons m-2-s-1 on a 12 hour day:night light regime.**

(A) Natural log of cell densities across 2 days of growth for biological replicates (A-C) of wild type and *npq4lhcsr1*.(B) Growth rate per day. Data in B represents the mean ± SD (n = 3).

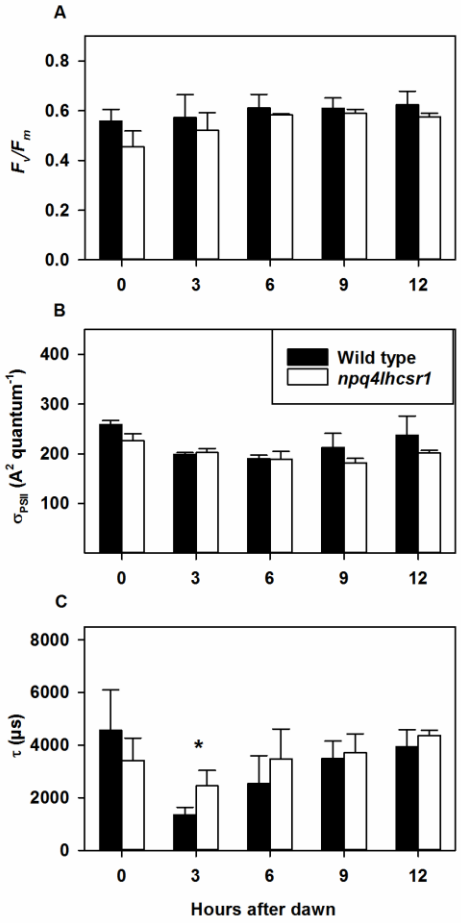


**Supplemental figure 2.5 Photophysiology of Photosystem II in ePPRs during growth in constant 2134 µmol photons $m^{-2}$ $s^{-1}$ on a 12 hour day:night light regime.**

(A) $F_v/F_m$ (B) Functional antenna size ($\sigma_{PSII}$, $A^2$ $quantum^{-1}$). (C) $Q_B$ re-oxidation kinetics ($\tau$, µs). Data represents the mean ± SD (n = 3). Symbols (*) represent significant differences from wild type within each timepoint based on an un-paired t-test ($p < 0.05$).

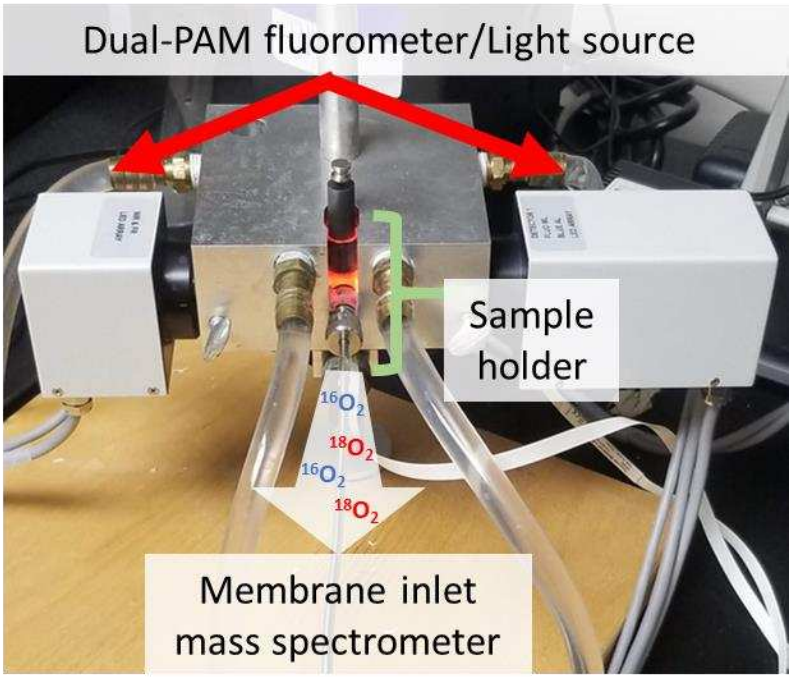


**Supplemental figure 3.1 Custom quartz cuvette and thermoregulated aluminum cuvette holder for parallel membrane inlet mass spectrometry and Dual-PAM fluorescence.** An aluminum block was custom machined to allow water re-circulation for thermoregulation in aluminum around the sample holder. Samples were illuminated with red light by a Dual-PAM in a custom quartz cuvette with glass side port for MIMS, which facilitated mixing by a bottom mounted magnetic stir plate. A PEEK carbon stopper machined for the cuvette with a purge whole was used in combination with a steel or glass stopper to maintain vacuum during MIMS experiments.

**Chapter 3 supplemental information**

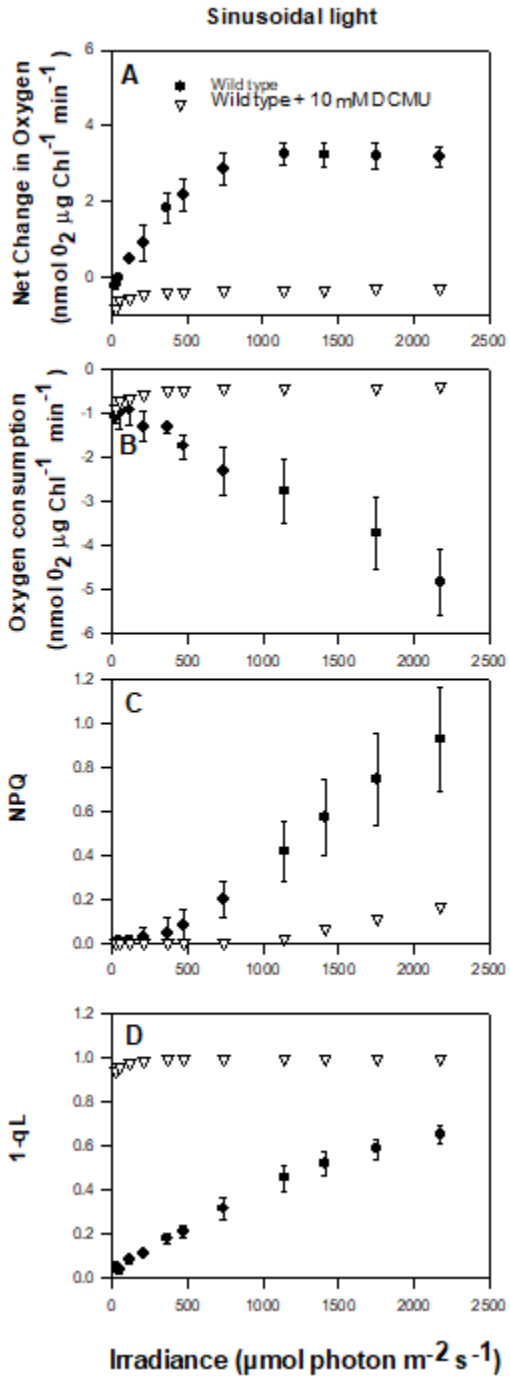


**Supplemental figure 3.2 Light dependent oxygen consumption capacity vs Irradiance for DCMU treated wild type acclimated to sinusoidal light.**
Wild type was harvested 6 hours after dawn and incubated with 10 µM DCMU for 5 minutes before the start of the P vs I light regime. Net photosynthesis, oxygen consumption, NPQ and 1-qL were measured simultaneously. Data for DCMU treatment represents n = 1.

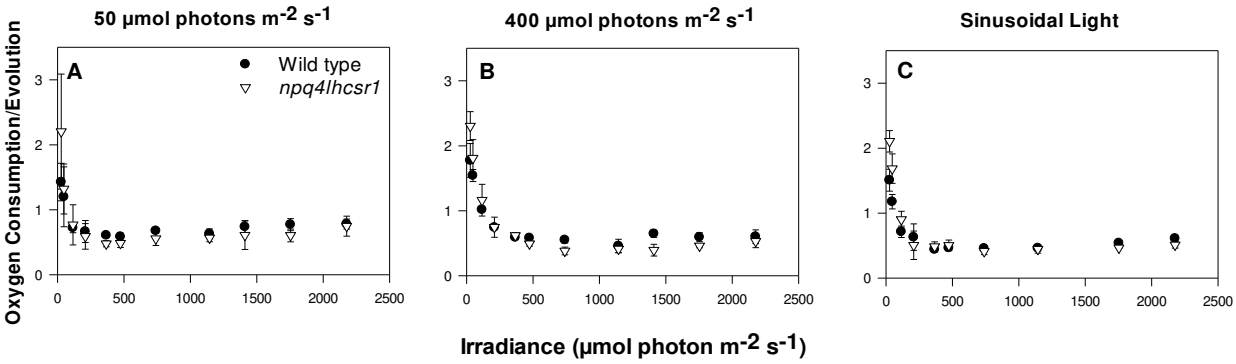


**Supplemental figure 3.3 Light dependent oxygen consumption capacity vs Irradiance for wild type and *npq4lhcsr1* acclimated to different light regimes.**

Wild type (black circles) and the *npq4lhcsr1* mutant (White triangles) acclimated to either 50 (a-d), 400 (e-h) µmol photon $m^{-2}$ $s^{-1}$ or a sinusoidal light regime (I-L, data collected 6 hours after dawn) were exposed to consecutive, increasing intensities of red light for a 3-minute duration. Net photosynthesis, oxygen consumption, NPQ and 1-qL were measured simultaneously. Data represents means ± s.d. (n = 3-4).

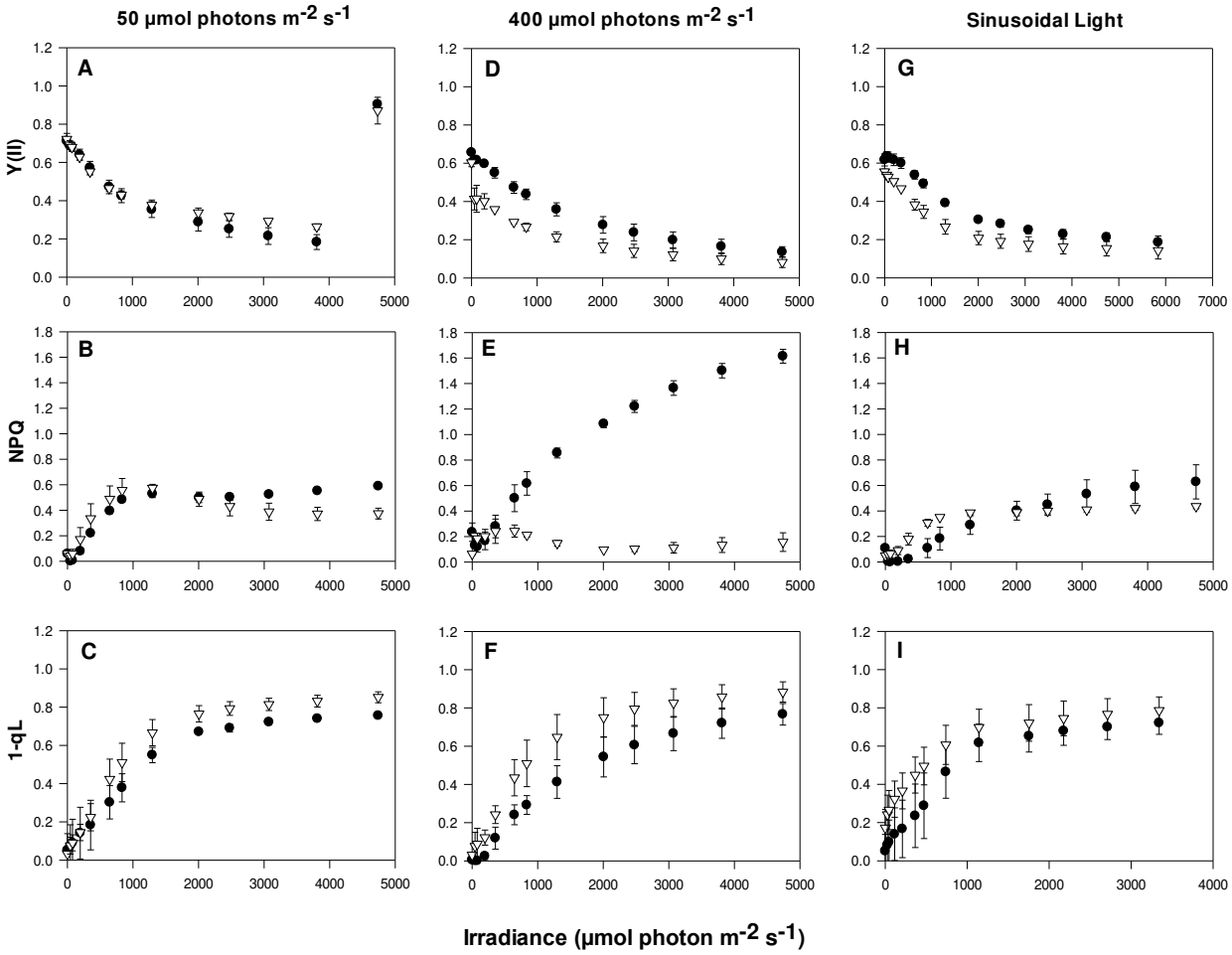


**Supplemental figure 3.4 Light irradiances impact on PSII quantum yields using an artificial leaf.**

Wild type (black circles) and the *npq4lhcsr1* mutant (White triangles) acclimated to either 50 (A-C), 400 (D-F) µmol photon $m^{-2}$ $s^{-1}$ or a sinusoidal light regime (G-I, data collected 6 hours after dawn) were exposed to consecutive, increasing intensities of red light for a 3-minute duration. Data represents means ± s.d. (n = 3-4).

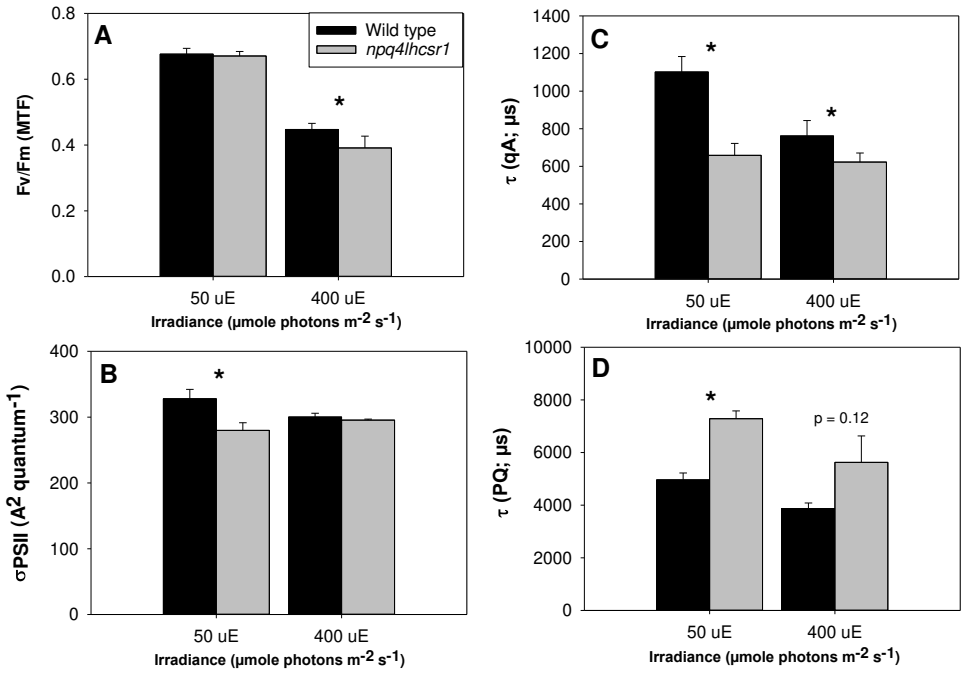


**Supplemental figure 3.5 Photophysiology of photosystem II in wild type and *npq4lhcsr1* acclimated to either 50 or 400 µmol photon $m^{-2}$ $s^{-1}$.**

Effective quantum yield (A), functional antenna size (B), qA re-oxidation kinetics (C) and qB re-oxidation kinetics (D) were measured within 1 minute of harvest by using a Fluorescence Induction and Relaxation (FIRe) fluorometer. Data represents means ± s.d. (n = 3). Symbols (*) represent significant differences from wild type within light acclimated states based on an un-paired t-test ($p<0.05$).

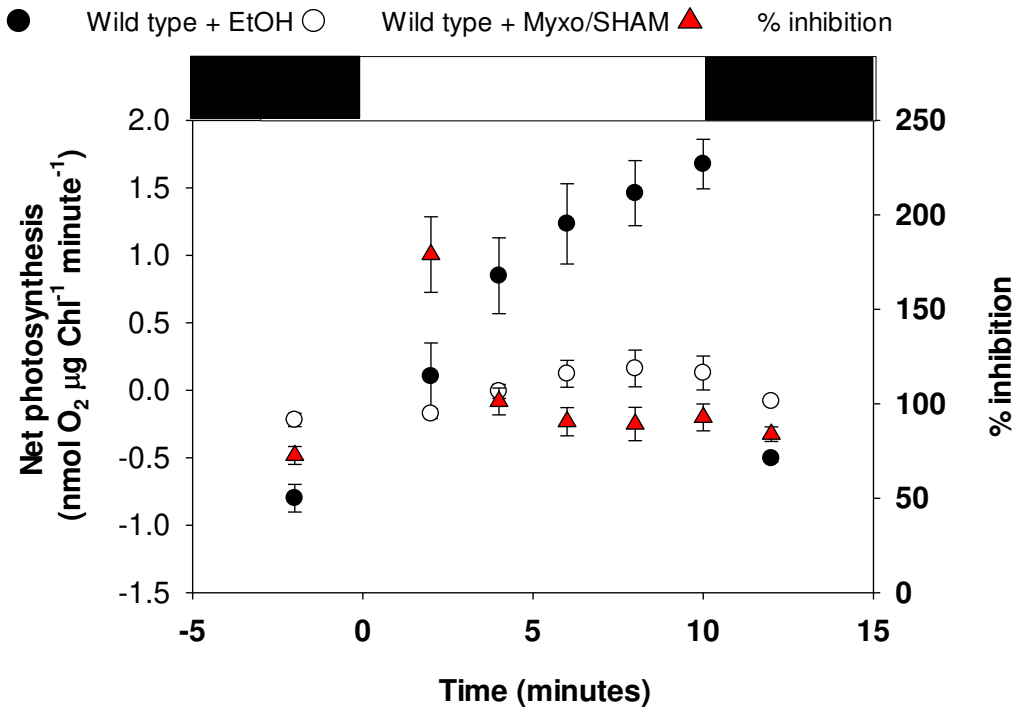


**Supplemental figure 3.6 Impact of dark incubation with Myxothiazol and SHAM on net photosynthesis in wild type Chlamydomonas.**

Wild type cells incubated for 8 minute with either ethanol (Filled circles) or Myxothiazol and SHAM (Myxo/SHAM) Empty circles) were illuminated for 10 minutes with 2000 µmol photon $m^{-2}$ $s^{-1}$ red light. % inhibition shown in red triangles reflects reduction in net photosynthesis between Myxo/SHAM.

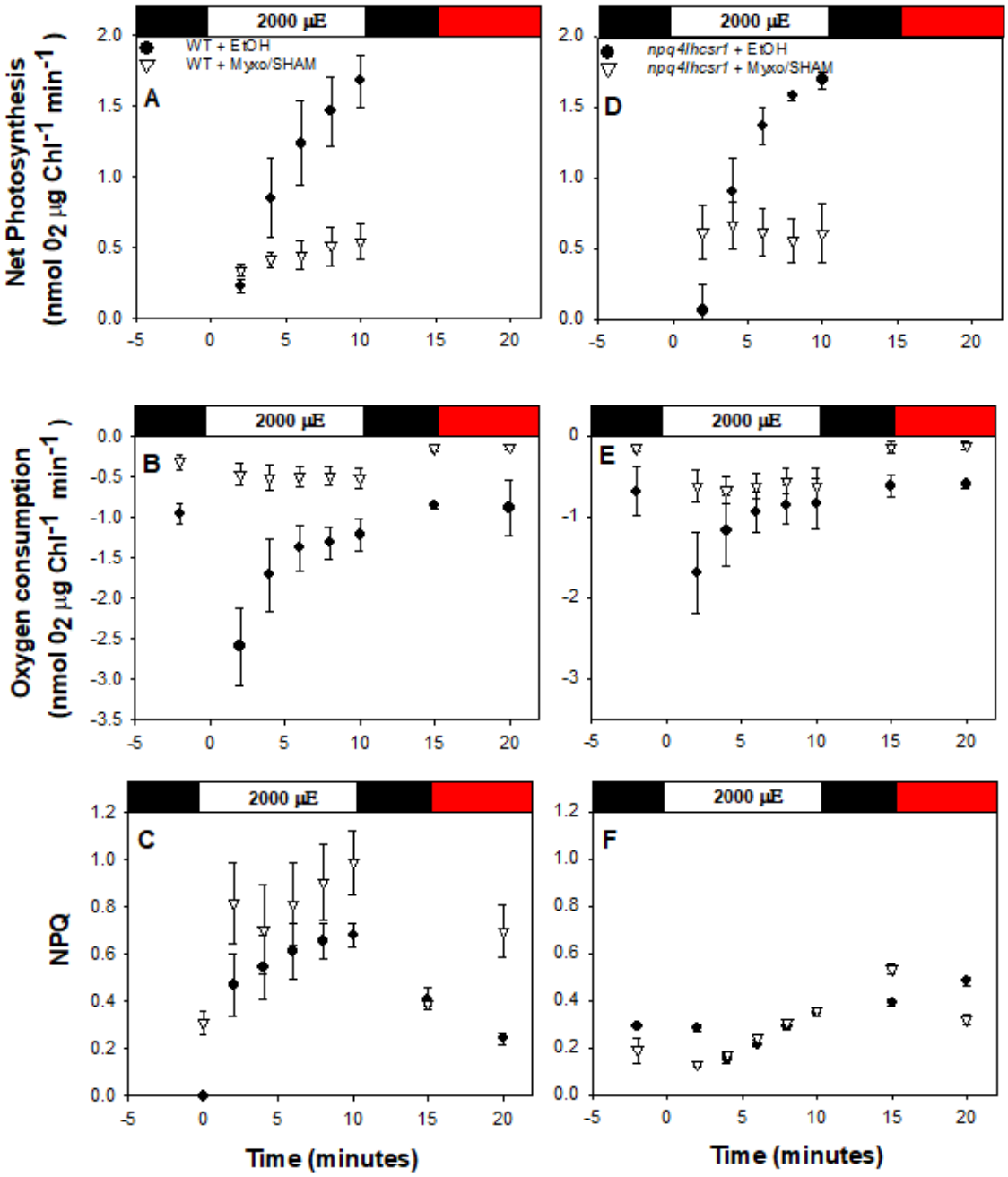


**Supplemental figure 3.7 Impact of the mitochondrial inhibitors (Myxothiazol and SHAM) on light dependent oxygen consumption in cultures acclimated to 400 µmol photon $m^{-2}$ $s^{-1}$ continuous light.**

Samples were pre-incubated with either ethanol or 2 µM myxothiazol (myxo) and 0.4 mM SHAM for 8 minutes in the dark prior to 10 minutes of 2000 µmol photon $m^{-2}$ $s^{-1}$ red light. Fluorescence was then allowed to recover for 5 minutes darkness followed by 5 minutes of far red light. Net photosynthesis, oxygen consumption, NPQ and 1-qL were collected simultaneously. Data represents means ± s.d. (n = 3-4).

**Supplemental Table 3.1 Wild type two-way ANOVA for comparisons of net photosynthesis between treatments**

Comparisons for factor: **treatment within dark respiration**

| **Comparison** | **Diff of Means** | **t** | **P** | **P<0.050** |
|---|---|---|---|---|
| EtOH vs. Myxo/SHAM | 0.125 | 0.479 | 0.867 | No |
| EtOH vs. PG | 0.0662 | 0.253 | 0.802 | No |

Comparisons for factor: **treatment within FR treatment**

| **Comparison** | **Diff of Means** | **t** | **P** | **P<0.050** |
|---|---|---|---|---|
| EtOH vs. Myxo/SHAM | 0.144 | 0.549 | 0.829 | No |
| EtOH vs. PG | 0.141 | 0.539 | 0.593 | No |

Comparisons for factor: **treatment within 2**

| **Comparison** | **Diff of Means** | **t** | **P** | **P<0.050** |
|---|---|---|---|---|
| EtOH vs. PG | 0.222 | 0.847 | 0.643 | No |
| EtOH vs. Myxo/SHAM | 0.102 | 0.391 | 0.698 | No |

Comparisons for factor: **treatment within 4**

| **Comparison** | **Diff of Means** | **t** | **P** | **P<0.050** |
|---|---|---|---|---|
| EtOH vs. Myxo/SHAM | 0.276 | 1.055 | 0.507 | No |
| EtOH vs. PG | 0.169 | 0.647 | 0.522 | No |

Comparisons for factor: **treatment within 6**

| **Comparison** | **Diff of Means** | **t** | **P** | **P<0.050** |
|---|---|---|---|---|
| EtOH vs. Myxo/SHAM | 0.317 | 1.212 | 0.411 | No |
| EtOH vs. PG | 0.113 | 0.430 | 0.669 | No |

Comparisons for factor: **treatment within 8**

| **Comparison** | **Diff of Means** | **t** | **P** | **P<0.050** |
|---|---|---|---|---|
| EtOH vs. PG | 0.718 | 2.741 | 0.018 | Yes |
| EtOH vs. Myxo/SHAM | 0.149 | 0.567 | 0.574 | No |

Comparisons for factor: **treatment within 10**

| **Comparison** | **Diff of Means** | **t** | **P** | **P<0.050** |
|---|---|---|---|---|
| EtOH vs. Myxo/SHAM | 0.411 | 1.568 | 0.234 | No |
| EtOH vs. PG | 0.398 | 1.519 | 0.137 | No |

Comparisons for factor: **treatment within 11**

| **Comparison** | **Diff of Means** | **t** | **P** | **P<0.050** |
|---|---|---|---|---|
| EtOH vs. Myxo/SHAM | 1.146 | 4.377 | <0.001 | Yes |
| EtOH vs. PG | 0.398 | 1.519 | 0.137 | No |

Comparisons for factor: **treatment within 12**

| **Comparison** | **Diff of Means** | **t** | **P** | **P<0.050** |
|---|---|---|---|---|
| EtOH vs. Myxo/SHAM | 1.519 | 5.800 | <0.001 | Yes |
| EtOH vs. PG | 0.979 | 3.739 | <0.001 | Yes |

Comparisons for factor: **treatment within 14**

| **Comparison** | **Diff of Means** | **t** | **P** | **P<0.050** |
|---|---|---|---|---|
| EtOH vs. PG | 0.807 | 3.083 | 0.007 | Yes |
| EtOH vs. Myxo/SHAM | 0.541 | 2.067 | 0.045 | Yes |

Comparisons for factor: **treatment within 16**

| **Comparison** | **Diff of Means** | **t** | **P** | **P<0.050** |
|---|---|---|---|---|
| EtOH vs. PG | 0.814 | 3.108 | 0.007 | Yes |

| | | | | |
|---|---|---|---|---|
| EtOH vs. Myxo/SHAM | 0.282 | 1.077 | 0.288 | No |

Comparisons for factor: **treatment within 18**

| **Comparison** | **Diff of Means** | **t** | **P** | **P<0.050** |
|---|---|---|---|---|
| EtOH vs. PG | 0.759 | 2.899 | 0.012 | Yes |
| EtOH vs. Myxo/SHAM | 0.0715 | 0.273 | 0.786 | No |

Comparisons for factor: **treatment within 20**

| **Comparison** | **Diff of Means** | **t** | **P** | **P<0.050** |
|---|---|---|---|---|
| EtOH vs. PG | 0.625 | 2.388 | 0.043 | Yes |
| EtOH vs. Myxo/SHAM | 0.0616 | 0.235 | 0.815 | No |

Comparisons for factor: **treatment within 25**

| **Comparison** | **Diff of Means** | **t** | **P** | **P<0.050** |
|---|---|---|---|---|
| EtOH vs. PG | 0.359 | 1.370 | 0.325 | No |
| EtOH vs. Myxo/SHAM | 0.224 | 0.854 | 0.398 | No |

Comparisons for factor: **treatment within 30**

| **Comparison** | **Diff of Means** | **t** | **P** | **P<0.050** |
|---|---|---|---|---|
| EtOH vs. Myxo/SHAM | 0.285 | 1.089 | 0.486 | No |
| EtOH vs. PG | 0.0771 | 0.294 | 0.770 | No |

## Supplemental Table 3.2 Wild type two-way ANOVA for comparisons of oxygen consumption between treatments

Comparisons for factor: **treatment within dark respiration**

| **Comparison** | **Diff of Means** | **t** | **P** | **P<0.050** |
|---|---|---|---|---|
| EtOH vs. Myxo/SHAM | 0.166 | 0.663 | 0.760 | No |
| EtOH vs. PG | 0.0595 | 0.238 | 0.813 | No |

Comparisons for factor: **treatment within FR treatment**

| **Comparison** | **Diff of Means** | **t** | **P** | **P<0.050** |
|---|---|---|---|---|
| EtOH vs. Myxo/SHAM | 0.220 | 0.880 | 0.620 | No |
| EtOH vs. PG | 0.196 | 0.783 | 0.437 | No |

Comparisons for factor: **treatment within 2**

| **Comparison** | **Diff of Means** | **t** | **P** | **P<0.050** |
|---|---|---|---|---|
| EtOH vs. PG | 0.162 | 0.649 | 0.769 | No |
| EtOH vs. Myxo/SHAM | 0.120 | 0.481 | 0.633 | No |

Comparisons for factor: **treatment within 4**

| **Comparison** | **Diff of Means** | **t** | **P** | **P<0.050** |
|---|---|---|---|---|
| EtOH vs. Myxo/SHAM | 0.421 | 1.683 | 0.189 | No |
| EtOH vs. PG | 0.00468 | 0.0187 | 0.985 | No |

Comparisons for factor: **treatment within 6**

| **Comparison** | **Diff of Means** | **t** | **P** | **P<0.050** |
|---|---|---|---|---|
| EtOH vs. Myxo/SHAM | 0.479 | 1.919 | 0.119 | No |
| EtOH vs. PG | 0.395 | 1.580 | 0.121 | No |

Comparisons for factor: **treatment within 8**

| **Comparison** | **Diff of Means** | **t** | **P** | **P<0.050** |
|---|---|---|---|---|
| EtOH vs. PG | 0.183 | 0.731 | 0.717 | No |
| EtOH vs. Myxo/SHAM | 0.139 | 0.556 | 0.581 | No |

Comparisons for factor: **treatment within 10**

| Comparison | Diff of Means | t | P | P<0.050 |
|---|---|---|---|---|
| EtOH vs. Myxo/SHAM | 0.134 | 0.537 | 0.835 | No |
| EtOH vs. PG | 0.0347 | 0.139 | 0.890 | No |

Comparisons for factor: **treatment within 11**

| Comparison | Diff of Means | t | P | P<0.050 |
|---|---|---|---|---|
| EtOH vs. Myxo/SHAM | 0.737 | 2.951 | 0.010 | Yes |
| EtOH vs. PG | 0.460 | 1.841 | 0.072 | No |

Comparisons for factor: **treatment within 12**

| Comparison | Diff of Means | t | P | P<0.050 |
|---|---|---|---|---|
| EtOH vs. Myxo/SHAM | 0.437 | 1.748 | 0.167 | No |
| EtOH vs. PG | 0.366 | 1.463 | 0.150 | No |

Comparisons for factor: **treatment within 14**

| Comparison | Diff of Means | t | P | P<0.050 |
|---|---|---|---|---|
| EtOH vs. Myxo/SHAM | 0.339 | 1.357 | 0.330 | No |
| EtOH vs. PG | 0.179 | 0.715 | 0.478 | No |

Comparisons for factor: **treatment within 16**

| Comparison | Diff of Means | t | P | P<0.050 |
|---|---|---|---|---|
| EtOH vs. Myxo/SHAM | 0.577 | 2.308 | 0.051 | No |
| EtOH vs. PG | 0.272 | 1.089 | 0.282 | No |

Comparisons for factor: **treatment within 18**

| Comparison | Diff of Means | t | P | P<0.050 |
|---|---|---|---|---|
| EtOH vs. Myxo/SHAM | 0.877 | 3.511 | 0.002 | Yes |
| EtOH vs. PG | 0.640 | 2.563 | 0.014 | Yes |

Comparisons for factor: **treatment within 20**

| Comparison | Diff of Means | t | P | P<0.050 |
|---|---|---|---|---|
| EtOH vs. Myxo/SHAM | 1.358 | 5.435 | <0.001 | Yes |
| EtOH vs. PG | 1.131 | 4.529 | <0.001 | Yes |

Comparisons for factor: **treatment within 25**

| Comparison | Diff of Means | t | P | P<0.050 |
|---|---|---|---|---|
| EtOH vs. Myxo/SHAM | 0.800 | 3.201 | 0.005 | Yes |
| EtOH vs. PG | 0.574 | 2.296 | 0.026 | Yes |

Comparisons for factor: **treatment within 30**

| Comparison | Diff of Means | t | P | P<0.050 |
|---|---|---|---|---|
| EtOH vs. Myxo/SHAM | 0.734 | 2.940 | 0.010 | Yes |
| EtOH vs. PG | 0.487 | 1.947 | 0.058 | No |

## Supplemental Table 3.3 Wild type two-way ANOVA for comparisons of 1-qL between treatments.

Comparisons for factor: **treatment within dark respiration**

| Comparison | Diff of Means | t | P | P<0.050 |
|---|---|---|---|---|
| EtOH vs. Myxo/SHAM | 0.000 | 0.000 | 1.000 | No |
| EtOH vs. PG | 0.000 | 0.000 | 1.000 | No |

Comparisons for factor: **treatment within FR treatment**

| Comparison | Diff of Means | t | P | P<0.050 |
|---|---|---|---|---|

| | | | | |
|---|---|---|---|---|
| EtOH vs. Myxo/SHAM | 0.000 | 0.000 | 1.000 | No |
| EtOH vs. PG | 0.000 | 0.000 | 1.000 | No |

Comparisons for factor: **treatment within 2**

| **Comparison** | **Diff of Means** | **t** | **P** | **P<0.050** |
|---|---|---|---|---|
| EtOH vs. PG | 0.00600 | 0.0837 | 0.996 | No |
| EtOH vs. Myxo/SHAM | 0.00133 | 0.0186 | 0.985 | No |

Comparisons for factor: **treatment within 4**

| **Comparison** | **Diff of Means** | **t** | **P** | **P<0.050** |
|---|---|---|---|---|
| EtOH vs. Myxo/SHAM | 0.0170 | 0.237 | 0.966 | No |
| EtOH vs. PG | 0.00300 | 0.0419 | 0.967 | No |

Comparisons for factor: **treatment within 6**

| **Comparison** | **Diff of Means** | **t** | **P** | **P<0.050** |
|---|---|---|---|---|
| EtOH vs. Myxo/SHAM | 0.282 | 3.930 | 0.002 | Yes |
| EtOH vs. PG | 0.110 | 1.530 | 0.143 | No |

Comparisons for factor: **treatment within 8**

| **Comparison** | **Diff of Means** | **t** | **P** | **P<0.050** |
|---|---|---|---|---|
| EtOH vs. Myxo/SHAM | 0.402 | 5.605 | <0.001 | Yes |
| EtOH vs. PG | 0.112 | 1.558 | 0.137 | No |

Comparisons for factor: **treatment within 10**

| **Comparison** | **Diff of Means** | **t** | **P** | **P<0.050** |
|---|---|---|---|---|
| EtOH vs. Myxo/SHAM | 0.443 | 6.182 | <0.001 | Yes |
| EtOH vs. PG | 0.112 | 1.563 | 0.136 | No |

Comparisons for factor: **treatment within 12**

| **Comparison** | **Diff of Means** | **t** | **P** | **P<0.050** |
|---|---|---|---|---|
| EtOH vs. Myxo/SHAM | 0.0930 | 1.298 | 0.377 | No |
| EtOH vs. PG | 0.0273 | 0.381 | 0.707 | No |

Comparisons for factor: **treatment within 14**

| **Comparison** | **Diff of Means** | **t** | **P** | **P<0.050** |
|---|---|---|---|---|
| EtOH vs. Myxo/SHAM | 0.100 | 1.400 | 0.325 | No |
| EtOH vs. PG | 0.0210 | 0.293 | 0.773 | No |

Comparisons for factor: **treatment within 16**

| **Comparison** | **Diff of Means** | **t** | **P** | **P<0.050** |
|---|---|---|---|---|
| EtOH vs. Myxo/SHAM | 0.103 | 1.433 | 0.310 | No |
| EtOH vs. PG | 0.0213 | 0.298 | 0.769 | No |

Comparisons for factor: **treatment within 18**

| **Comparison** | **Diff of Means** | **t** | **P** | **P<0.050** |
|---|---|---|---|---|
| EtOH vs. Myxo/SHAM | 0.0973 | 1.358 | 0.346 | No |
| EtOH vs. PG | 0.0237 | 0.330 | 0.745 | No |

Comparisons for factor: **treatment within 20**

| **Comparison** | **Diff of Means** | **t** | **P** | **P<0.050** |
|---|---|---|---|---|
| EtOH vs. Myxo/SHAM | 0.0953 | 1.330 | 0.360 | No |
| EtOH vs. PG | 0.0247 | 0.344 | 0.735 | No |

Comparisons for factor: **treatment within 25**

| **Comparison** | **Diff of Means** | **t** | **P** | **P<0.050** |
|---|---|---|---|---|
| EtOH vs. PG | 0.272 | 3.795 | 0.003 | Yes |

| | | | | |
|---|---|---|---|---|
| EtOH vs. Myxo/SHAM | 0.221 | 3.088 | 0.006 | Yes |

Comparisons for factor: **treatment within 30**

| **Comparison** | **Diff of Means** | **t** | **P** | **P<0.050** |
|---|---|---|---|---|
| EtOH vs. Myxo/SHAM | 0.385 | 5.377 | <0.001 | Yes |
| EtOH vs. PG | 0.155 | 2.158 | 0.045 | Yes |

## Supplemental Table 3.4 Wild type two-way ANOVA for comparisons of NPQ between treatments.

Comparisons for factor: **treatment within dark respiration**

| **Comparison** | **Diff of Means** | **t** | **P** | **P<0.050** |
|---|---|---|---|---|
| EtOH vs. PG | 0.632 | 5.273 | <0.001 | Yes |
| EtOH vs. Myxo/SHAM | 0.0162 | 0.135 | 0.894 | No |

Comparisons for factor: **treatment within FR treatment**

| **Comparison** | **Diff of Means** | **t** | **P** | **P<0.050** |
|---|---|---|---|---|
| EtOH vs. Myxo/SHAM | 0.0162 | 0.135 | 0.989 | No |
| EtOH vs. PG | 0.000 | 0.000 | 1.000 | No |

Comparisons for factor: **treatment within 2**

| **Comparison** | **Diff of Means** | **t** | **P** | **P<0.050** |
|---|---|---|---|---|
| EtOH vs. Myxo/SHAM | 0.0393 | 0.328 | 0.936 | No |
| EtOH vs. PG | 0.0127 | 0.106 | 0.917 | No |

Comparisons for factor: **treatment within 4**

| **Comparison** | **Diff of Means** | **t** | **P** | **P<0.050** |
|---|---|---|---|---|
| EtOH vs. Myxo/SHAM | 0.0387 | 0.323 | 0.938 | No |
| EtOH vs. PG | 0.0120 | 0.100 | 0.921 | No |

Comparisons for factor: **treatment within 6**

| **Comparison** | **Diff of Means** | **t** | **P** | **P<0.050** |
|---|---|---|---|---|
| EtOH vs. Myxo/SHAM | 0.214 | 1.783 | 0.175 | No |
| EtOH vs. PG | 0.00833 | 0.0695 | 0.945 | No |

Comparisons for factor: **treatment within 8**

| **Comparison** | **Diff of Means** | **t** | **P** | **P<0.050** |
|---|---|---|---|---|
| EtOH vs. Myxo/SHAM | 0.437 | 3.649 | 0.004 | Yes |
| EtOH vs. PG | 0.0343 | 0.286 | 0.778 | No |

Comparisons for factor: **treatment within 10**

| **Comparison** | **Diff of Means** | **t** | **P** | **P<0.050** |
|---|---|---|---|---|
| EtOH vs. Myxo/SHAM | 0.592 | 4.942 | <0.001 | Yes |
| EtOH vs. PG | 0.0467 | 0.389 | 0.702 | No |

Comparisons for factor: **treatment within 12**

| **Comparison** | **Diff of Means** | **t** | **P** | **P<0.050** |
|---|---|---|---|---|
| EtOH vs. Myxo/SHAM | 0.539 | 4.500 | <0.001 | Yes |
| EtOH vs. PG | 0.508 | 4.236 | <0.001 | Yes |

Comparisons for factor: **treatment within 14**

| **Comparison** | **Diff of Means** | **t** | **P** | **P<0.050** |
|---|---|---|---|---|
| EtOH vs. PG | 0.456 | 3.805 | 0.003 | Yes |
| EtOH vs. Myxo/SHAM | 0.419 | 3.496 | 0.003 | Yes |

Comparisons for factor: **treatment within 16**

| Comparison | Diff of Means | t | P | P<0.050 |
|---|---|---|---|---|
| EtOH vs. Myxo/SHAM | 0.466 | 3.888 | 0.002 | Yes |
| EtOH vs. PG | 0.441 | 3.679 | 0.002 | Yes |

Comparisons for factor: **treatment within 18**

| Comparison | Diff of Means | t | P | P<0.050 |
|---|---|---|---|---|
| EtOH vs. Myxo/SHAM | 0.551 | 4.597 | <0.001 | Yes |
| EtOH vs. PG | 0.531 | 4.428 | <0.001 | Yes |

Comparisons for factor: **treatment within 20**

| Comparison | Diff of Means | t | P | P<0.050 |
|---|---|---|---|---|
| EtOH vs. Myxo/SHAM | 0.652 | 5.443 | <0.001 | Yes |
| EtOH vs. PG | 0.638 | 5.326 | <0.001 | Yes |

Comparisons for factor: **treatment within 25**

| Comparison | Diff of Means | t | P | P<0.050 |
|---|---|---|---|---|
| EtOH vs. PG | 1.019 | 8.499 | <0.001 | Yes |
| EtOH vs. Myxo/SHAM | 0.0847 | 0.706 | 0.489 | No |

Comparisons for factor: **treatment within 30**

| Comparison | Diff of Means | t | P | P<0.050 |
|---|---|---|---|---|
| EtOH vs. Myxo/SHAM | 0.721 | 6.013 | <0.001 | Yes |
| EtOH vs. PG | 0.154 | 1.285 | 0.215 | No |

## Supplemental Table 3.5 *npq4lhcsr1* two-way ANOVA for comparisons of net photosynthesis between treatments.

Comparisons for factor: **Treatment within dark respiration**

| Comparison | Diff of Means | t | P | P<0.050 |
|---|---|---|---|---|
| EtOH vs. PG | 0.107 | 0.551 | 0.827 | No |
| EtOH vs. Myxo/SHAM | 0.0552 | 0.285 | 0.777 | No |

Comparisons for factor: **Treatment within FR treatment**

| Comparison | Diff of Means | t | P | P<0.050 |
|---|---|---|---|---|
| EtOH vs. Myxo/SHAM | 0.302 | 1.563 | 0.234 | No |
| EtOH vs. PG | 0.103 | 0.531 | 0.598 | No |

Comparisons for factor: **Treatment within 2**

| Comparison | Diff of Means | t | P | P<0.050 |
|---|---|---|---|---|
| EtOH vs. PG | 0.0332 | 0.172 | 0.982 | No |
| EtOH vs. Myxo/SHAM | 0.0239 | 0.124 | 0.902 | No |

Comparisons for factor: **Treatment within 4**

| Comparison | Diff of Means | t | P | P<0.050 |
|---|---|---|---|---|
| EtOH vs. Myxo/SHAM | 0.165 | 0.852 | 0.638 | No |
| EtOH vs. PG | 0.0150 | 0.0778 | 0.938 | No |

Comparisons for factor: **Treatment within 6**

| Comparison | Diff of Means | t | P | P<0.050 |
|---|---|---|---|---|
| EtOH vs. Myxo/SHAM | 0.0949 | 0.491 | 0.860 | No |
| EtOH vs. PG | 0.0888 | 0.459 | 0.648 | No |

Comparisons for factor: **Treatment within 8**

| Comparison | Diff of Means | t | P | P<0.050 |
|---|---|---|---|---|
| EtOH vs. Myxo/SHAM | 0.211 | 1.091 | 0.483 | No |

| | | | | |
|---|---|---|---|---|
| EtOH vs. PG | 0.0314 | 0.162 | 0.872 | No |

Comparisons for factor: **Treatment within 10**

| **Comparison** | **Diff of Means** | **t** | **P** | **P<0.050** |
|---|---|---|---|---|
| EtOH vs. PG | 0.188 | 0.813 | 0.664 | No |
| EtOH vs. Myxo/SHAM | 0.131 | 0.676 | 0.502 | No |

Comparisons for factor: **Treatment within 11**

| **Comparison** | **Diff of Means** | **t** | **P** | **P<0.050** |
|---|---|---|---|---|
| EtOH vs. Myxo/SHAM | 0.733 | 3.793 | <0.001 | Yes |
| EtOH vs. PG | 0.459 | 1.982 | 0.053 | No |

Comparisons for factor: **Treatment within 12**

| **Comparison** | **Diff of Means** | **t** | **P** | **P<0.050** |
|---|---|---|---|---|
| EtOH vs. Myxo/SHAM | 0.221 | 1.145 | 0.449 | No |
| EtOH vs. PG | 0.0236 | 0.102 | 0.919 | No |

Comparisons for factor: **Treatment within 14**

| **Comparison** | **Diff of Means** | **t** | **P** | **P<0.050** |
|---|---|---|---|---|
| EtOH vs. Myxo/SHAM | 0.439 | 2.275 | 0.054 | No |
| EtOH vs. PG | 0.492 | 2.125 | 0.039 | Yes |

Comparisons for factor: **Treatment within 16**

| **Comparison** | **Diff of Means** | **t** | **P** | **P<0.050** |
|---|---|---|---|---|
| EtOH vs. PG | 0.639 | 2.757 | 0.017 | Yes |
| EtOH vs. Myxo/SHAM | 0.371 | 1.921 | 0.061 | No |

Comparisons for factor: **Treatment within 18**

| **Comparison** | **Diff of Means** | **t** | **P** | **P<0.050** |
|---|---|---|---|---|
| EtOH vs. Myxo/SHAM | 0.267 | 1.380 | 0.318 | No |
| EtOH vs. PG | 0.292 | 1.262 | 0.213 | No |

Comparisons for factor: **Treatment within 20**

| **Comparison** | **Diff of Means** | **t** | **P** | **P<0.050** |
|---|---|---|---|---|
| EtOH vs. Myxo/SHAM | 0.660 | 3.416 | 0.003 | Yes |
| EtOH vs. PG | 0.259 | 1.119 | 0.269 | No |

Comparisons for factor: **Treatment within 25**

| **Comparison** | **Diff of Means** | **t** | **P** | **P<0.050** |
|---|---|---|---|---|
| EtOH vs. PG | 0.234 | 1.001 | 0.540 | No |
| EtOH vs. Myxo/SHAM | 0.0826 | 0.358 | 0.722 | No |

Comparisons for factor: **Treatment within 30**

| **Comparison** | **Diff of Means** | **t** | **P** | **P<0.050** |
|---|---|---|---|---|
| EtOH vs. Myxo/SHAM | 0.755 | 3.910 | <0.001 | Yes |
| EtOH vs. PG | 0.435 | 1.876 | 0.067 | No |

## Supplemental Table 3.6 *npq4lhcsr1* two-way ANOVA for comparisons of oxygen consumption between treatments.

Comparisons for factor: **Treatment within dark respiration**

| **Comparison** | **Diff of Means** | **t** | **P** | **P<0.050** |
|---|---|---|---|---|
| EtOH vs. PG | 0.153 | 0.812 | 0.669 | No |
| EtOH vs. Myxo/SHAM | 0.0825 | 0.440 | 0.664 | No |

Comparisons for factor: **Treatment within FR treatment**

| Comparison | Diff of Means | t | P | P<0.050 |
|---|---|---|---|---|
| EtOH vs. Myxo/SHAM | 0.279 | 1.485 | 0.279 | No |
| EtOH vs. PG | 0.185 | 0.988 | 0.333 | No |

Comparisons for factor: **Treatment within 2**

| Comparison | Diff of Means | t | P | P<0.050 |
|---|---|---|---|---|
| EtOH vs. PG | 0.167 | 0.890 | 0.619 | No |
| EtOH vs. Myxo/SHAM | 0.147 | 0.782 | 0.442 | No |

Comparisons for factor: **Treatment within 4**

| Comparison | Diff of Means | t | P | P<0.050 |
|---|---|---|---|---|
| EtOH vs. PG | 0.156 | 0.831 | 0.657 | No |
| EtOH vs. Myxo/SHAM | 0.0300 | 0.160 | 0.874 | No |

Comparisons for factor: **Treatment within 6**

| Comparison | Diff of Means | t | P | P<0.050 |
|---|---|---|---|---|
| EtOH vs. PG | 0.260 | 1.387 | 0.326 | No |
| EtOH vs. Myxo/SHAM | 0.0894 | 0.476 | 0.638 | No |

Comparisons for factor: **Treatment within 8**

| Comparison | Diff of Means | t | P | P<0.050 |
|---|---|---|---|---|
| EtOH vs. Myxo/SHAM | 0.344 | 1.833 | 0.153 | No |
| EtOH vs. PG | 0.246 | 1.309 | 0.203 | No |

Comparisons for factor: **Treatment within 10**

| Comparison | Diff of Means | t | P | P<0.050 |
|---|---|---|---|---|
| EtOH vs. Myxo/SHAM | 0.205 | 1.091 | 0.491 | No |
| EtOH vs. PG | 0.0835 | 0.371 | 0.714 | No |

Comparisons for factor: **Treatment within 11**

| Comparison | Diff of Means | t | P | P<0.050 |
|---|---|---|---|---|
| EtOH vs. PG | 0.697 | 3.095 | 0.010 | Yes |
| EtOH vs. Myxo/SHAM | 0.0845 | 0.450 | 0.657 | No |

Comparisons for factor: **Treatment within 12**

| Comparison | Diff of Means | t | P | P<0.050 |
|---|---|---|---|---|
| EtOH vs. PG | 1.004 | 4.459 | <0.001 | Yes |
| EtOH vs. Myxo/SHAM | 0.800 | 4.262 | <0.001 | Yes |

Comparisons for factor: **Treatment within 14**

| Comparison | Diff of Means | t | P | P<0.050 |
|---|---|---|---|---|
| EtOH vs. PG | 0.306 | 1.362 | 0.338 | No |
| EtOH vs. Myxo/SHAM | 0.0803 | 0.428 | 0.673 | No |

Comparisons for factor: **Treatment within 16**

| Comparison | Diff of Means | t | P | P<0.050 |
|---|---|---|---|---|
| EtOH vs. Myxo/SHAM | 0.422 | 2.248 | 0.068 | No |
| EtOH vs. PG | 0.116 | 0.515 | 0.611 | No |

Comparisons for factor: **Treatment within 18**

| Comparison | Diff of Means | t | P | P<0.050 |
|---|---|---|---|---|
| EtOH vs. Myxo/SHAM | 0.890 | 4.742 | <0.001 | Yes |
| EtOH vs. PG | 1.009 | 4.485 | <0.001 | Yes |

Comparisons for factor: **Treatment within 20**

| Comparison | Diff of Means | t | P | P<0.050 |
|---|---|---|---|---|

| | | | | |
|---|---|---|---|---|
| EtOH vs. Myxo/SHAM | 0.886 | 4.721 | <0.001 | Yes |
| EtOH vs. PG | 0.925 | 4.110 | <0.001 | Yes |

Comparisons for factor: **Treatment within 25**

| **Comparison** | **Diff of Means** | **t** | **P** | **P<0.050** |
|---|---|---|---|---|
| EtOH vs. Myxo/SHAM | 1.234 | 5.500 | <0.001 | Yes |
| EtOH vs. PG | 0.639 | 2.811 | 0.010 | Yes |

Comparisons for factor: **Treatment within 30**

| **Comparison** | **Diff of Means** | **t** | **P** | **P<0.050** |
|---|---|---|---|---|
| EtOH vs. Myxo/SHAM | 0.744 | 3.962 | 0.001 | Yes |
| EtOH vs. PG | 0.393 | 1.745 | 0.094 | No |

## Supplemental Table 3.7 *npq4lhcsr1* two-way ANOVA for comparisons of 1-qL between treatments.

Comparisons for factor: **Treatment within dark respiration**

| **Comparison** | **Diff of Means** | **t** | **P** | **P<0.050** |
|---|---|---|---|---|
| EtOH vs. Myxo/SHAM | 0.000 | 0.000 | 1.000 | No |
| EtOH vs. PG | 0.000 | 0.000 | 1.000 | No |

Comparisons for factor: **Treatment within FR treatment**

| **Comparison** | **Diff of Means** | **t** | **P** | **P<0.050** |
|---|---|---|---|---|
| EtOH vs. Myxo/SHAM | 0.000 | 0.000 | 1.000 | No |
| EtOH vs. PG | 0.000 | 0.000 | 1.000 | No |

Comparisons for factor: **Treatment within 2**

| **Comparison** | **Diff of Means** | **t** | **P** | **P<0.050** |
|---|---|---|---|---|
| EtOH vs. PG | 0.0250 | 0.840 | 0.646 | No |
| EtOH vs. Myxo/SHAM | 0.0160 | 0.537 | 0.593 | No |

Comparisons for factor: **Treatment within 4**

| **Comparison** | **Diff of Means** | **t** | **P** | **P<0.050** |
|---|---|---|---|---|
| EtOH vs. Myxo/SHAM | 0.0240 | 0.806 | 0.668 | No |
| EtOH vs. PG | 0.0217 | 0.728 | 0.470 | No |

Comparisons for factor: **Treatment within 6**

| **Comparison** | **Diff of Means** | **t** | **P** | **P<0.050** |
|---|---|---|---|---|
| EtOH vs. Myxo/SHAM | 0.329 | 11.040 | <0.001 | Yes |
| EtOH vs. PG | 0.108 | 3.628 | <0.001 | Yes |

Comparisons for factor: **Treatment within 8**

| **Comparison** | **Diff of Means** | **t** | **P** | **P<0.050** |
|---|---|---|---|---|
| EtOH vs. Myxo/SHAM | 0.408 | 13.716 | <0.001 | Yes |
| EtOH vs. PG | 0.141 | 4.747 | <0.001 | Yes |

Comparisons for factor: **Treatment within 10**

| **Comparison** | **Diff of Means** | **t** | **P** | **P<0.050** |
|---|---|---|---|---|
| EtOH vs. Myxo/SHAM | 0.453 | 15.228 | <0.001 | Yes |
| EtOH vs. PG | 0.132 | 4.434 | <0.001 | Yes |

Comparisons for factor: **Treatment within 12**

| **Comparison** | **Diff of Means** | **t** | **P** | **P<0.050** |
|---|---|---|---|---|
| EtOH vs. Myxo/SHAM | 0.0270 | 0.907 | 0.601 | No |
| EtOH vs. PG | 0.0113 | 0.381 | 0.705 | No |

Comparisons for factor: **Treatment within 14**

| Comparison | Diff of Means | t | P | P<0.050 |
|---|---|---|---|---|
| EtOH vs. Myxo/SHAM | 0.0470 | 1.579 | 0.226 | No |
| EtOH vs. PG | 0.0153 | 0.515 | 0.609 | No |

Comparisons for factor: **Treatment within 16**

| Comparison | Diff of Means | t | P | P<0.050 |
|---|---|---|---|---|
| EtOH vs. Myxo/SHAM | 0.0587 | 1.971 | 0.105 | No |
| EtOH vs. PG | 0.0227 | 0.761 | 0.450 | No |

Comparisons for factor: **Treatment within 18**

| Comparison | Diff of Means | t | P | P<0.050 |
|---|---|---|---|---|
| EtOH vs. Myxo/SHAM | 0.0713 | 2.396 | 0.040 | Yes |
| EtOH vs. PG | 0.0333 | 1.120 | 0.268 | No |

Comparisons for factor: **Treatment within 20**

| Comparison | Diff of Means | t | P | P<0.050 |
|---|---|---|---|---|
| EtOH vs. Myxo/SHAM | 0.0793 | 2.665 | 0.020 | Yes |
| EtOH vs. PG | 0.0460 | 1.545 | 0.128 | No |

Comparisons for factor: **Treatment within 25**

| Comparison | Diff of Means | t | P | P<0.050 |
|---|---|---|---|---|
| EtOH vs. PG | 0.334 | 11.230 | <0.001 | Yes |
| EtOH vs. Myxo/SHAM | 0.258 | 8.655 | <0.001 | Yes |

Comparisons for factor: **Treatment within 30**

| Comparison | Diff of Means | t | P | P<0.050 |
|---|---|---|---|---|
| EtOH vs. Myxo/SHAM | 0.347 | 11.667 | <0.001 | Yes |
| EtOH vs. PG | 0.163 | 5.486 | <0.001 | Yes |

## Supplemental Table 3.8 *npq4lhcsr1* two-way ANOVA for comparisons of NPQ between treatments.

Comparisons for factor: **Treatment within dark respiration**

| Comparison | Diff of Means | t | P | P<0.050 |
|---|---|---|---|---|
| EtOH vs. Myxo/SHAM | 0.000 | 0.000 | 1.000 | No |
| EtOH vs. PG | 0.000 | 0.000 | 1.000 | No |

Comparisons for factor: **Treatment within FR treatment**

| Comparison | Diff of Means | t | P | P<0.050 |
|---|---|---|---|---|
| EtOH vs. Myxo/SHAM | 0.000 | 0.000 | 1.000 | No |
| EtOH vs. PG | 0.000 | 0.000 | 1.000 | No |

Comparisons for factor: **Treatment within 2**

| Comparison | Diff of Means | t | P | P<0.050 |
|---|---|---|---|---|
| EtOH vs. Myxo/SHAM | 0.0197 | 0.481 | 0.865 | No |
| EtOH vs. PG | 0.0180 | 0.440 | 0.662 | No |

Comparisons for factor: **Treatment within 4**

| Comparison | Diff of Means | t | P | P<0.050 |
|---|---|---|---|---|
| EtOH vs. PG | 0.0217 | 0.530 | 0.839 | No |
| EtOH vs. Myxo/SHAM | 0.0150 | 0.367 | 0.715 | No |

Comparisons for factor: **Treatment within 6**

| Comparison | Diff of Means | t | P | P<0.050 |
|---|---|---|---|---|
| EtOH vs. Myxo/SHAM | 0.110 | 2.684 | 0.020 | Yes |

| | | | | |
|---|---|---|---|---|
| EtOH vs. PG | 0.0213 | 0.522 | 0.604 | No |

Comparisons for factor: **Treatment within 8**

| **Comparison** | **Diff of Means** | **t** | **P** | **P<0.050** |
|---|---|---|---|---|
| EtOH vs. Myxo/SHAM | 0.180 | 4.413 | <0.001 | Yes |
| EtOH vs. PG | 0.00200 | 0.0489 | 0.961 | No |

Comparisons for factor: **Treatment within 10**

| **Comparison** | **Diff of Means** | **t** | **P** | **P<0.050** |
|---|---|---|---|---|
| EtOH vs. Myxo/SHAM | 0.219 | 5.367 | <0.001 | Yes |
| EtOH vs. PG | 0.0170 | 0.416 | 0.679 | No |

Comparisons for factor: **Treatment within 12**

| **Comparison** | **Diff of Means** | **t** | **P** | **P<0.050** |
|---|---|---|---|---|
| EtOH vs. Myxo/SHAM | 0.0627 | 1.534 | 0.246 | No |
| EtOH vs. PG | 0.0247 | 0.604 | 0.549 | No |

Comparisons for factor: **Treatment within 14**

| **Comparison** | **Diff of Means** | **t** | **P** | **P<0.050** |
|---|---|---|---|---|
| EtOH vs. Myxo/SHAM | 0.0260 | 0.636 | 0.777 | No |
| EtOH vs. PG | 0.00933 | 0.228 | 0.820 | No |

Comparisons for factor: **Treatment within 16**

| **Comparison** | **Diff of Means** | **t** | **P** | **P<0.050** |
|---|---|---|---|---|
| EtOH vs. Myxo/SHAM | 0.0420 | 1.028 | 0.523 | No |
| EtOH vs. PG | 0.0243 | 0.595 | 0.554 | No |

Comparisons for factor: **Treatment within 18**

| **Comparison** | **Diff of Means** | **t** | **P** | **P<0.050** |
|---|---|---|---|---|
| EtOH vs. Myxo/SHAM | 0.0487 | 1.191 | 0.422 | No |
| EtOH vs. PG | 0.0360 | 0.881 | 0.383 | No |

Comparisons for factor: **Treatment within 20**

| **Comparison** | **Diff of Means** | **t** | **P** | **P<0.050** |
|---|---|---|---|---|
| EtOH vs. Myxo/SHAM | 0.0520 | 1.273 | 0.375 | No |
| EtOH vs. PG | 0.0467 | 1.142 | 0.259 | No |

Comparisons for factor: **Treatment within 25**

| **Comparison** | **Diff of Means** | **t** | **P** | **P<0.050** |
|---|---|---|---|---|
| EtOH vs. Myxo/SHAM | 0.178 | 4.348 | <0.001 | Yes |
| EtOH vs. PG | 0.0947 | 2.317 | 0.025 | Yes |

Comparisons for factor: **Treatment within 30**

| **Comparison** | **Diff of Means** | **t** | **P** | **P<0.050** |
|---|---|---|---|---|
| EtOH vs. Myxo/SHAM | 0.0447 | 1.093 | 0.481 | No |
| EtOH vs. PG | 0.0267 | 0.653 | 0.517 | No |

**Chapter 4 supplemental information**

**Supplemental table 4.3 Screening primers for confirmation of chloroplast genome insertion.**

| Primer | Description | Sequence (5'-3') |
|---|---|---|
| LEMS_3f | c*odA* insertion | AATAACATTTTATGTCTAACAACGCTTTAC |
| LEMS_4r | c*odA* insertion | TTAGATTATTTTTATTAAGCGTAATCTGGAAC |
| mbc_198f | No CodA *(psaA*) | AGATTTTATTTTTCTGGCACATCGT |
| mbc_199f | TN72 background (forward) | GTCATTGCGAAAATACTGGTGC |
| mbc_200r | TN72 background (reverse 1) | CGGATGTAACTCAATCGGTAG |
| R3r | No CodA *(ChlB)* | AGCAACCCCTTGACGAGAGA |

**Supplemental table 4.4 Primers for flanking sequence amplification.**

| Primer | Description | Sequence (5'-3') |
|---|---|---|
| AP1 | Adaptor Primer for primary reactions | GTAATACGACTCACTATAGAGT |
| AP2 | Adaptor primer for secondary reactions | ACTATAGAGTACGCGTGGT |
| RIM_3-1 | 3' insert primer for primary reactions | CGGTATCGGAGGAAAAGCTG |
| RIM_3-2 | 3' insert primer for secondary reactions | GCTGTTGGACGAGTTCTTCTG |
| RX1 | 5' insert primer for secondary reactions | GCCCTCATAGCCCGCCAAATCAG |
| RX2 | 5' insert primer for primary reactions | AAGCCGATAAACACCAGCCC |

**Supplemental table 4.5 Amplification primers vector backbones used in cloning.**

| Primer | Description | Sequence (5'-3') |
|---|---|---|
| LEM16_pRY127Df | Vector backbone amplification primer for *psaA::codA* | ATTTTTATTTTTCATGATGTTTATGTG |
| LEM13_pRY127Dr | Vector backbone amplification primer for *psaA::codA* | TGGATTTCTCCTTATAATAACAATTATTTAATTTAATAAATAC |
| LEM16_pRY127Df | Vector backbone amplification primer for *chlB::codA* | ATTTTTATTTTTCATGATGTTTATGTG |
| LEM2_5'_ChlB_rev_v2 | Vector backbone amplification primer for *chlB::codA* | TGTTAGACATAAAATGTTATTTTGTAGTCAAAACGCAC |

**Supplemental table 4.6 Table of plasmid vector maps used in study.**

| Plasmid Name | Plasmid Map |
|---|---|
| pRY127D *psaA::codA* | 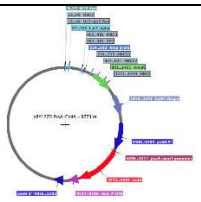 |
| pRY127D *chlB::codA* | 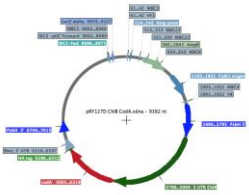 |
| pRY127D empty vector Control | 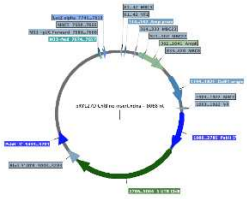 |

# APPENDIX B: CHARACTERIZATION OF *CHLAMYDOMONAS* PHYSIOLOGY IN THE ABSENCE OF EXCITATION DEPENDENT QUENCHING AND STATE TRANSITIONS

## Preface

The following appendix presents work on the qE mutant, *npq4lhcsr1*, qT mutant (*stt7-9*) and qE and qT mutant (*nqp4lhcsr1stt7-9*). In 2016 we discovered that the *stt7-9* line generated originally in 1999 had a background mutation in one of the two nuclear genes encoding the small subunit of rubisco and a protein of unknown function (g2496). Unfortunately, by this time several studies had used this mutant to characterized qT (Lucker *et al.*, 2013, Cardol *et al.*, 2009, Allorent *et al.*, 2013, Ghysels *et al.* 2013, Alric *et al.*, 2014, Johnson *et al.,* 2012, Nagy *et al.*, 2014, Roach *et al.*, 2015, Kodru *et al.*, 2015*)*. Most of these studies focused on biochemical analysis of the *stt7-9* mutant and crosses derived from this background. Consequently, the potential impact of these background mutations is minimal, but likely had an affect on questions that were associated with the acclimation or physiological state – which may be impaired in the absence of the *rbcS2* subunit or this protein of unknown function. Work on the mutant lines *stt7-9* and *npq4lhcsr1stt7-9* was subsequently discontinued due to concerns over possible artifacts generated by these background deletions. The following section details the physiological characterization conducted up to 2016 on these mutants.

## Introduction

Research on excitation dependent quenching in *Chlamydomonas* has focused on characterizing LHCSR3.1 and LHCSR3.2 mutant, *npq4*, to avoid pleiotropic affects associated with mutants of the xanthophyll cycle. The initial study characterizing the LHCSR3.1 and LHCSR3.2 mutant, *npq4*, demonstrated that LHCSR3 is required for approximately 50% of the non-photochemical quenching of chlorophyll fluorescence (NPQ) and that in their absence, *npq4*

experiences reduced fitness when shifted from a low-light acclimated state to excess light (1,100 µmole photon $m^{-2}$ $s^{-1}$)(Peers *et al.*, 2009). In high light acclimated conditions (325 µmole photon $m^{-2}$ $s^{-1}$), Peers *et al.* found no difference in reproductive fitness measured by growth rate per day. This suggested that while loss of qE is required during a shift to high light, long-term acclimation responses can effectively compensate for its loss under relatively low, high light growth conditions.

Research on state transitions role in fitness in *Chlamydomonas* has used the *stt7-9* mutant. Initial studies characterizing *stt7-9* found no difference in growth rate or photosensitivity when compared with wild type (Depège *et al.*, 2003). It was later shown that loss state transitions impacts fitness when respiration is impaired (Cardol *et al.*, 2009). Cardol *et al.* (2009) showed that this was due to reduced cyclic electron transport in a mutant impaired in both respiration and state transitions. This suggests that state transitions may adjust photosystem I turnover to increase ATP production when cellular ATP levels are depleted.

Comparison of PSII photophysiology in *npq4* with *stt7-9* and a double mutant, *npq4stt7-9,* showed that both are required to maintain PSII efficiency during light stress. Allorent *et al.* (2013) showed that shifting cells to high light (500 µmole photon $m^{-2}$ $s^{-1}$) for 4 hours lead to a significant decrease in the yield of fluorescence from PSII (measured as the variable fluorescence (Fv) /maximum fluorescence (Fm)) in both single and double mutant. This parameter, $F_v/F_m$, reflects the number of PSII reaction centers open to photochemistry with lower values indicating increased PSII photoinhibition (qI). Significant reductions in PSII efficiency observed in *npq4stt7-9* over *npq4* or *stt7-9* alone suggested that both processes cooperate in protecting PSII from damage(Allorent *et al.*, 2013a). Enhanced $H_2O_2$ production generated in *stt7-9* during the first hours of high light acclimation relative to wild type indicates that state

transitions play a photoprotective role prior to significant LHCSR accumulation(Allorent *et al.*, 2013a). Together these observations suggest an overlap between light energy dissipation by excitation dependent quenching and state transitions and may indicate that they cooperate in excess light conditions to avoid excess damage to the photosynthetic apparatus.

To test the hypothesis that excitation dependent quenching and state transitions cooperate to maintain fitness in excess light, I am comparing the uncharacterized LHCSR-less mutant, *npq4lhcsr1,* the state transition mutant, *stt7-9,* and a triple mutant, *npq4lhcsr1stt7-9 #4*.

**Methods**

Methods for this section are presented in chapter 2.

**Results and discussion**

To evaluate the role of excitation dependent quenching and state transitions on fitness in excess light conditions. Physiology was assessed in cultures acclimated to saturating constant irradiance (860 µmole photon $m^{-2}$ $s^{-1}$) in shake flasks and compared with sub-saturating conditions (50 µmole photon $m^{-2}$ $s^{-1}$ ). Constant light was used for this initial characterization to avoid variability in LHCSR expression during natural diurnal cycling (Savard *et al.*, 1996). Under these conditions, significant reductions in exponential growth rate per day were observed for in *npq4lhcsr1 and stt7-9* compared with wild type and loss of both qE and qT in *npq4lhcsr1stt7-9 #4* lead to even greater growth inhibition than loss of qE or qT alone (Figure A.1). This shows that qE and qT cooperate to maintain reproductive fitness in excess light. The magnitude of the reductions observed though also suggests that in the absence of light energy dissipation other mechanisms compensate by either reducing light absorption or dissipating excess reductant.

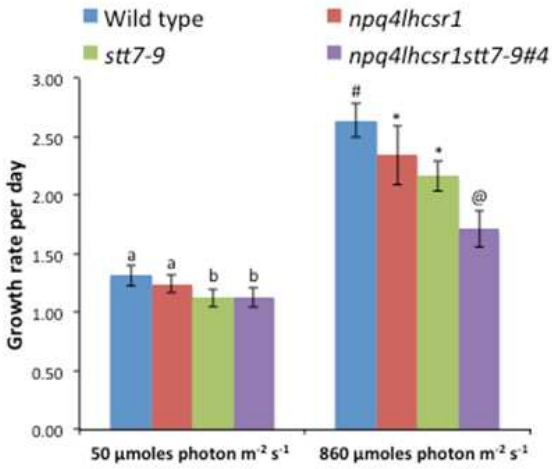


**Figure B.1 Exponential growth rates qE and qT mutants.**
Data represents means ± s.d. (n=8). Symbols denote statistically significant differences ($p < 0.05$) based on a one-way ANOVA followed by a tukey multiple comparison test.

PAM fluorometry was used to determine if reductions in growth rate are associated with changes in PSII photochemistry. Reductions in growth rate were correlated with significant decreases in the photosystem II efficiency (measured by $F_v/F_m$) for *npq4lhcsr1* and *npq4lhcsr1stt7-9 #4*, but not for *stt7-9* (Figure A.2). These results indicate that reductions in growth rate observed in excitation dependent quenching mutants might be due to increased PSII damage. While increased PSII efficiency in *stt7-9* (Figure A.2) may be explained by its increased capacity for excitation dependent quenching compared with wild type (Figure A.3B). Excitation dependent quenching is measured by NPQ that is rapidly induced by excess light (white box) and undergoes rapid reversion during subsequent darkness (black box) NPQ induced during excess light exposure in *npq4lhcsr1* and *npq4lhcsr1stt7-9 #4* does not relax after the lights are turned off (black box), indicating that NPQ induced during these time courses is predominately from PSII photoinhibition (qI). Initial measurements of relative qT indicate that the relative capacity

for transitions is significantly reduced in both light conditions for *stt7-9* and *npq4lhcsr1stt7-9 #4* mutants. This was measured by comparing the maximum PSII fluorescence after incubating cultures in the dark for 20 minutes without aeration (state II favoring) followed by 10 minutes of far red light to oxidize the plastoquinone pool and induce a transition to state I where LHCII should be associated with PSII. However, these measurements do not reflect a quantitative measure of state transition capacity.

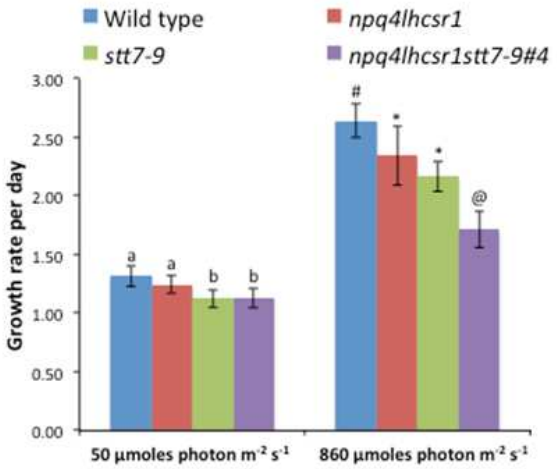


**Figure B.2 Exponential growth rates qE and qT mutants.**
Data represents means ± s.d. (n=8). Symbols denote statistically significant differences ($p < 0.05$) based on a one-way ANOVA followed by a tukey multiple comparison test.

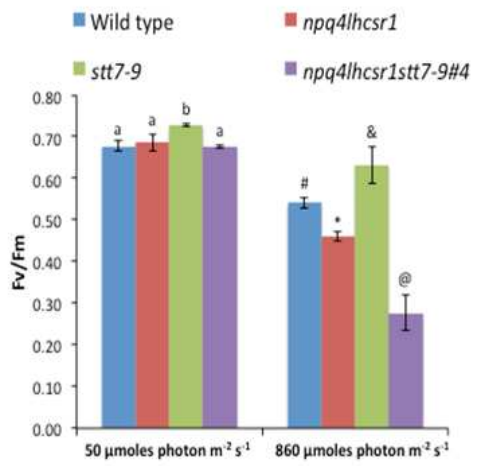


**Figure B.3 PSII efficiency for qE and qT mutants.**
Data represents means ± s.d. (n=3). Symbols denote statistically significant differences ($p < 0.05$) based on a one-way ANOVA followed by a tukey multiple comparison test.

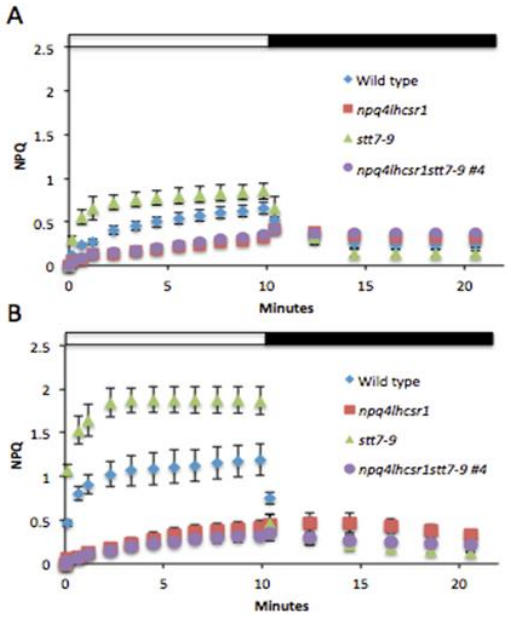


**Figure B.4 NPQ in qE and qT mutants.**
Relative excitation dependent quenching (qE) and PSII photoinhibition (qI) was assessed in light limited (A; 50 µmole photon $m^{-2}$ $s^{-1}$) or excess light (B; 860 µmole photon $m^{-2}$ $s^{-1}$) acclimated cultures. A Dual-PAM fluorometer was used to measure non-photochemical quenching of chlorophyll (NPQ) fluorescence induced during exposure to excess light shown under the white box (Light limited = 600 µmole photon $m^{-2}$ $s^{-1}$; Excess light= 2005 µmole photon $m^{-2}$ $s^{-1}$) followed by dark relaxation with far red light to re-oxidize the plastoquinone pool by preferential PSI excitation. This was used to separate qI from qT. Data represents means ± s.d. (n=3).

To test whether growth reductions are due to increased ROS generation, the fluorescent probe, cellROX (Life Tech), was used to measure reactive species. No significance differences were observed between cultures under either growth condition tested (Table A.1). While this suggests that oxidative stress is not responsible for the reductions in growth rate observed, cellROX does not react with $^1O_2$ produced by PSII during over excitation(Roach and Krieger-Liszkay, 2012).

Gross oxygen evolution by photosynthesis and oxygen consumption by respiration were measured in cultures acclimated to 860 µmole photon $m^{-2}$ $s^{-1}$ to determine if the relative rates of photosynthesis or respiration per cell were affected. No significant differences were observed during the 10-minute period used to measure oxygen consumption by respiration in the dark or oxygen evolution measured during exposure to 900 µmole photon $m^{-2}$ $s^{-1}$ (Table A.1B). This suggests that loss of excitation dependent quenching and/or state transitions does not significantly impair the rates of photosynthesis or respiration under their respective culture conditions.

**Table B.1 Effects of light level on *Chlamydomonas* qE and qT mutants.**
Data represent mean ± s.d. for low light (50 µmole photon $m^{-2}$ $s^{-1}$) acclimated (A) and high light (860 µmole photon $m^{-2}$ $s^{-1}$) acclimated cultures (B) Symbols denote statistically significant differences ($p < 0.05$) based on a one-way ANOVA followed by a tukey multiple comparison test for n = 3-8. (-) denotes measurements not yet performed. Note that chlorophyll measurements provided in this table are performed via methanol extraction and are not comparible to the acetone extractions performed in Chapter 2. Methanol extraction increasing the rate of chlorophyll degradation and lead to inaccurate calculations of chlorophyll a/b ratios in this study(Porra, 2002).

A

| | units | 50 µmol photon $m^{-2}$ $s^{-1}$ | | | |
|---|---|---|---|---|---|
| | | Wild type | *npq4lhcsr1* | *stt7-9* | *npq4lhcsr1stt7-9#4* |
| Chlorophyll a + b | Fmol/cel | 3.23 ± 0.30 @,* | 2.61 ± 0.22 #,* | 3.67 ± 0.34 @ | 2.17 ± 0.18 * |
| chlorophylla/b | mol:mol | 3.66 ± 0.07 | 4.03 ± 0.26 | 4.19 ± 0.35 | 3.80 ± 0.09 |
| State transitions | $100*(Fm^{oxi}-Fm^{red})/Fm^{oxi}$ | 25.9 ± 1.6@ | 21.2 ± 1.7 * | -0.3 ± 0.7 # | -3.3 ± 0.8 # |
| Cell size | $\mu m^3$ | - | - | - | - |
| Gross oxygen evolution | fmol $O_2$ $cell^{-1}$ $day^{-1}$ | - | - | - | - |
| Respiration | fmol $O_2$ $cell^{-1}$ $day^{-1}$ | - | - | - | - |
| Relative CellROX | RFU (X1000) per cell | 9.6 ± 2.4 | 7.1 ± 0.8 | 5.3 ± 0.8 | 8.1 ± 4.2 |

B

| | units | 860 µmol photon $m^{-2}$ $s^{-1}$ | | | |
|---|---|---|---|---|---|
| | | Wild type | *npq4lhcsr1* | *stt7-9* | *npq4lhcsr1stt7-9#4* |
| Chlorophyll a + b | Fmol/cel | 0.89 ± 0.14 @ | 1.21 ± 0.34 * | 1.93 ± 0.35 # | 0.601 ± 0.15 @ |
| chlorophylla/b | mol:mol | 4.96 ± 1.3 | 3.63 ± 0.87 | 3.97 ± 1.16 | 3.92 ± 0.82 |
| State transitions (% change) | $100*(Fm^{oxi}-Fm^{red})/Fm^{oxi}$ | 28.9 ± 2.5 @ | 25.6 ± 5 @ | 8.0 ± 5.7 * | -0.5±+0.3 * |
| Cell size | $\mu m^3$ | 198.0 ± 13.1 | 160.6 ± 26.3 | 266.4 ± 42.9 | 139.7 ± 10.2 |
| Gross oxygen evolution | fmol $O_2$ $cell^{-1}$ $day^{-1}$ | 6.9 ± 2.2 | 7.8 ± 3.2 | 10.6 ± 3.0 | 7.3 ± 1.3 |
| Respiration | fmol $O_2$ $cell^{-1}$ $day^{-1}$ | 3.1 ± 1.2 | 3.3 ± 1.2 | 3.5 ± 1.3 | 2.4 ± 1.7 |
| Relative CellROX | RFU (X1000) per cell | 1296.7 ± 85.5 | 1336.2 ± 96.1 | 1145.2 ± 100.0 | 1251.3 ± 38.7 |

Previous characterization of the stt7-9 mutant has proceeded in the absence of concrete genotype verification (Lucker *et al.*, 2013, Cardol *et al.*, 2009, Allorent *et al.*, 2013, Ghysels *et al.* 2013, Alric *et al.*, 2014, Johnson *et al.,* 2012, Nagy *et al.*, 2014, Roach *et al.*, 2015, Kodru *et al.*, 2015). Figure A.5A and B provide representations of the chloroplast genome location for the *stt7* gene. We used overlapping amplicons to map the site of the *arg7* insertion cassette used to generate this mutant. We found that amplicons 6-9 were missing in the *stt7-9* mutant line. Additionaly, we failed to obtain amplicons to test PCRs for 5' genes encoding the small subunit of Rubisco (*rbcS2*) and the uncharacterized ORF g2496. This indicates the *stt7-9* mutant has a

background mutation that likely effects the phenotype observed.

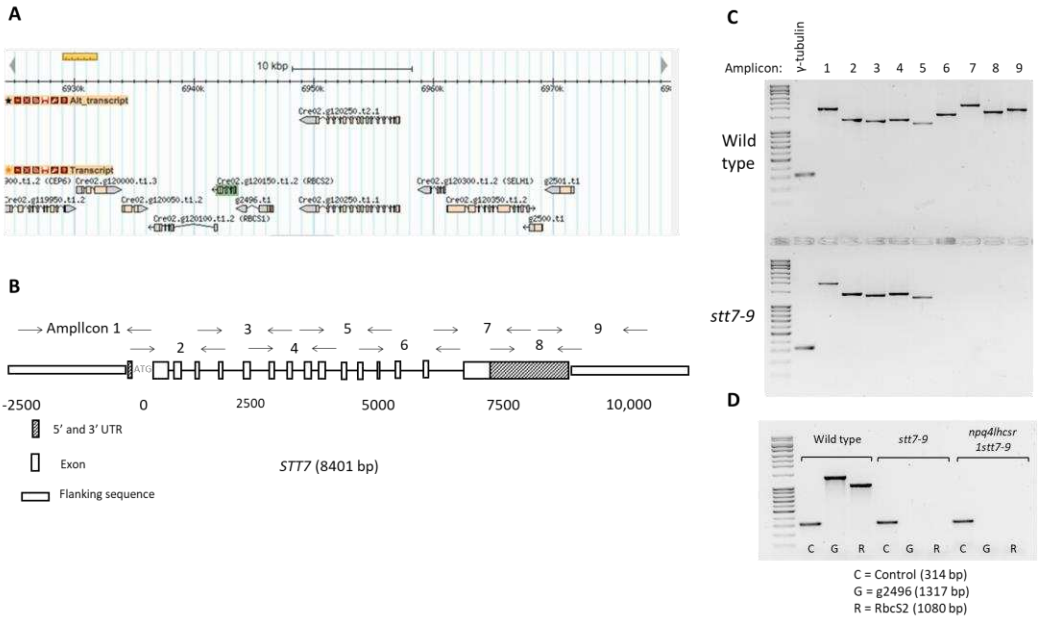


**Figure B.5 PCR based investigation of the putative mutation in the *stt7-9* background.** (A) JGI genome map of the *stt7* (Cre02.g120250) gene sequence - boxe. (B) Representation of PCR strategy for identification of the mutation site in the *stt7* gene. (C) Gel electrophoresis of PCR reactions for wild type and the *stt7-9.* (D) Gel electrophoresis of PCR tests used for assessing the presence of the g2496 and *rbcS2* coding regions.

## Conclusions

Background mutations identified by PCR in the *stt7-9* mutant suggested that phenotypes observed may be impacted by factors outside of the inhibition of *stt7-9* protein accumulation. We proceeded as reported in Chapter #2 by focusing our characterization on the qE mutant *npq4lhcsr1*. It was later shown that the *stt7-9* mutant produced a STT7 protein fused to the ARG7 resistance cassette used in its construction (Bergner *et al.*, 2015). This mutant showed extremely low Kinase activity and has not been used in the literature since.